DOTTORATO DI RICERCA IN BIOLOGIA

(XXX CICLO)

Human dental tissues: Advancement in virtual dental analysis

Tesi di
Gregorio Oxilia

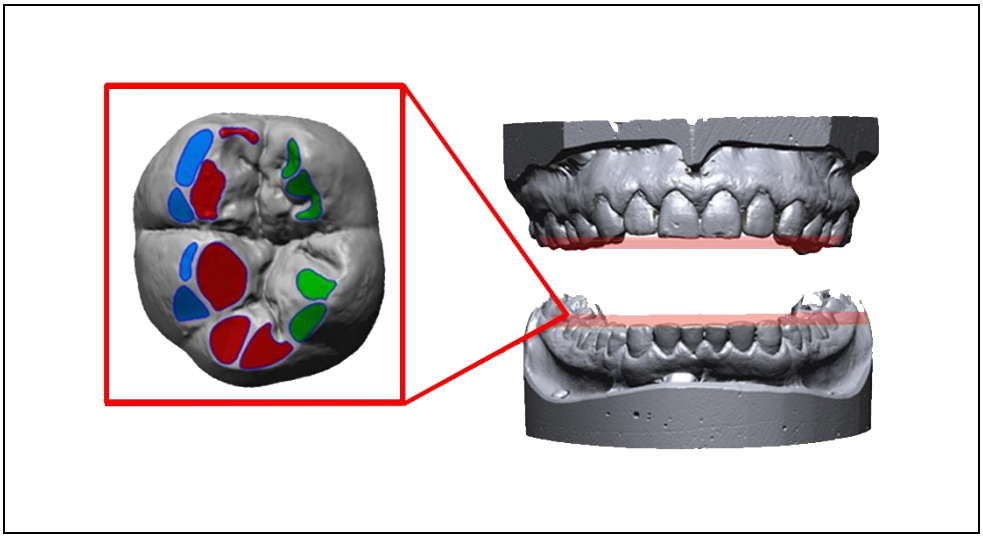

Coordinatore Prof. Alberto Ugolini

Tutor Prof. Jacopo Moggi Cecchi
Co-tutor Prof. Stefano Benazzi

(2018)

UNIVERSITÀ
DEGLI STUDI
FIRENZE

DOTTORATO DI RICERCA IN BIOLOGIA

(Antropologia e Primatologia)

CICLO XXX

Human dental tissues: Advancement in virtual dental analysis.

Settore Scientifico Disciplinare BIO/08

Dottorando:
Dott. Oxilia Gregorio

Tutore:
Prof. Jacopo MoggiCecchi

Co-tutore:
Prof. Stefano Benazzi

Coordinatore:
Prof. Alberto Ugolini

Anni 2014/2017

TABLE OF CONTENTS

Abstract

The subject of this doctoral dissertation concerns the usefulness of virtual analysis approach in studies of dental tissues and their defects.

The real symmetry and perfect balance between opposite jaw halves and antagonistic teeth is not the reality in the masticatory system. The sample of Yuendumu Aboriginal people used in **Paper I** consists of complete maxillary and mandibular dental arch 3D models from 19 individuals (young and adult). The analysis was carried out on first molars from all quadrants and only individuals with similar levels of wear were selected (76 teeth in total). Virtual methods were applied in order to inspect the palatal arch asymmetries in relation to the alveolar bones inclination and consequently, the alteration of dental crown.

Crown alteration (Enamel and Dentine) could be produced by several factors such as masticatory activity, pathological, anthropic and cultural alterations. However, anthropological studies are sometimes not able to distinguish differences among them without an interdisciplinary approach.

Particularly, pathological alterations (pits and fissures) are extremely difficult to interpret without microscopy analysis. That is the reason why a virtual approach in dental studies is useful to understand and distinguish any natural or anthropic alteration. Two examples are shown in **Paper II** and **Paper III** where two dental treatments discovered in two Italian sites have been described: Villabruna specimen and Fredian shelters.

The modern human specimen Villabruna (Paper II) from a burial in Northern Italy is the earliest evidence of dental therapeutic intervention on a Late Upper Paleolithic (ca. 14,000 yr BP). Using Scanning Electron Microscopy (SEM) we showed the presence of striations deriving from the manipulation of a large occlusal carious cavity of the lower right third molar. The striations have a "V''-shaped transverse section and several parallel micro-scratches at their

base, as typically displayed by cutmarks on teeth. Based on in vitro experimental replication and a complete functional reconstruction of the Villabruna dental arches, we confirmed that the identified striations and the associated extensive enamel chipping on the mesial wall of the cavity were produced ante-mortem by pointed flint tools during scratching and chiseling activities.

Similar situation was identified at the Fredian shelter (Paper III). The two upper incisors display exposed pulp chambers with circumferential enlargement, chipped dentine on the cavity margins and striations on the cavity walls. Histochemical analysis of the material embedded at the bottom of the cavities revealed a conglomerate of vegetal fibers and probably hairs. Moreover, Fourier transform infrared spectroscopy (FTIR), energy dispersion X-ray spectroscopy (EDS), and Raman microscopy analysis of black residue adhering to the walls of both cavities is consistent with organic substances, specifically bitumen. A direct chronometric date for Fredian 5 confirms a Late Upper Paleolithic context (between 13,000-12,735 calendar years ago). Overall, our results are consistent with in vivo dental drilling to remove necrotic or infected pulp tissue (pulpitis) and the subsequent use of a composite, organic dental filling in the cavity.

The conservation of human remains is the main interest of good anthropological research and any organic matter identified within a dental cavity needs to be conserved. This is the topic of **paper IV**: Letter to the Editor I had written in order to clarify the reason why we have decided to use three different methods (infrared spectroscopy (FTIR), energy dispersion X-ray spectroscopy (EDS), and Raman microscopy analysis) rather than gas-chromatography.

Finally, when a tooth does not show any pathological alteration or exhibits a normal/slight wear pattern on the occlusal surface (wear stage 1-2, 3 Smith, 1974) it is possible to obtain information regarding taxonomy based on volume

(3D) or areas (2D) of Enamel, Dentine (**paper V, VI, VII. VIII**) and morphometric analysis of teeth's root (**paper IX**).

This thesis therefore strives to provide a contribution to understanding how virtual approach to dental studies can be used to increase the knowledge of dental tissues and their defects.

List of Publications

Paper I – Journal of Dental Research

G. Oxilia, O. Kullmer, G. Townsend, J. Kaidonis, Marco Boggioni, Andrea Papini, J. Moggi-Cecchi, L. Fiorenza, S. Benazzi. Asymmetry, balance and dental macrowear patterns of Yuendumu Aboriginals: a case study. *Journal of Dental Research* (Under-Review).

Paper II – Scientific Reports - Nature

Gregorio Oxilia, Marco Peresani, Matteo Romandini, Chiara Matteucci, Cynthianne Debono Spiteri, Amanda G. Henry, Dieter Schulz, Will Archer, Jacopo Crezzini, Francesco Boschin, Paolo Boscato, Klervia Jaouen, Tamara Dogandzic, Alberto Broglio, Jacopo Moggi-Cecchi, Luca Fiorenza, Jean-Jacques Hublin, Ottmar Kullmer & Stefano Benazzi (2015). Earliest evidence of dental caries manipulation in the Late Upper Palaeolithic. *S*cientific Reports **5**, 12150; doi: 10.1038/srep12150.

Paper III – American Journal of Physical Anthropology

Gregorio Oxilia, Flavia Fiorillo, Francesco Boschin, Elisabetta Boaretto, Salvatore A. Apicella, Chiara Matteucci, Daniele Panetta, Rossella Pistocchi, Franca Guerrini, Cristiana Margherita, Massimo Andretta, Rita Sorrentino, Giovanni Boschian, Simona Arrighi, Irene Dori, Giuseppe Mancuso, Jacopo Crezzini, Alessandro Riga, Maria C. Serrangeli, Antonino Vazzana, Piero A. Salvadori, Mariangela Vandini, Carlo Tozzi, Adriana Moroni, Robin N. M. Feeney, John C. Willman, Jacopo Moggi-Cecchi, Stefano Benazzi (2017a). The dawn of dentistry in the late upper Paleolithic: An early case of pathological intervention at Riparo Fredian. *American Journal of Physical Anthropology.* 00:1–16. https://doi.org/10.1002/ajpa.23216.

Paper IV – American Journal of Physical Anthropology

Gregorio Oxilia, Flavia Fiorillo, Francesco Boschin, Elisabetta Boaretto, Salvatore A. Apicella, Chiara Matteucci, Daniele Panetta, Rossella Pistocchi, Franca Guerrini, Cristiana Margherita, Massimo Andretta, Rita Sorrentino, Giovanni Boschian, Simona Arrighi, Irene Dori, Giuseppe Mancuso, Jacopo Crezzini, Alessandro Riga, Maria C. Serrangeli, Antonino Vazzana, Piero A. Salvadori, Mariangela Vandini, Carlo Tozzi, Adriana Moroni, Robin N. M. Feeney, John C. Willman, Jacopo Moggi-Cecchi, Stefano Benazzi (2017b). Letter to the editor: Reply to Hardy & Buckley: Earliest evidence of bitumen from Homo sp. teeth is from El Sidron. *American Journal of Physical Anthropology*. DOI: 10.1002/ajpa.23254.

Paper V – Journal of Human Evolution

Cristiana Margherita, Sahra Talamo, Karin Wiltschke-Schrotta, Sascha Senck, **Gregorio Oxilia**, Rita Sorrentino, Giuseppe Mancuso, Giorgio Gruppioni, Robert Lindner, Jean-Jacques Hublin, Stefano Benazzi (2016). A reassessment of the presumed Torrener Bärenhöhle's Paleolithic human tooth. *Journal of Juman Evolution*, 30; 1e6.

Paper VI – Quaternary International

Julie Arnaud, Carlo Peretto, Daniele Panetta, Maria Tripodi, Federica Fontana, Marta Arzarello, Ursula Thun Hohenstein, Claudio Berto, Benedetto Sala, **Gregorio Oxilia**, Piero A Salvadori, Stefano Benazzi (2016). A reexamination of the Middle Paleolithic human remains from Riparo Tagliente, Italy. *Quaternary International*, 425; 437-444.

Paper VII – Journal of Human Evolution

Cristiana Margherita, **Gregorio Oxilia**, Veronica Barbi, Daniele Panetta, Jean – Jacques Hublin, David Lordkipanidze, Tengiz Meshveliani, Nino Jakeli, Zinovi

Matskevich, Ofer Bar-Yosef, Anna Belfer-Cohen, Ron Pinhasi, Stefano Benazzi (2017). Morphological description and morphometric analyses of the Upper Palaeolithic human remains from Dzudzuana and Satsurblia caves, western Georgia. *Journal of Human Evolution*, 113, 83-90.

Paper VIII – Scientific Reports – Nature

Ella Been, Erella Hovers, Ravid Ekshtain, Ariel Malinski-Buller, Nuha Agha, Alon Barash, Daniella E. Bar-Yosef Mayer, Stefano Benazzi, Jean-Jacques Hublin, Lihi Levin, Noam Greenbaum, Netta Mitki, **Gregorio Oxilia**, Naomi Porat, Joel Roskin, Michalle Soudack, Reuven Yeshurun, Ruth Shahack-Gross, Nadav Nir, Mareike C. Stahlschmidt, Yoel Rak, Omry Barzilai (2017). The first Neanderthal remains from an open-air Middle Palaeolithic site in the Levant. *Scientific Reports*. 7 – 2958 doi:10.1038/s41598-017-03025-z

Paper IX – Journal of Anthropological Sciences

Alessandro Riga, **Gregorio Oxilia**, Daniele Panetta, Piero A. Salvadori, Stefano Benazzi, Lyn Wadley, Jacopo Moggi-Cecchi. Human deciduous teeth from the Middle Stone Age layers of Sibudu Cave (South Africa). *Journal of Anthropological Sciences* (Under-Review).

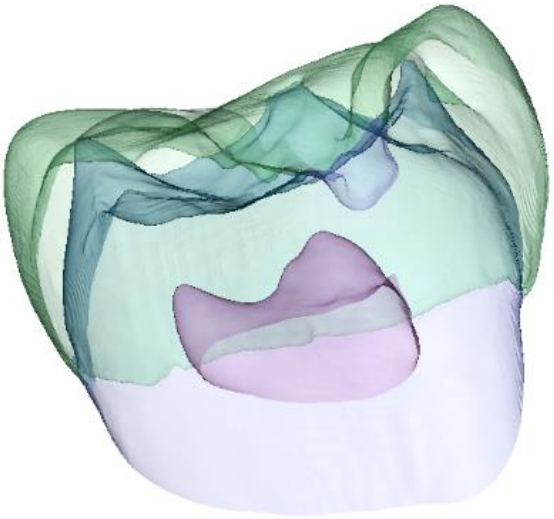

“It is always advisable to perceive clearly our ignorance.”
(Charles R. Darwin)

Introduction

A tooth consists of two main tissues: 1) Enamel, 2) Dentine.

Enamel is the hardest mineralized tissue in the human body covering the dentine in the crown of tooth. It contains only 4% of organic (1% protein and about 3% of water) and 96% of inorganic matter mainly composed by hydroxyapatite crystals (Eastoe 1960, Cuy et al. 2002, Hillson 1996, Nanci 2012). Enamel has no vascular supply and no cells thus tooth enamel cannot repair damage from decay or from wear.

Dentine is composed by 70% hydroxyapatite, 20% collagen and 10% water and it is less mineralized than the enamel, making this tissue more brittle (Nanci 2012). It partially contributes to the crown and forms the root in which nerve is hosted (Weber 2010).

Dentine is avascular but has cells (odontoblasts) lining its inner surface. When Enamel looses thickness, dentine surface is exposed, increasing the sensitivity due to the the tubules which stimulate the nerves and cells inside the tooth. Pulp chamber is at the center of the teeth containing innervation, blood vessels and connective tissue. Finally, a thin cementum layer coats the root to the jawbone through a system of collagenous connective tissue fibers called periodontal fibers (Hillson 1996, Wittwer-Backofen et al. 2003).

1. OCCLUSAL SURFACE ALTERATIONS

1.1 Masticatory activity

Masticatory activities are one of the many factors producing the gradual loss of enamel tissues; it is possible to distinct three processes: attrition, abrasion and erosion that act together, each with a varying intensity and duration to produce a multitude of different wear patterns (Kaidonis, 2008).

The first (attrition) is a mechanical wear produced by occlusal surfaces contact of antagonist teeth and it produce flat and shiny areas with well-defined borders called wear facets (Every, 1972; Kaidonis et al., 1993; Imfeld, 1996; Hillson, 2003; Kaidonis, 2008).

The second (abrasion) is generated by frictions of exogenous materials (Kaifu et al., 2003; Kaidonis, 2008). In fact, the food or dust usually contain some abrasive particles, which produce some striations on the occlusal surface of a tooth.

Finally, the loss of enamel tissue can be also induced by chemical dissolution (Erosion) (Kaifu et al., 2003; Addy & Shellis, 2006; Kaidonis, 2008). Wear facets produced by this dissolution are different from those produced by attrition. In fact, defects produced by erosion are sharply defined, wedge-shaped depressions often in facial and cervical areas. Although dentinal scooping is commonly associated with erosion, the eroded occlusal surface displays significant differences in shape compared with that caused mainly by abrasion (Bell et al., 1998).

1.2 Pathological alteration

Pathological defects such as infection caries are the most intrusive cause of dental crown alteration. Dental caries are a major oral health problem in modern human societies, representing one of the most common chronic dental diseases

around the world. This transmissible disease is the result of an imbalance of the indigenous oral biota rather than a nonindigenous, exogenous pathogen (Caufield et al. 2000). Dental caries develops by the localized dissolution of the tooth hard tissues, caused by acids that are produced by bacteria in the biofilms (dental plaque) on the teeth and eventually lead to "cavities." Microbe communities attach to tooth surface and create a biofilm (Velusamy et al. 2016) and it use sucrose and other dietary sugars as a food source to grow (Marsh et al. 1999). The dietary sugars go through anaerobic fermentation pathways producing lactate. The lactate is excreted from the cell onto the tooth enamel then ionizes. The lactate ions demineralize the hydroxyapatite crystals causing the tooth to be degraded (Yadav et al. 2017). The biofilm consists of microorganisms, including the highly cariogenic mutants streptococci, and a matrix made up mainly of extracellular polysaccharides (Figure 2). The destructive acids are produced when fermentable carbohydrates (sugars) reach these biofilms, each episode resulting in tooth damage (attack). If this process does not occur frequently, then the natural capacity of the body (through saliva) to remineralize will prevent formation of a cavity (Kreth et al. 2015). Thus, the main risk factors include presence of cariogenic biofilms and frequent consumption of fermentable carbohydrates

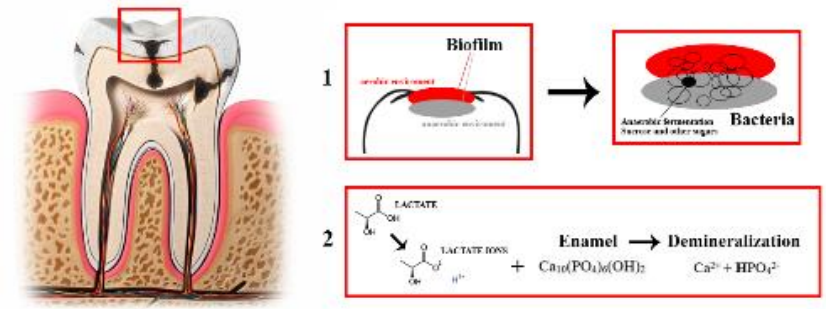

Figure 2. Formation process of infection caries.

1.3 Anthropic alteration

Dental caries is a major oral health problem in modern human societies (Cummins, 2013), representing one of the most common chronic dental disease around the world. The need to treat carious teeth was well-known during historical time as well. To improve pain relief, medieval treatments were based on either humoral theory using herbal remedies or anatomical principles (Anderson, 2004; Khodadoust et al., 2013). Ancient Greeks and mainly Romans were acquainted with caries removal by drilling and emptying the painful teeth (Guerini, 1909), and Egyptian texts confirm this practice was established at least in the third millennia BC (Ring, 1985).

The most ancient evidence of dentistry dates back to the Neolithic period, probably caused by the increase in carbohydrate-rich diets typical of agricultural societies when compared with the more varied diet of hunter-gatherers (Braidwood et al., 1961; Oelzea et al., 2011). Indeed, beeswax dental filling was discovered in ca. 6,500 ya old human tooth from Slovenia (Bernardini et al., 2012), while tooth perforation with bow drills, presumably to remove decayed tissues, was observed in ca. 9,000 ya old molars from a Neolithic graveyard in Pakistan (Coppa et al., 2006).

Before the Neolithic, primitive forms of oral hygiene were represented by the use of toothpicks (hard, thin and rigid probe, such as small piece of wood or bone) maybe to remove food particles between teeth, leaving characteristic interproximal grooves (in the mesial and distal surface of the teeth) bucco-lingually elongated (Lozano et al., 2013). This practice, documented from the beginning of the genus Homo to present day aboriginal populations (Brown and Molnar, 1990), has been suggested as a measure to alleviate sore gums (Lozano et al., 2013), but does not represent a real dental treatment.

Indeed, beeswax dental filling was discovered in ca. 6,500 yr BP human tooth from Slovenia (8), while tooth perforation with bow drills, presumably to

remove decayed tissues, was observed in ca. 9,000 yr BP molars from a Neolithic graveyard in Pakistan (Coppa et a.- 2006).

This thesis provides new evidence of dental manipulation backdating the earliest evidence of caries treatment to the Late Upper Paleolithic.

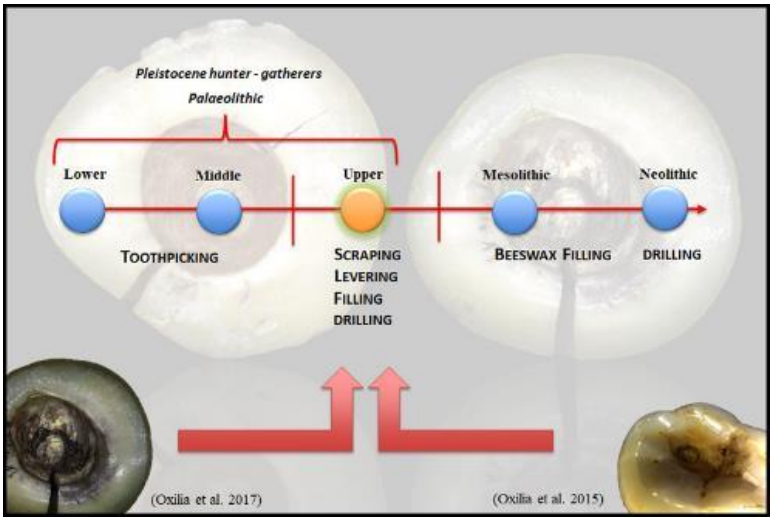

Figure 3. Short timeline of anthropic treatment.

1.4 Cultural expression

Regional traditions of intentional dental modification for purposes of cultural expression of social identities are well documented. Non-therapeutic dental modifications are major cultural expressions in recent hunter-gatherers groups (Milner et al. 1991, Pinchi et al. 2015), representing one of the most common body manipulation used to communicate symbolic messages. Various forms of dental modification have been documented (Vukovic et al. 2009, Pinchi et al. 2015), most of them involving the ablation (i.e., mutilation) and reshaping (e.g., filing, perforation, inlay) of the anterior teeth, in particular the upper central

incisors (González et al. 2010, Roksandic et al. 2016). Likewise various are the symbolic meaning that this practice conveys, which may be related to religious purposes, initiation and rites of passage, markings of social status or rank, group identity, or to imitate attributes of specific animals (Benedix 1998, Zumbroich 2009).

Dental ablation represents the oldest evidence, a rudimentary practice observed in North Africa (Humphrey et al. 2008) and Southeast Asia (Willman et al. 2016) since the Late Upper Paleolithic. More complex patterns that envisage the intentional reshaping of the anterior teeth, rather than ablation, emerged later, the most ancient one dating to the Late Stone Age (ca. 4500–4200 BP) of Karkarichinkat in the lower Tilemsi Valley, Eastern Mali (Finucane et al. 2008). Subsequently, dental reshaping was observed in some early civilizations dating to the 2nd millennium BC (Tisler et al. 1999), and from this time period onward it was recognized in several past societies around the world (Arcini 2005, Becker, 1994)

2 TAXONOMICAL IDENTIFICATION

2.1 Crown

Enamel thickness analysis plays an important role in the taxonomic, phylogenetic, and dietary assessment of extant and fossil primates (Schwartz, 2000; Martin et al., 2003; Grine et al., 2005; Olejniczak et al., 2007; Smith et al., 2012).

Enamel Thickness can be studied in 2D and 3D analysis. The methods used to measure 2D Enamel thickness follow the pioneer method provided by Martin (1985) which was based on a single physical cross-section on primate teeth. The need to maintain dental remains intact, pushed scholars to rethink new analytical methods, such as synchrotron and standard micro-computed tomography (micro-CT) based on non-destructive analysis. Two-dimensional (2D) enamel thickness analysis was refined and the study of dental enamel thickness began to be studied in three dimensional (3D) form (Kono, 2004; Tafforeau, 2004; Olejniczak, 2006; Olejniczak et al., 2008). With the exception of *Ardipithecus ramidus* (White et al., 1994), hominins are generally considered to be a thick-enameled clade (e.g., Martin, 1985; Grine and Martin, 1988; Kono, 2004; Tafforeau, 2004; Smith et al., 2005, 2006a; Olejniczak et al., 2008, Grine and Martin, 1988; Macchiarelli et al., 2006; Smith et al., 2006b). Despite this characterization, enamel thickness variation within the genus *Homo* is poorly understood.

Neandertal molars show a derived condition of thinner enamel than fossil *Homo sapiens* and modern human molars (e.g., Zilberman and Smith, 1992; Zilberman et al., 1992; Molnar et al., 1993; Smith and Zilberman, 1994; Ramirez Rozzi, 1996; Grine, 2004), showing that enamel thickness range of genus *Homo* may be broader than is commonly stated, and that Neandertals occupy the thin end of this range. Therefore, thinner enamel in Neandertals has been used to support

their specific distinction from relatively thicker-enameled *Homo sapiens* (Grine, 2004).

Besides the taxonomical identification of the tissues of dental crown, the taxonomical identification can be identified also on teeth's roots.

2.2 Root

Anthropic and masticatory alterations are the main causes of crown reduction. Although there is a variable deposition of cementum layers at the root apex (Azaz et al., 1974; Ainamo and Talari, 1975; Dean et al., 1992; Lieberman, 1994), there are less change in tooth root than crown. This is the reason why taxonomical analysis has focused also on root metric analysis. There have been several functional, pathological and taxonomical studies on teeth roots in order to understand shapes variation among species.

The bifurcation (mandibular molar) or trifurcation (maxillary teeth) seems to be lesser functional than roots where this separation is more apically positioned (Blumberg et al., 1971; Kovacs, 1971). Two hypotheses have been put forward to explain the selective advantage of taurodont molars (Benazzi et al. 2015).

It has been argued that a large pulp chamber could be useful in high-attritional populations because the increasing of deposition of secondary dentine prolongs the tooth longevity (Coon, 1962; Hamner et al., 1964; Blumberg et al., 1971; Hillson, 1996).

Neanderthal teeth show some morphological and morphometric differences if compared to Sapiens. In fact, It has been observed an enlargement of crown size of neandertal teeth attained by expanding the crown (or cervical) base or by increasing cusp height, through a steeper topography of the enamel-dentine junction (EDJ) (Macchiarelli et al., 2006; Olejniczak et al., 2008).

Considering tooth crown as strictly related to root dimensions as observed in anthropoid primates (Kupczik et al., 2009) it would be expect that Neanderthal

exhibit large root surface areas compared to *H. sapiens*. Sure enough, many scholars support this prediction. Neandertals teeth have significantly greater dimension in tooth's root than Upper Palaeolithic and recent *H. sapiens* (Smith and Paquette, 1989; Bailey, 2005; Walker et al., 2008). In this thesis, taxonomical analysis (crown and root analysis) was useful in order to investigate appropriate attribution of some teeth.

3 OBJECTIVES

This thesis is focused on the potential of virtual dental analysis. The objectives are as follows:

(1) **Enamel tissue**: virtual analysis of dental wear pattern related to the dynamic context of the masticatory system.

(2) **Enamel and Dentine tissues**: detailed understanding of cavities identified on dental crown using microCT scan and virtual analysis.

(3) **Enamel, Dentine, pulp chamber and root**: 2D and 3D virtual analysis of teeth. Morphological and morphometric analysis of dental tissues were studied in order to obtain information about taxonomy.

4 MATERIALS

Masticatory, pathological and functional studies:

- Paleolithic specimen: **Riparo Villabruna** (Italy);
- Paleolithic specimen: **Riparo Fredian** (Italy);
- Recent human group: **Yuendumu Aboriginal people** (Australia).

Taxonomical studies:

- Paleolithic specimen: **Torrener Bärenhöhle** (Austria);
- Paleolithic specimen: **Riparo Tagliente** (Italy);
- Paleolithic specimen: **Dzudzuana and Satsurblia** (Georgia);
- Paleolithic specimen: **Quashish** (Israel).
- Paleolithic specimen: **Sibudu** (Africa)

Figure 4. Geographic provenance of samples.

5 RESULTS

This thesis consists of nine papers:

Paper I: The physiologicial linkage between dental arch asymmetry, alveolar inclination and dental macrowear pattern.

Journal of Dental Research (Under-Review).
G. Oxilia, E. Bortolini, S. Martini, A. Papini, M. Boggioni, L. Buti, G. Townsend, J. Kaidonis, L. Fiorenza, Emanuela Cristiani, O. Kullmer, J. Moggi-Cecchi, S. Benazzi.

Exact symmetry and perfect balance between opposite jaw halves as well as between antagonistic teeth is not frequently observed in natural masticatory systems. Research results show that asymmetry in our body, skull, and jaws is often related to genetic environmental and individual ontogenetic factors. However, modern humans exhibit increased variability in tooth positions and asymmetry compared to non-human primates and most fossil hominins. The present work investigates the relationship between dental macrowear patterns and alveolar inclinations on a sample of complete maxillary and mandibular 3D models of dental arches from 19 young and adult Yuendumu Aboriginal individuals. The analysis was carried out on first molars (M1) from all quadrants. Virtual models were oriented identifying a standard reference plane for each jaw. Occlusal Fingerprint Analysis was used for the analysis of macrowear patterns, and 2D cross-sectional geometric analysis of the jaws was carried out to investigate asymmetry in dental arches. The asymmetry observed in the present sample is highly variable on both arches, and it is associated with differences in the inclination of upper M1 crowns. Wear facet position on opposite teeth also reflects differences in inclination of the molars between left

and right sides. Our results suggest that overall asymmetry in the masticatory apparatus of modern humans affects occlusal contacts of wear facets between opposing teeth.

Paper II: Earliest evidence of dental caries manipulation in the Late Upper Palaeolithic.

Scientific Reports 5, 12150 (2015).
Gregorio Oxilia, Marco Peresani, Matteo Romandini, Chiara Matteucci, Cynthianne Debono Spiteri, Amanda G. Henry, Dieter Schulz, Will Archer, Jacopo Crezzini, Francesco Boschin, Paolo Boscato, Klervia Jaouen, Tamara Dogandzic, Alberto Broglio, Jacopo Moggi-Cecchi, Luca Fiorenza, Jean-Jacques Hublin, Ottmar Kullmer & Stefano Benazzi

Prehistoric dental treatments were extremely rare, and the few documented cases are known from the Neolithic, when the adoption of early farming culture caused an increase of carious lesions. Here we report the earliest evidence of dental caries intervention on a Late Upper Palaeolithic modern human specimen (Villabruna) from a burial in Northern Italy. Using Scanning Electron Microscopy we show the presence of striations deriving from the manipulation of a large occlusal carious cavity of the lower right third molar. The striations have a “V”-shaped transverse section and several parallel micro-scratches at their base, as typically displayed by cutmarks on teeth. Based on in vitro experimental replication and a complete functional reconstruction of the Villabruna dental arches, we confirm that the identified striations and the associated extensive enamel chipping on the mesial wall of the cavity were produced ante-mortem by pointed flint tools during scratching and levering activities. The Villabruna specimen is therefore the oldest known evidence of dental caries intervention, suggesting at least some knowledge of disease

treatment well before the Neolithic. This study suggests that primitive forms of carious treatment in human evolution entail an adaptation of the well-known toothpicking for levering and scratching rather than drilling practices.

Paper III: The dawn of dentistry in the Late Upper Paleolithic: An early case of pathological intervention at Riparo Fredian.

American Journal of Physical Anthropology 163, 1096-8644 (2017).
Gregorio Oxilia, Flavia Fiorillo, Francesco Boschin, Elisabetta Boaretto, Salvatore A. Apicella, Chiara Matteucci, Daniele Panetta, Rossella Pistocchi, Franca Guerrini, Cristiana Margherita, Massimo Andretta, Rita Sorrentino, Giovanni Boschian, Simona Arrighi, Irene Dori, Giuseppe Mancuso, Jacopo Crezzini, Alessandro Riga, Maria C. Serrangeli, Antonino Vazzana, Piero A. Salvadori, Mariangela Vandini, Carlo Tozzi, Adriana Moroni, Robin N. M. Feeney, John C. Willman, Jacopo Moggi-Cecchi and Stefano Benazzi.

Early evidence for the treatment of dental pathology is found primarily among food-producing societies associated with high levels of oral pathology. However, some Late Pleistocene hunter-gatherers show extensive oral pathology, suggesting that experimentation with therapeutic dental interventions may have greater antiquity. Here we report the second earliest probable evidence for dentistry in a Late Upper Paleolithic hunter-gatherer recovered from Riparo Fredian (Tuscany, Italy).
The Fredian 5 human consists of an associated maxillary anterior dentition with antemortem exposure of both upper first incisor (I1) pulp chambers. The pulp chambers present probable antemortem modifications that warrant in-depth analyses and direct dating. Scanning electron microscopy (SEM), microCT and residue analyses were used to investigate the purported modifications of external and internal surfaces of each I1.

The direct date places Fredian 5 between 13,000-12,740 calendar years ago. Both pulp chambers were circumferentially enlarged prior to the death of this individual. Occlusal dentine flaking on the margin of the cavities and striations on their internal aspects suggest anthropic manipulation. Residue analyses revealed a conglomerate of bitumen, vegetal fibers, and probable hairs adherent to the internal walls of the cavities.

The results are consistent with tool-assisted manipulation to remove necrotic or infected pulp in vivo and the subsequent use of a composite, organic filling. Fredian 5 confirms the practice of dentistry – specifically, a pathology-induced intervention – among Late Pleistocene hunter-gatherers. As such, it appears that fundamental perceptions of biomedical knowledge and practice were in place long before the socioeconomic changes associated with the transition to food production in the Neolithic.

Paper IV: Letter to the editor: Reply to Hardy & Buckley: Earliest evidence of bitumen from Homo sp. teeth is from El Sidron.

American Journal of Physical Anthropology. DOI: 10.1002/ajpa.23254 (2017).
Gregorio Oxilia, Flavia Fiorillo, Francesco Boschin, Elisabetta Boaretto, Salvatore A. Apicella, Chiara Matteucci, Daniele Panetta, Rossella Pistocchi, Franca Guerrini, Cristiana Margherita, Massimo Andretta, Rita Sorrentino, Giovanni Boschian, Simona Arrighi, Irene Dori, Giuseppe Mancuso, Jacopo Crezzini, Alessandro Riga, Maria C. Serrangeli, Antonino Vazzana, Piero A. Salvadori, Mariangela Vandini, Carlo Tozzi, Adriana Moroni, Robin N. M. Feeney, John C. Willman, Jacopo Moggi-Cecchi and Stefano Benazzi.

In Oxilia et al., 2017, we report the presence of antemortem modifications to both I1 pulp chambers from a single individual (Fredian 5) from the Epigravettian context of Riparo Fredian (Tuscany, Italy). The analysis included

the direct dating of the Fredian 5 in addition to microscopic, microCT, and residue analyses of the internal and external surfaces of the modified I1s. In respond to our article, Hardy and Buckley (in press) take issue with both the methods used to analyze the residues retrieved from the pulp cavities of Fredian 5 and our interpretation of the residue as "bitumen." Furthermore, they argue that we wrongfully attribute our findings as the earliest instance of bitumen found on Pleistocene human teeth given it was described earlier among the Neandertals from El Sidron (Hardy et al., 2012; Radini et al., 2016; Radini, Buckley, Nikita, Copeland, & Hardy, 2017). We address these concerns in the letter.

Paper V: A reassessment of the presumed Torrener Bärenhöhle's Paleolithic human tooth

Journal of Juman Evolution. 30, 1e6 (2016).
Cristiana Margherita, Sahra Talamo, Karin Wiltschke-Schrotta, Sascha Senck, Gregorio Oxilia, Rita Sorrentino, Giuseppe Mancuso, Giorgio Gruppioni, Robert Lindner, Jean-Jacques Hublin, Stefano Benazzi.

Torrener Bärenhöhle's cave cave is a corridor located about 810 m€ from Golling an der Salzach (Salzburg, Austria). The cave was discovered in 1924 by Hermann Gruber, an Austrian alpine guide. After the initial speleological survey, the cave was the subject of a paleontological excavation. The excavation unearthed an enormous amount of animal bones mostly belonging to Ursus spelaeus, for a total of more than 90 individuals. Until 1971, the publications about this cave had always mentioned animal bones only, but Gaisberger later reported the presence of a human molar attributed to the 1924 Torrener Bärenhöhle's collection difficult to attribute. In this contribution, we investigate the tooth from Torrener Bärenhöhle's cave (hereafter called T.B.I).

This tooth was microCT-scanned to digitally study its external and internal morphology, and sampled for AMS radiocarbon dating to establish its taxonomy and chronology.

Paper VI: A reexamination of the Middle Paleolithic human remains from Riparo Tagliente.

Quaternary International, 425; 437-444 (2016).
Julie Arnaud, Carlo Peretto, Daniele Panetta, Maria Tripodi, Federica Fontana, Marta Arzarello, Ursula Thun Hohenstein, Claudio Berto, Benedetto Sala, Gregorio Oxilia, Piero A Salvadori, Stefano Benazzi.

Despite new discoveries of human fossil remains, some aspects of paleoanthropological research are biased by the poor sample size, which limits our understanding of intra-species variability among the different hominin species. In this context, continuous assessment and reassessment of human fossil remains discovered decades ago, and often unknown to the scientific community, represent an opportunity to address this issue. Moreover, deciduous teeth are less studied than permanent dentitions, an aspect which contributes to limit our understanding. In the present study, we provide a detailed description of Tagliente 3 (upper right second deciduous molar) and Tagliente 4 (lower left deciduous canine), two deciduous teeth from Riparo Tagliente (Stallavena di Grezzana, Verona) attributed to Homo neanderthalensis. In terms of morphology and size, Tagliente 3 presents typical Neandertal derived features (e.g., likely large hypocone and complex topography of the enamel-dentine junction). Although deciduous canines usually do not provide substantial morphologically diagnostic information, Tagliente 4 falls in the upper range of the Neandertal variability for its bucco-lingual diameter. In terms of tissue proportions both teeth fall within the Neandertal range of variation: Tagliente 3 for the enamel thickness distribution and Tagliente 4 for the volume of the

crown dentine. This work contributes to increase our knowledge on the variability of Neandertal deciduous dentition.

Paper VII: Morphological description and morphometric analyses of the Upper Palaeolithic human remains from Dzudzuana and Satsurblia caves, western Georgia.

Journal of Human Evolution, 113, 83-90. (2017).
Cristiana Margherita, Gregorio Oxilia, Veronica Barbi, Daniele Panetta, Jean – Jacques Hublin, David Lordkipanidze, Tengiz Meshveliani, Nino Jakeli, Zinovi Matskevich, Ofer Bar-Yosef, Anna Belfer-Cohen8, Ron Pinhasi, Stefano Benazzi.

Located in the southern Caucasus, Georgia was a major geographic corridor for hominin dispersal into Eurasia since the Early Pleistocene. During the Late Pleistocene it has been suggested that the region was inhabited by Neandertals until 37 ka cal BP, potentially replaced by modern humans 38-34 ka cal BP. However, the scanty fossil human remains retrieved from Late Pleistocene deposits in Georgia did not provide to date sufficient information to identify the makers of specific technocomplexes. Here we use non-invasive digital methods to provide the first dental morphological description and morphometric analyses of Upper Paleolithic human remains from Dzudzuana and Satsurblia caves, in western Georgia. The Upper Palaeolithic sequence at Dzudzuana cave comprises three occupational episodes separated by millennia long hiatuses: the lowermost UP phase, Unit D, dated to 34.5 32.2 ka cal. BP; the following Unit C, dated to 27–24 ka cal. BP (the human teeth studied were retrieved from the lower part of this Unit); and the latest UP phase, Unit B dated to 16.5–13.2 ka cal. BP. Human occupational layers at Satsurblia Cave yielded a series of living surfaces dated to (a) prior to the Last Glacial Maximum (LGM) at 25.5–24.4 ka

cal. BP and (b) after the LGM at 17.9–16.2 ka cal. BP. Human remains were from Area B, from layers dated to the post LGM phases dated to 13 ka cal BP. Dzu 1 (Rdm, Layer C3) and Dzu 2 (Rdm2, Layer C4) from Dzudzuana, SATP5-2 (Rdi1, Area B) and a left fragment of a juvenile mandible (bearing an erupted Ldm D= SATP5-3, and LM1 and un-erupted LP3,LP4,andLM2, Area B) from Satsurblia were scanned using micro-CT system. The resulting image data were segmented in order to produce three-dimensional digital copies, which were used for both morphological description and morphometric analyses. Besides mesio-distal (MD) and bucco-lingual (BL) crown diameters, we used crown (for Dzu 1 and SATP5-3) and cervical (for SATP5-3) outline analyses and we assessed the 3D enamel thickness of the permanent teeth. The morphometric data were compared with a sample of Neandertals, Early H. sapiens , UP H. sapiens and recent /textitH. sapiens teeth available from the literature, except for MD and BL diameters of the permanent teeth as well as the 3D enamel thickness, for which an ex novo comparative dataset was created. All morphological features (e.g., cusp numbers, fissure pattern) observed in all teeth align with modern humans. BL crown diameters of Dzu 1 and Dzu 2 are small and fall closer to the modern human variability, as also confirmed by the crown outline analysis of Dzu 1. Similar morphometric results were obtained for the human remains from Satsurblia Cave. Crown diameters for deciduous and permanent teeth are closer to the modern human range of variation. In addition, the crown and cervical outlines of SATP5 3 fall within the modern human range of variability. Finally, all permanent teeth of the Satsurblia mandibular fragment show thick enamel, higher than the mean values computed for Neandertals but within modern human variability. Overall, our results support the attribution of the Upper Paleolithic technocomplexes of both Dzudzuana and Satsurblia caves to modern humans. Moreover, the human remains from Dzudzuana represent, up to now, the oldest evidence of modern humans from southern Caucasus.

Paper VIII: The first Neanderthal remains from an open-air Middle Palaeolithic site in the Levant.

Scientific Reports, 7 - 2958 doi:10.1038/s41598-017-03025-z (2017).
Ella Been, Erella Hovers, Ravid Ekshtain, Ariel Malinski-Buller, Nuha Agha, Alon Barash, Daniella E. Bar-Yosef Mayer, Stefano Benazzi, Jean-Jacques Hublin, Lihi Levin, Noam Greenbaum, Netta Mitki, Gregorio Oxilia, Naomi Porat, Joel Roskin, Michalle Soudack, Reuven Yeshurun, Ruth Shahack-Gross, Nadav Nir, Mareike C. Stahlschmidt, Yoel Rak, Omry Barzilai.

The late Middle Palaeolithic (MP) settlement patterns in the Levant included the repeated use of caves and open landscape sites. The fossil record shows that two types of hominins occupied the region during this period—Neandertals and Homo sapiens. Until recently, diagnostic fossil remains were found only at cave sites. Because the two populations in this region left similar material cultural remains, it was impossible to attribute any open-air site to either species. In this study, we present newly discovered fossil remains from intact archaeological layers of the open-air site ‘Ein Qashish, in northern Israel. The hominin remains represent three individuals: EQH1, a ondiagnostic skull fragment; EQH2, an upper right third molar (RM 3); and EQH3, lower limb bones of a young Neandertal male. EQH2 and EQH3 constitute the fist diagnostic anatomical remains of Neandertals at an open-air site in the Levant. The optically stimulated luminescence ages suggest that Neandertals repeatedly visited ‘Ein Qashish between 70 and 60 ka. The discovery of Neandertals at open-air sites during the late MP reinforces the view that Neandertals were a resilient population in the Levant shortly before Upper Palaeolithic Homo sapiens populated the region

Paper IX: Human deciduous teeth from the Middle Stone Age layers of Sibudu Cave (South Africa).

Journal of Anthropological Sciences (Under-Review).
Alessandro Riga, Gregorio Oxilia, Daniele Panetta, Piero A. Salvadori, Stefano Benazzi, Lyn Wadley, Jacopo Moggi-Cecchi.

In the African Pleistocene, the fossil evidence of early Homo sapiens populations is still relatively limited. Here we present two additional specimens (two deciduous teeth) recovered from the Middle Stone Age (MSA) deposits of Sibudu Cave (KwaZulu-Natal, South Africa). We describe their morphology and metrics, using three-dimensional models of the teeth obtained from high-resolution micro-CT images. The first specimen is a Ldm1 (HUM. TO 1) recovered in the BS5 layer dated at the top level at 77.3 ± 2.7 ka and the tools from this member are assigned to the "pre-Still Bay" assemblage. The other specimen is a Rdi1 (HUM. TO 2) coming from the Pinkish Grey Sand (PGS) member, dated at 64.7±2.3 ka, and associated with the Howieson's Poort industry.

Both teeth are well preserved, with minor post mortem cracks not affecting the overall morphology and they comprise the intact, worn crown and the remnants of the roots, naturally resorbed. A large carious lesion occupies most of the distal face and part of the occlusal surface in the Ldm1; also a chip of enamel is missing from the disto-buccal corner. In the Rdi1 average enamel thickness and relative enamel thickness values have been measured. For both teeth, we compared mesio-distal (MD) and bucco-lingual (BL) diameters with those of other Late Pleistocene deciduous teeth and extant Homo sapiens. The analysis has shown that they are comparable in size with the other MSA specimens described in the literature. For the dm1s an interesting pattern emerges, in particular for the MD diameter, confirming a trend towards dental reduction in

our species and suggesting the possibility that deciduous dental metrics can discriminate different fossil populations of H. sapiens.

6 CONCLUSIONS

- This dissertation presents a contribution to understanding how virtual approach to dental studies can be used to increase the knowledge of dental tissues and their defects. Virtual approach provides information regarding each dental tissue, from which it is possible to obtain information about masticatory and para-masticatory activity, pathological alteration, anthropic intervention, cultural expression and taxonomy;

- New perspective of dental macrowear studies (Paper I). Development of wear facets is related to the asymmetries, which affect masticatory apparatus. Thus, internal factors such as deglutition seem to be responsible for wear facet development besides external influence such as dietary abrasiveness, environment or technology, which influence the integrity of occlusal surface during lifespan of an individual;

- Interdisciplinary studies allowed us to discover more ancient evidence of dental caries manipulation (Paper II and III) than previously known;

- Taxonomical analysis of human teeth is extreme useful to determine the species which it belongs, a particular settlement pattern or territorial behavior (Paper IV-IX).

Future Works

The analyzed samples show a wide variability of interpretation (taxonomy, functional, para-functional, pathological, anthropic and cultural expression) distinguishable by distinct patterns of alteration. Only interdisciplinary studies together to virtual and traditional anthropological approach can provide holistic comprehension of past/present human life style. Future studies on dental macrowear should focus on understanding:

1) How asymmetries of masticatory system influence dental wear pattern, ultimately supporting a reevaluation of our interpretation of cultural and dietary habits deducted by macrowear analysis.

2) How inclinations of alveolar arches influence the tooth orientation. In fact, the real inclination of a tooth is variable and it is not always 90 degree as dental studies assume based on the cervical line (Benazzi et al. 2011). A proper evaluation of tooth inclination could also allow understanding the reason why some wear facets developed and where the pressure of masticatory apparatus focus on during maximum intercuspation.

As discussed in Paper I, many of the features identified on human casts and fossils record are probably related to the tongue pressure, which has an important role in dental asymmetries development. The role of each variable should be considered both in dental evolutionary studies and in modern dentistry. In the first case, the studies of orofacial disorders would be useful to increase the knowledge of parafunctional disorders in the fossils; on the other, a functional approach retrieving the correct posture and functional deglutition of the tongue in dental rehabilitation should be considered to harmonize functionally the mouth with the rest of the body.

A holistic vision of tooth analysis could be useful in anthropological and dentistry fields.

References

Addy, M. & Shellis, R.P. 2006. Interaction between attrition, abrasion and erosion in tooth wear. *Monographs in Oral Science*, 20, 17–31.

Ainamo, J. & Talari, A. 1975. Eruptive movements of teeth in human adults. In: Poole, D.G.F., Stack, M.V. (Eds.), Eruptive Movements of Teeth in Human Adults. Butterworths, London, pp. 97e107

Anderson, T. 2004. Dental treatment in Medieval England. *The British Dental Journal*, 197, 419–25.

Arcini, C. 2005. The Vikings bare their filed teeth. *American Journal of Physical Anthropology*, 128, 727–733.

Azaz, B., Ulmansky, M., Moshev, R. & Sela, J. 1974. Correlation between age and thickness of cementum in impacted teeth. *Oral Surgery, Oral Medicine, Oral Pathology, Oral Radiology*, 38, 691e694.

Bailey, S.E. 2005. Diagnostic dental differences between Neandertals and Upper Paleolithic modern humans: getting to the root of the matter. In: Zadzinska, E. (Ed.), Current Trends in Dental Morphology Research. University of qódz Press (Poland), qódz, pp. 201e210.

Bell, E.J., Kaidonis, J.A., Townsend, G.C. & Richards, L.C. 1998. Comparison of exposed dentinal surfaces resulting from abrasion and erosion. *Australian Dental Journal*, 43, 362–366.

Benazzi S, Nguyen HN, Kullmer O & Hublin J-J. 2015. Exploring the biomechanics of taurodontism, *Journal of Anatomy*, 226, 180-8.

Benedix, D. C. A Biocultural Analysis of Intentional Dental Modifications. (University of Tenessee, 1998).

Bernardini, F., Tuniz, C., Coppa, A., Mancini, L., Dreossi, D., Eichert, D., Turco, G., Biasotto, M., Terrasi, F., De Cesare, N., Hua, Q. & Levchenko, V. 2012. Beeswax as Dental Filling on a Neolithic Human Tooth. *PLoS ONE*, 7.

Blumberg, J.E., Hylander, W.L., Goepp, R.E. 1971. Taurodontism: a biometric study. *American Journal of Physical Anthropology*, 34, 243e256.

Braidwood, R., Howe, B. & Reed, C. 1961. The Iranian Prehistoric Project: new problems arise as more is learned of the first attempts at food production and settled village life. *Science*, 133, 2008–2010.

Brown, T, Molnar, S. 1990. Interproximal grooving and task activity in Australia. *American Journal of Physical Anthropology*, 81, 545–553.

Caufield, P.W. & Griffen, A.L. 2000. Dental caries. An infectious and transmissible disease. *Pediatric Clinics of North America*, 47, 1001–1019

Coon, C.S. 1962. The Origin of Races. Alfred A. Knopf, Inc., New York

Coppa, A., Bondioli, L., Cucina, A., Frayer, D., Jarrige, C., Jarrige, J.F., Quivron, G., Rossi, M., Vidale, M., Macchiarelli, R. 2006. Early Neolithic tradition of dentistry. *Nature* 440, 755-756.

Cummins, D. 2013. Dental caries: a disease, which remains a public health concern in the 21st century the exploration of a breakthrough technology for caries prevention. *Journal of Clinical Dentistry*, 24, 1-14

Cuy, J. L., Mann, A. B., Livi, K. J., Teaford, M. F. & Weihs, T. P. 2002. Nanoidentation mapping of the mechanical properties of human molar tooth enamel. *Archives of Oral Biology*, 47, 281 – 291.

Dean, M.C., Jones, M.E., Pilley, J.R. 1992. The natural history of tooth wear, continuous eruption and periodontal disease in wild shot great apes. *Journal of Human Evolution*, 22, 23e39.

Every, R.G. 1972. A new terminology for mammalian teeth: founded on the phenomenon of thegosis. Parts 1 & 2. Pegasus, Christchurch

Finucane, B. C., Manning, K. & Touré, M. 2008. Prehistoric dental modification in West Africa - Early evidence from Karkarichinkat Nord, Mali. *International Journal of Osteoarchaeology*, 18, 632–640

González, E. L., Pérez, B. P., Sánchez, J. A. S. & Acinas, M. M. R. 2010. Dental aesthetics as an expression of culture and ritual. *British Dental Journal*, 208, 77–80.

Grine, F.E. 2004. Geographic variation in human tooth enamel thickness does not support Neandertal involvement in the ancestry of modern Europeans. *South African Journal of Science*, 100, 389 e394.

Grine, F.E. 2005. Enamel thickness of deciduous and permanent molars in modern Homo sapiens. *American Journal of Physical Anthropology*, 126, 14e31.

Grine, F.E. & Martin, L.B. 1988. Enamel thickness and development in Australopithecus and Paranthropus. In: Grine, F.E. (Ed.), Evolutionary History of the 'Robust' Australopithecines. Aldine de Gruyter, New York, pp. 3e42.

Guerini V. 1909. A History of Dentistry from The Most Ancient Times until the End of The eighteenth Century. Philadelphia: Lea & Febiger.

Hamner, J.E., Witkop, C.J. & Metro, P.S. 1964. Taurodontism. Oral Surgery, 18, 409e418

Hillson S. 2003. Dental Anthropology. Cambridge University Press, Cambridge.

Hillson, S. 1996. Dental Anthropology. Cambridge University Press, Cambridge, New York, Port Melbourne, Madrid, Cape Town.

Hillson, S. 1996. Dental Anthropology. Cambridge University Press, Cambridge.

Humphrey, L. T. & Bocaege, E. 2008. Tooth evulsion in the Maghreb: Chronological and geographical patterns. *African Archaeological Review*, 25, 109–123.

Imfeld, T. 1996. Dental erosion. Definition, classification and links. Eur. Journal of Oral Science, 104, 151-155.

Kaidonis, J.A. 2008. Tooth wear: the view of the anthropologist. *Clinical Oral Investigations*, 12, supp. 1, 21-26.

Kaidonis, J.A., Townsend, G.C. & Richards, L.C. 1993. Nature and frequency of dental wear facets in an Australian Aboriginal population. *Journal* of *Oral Rehabilitation,* 20, 333–340.

Kaifu Y., Kasai K., Townsend G.C. & Richards L.C. 2003. Tooth Wear and the ―Design‖ of the Human Dentition: A Perspective From Evolutionary Medicine. *Yearbook of Physical Anthropology*, 46, 47-61.

Khodadoust, K., Ardalan, M., Pourabbas, R. & Abdolrahimi, M. 2013. Dental and oral diseases in Medieval Persia, lessons from Hedayat Akhawayni. *Journal* of *Medical Ethics and History* of *Medicine,* 6, 9.

Kono, R.T. 2004. Molar enamel thickness and distribution patterns in extant great apes and humans: new insights based on a 3-dimensional whole crown perspective. *Anthropological Science*, 112, 121e146.

Kovacs, I. 1971. A systematic description of dental roots. In: Dahlberg, A.A. (Ed.), Dental Morphology and Evolution. The University of Chicago Press, Chicago and London, pp. 211e256

Kreth J. & Herzberg M.C. 2015. Molecular Principles of Adhesion and Biofilm Formation. In: Chávez de Paz L., Sedgley C., Kishen A. (eds) The Root Canal Biofilm. Springer Series on Biofilms, vol 9. Springer, Berlin, Heidelberg

Kupczik, K., Olejniczak, A.J., Skinner, M.M. & Hublin, J.-J. 2009. Molar crown and root size relationship in anthropoid primates. In: Koppe, T., Meyer, G., Alt, K.W. (Eds.), Interdisciplinary Dental Morphology. Frontiers of Oral Biology Series, vol. 13. Karger, Basel,, pp. 16e22.

Lebel, S., Trinkaus, E., Faure, M., Fernandez, P., Guérin, C., Richter, D., Mercier, N., Valladas, H. & Wagner G.A. 2001. Comparative morphology and paleobiology of Middle Pleistocene human remains from the Bau de l'Aubesier, Vaucluse, France. *Proceedings of the National Academy of Sciences.* USA 98, 11097-102.

Lieberman, D.E. 1994. The biological basis for seasonal increments in dental cementum and their application to archaeological research. *Journal of Archaeological Science*, 21, 525e539

Lozano, M., Subirà, M., Aparicio, J., Lorenzo, C. & Gómez-Merino, G. 2013. Toothpicking and periodontal disease in a Neanderthal specimen from Cova Foradà site (Valencia, Spain). *PLoS One* 8, e76852.

Macchiarelli, R., Bondioli, L., Debenath, A., Mazurier, A. & Tournepiche, J.-F., Birch, W. & Dean, M.C. 2006. How Neanderthal molar teeth grew. *Nature* 444, 748e751.

Marsh, P & Martin, MV. Oral Microbiology. 4th edn. Wright, Oxford; 1999

Marshall Joseph Becker. 1994. Etruscan Gold Dental Appliances: Origins and Functions as Indicated by an Example from Orvieto, Italy, in the Danish National Museum. *Dental Anthropology Newsletter*, 3, 2–8.

Martin, L. 1985. Significance of enamel thickness in hominoid evolution. *Nature* 314, 260e263

Martin, L.B., Olejniczak, A.J. & Maas, M.C. 2003. Enamel thickness and microstructure in pitheciin primates, with comments on dietary adaptations of the middle Miocene hominoid Kenyapithecus. *Journal of Human Evolution*, 45, 351e367.

Milner, G. R. & Larsen, C. S. 1991. Teeth as artefacts of human behaviour: intentional mutilation and accidental modification. *Advances in Dental Anthropology*, 357–378.

Molnar, S., Hildebolt, C., Molnar, I.M., Radovcic´, J. & Gravier, M. 1993. Hominid enamel thickness. I. The Krapina Neandertals. *American Journal of Physical Anthropology*, 92, 131 e138.

Nanci, A. 2012. Ten Cate's Oral Histology, 8th Edition. Development, Structure and Function. Elsevier, Mosby, St. Louis, Missouri.

Oelzea, V., Siebert A., Nicklisch, N., Meller, H., Dresely, V., Alt, K.W. 2011. Early Neolithic diet and animal husbandry: stable isotope evidence from three Linearbandkeramik (LBK) sites in Central Germany. *Journal of Archaeological Science*, 38, 270–279.

Olejniczak, A.J., Gilbert, C.C., Martin, L.B., Smith, T.M., Ulhaas, L. & Grine, F.E. 2007. Morphology of the enamel-dentine junction in sections of anthropoid primate maxillary molars. *Journal of Human Evolution*, 53, 292e301

Olejniczak, A.J. & Grine, F.E. 2006. Assessment of the accuracy of dental enamel thickness measurements using microfocal X-ray computed tomography. *The Anatomical Record. Part A, Discoveries* in *Molecular, Cellular*, and *Evolutionary Biology*, 288, 263e275.

Olejniczak, A.J., Smith, T.M., Skinner, M.M., Grine, F.E., Feeney, R.N.M., Thackeray, J.F. & Hublin, J.-J. 2008a. Three-dimensional molar enamel distribution and thickness in Australopithecus and Paranthropus. *Biology Letters*, 4, 406e410.

Pinchi, V., Barbieri, P., Pradella, F., Focardi, M., Bartolini, V. & Norelli, G.A. 2015. Dental Ritual Mutilations and Forensic Odontologist Practice: a Review of the Literature. *Acta Stomatologica Croatica*, 49, 3–13.

Ramirez Rozzi, F.V. 1996. Comment on the causes of thin enamel in Neandertals. *American Journal of Physical Anthropology*, 99, 625 e626.

Ring, M. 1985. Dentistry: An Illustrated History. New York: Harry N. Abrams.

Roksandic, M., Alarie, K., Rodríguez Suárez, R., Huebner, E. & Roksandic, I. 2016. Not of African Descent: Dental Modification among Indigenous Caribbean People from Canímar Abajo, Cuba. *PLoS One* 11, e0153536.

Ricci, S., Capecchi, G., Boschin, F., Arrighi, S., Ronchitelli, A. & Condemi, S. 2014. Toothpick use among Epigravettian Humans from Grotta Paglicci (Italy). *International Journal of Osteoarchaeology* Doi:10.1002/oa.2420.

Schwartz, G.T. 2000a. Taxonomic and functional aspects of the patterning of enamel thickness distribution in extant large-bodied hominoids. *American Journal of Physical Anthropology*, 111, 221e244.

Smith, T.M., Olejniczak, A.J., Martin, L.B. & Reid, D.J. 2005. Variation in hominoid molar enamel thickness. *Journal of Human Evolution*, 48, 575– 592.

Smith, F.H. & Paquette, S.P. 1989. The adaptive basis of Neandertal facial form, with some thoughts on the nature of modern human origins. In: Trinkaus, E. (Ed.), The Emergence of Modern Humans. Cambridge University Press, Cambridge, pp. 181e210.

Smith, P. & Zilberman, U. 1994. Thin enamel and other tooth components in Neanderthals and other hominids. *American Journal of Physical Anthropology*, 95, 85 e87.

Smith, T.M., Olejniczak, A.J., Reid, D.J., Ferrell, R.J. & Hublin, J.J. 2006. Modern human molar enamel thickness and enamel-dentine junction shape. *Archives of Oral Biology*, 51, 974e995

Smith, T.M., Olejniczak, A.J., Tafforeau, P., Reid, D.J., Grine, F.E. & Hublin, J.J. 2006b. Molar crown thickness, volume, and development in South African Middle Stone Age humans. *The South African Journal of Science*, 102, 513 e517.

Smith, T.M., Olejniczak, A.J., Zermeno, J.P., Tafforeau, P., Skinner, M.M., Hoffmann, A., Radovcic, J., Toussaint, M., Kruszynski, R., Menter, C., Moggi-Cecchi, J., Glasmacher, U.A., Kullmer, O., Schrenk, F., Stringer, C. & Hublin, J.J. 2012. Variation in enamel thickness within the genus Homo. *Journal of Human Evolution*, 62, 395e411.

Tafforeau P. 2004. Phylogenetic and functional aspects of tooth enamel microstructure and three-dimensional structure of modern and fossil primate molars. Ph.D. Dissertation, Universit e de Montpellier II.

Tiesler, V. 1999. Head Shaping and Dental Decoration Among the Ancient Maya : Archeological and Cultural Aspects. Society 1–11.

Velusamy, S.K., Markowitz, K., Fine, D.H & Velliyagounder, K. 2016. Human lacto ferrin protects against Streptococcus mutans-induced caries in mice. *Oral Diseases,* 22,148-54.

Vukovic, A., Bajsman, A., Zukic, S. & Secic, S. 2009. Cosmetic Dentistry in Ancient Times – a Short Review. *Bulletin of the International Association for Paleodontology*, 3, 9–13.

Walker, M.J., Gibert, J., López, M.V., Lombardi, V.A ., Pérez-Pérez, A ., Zapata, J., Ortega, J., Higham, T., Pike, A ., Schwenninger, J.-L., Zilhão, J. & Trinkaus, E. 2008. Late Neandertals in Southeastern Iberia: Sima de las Palomas del Cabezo Gordo, Murcia, Spain. *Proceeding of the National. Academy of Sciences*. U.S.A. 105, 20631e20636

Weber T. 2010. Zahnmedizin. 3rd Issue, Georg Thieme Verlag, Stuttgart, New York.

Willman, J. C., Shackelford, L. & Demeter, F. 2016. Incisor ablation among the late upper paleolithic people of Tam Hang (Northern Laos): Social identity, mortuary practice, and oral health. *American Journal of Physical Anthropology*, 00.

Wittwer-Backofen, U., Gampe, J., Vaupel, J. W. 2003. Tooth cementum annulation for age estimation: Results from a large known-age validation study. *American Journal of Physical Anthropolog*, 123, 119 – 129.

Yadav, K & Prakash, S. 2017. Dental Caries: A Microbiological Approach. *Journal* of *Clinical Infectious Diseases and Practice,* 2, 118. doi: 10.4172/2476-213X.1000118

Zilberman, U., Skinner, M. & Smith, P. 1992. Tooth components of mandibular deciduous molars of Homo sapiens sapiens and Homo sapiens neanderthalensis: a radiographic study. *American Journal of Physical Anthropolog*, 87, 255 e 262.

Zilberman, U. & Smith, P. 1992. A comparison of tooth structure in Neanderthals and early Homo sapiens sapiens: a radiographic study. *Journal of Anatomy*, 180, 387 e393

Zumbroich, T. J. 2009. Teeth as black as a bumble bee's wings: The ethnobotany of teeth blackening in Southeast Asia. *Ethnobotany Research and Applications*, 7, 381–398.

Journal of Dental Research

The physiological linkage between dental arch asymmetry, alveolar inclination and dental macrowear pattern

G. Oxilia[1,2], E. Bortolini[2], S. Martini[3], A. Papini[4], M. Boggioni[5], L. Buti[2], C. Figus[2], R. Sorrentino[2], G. Townsend[6], J. Kaidonis[6], L. Fiorenza[7,8], E. Cristiani[9], O. Kullmer[10,11,] J. Moggi-Cecchi[1], S. Benazzi[2,12].

[1]Department of Biology, University of Florence, Via del Proconsolo, 12, 50122 Firenze, Italy

[2]Department of Cultural Heritage, University of Bologna, Via degli Ariani 1, 48121 Ravenna, Italy.

[3]Dental Lab Technician, via Milani, 1, 37124, Parona (Verona), Italy.

[4]Dentist's surgery, via Walter Tobagi 35, 59100, Prato, Italy.

[5]Dentist's surgey, via D'Andrade 34/207, 16154, Genova Sestri Ponente, Italy.

[6]School of Dentistry, The University of Adelaide, Adelaide, Australia.

[7]Department of Anatomy and Developmental Biology, Monash University, Melbourne VIC 3800, Australia;

[8]Earth Sciences, University of New England, Armidale NSW 2351, Australia;

[9]Department of Oral and Maxillo Facial Sciences, Sapienza University, Via Caserta 6 00161, Rome

[10]Senckenberg Research Institute, Senckenberganlage 25, 60325 Frankfurt am Main, Germany;

[11]Department of Paleobiology and Environment, Institute of Ecology, Evolution, and Diversity, Johann Wolfgang Goethe University, Max-von-Laue-Str. 13, 60438 Frankfurt, Germany

[12]Department of Human Evolution, Max Planck Institute for Evolutionary Anthropology, Deutscher Platz 6, 04103 Leipzig, Germany

Corresponding Authors:

G. Oxilia, Department of Biology, University of Florence, Via del Proconsolo, 12, 50122 Firenze, Italy. Email: Gregorio.oxilia@unifi.it

Introduction

Tooth wear is a physiological and adaptive phenomenon of dental tissue loss (Benazzi et al., 2013). In anatomically modern humans numerous factors such as tooth position in the dental arch (Molnar, 1990), diet (Fiorenza et al. 2015), foreign abrasive substances (Lucas et al. 2014), endogenous and exogenous chemical factors (Grippo et al. 2004), bruxism (Sameera et al. 2017), para-masticatory activities (Fiorenza et al. 2011a) and cultural practices such as dental treatment (Oxilia et al. 2015, 2017), are involved. Overall, these factors contribute in creating and modifying wear on the occlusal surface of teeth. Owing to the link between above mentioned factors and the inevitable appearance of wear facets, the latter are useful, e.g. to reconstruct dietary habits and behavioral patterns in great ape species and ancestral hominin groups (Molnar, 1971 Smith, 1984; Fiorenza et al., 2011b), to evaluate predominant occlusal movements performed during masticatory activity (Kullmer et al. 2012, Oxilia et al. 2015), and to reconstruct biomechanical effects of occlusal loading scenarios in teeth and supporting structures (Dejak et al. 2003).

However, at present there has been no substantial contribution to explore the effects of asymmetry in the masticatory system in respect to its impact wear facet creation and wear pattern appearance.

Many factors can be responsible for asymmetries in the masticatory apparatus such as tongue movements involved in deglutition, speech and postural stability beside others, all of which produce an alteration of both upper and lower jaw

morphology (Palmer et al. 1997, Hiiemae et al. 2003, Gokce et al. 2012, Hori et al. 2013, Alghadir et al. 2015,).

In particular, deglutition consists of four stages that can be divided into voluntary and involuntary control (Mosier et al. 1999, Anagnostara et al. 2001, Hartl et al. 2003). During voluntary control phases, the jaws remain fixed with teeth in maximum intercuspation (Pameijer et al. 1970) by the bilateral recruitment of muscles *M. masseter*, *M. temporalis* and *M. pterygoideus medialis* and the tongue lift up because of the contraction produced by *M. mylohyoideus* (Palmer et al. 1997, 2008).

The tongue pushing upwards exerts a pressure on the palate, which is then transmitted through the maxillary bones producing an adaptation in the position of the teeth (Proffit 1978). At the same time, this alteration involves the palate, vomer and the sphenoid bones. These bones are part of greater context where all the other cranial bones interact generating alterations in the skull morphology (Fishman 1969, Rakosi 1978, Kapoor et al. 1979, Brodie 1946).

There are three main forces responsible for mandibular tooth inclination: a) lingual force (the muscles of the tongue); b) buccal force (*M. buccinator* and *M. masseter*); and c) occlusal force (loading during mastication). The spatial positions of teeth and jawbones depend on the combination of these three forces. Initially, mandibular molars erupt lingually, then they move buccally due to tongue pressure and *M. masseter* function (Janson et al., 2004). Finally, the molars reach a balance position (Masumoto et al., 2001) which will change during life due to the pressure of tongue and other muscles, and other factors.

In our study we use digital casts of upper and lower dental arches from Yuendumu Aboriginal individuals (Brown et al. 2011) to explore the relationship between alveolar inclination and macrowear patterns in first molars (M1). Our results provide evidence of a significant link between the general architecture of dental arch and the distribution of abrasive wear facets on the occlusal surface.

Materials and Methods

Sample

The Yuendumu collection consists of measurements, radiographs, family data, and 1717 sets of dental casts representing 446 individuals that were produced from alginate impressions (Brown et al., 2011).

The sample used in this study consists of complete casts of maxillary and mandibular dental arches belonging to 19 adult and sub-adult individuals (Appendix Table 1), all of which are characterized by slight or moderate M1s wear (up to wear stage 2 and 3 based on Smith, 1984).

Casting and digital acquisition of upper and lower dental arches

We digitize the dental cast collection using a white-light scanning system with an *xy* resolution of 45 μm based on structured-light technology (smartSCAN3D C-5, Breuckmann, GmbH). Collection and alignment of the scan-data was carried out using the integrated scanning software optoCAT (Breuckmann, GmbH). The 3D virtual models were further post-processed using PolyWorks® V12 (InnovMetric Software Inc.), a 3D metrology platform software. The unfinished polygonal model was imported into the IMEdit™ module where topology errors, artifacts, and degenerate/duplicate triangles were manually identified and removed.

For each specimen, the macrowear pattern of the maxillary/mandibular, left/right first molars (i.e., 76 M1s), the alveolar inclination at the level of the M1s, and the quantification of the jaw asymmetry, were obtained as detailed below.

Macrowear pattern of the M1s

M1 wear facets were manually outlined on each digital 3D surface models and were labeled according to the wear facet terminology and numbering system created by Maier and Schneck (1981). Areas that were affected by wear were

then grouped into their respective masticatory cycle phases, i.e. phase I buccal facets (1, 1.1, 2, 2.1, 3, 4), phase II (9, 10, 11, 12, 13, 10.1), and phase I lingual facets (5, 6, 7, 8) (Kay and Hiiemae, 1974). The relative wear area of each chewing phase was computed by summing the absolute areas (in mm^2) belonging to the same phase, and dividing this sum with to the total occlusal wear area. The resulting values (proportions) were visually represented by the ternary plot.

Alveolar inclination – a proxy for M1 crown inclination.

A reference plane (hereafter called "RP") was identified on virtual models. The xy-plane of a Cartesian coordinate system was transformed parallel to the RP. The RP was obtained by observing: i) the apex of the septum between the central incisors; and ii) two points marked respectively on the left and right hypoconid (mandibular M1s) and metacone (maxillary M1s) (Appendix Figure 1a,e).

Then, a plane perpendicular to the RP, passing through the hypoconid (mandibular M1s) and metacone (maxillary M1s) (Appendix Figure 1c,g), was created in order to obtain a cross-section of dental arch (Appendix Figure 1d,h). On the cross-section, a line was drawn for each M1 between the buccal and lingual gingival sulcus (hereafter called "Gingival Line"). Finally, further an additional line was located at the cross-section perpendicular to the Gingival Line (hereafter called "Vertical Line"). The lingual angle measured at the cross-section between the Vertical Line and the RP was used to establish the buccal or lingual inclination of the alveolar arch at the level of M1s (Appendix Figure 1d,h). This measurement is taken as a proxy for the inclination of the M1 crowns. An angle higher or lower than 90° suggests a lingual or buccal inclination of the M1 crowns respectively.

Quantifying palatal arch asymmetry

The cross-sections described above were also used to quantify the asymmetry of the palatal arch. In detail, for both mandibular and maxillary cross-sections, the midpoint (MP) between the left and right M1 lingual gingival sulcus was computed. The line passing through MP and connected to projected MP on the perpendicular reference plane (PRP), was used to split the palatal arch in a left and right half-component (Appendix Figure 2). The relative area of each half-component (Appendix Figure 2b) was calculated by dividing the absolute area of each half side by the total palatal area.

Measures of statistical association

The relatively small size of the present sample (n=19) does not allow to appropriately ascertain a normal distribution in the values. We therefore used a non-parametric Mann-Whitney-Wilcoxon signed-rank test for two-sample, paired study design in order to see whether the wear patterns observed in the different masticatory phases of each dental arch are significantly different from one another.

The potential relationship among dental alveolar inclinations was analysed using Spearman rank correlation coefficient (rho) which was preferred to linear correlation because of the presence of angular measures and the impossibility of confidently test for normality of the observed variables. The same statistical analysis was performed to test for significant relationships between alveolar inclination and macrowear in each masticatory phase in each quadrant. For significant cases identified through correlation, we ascertained the presence of linear relationship between variables. Once the existence of such condition was verified for all variable pairs, which had presented with significant correlation, we performed a linear regression analysis to assess the explanatory power of

alveolar inclination with respect to wear patterns, and to determine whether this conclusion could be generalized in future studies.

Finally, the relationship between palatal area and alveolar inclination was explored using a Chi-square test of independence and Correspondence Analysis. All analyses were performed in R version 3.2.3 (R Core Team 2015) using built-in functions and the package *ca* (Nenadic and Greenacre 2007).

Results

Macrowear pattern phase distribution of the M1s

The relative proportion (percentage) of the three masticatory phases identified on the M1s were graphically represented in the ternary plots (Figure 1). Overall distributions of mandibular and maxillary M1s overlap (Figure 1a), even though the latter (black circle) is more scattered than the former (red circle). Indeed, significant differences between antagonists (Mann-Whitney-Wilcoxon signed-rank test) were observed for some masticatory phases. The only significant results were obtained for buccal and lingual Phase I antagonist arches of both the Left (p=0.04) and Right (p=0.03) side (Table 1).

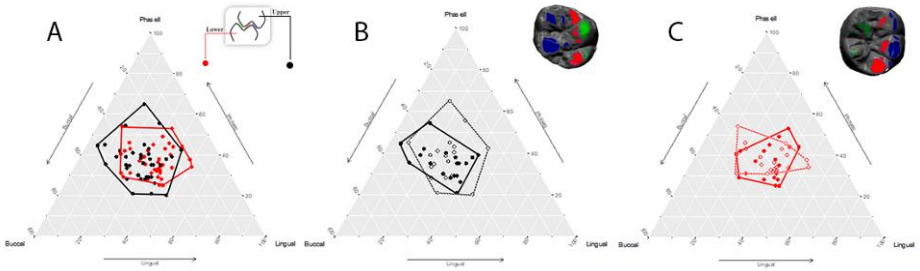

Figure 1. Ternary diagrams showing the proportions (in %) of relative wear areas of buccal phase I facets, lingual phase I facets, and phase II facets, which are positioned in an equilateral triangle. Each base of the triangle represents a ratio of 0% while the vertices correspond to a percentage of 100%. A) Relation between upper (black) and lower (red) molars. B) Relation between right (filled

points) and left (empty points) upper molars. C) Relation between right (filled points) and left (empty points) lower molars.

Table 1. Relationship between masticatory phases of each dental arch measured using Mann-Whitney-Wilcoxon signed-rank test for two-sample, paired study design (T= test statistic; α=0.05)

	Phase II	Buccal Phase I	Lingual Phase I
UL - UR	T=109.5 p=0.3	T=64 p=0.6	T=76 p=0.7
UL - LL	T=102 p=0.8	**T=134 p=0.04**	**T=44 p=0.042**
LR - UR	T=103.5 p=0.75	**T=43 p=0.034**	**T=131 p=0.05**
LR - LL	T=68 p=0.46	T=107.5 p=0.63	T=88 p=0.93

UL = Upper Left; UR = Upper right; LL = Lower Left; LR = Lower right

When maxillary and mandibular M1s of the same individual are considered separately, there are no significant differences in the pattern of masticatory phases between left and right side (Fig. 1b,c, Table 1). Overall, we observed that right maxillary M1s (points) are more variable than left maxillary M1s (circles) (Figure 1b), while such difference was not observed for mandibular molars (Figure 1c).

Alveolar inclination – a proxy for M1 crown inclination

The inclination of maxillary and mandibular M1 crowns are listed in appendix Table 2. Even though we observe variability between opposite (left and right; Appendix Table 3) and antagonist teeth (Appendix Table 4), the only significant

relationship emerges between alveolar inclinations of opposite sides of the upper (rho = 0.55, p = 0.016) and lower (ρ = 76, p = 0.00016) dental arch respectively (Table 2).

Table 2. Potential relationship among dental alveolar inclinations expressed as Spearman rank correlation coefficients (rho). Significant values in bold (**α**=0.05)).

	rho	p
UR~UL	**0.55**	**0.016**
UR~LR	-0.18	0.46
UR~LL	-0.17	0.46
UL~LR	0.2	0.39
UL~LL	0	1
LR~LL	**0.76**	**0.00016**

UL = Upper Left; UR = Upper right; LL = Lower Left; LR = Lower right

Relationship between alveolar arches and dental wear development

The relationships between alveolar inclination of each position and the wear patterns in each masticatory phase at each position is shown in Table 3. Significant correlations are identified only for the right side, in both the upper and lower arch (quadrants 1 and 4). More specifically, significant negative relationship is identified for Phase II in UR position and buccal phase I in LR position. On the other hand, lingual Phase I of the right side always exhibits positive correlation with alveolar inclination.

Table 3. Relationship between alveolar inclination of each position and the relative masticatory phases measured as Spearman rank correlation coefficient (rho). Significant values in bold (α=0.05)).

	Phase II	Buccal Phase I	Lingual Phase I
UR	rho= **-0.65 p=0.0026**	rho= -0.38 p=0.1	**rho= 0.73 p=0.00035**
UL	rho= -0.09 p=0.7	rho= 0.14 p=0.55	rho= 0.006 p=0.98
LR	rho= 0.18 p=0.44	**rho= -0.56 p=0.011**	**rho= 0.52 p=0.025**
LL	rho= -0.056 p=0.82	rho= -0.19 p=0.439	rho= 0.14 p=0.55

UL = Upper Left; UR = Upper right; LL = Lower Left; LR = Lower right

All four cases confirm the presence of a significant relationship (Table 4). The coefficient of determination (R^2) and the relative F statistic underline that variability in alveolar inclination is one of the mechanisms driving wear area distribution in the masticatory phases and the significance of the obtained values suggests that these results probably can be generalized also for a broader sample.

Table 4. Coefficient of determination (R^2) and the relative F statistic produced by linear regression to infer the proportion of variability in wear masticatory phases that could be explained by alveolar inclination.

	R^2	*p*-value	F-statistic for 1 and 17 df
UR_Phase II ~ UR inclination	0.32	0.006	9.579
UR_Lingua Phase l ~ UR inclination	0.42	0.0016	14.09
LR_Buccal Phase I~ LR inclination	0.33	0.006	9.881
LR_Lingual Phase I~ LR inclination	0.17	0.05	4.654

UL = Upper Left; UR = Upper right; LL = Lower Left; LR = Lower right

Relation between Palatal arch and alveolar inclination

The values of the relative areas of palatal process (Appendix Table 5) show only six individuals with no difference (50%) between each half. To preliminary explore the possible relationship between palatal arch and alveolar inclination we grouped upper alveolar inclinations into categorical variables and observed their occurrence across three palatal configurations (Appendix Table 8). Given the small sample size, no significant difference emerged from a Chi-squared test. However, Correspondence Analysis explains the variability in the data with the first two axes (96.7% and 3.3% respectively; Appendix Figure 4), and clearly points to a difference between cases in which alveolar inclinations are divergent and cases in which opposite sides exhibit parallel inclination (Appendix Figure 4).

Discussion

The results described in this study provides evidence that alveolar arch inclination (lingual or buccal) has an impact on the distribution of dental wear. Present results suggest that upper and lower alveolar arches produce an increase in tooth wear facet areas. Lingual phase I when alveolar arches present with an angle greater than 90 degree (buccal tendency), while an angle of less than 90 degrees (lingual tendency) tends to increase wear area of the buccal slope.

The values of dental masticatory phases show differences in wear between antagonistic molars (Table 1). In this respect, it is recommended to separately analyze maxillary and mandible molars wear facet areas for comparative group studies in order to greatly reduce the variability. Whether this effect depends on the sample per se or on the sample size needs to be tested in the future with larger sample.

Alveolar inclination values exhibit a high degree of inter-individual variability (Appendix Table 2). Correlation analysis between inclinations of right and left sides of upper molars shows lower values of correlation than mandible molars could be related to the interference of palatal arch asymmetry. Different results were observed for mandible alveolar arches. In fact, the inclination of lower jaw ($p = 0.00016$) seems not to be influenced by palatal arch than upper jaw arches ($p = 0.016$) (Table 2). In view of these results, upper and lower jaws seem to be two separate and yet interdependent elements, and the lack of relationship between upper and lower jaws (Appendix Table 2, 6 and 7) is also supported by the absence of statistical significance (Table 1 and 2). These analyses demonstrate a mismatch between antagonist occlusal surfaces contact (misaligned bite in extreme case) which is entered by the occlusal sequence and maximum intercuspation produced during deglutition that is performed more than one thousand times a day (Lear et al. 1965).

The absence of a quantifiable relationship between upper and lower masticatory phases seems not to be confirmed by the significant values of statistical analysis

showed in Table 3, where the relationship between alveolar inclination and masticatory phases seems to be evident only on the right side. This result can be explained based on the characteristic mode of occlusion observed among Australian Aborigines called: “X-occlusion” or “alternate intercuspation” (Barret 1953). When there is a normal maximum intercuspation on the right side, the left side can display a large overjet, and vice versa. The upper dental arch of human groups is wider than the lower. In this research, Aboriginal individuals included in the present research probably have a tendency to occlude on the right side (“individuals sunny side of occlusion”) producing an increase in occlusal force and thus a more localized evidence of the relationship between wear development and alveolar inclination.

Although no statistically significant relationship between palate shape and alveolar inclination emerged in the present study – due to small size of the studied sample, or functionally, to the absence of pathological condition, which can increase the asymmetries of palatal bone development e.g. by a wrong tongue posture and pressure (Palmer et al. 1997, Hiiemae et al. 2003, Gokce et al. 2012, Hori et al. 2013, Alghadir et al. 2015,). Exploratory data analysis (CA), however, suggested that distinctive patterns may emerge for diverging and parallel alveolar inclinations across different palatal settings. This intriguing correspondence may point to a genuine effect of palate shape on alveolar inclination, and will deserve to be further investigated. In fact, the tongue acts in concert with all the other muscles involved in swallowing while the hard palate absorbs the force created by the tongue. In a normal swallowing, the tip of the tongue presses firmly against the roof of the mouth or hard palate, located slightly behind the front teeth. During an incorrect deglutition, on the other hand, the tip and/or sides of the tongue press against or spread between the teeth producing an increasing of loading asymmetries, likely also effecting bone asymmetry. Orofacial Myofunctional Disorders (OMDs) result from similar processes.

The latter are functional disorders of facial and masticatory apparatus, and may directly or indirectly affect many factors such as breastfeeding, facial skeletal growth, speech, temporomandibular joint movement, in addition to the insurgence of an abnormal bite. Tongue thrust is a common kind of OMD where constant pressure from resting or incorrectly thrusting the tongue away from the hard palate may push teeth out of place and that pressure may later prevent teeth from erupting (breaking through the gum). Retrieving the correct posture and functional deglutition of the tongue (Van Dyck, 2015) seems one of the main solutions to this problem.

The analysis of masticatory context has shown a new perspective of dental macrowear studies. Internal factors such as bone growth and dental crown asymmetries are responsible factors influencing the appearance of wear facet patterns besides multifactorial external influences, such as dietary abrasiveness, environment and cultural technologies. Throughout the evolutionary pathway towards *Homo sapiens*, food quality and physical properties have reciprocal proportional changed through cultural progress in particular with an increased invention of sophisticated external food preparation technics. This general trend has led to a reduction of biomechanical loading and forces in our masticatory system during food ingestion and dental processing. From a biological perspective it is likely that through the continuing relieve of biomechanical pressure on our masticatory system the human organism reacts with a reduction in the affected system, and an increase in variability and asymmetry in development, growth and remodeling in the masticatory apparatus as a whole.

Based on our result we can conclude that: a) Upper and lower jaw are intertwined and yet show differential wear and inclinations, b) there is a correlation between alveolar inclination and dental crown tilting and macrowear, in some cases (right side in our sample) inclination explains part of the variability observed in wear facet patterns, c) of course there are other factors, that probably determine the residual variability, the one not explained

by inclination, d) there is a possible correspondence between palatal shape and alveolar inclination – this may allow us to formulate some intriguing hypotheses concerning the role of deglutition – which will be tested with a more appropriate sample in future studies.

Finally, dental macrowear studies should focus on understanding 1) how asymmetries of masticatory system influence dental wear pattern and how the expression of asymmetry has changed through time due to the development of various cultural and dietary habits in human societies.

2) How inclinations of alveolar arches influence and corresponds to the tooth crown orientation. In fact, the real inclination of a tooth is variable and it is not always 90 degree as dental studies assume based on the cervical line (Benazzi et al. 2009). A proper evaluation of tooth inclination will also help to understand why some individual wear facets have developed, and where the pressure of masticatory apparatus focus on during occlusal dynamics.

The role of asymmetry in the masticatory apparatus should be considered both in dental evolutionary studies and in modern dentistry. In the first case, studies of orofacial disorders and temporomandibular joint asymmetry would be useful to increase the knowledge of parafunctional influences of jaw asymmetries. A functional approach retrieving data on postcranial posture, chewing and functional deglutition of the tongue in dental rehabilitation should be considered to harmonize functionality in the mouth with the full body.

A more holistic view in future occlusal research, clinical diagnoses and therapies is demanded to understand development of the variability and asymmetry in our masticatory system and to evaluate individual patient situations.

The datasets supporting this article have been uploaded as part of the Supplementary Material.

Acknowledgements

These authors wish to thank the University of Adelaide and Monash University for making this rare sample available to study. The authors declare no potential conflicts of interest with respect to the authorship and/or publication of this article.

Author Contributions G.O., S.M., SB conceived the idea for the study. J.K., G.T., L.F. provided the scan of the jaws. G.O., O.K. L.F carried out macrowear analysis. E.B. and G.O. performed statistical analysis. G.O. carried out the virtual analysis of the masticatory apparatus. G. O., E.B., A.P., M. B., L.B., G. T, J. K., L. F., E. C., O. K., J. M-C, S. B. wrote the manuscript and supplements.

References

Alghadir AH, Zafar H, Iqbal ZA. 2015. Effect of tongue position on postural stability during quiet standing in healthy young males. *Somatosens Mot Res.* 32 (3):183-6

Anagnostara A, Stoeckli S, Weber OM, Kollias SS. 2001. Evaluation of the anatomical and functional properties of deglutition with various kinetic high-speed MRI sequences. *J Magn Reson Imaging.* 14: 194–199.

Barrett MJ. 1953. X-occlusion. Dent Mag Oral Top. 70: 279

Benazzi S, Fantini M, De Crescenzio F, Persiani F, Gruppioni G. 2009. Improving the spatial orientation of human teeth using a virtual 3D approach. J Hum Evol 56: 286–293.

Benazzi S, Nguyen HN, Schulz D, Grosse IR, Gruppioni G et al. 2013. The Evolutionary Paradox of Tooth Wear: Simply Destruction or Inevitable Adaptation? PLOS ONE 8: e62263. doi:10.1371/journal.pone.0062263.

Brodie AG. 1946. "Facial Pattern". A theme on variation. *Angle Orthod.* 16: 75–86.

Brown, Tasman. 2011. Yuendumu : legacy of a longitudinal growth study in Central Australia / by Tasman Brown ... [et al] University of Adelaide Press Adelaide

Dejak B, Młotkowski A, Romanowicz M. 2003. Finite element analysis of stresses in molars during clenching and mastication. *J Prosthet Dent.* 90: 591–597.

Fiorenza L, Benazzi S, Tausch J, Kullmer O, Bromage TG, Schrenk F. 2011a. Molar macrowear reveals Neanderthal eco-geographic dietary variation. 6 (3): e14769.

Fiorenza, L., Benazzi, S., Kullmer, O., 2011b. Para-masticatory wear facets and their functional significance in hunter-gatherer maxillary molars. J. Archaeol. Sci. 38: 2182-2189.

Fiorenza, L., 2015. Reconstructing diet and behaviour of Neanderthals from Central Italy through dental macrowear analysis. J. Anthropol. Sci, 93: 1-15.

Fishman LS. 1969. Postural and dimensional changes in the tongue from rest position to occlusion. Angle Orthod. 39: 109–13.

Gokce HS, Gokce SM, Akin E, Bulakbasi N, and Akyol M. 2012. Effect of complete denture wearing on deglutition time: a cine-magnetic resonance imaging study. *Journal of Oral Rehabilitation*, 39: 198–209. doi:10.1111/j.1365-2842.2011.02272

Grippo JO, Simring M, Schreiner S. 2004. Attrition, abrasion, corrosion and abreaction revisited: a new perspective on tooth surface lesions. *J Am Dent Assoc.* 135(8):1109–1118.

Hartl DM, Albiter M, Kolb F, Luboinski B, Sigal R. 2003. Morphologic parameters of normal swallowing events using singleshot fast spin echo dynamic MRI. *Dysphagia.* 18: 255–262.

Hiiemae KM, Palmer JB. 2003. Tongue movements in feeding and speech. Review. *Crit Rev Oral Biol Med.*14: 413–429.

Hori K, Taniguchi H, Hayashi H, Magara J, Minagi Y, Li Q, et al. 2013. Role of tongue pressure production in oropharyngeal swallow biomechanics. *Physiol Rep.* 1:191–8. doi: 10.1002/phy2.167.

Janson G, Bombonatti R, Cruz KS, Hassunuma CY, Del Santo MJ. 2004. Buccolingual inclinations of posterior teeth in subjects with different facial patterns. *Am J Orthod Dentofacial Orthop.* 125(3): 316–322.

Kay, R.F., Hiiemae, K.M., 1974. Jaw movement and tooth use in recent and fossil primates. Am. J. Phys. Anthropol. 40, 227–256.

Kapoor DN, Sharma VP, Grover CM. 1979. Dentofacial pattern of tongue thrusters - a cephalometric study. *J lnd Dent Assoc.* 51: 295–7.

Kullmer O., Schulz D. and Benazzi S. 2012. An Experimental Approach to Evaluate the Correspondence Between Wear Facet Position and Occlusal Movements. *Anat Rec.* 295: 846–852.

Van Dyck C., Dekeyser A., Vantricht E., Manders E., Goeleven A., Fieuws S., Willems G. 2016. The effect of orofacial myofunctional treatment in children with anterior open bite and tongue dysfunction: a pilot study, *European Journal of Orthodontics*, 38: 227–234.

Lear CS, Flanagan JB, Moorrees CF. 1965. The frequency of deglutition in man. *Arch Oral Biol.* 10: 83-89.

Lucas, PW, Van Casteren A, Al-Fadhalah K, Almusallam AS, Henry AG, Michael S, Watzke J, Reed DA, Diekwisch TGH, Strait D, Atkins AG. 2014. The role of dust, grit and phytoliths in tooth wear. Ann. Zool. Fennici 51: 143-152.

Maier W, Schneck G. 1981. Konstruktionsmorphologische Untersuchungen am Gebiß der hominoiden Primaten. Z. Morph. Anthrop. 72: 127-169.

Masumoto T, Hayashi I, Kawamura A, Tanaka K, Kasai K. 2001. Relationships among facial type, buccolingual molar inclination, and cortical bone thickness of the mandible. Eur J Orthod. 23(1): 15–23.

Molnar S. 1971. Human tooth wear, tooth function and cultural variability. Am. J. Phys. Anthropol. 34: 175-189.

Molnar S. and Molnar IM. 1990. Dental arch shape and tooth wear variability. Am. J. Phys. Anthropol., 82: 385–395.

Mosier KM, Liu W, Maldjian JA, Shah R, Modi B. 1999. Lateralization of cortical function in swallowing: a functional MR imaging study. Am J Neuroradiol. 20: 1520–1526.

Nenadic, O., Greenacre, M. 2007. Correspondence Analysis in R, with two- and threedimensional graphics: The capackage. Journal of Statistical Software 20(3):1-13

Oxilia G, Fiorillo F, Boschin F, et al. 2017. The dawn of dentistry in the late upper Paleolithic: An early case of pathological intervention at Riparo Fredian. Am J Phys Anthropol. 163: 446-461.

Oxilia, G. *et al.* 2015. Earliest evidence of dental caries manipulation in the Late Upper Palaeolithic. *Sci. Rep.* **5**, 12150.

Palmer PM, Jaffe DM, McCulloch TM, Finnegan EM, Van Daele DJ, & Luschei ES. 2008. Quantitative Contributions of the Muscles of the Tongue, Floor-of-Mouth, Jaw, and Velum to Tongue-to-Palate Pressure Generation. *J Speech Lang Hear Res*, 51(4): 828-835.

Palmer, J.B., Hiiemae, K.M., Liu, J.1997. Tongue–jaw linkages in feeding: a preliminary videofluorographic study. Arch. Oral Biol. 42: 429–441.

Pameijer JH, Glickman I, Roeber FW. 1970. Intraoral occlusal telemetry. Part IV. Tooth contact during swallowing *J. Prosth. Dent.* 24: 396-400.

Proffit WR. 1978. Equilibrium theory revisited: factors influencing position of the teeth. Angle Orthod. 48: 175–186.

R Core Team. 2015. R: A language and environment for statistical computing. R Foundation for Statistical Computing, Vienna, Austria. URL https://www.R-project.org/.

Rakosi T. 1978. An atlas and manual of cephalometric radiography. London: Wolf Medical Publication Limited. pp. 96–8.

Sameera Singh D, Singh DP, Nitya D. 2017. Bruxism: Its multiple causes and its effects on Dental Implants: A Review. J Oral Health Craniofac Sci. 2: 057-063.

Smith BH, 1984. Patterns of molar wear in hunter-gatherers and agriculturists. Am. J. Phys. Anthropol. 63: 39–56.

SUPPLEMENTARY INFORMATIONS

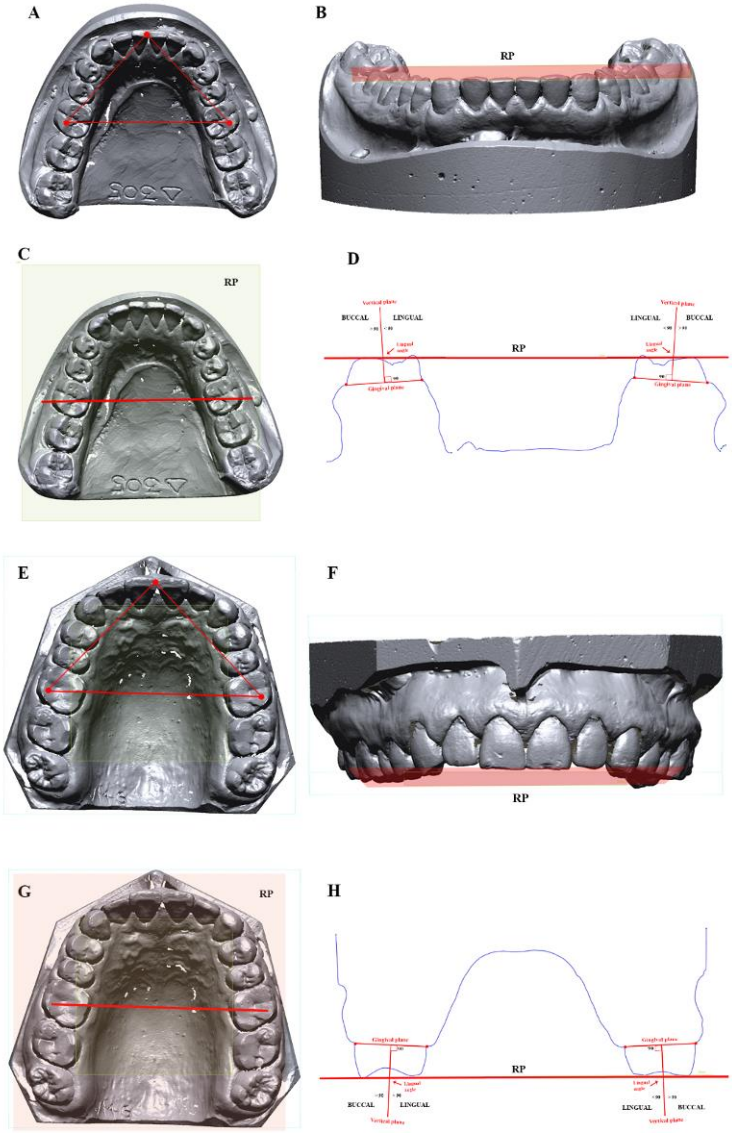

Appendix Figure 1. Occlusal reference plane. Three anatomical points were identified on the occlusal surface (A, E) and the plane crated form them was taken as reference plane (RP) (B, F). Afterwards a plane was draw between

Hypoconid (C) and Metacone (G) of first molars perpendicular to the RP. A cross-section of the entire virtual model was obtained (D, H) in order to calculate the inclinations of alveolar bone (vertical plane perpendicular to the gingival plane) in relation to RP.

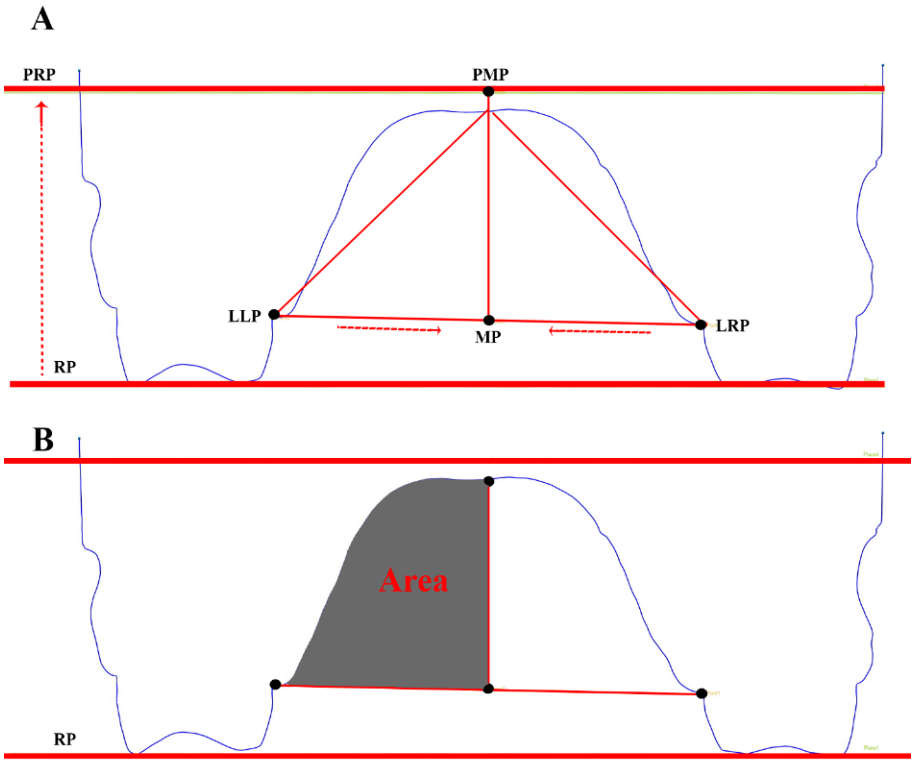

Appendix Figure 2. Cross-section of upper jaw. A) Points used to calculate the relative areas of the palatal arch. B) Areas of the palatal arch. (RP = Reference plane; PRP = Projected Reference Plane; LLP = Lingual Left Point; LRP = Lingual right point; MP = Middle point; PMP = Projected middle point).

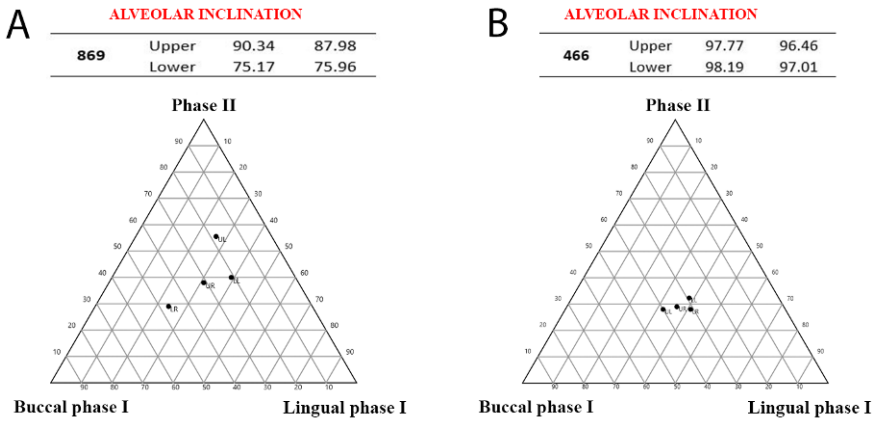

Appendix Figure 3. Ternary diagram of individuals with asymmetric (A) and symmetric (B) alveolar inclinations (degree). Asymmetric (A) masticatory apparatus produce more differences in wear pattern development than symmetric (B).

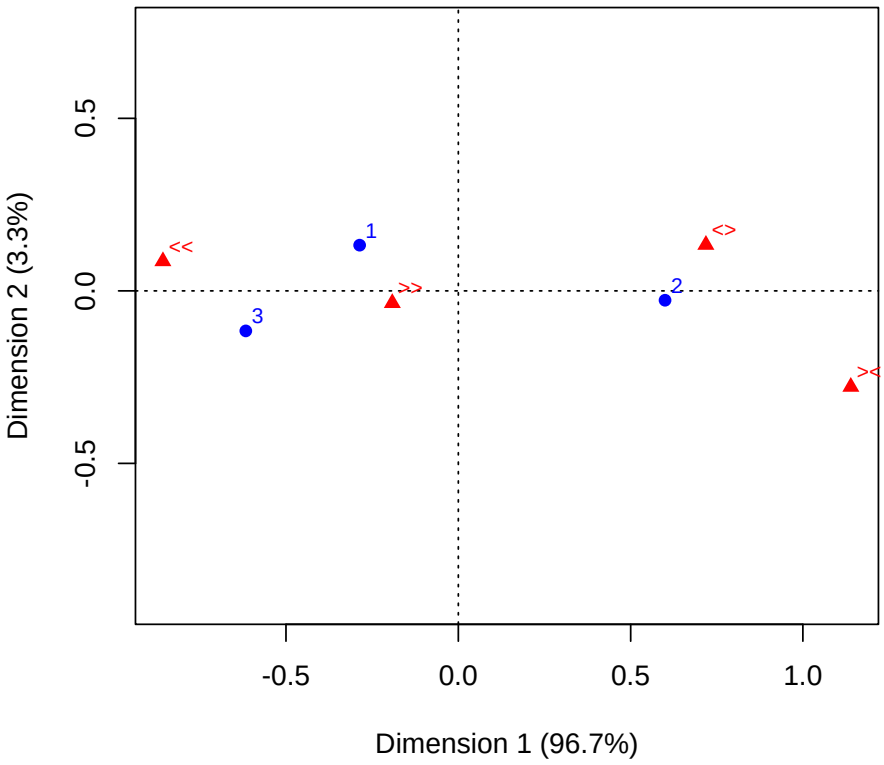

Appendix Figure 4. Correspondence Analysis of alveolar inclinations classes distributed across three different palatal configurations (as described in Appendix Table 8). Dots represent palatal configurations (1. L=R; 2. L>R; 3. R>L) while triangles represent alveolar inclination classes (UR>90 UL >90; UR> UL<; UR< UL>; UR< UL<).

Appendix Table 1. Individuals analyzed from the Yuendumu Aboriginal group.

			Mandible	Maxilla
Specimen	**Age**	**Sex**	**dentition**	**dentition**
751	8	male	mixed	mixed
640	9	male	mixed	mixed
247	10	male	mixed	mixed
716	10	male	mixed	mixed
869	10	male	mixed	mixed
288	11	male	mixed	mixed
634	11	female	mixed	mixed
859	12	male	permanent	permanent
359	15	male	permanent	permanent
251	16	male	permanent	permanent
183	17	male	permanent	permanent
305	17	male	permanent	permanent
307	17	male	permanent	permanent
549	17	female	permanent	permanent
243	19	male	permanent	permanent
294	21	female	permanent	permanent
421	26	male	permanent	permanent
338	29	male	permanent	permanent
466	30	male	permanent	permanent

Appendix Table 2. Inclinations (degree) of antagonist M1s

Specimen	M1	right	Left
183	Maxilla	86.02	91.23
	Mandible	83.38	82.52
247	Maxilla	95.91	90.38
	Mandible	72.71	78.08
251	Maxilla	93.17	93.64
	Mandible	89.39	90
288	Maxilla	101.1	102.5
	Mandible	83.35	86.99
294	Maxilla	88.42	100.78
	Mandible	93.51	89.96
305	Maxilla	89.75	91.31
	Mandible	93.51	93.68
307	Maxilla	91.58	94.87
	Mandible	93.65	90.42
634	Maxilla	90.09	91.36
	Mandible	84.14	88.17
640	Maxilla	84.24	88.5
	Mandible	92.15	95.92
716	Maxilla	90	93.46
	Mandible	87.03	94.75
751	Maxilla	91.71	91.95
	Mandible	72.04	76.5
859	Maxilla	89.78	85.29
	Mandible	80.59	91.43
869	Maxilla	90.34	87.98

	Mandible	75.17	75.96
338	Maxilla	92.19	100.75
	Mandible	93.07	93.84
359	Maxilla	90.84	90.23
	Mandible	104.82	103.7
421	Maxilla	96.4	100.02
	Mandible	90.38	97.12
466	Maxilla	97.77	96.46
	Mandible	98.19	97.01
243	Maxilla	101.31	99.92
	Mandible	75.03	74.78
549	Maxilla	93.66	97.17
	Mandible	91.2	87.38
Range	**Maxilla**	**84.24 - 102.5**	
	Mandible	**72.04 - 104.82**	

Appendix Table 3. Difference in inclinations (degree) between opposite alveolar bones belonging to maxilla and mandible.

Specimen	Uppers	Lowers
183	-5.21	0.86
247	5.53	-5.37
251	-0.47	-0.61
288	-1.4	-3.64
294	-12.36	3.55
305	-1.56	-0.17
307	-3.29	3.23
634	-1.27	-4.03
640	-4.26	-3.77
716	-3.46	-7.72
751	-0.24	-4.46
859	4.49	-10.84
869	2.36	-0.79
338	-8.56	-0.77
359	0.61	1.12
421	-3.62	-6.74
466	1.31	1.18
243	1.39	0.25
549	-3.51	3.82

Appendix Table 4. Difference in inclinations (degree) between antagonist M1 crowns, for both right and left side.

Specimen	Right	Left
183	2.64	8.71
247	23.2	12.3
251	3.78	3.64
288	17.75	15.51
294	-5.09	10.82
305	-3.76	-2.37
307	-2.07	4.45
634	5.95	3.19
640	-7.91	-7.42
716	2.97	-1.29
751	19.67	15.45
859	9.19	-6.14
869	15.17	12.02
338	-0.88	6.91
359	-13.98	-13.47
421	6.02	2.9
466	-0.42	-0.55
243	26.28	25.14
549	2.46	9.79

Appendix Table 5. Values of relative areas of palatal arch. The relative palatal area of each side (left and right) was computed by summing the absolute areas (in mm^2) belonging to the same side, and dividing this sum with to the total palatal area.

Specimen	Palatal Left	Palatal Right
183	0.47	0.53
247	0.52	0.48
251	0.51	0.49
288	0.51	0.49
294	0.49	0.51
305	0.50	0.50
307	0.49	0.51
634	0.50	0.50
640	0.50	0.50
716	0.48	0.52
751	0.50	0.50
859	0.51	0.49
869	0.49	0.51
338	0.48	0.52
359	0.50	0.50
421	0.48	0.52
466	0.50	0.50
243	0.51	0.49
549	0.48	0.52

Appendix Table 6. Upper first molars. Difference between right and left absolute areas of wear pattern.

Specimen	Phase II	Buccal phase I	Lingual phase I
183	-2.15	-3.49	0.64
247	-2.16	0.10	5.64
251	2.57	-1.11	2.19
288	0.88	0.92	-1.49
294	-3.18	-6.53	0.05
305	0.75	-6.53	4.36
307	6.23	3.70	-5.18
634	-3.42	-1.83	0.91
640	-5.22	-2.63	2.68
716	0.91	-3.63	1.54
751	5.65	-0.77	-2.99
859	-0.06	6.82	2.38
869	4.90	-2.36	-0.28
338	-8.96	6.17	-2.85
359	0.00	0.57	-1.45
421	5.25	3.42	-2.59
466	-2.67	-1.70	-3.76
243	-2.10	-3.16	-1.10
549	6.83	2.02	-5.78

Appendix Table 7. Lower first molars. Difference between right and left absolute areas of wear pattern.

Specimen	Phase II	Buccal Phase I	Lingual Phase I
183	-4.42	-1.08	0.24
247	3.92	0.37	3.57
251	3.46	-2.09	-0.03
288	-3.65	0.85	-1.90
294	3.95	-2.55	9.10
305	-4.13	3.60	4.33
307	2.17	2.00	1.15
634	1.96	0.70	-1.31
640	-0.42	2.79	0.62
716	3.84	1.43	1.10
751	4.52	2.78	-1.29
859	5.13	2.18	4.37
869	0.60	-10.13	1.98
338	0.62	0.10	-2.86
359	1.20	3.70	-1.05
421	-0.61	0.06	10.49
466	-2.66	-4.71	-5.99
243	3.22	0.84	0.83
549	2.52	-2.83	-5.14

Appendix Table 8. Occurrence of different classes of alveolar inclinations in the upper dental arch, based on the angle of each side being higher or lower than 90 degrees. Different palatal sets (rows) are determined according the relative proportion of the two palatal halves. The only case exhibiting UR angle exactly equal to 90 degrees has been treated as a measurement error and randomly assigned to one of the alveolar inclination classes (in this case UR<90 UL>90).

	UR>90 UL>90	**UR>90 UL<90**	**UR<90 UL>90**	**UR<90 UL<90**
L=R (1)	4	0	1	1
L>R (2)	4	1	3	0
R>L (3)	4	0	0	1

Scientific Reports – Nature
Sci. Rep. 5, 12150; doi: 10.1038/srep12150 (2015).

Earliest evidence of dental caries manipulation in the Late Upper Palaeolithic

Gregorio Oxilia[1,2,3], Marco Peresani[3], Matteo Romandini[3], Chiara Matteucci[2], Cynthianne Debono Spiteri[4,5], Amanda G. Henry[4,6], Dieter Schulz[7], Will Archer[6], Jacopo Crezzini[8], Francesco Boschin[8], Paolo Boscato[9], Klervia Jaouen[6], Tamara Dogandzic[6], Alberto Broglio[3], Jacopo Moggi-Cecchi[1], Luca Fiorenza[10,11], Jean-Jacques Hublin[6], Ottmar Kullmer[12] & Stefano Benazzi[2,6]*

[1]Department of Biology, University of Florence, Via del Proconsolo, 12, 50122 Firenze, Italy

[2]Department of Cultural Heritage, University of Bologna, Via degli Ariani 1, 48121 Ravenna, Italy

[3]Sezione di Scienze Preistoriche e Antropologiche, Dipartimento di Studi Umanistici, Corso Ercole I d'Este 32, Università di Ferrara, 44100 Ferrara, Italy.

[4]Plant Foods in Hominin Dietary Ecology Research Group, Max Planck Institute for Evolutionary Anthropology, Deutscher Platz 6, 04103 Leipzig, Germany

[5]Institut für Ur- und Frühgeschichte und Archäologie des Mittelaters, Eberhard Karls Universität Tübingen, Schloss Hohentübingen, 72070 Tübingen, Germany.

[6]Department of Human Evolution, Max Planck Institute for Evolutionary Anthropology, Deutscher Platz 6, 04103 Leipzig, Germany

[7]Dental Workshop Bensheim, Private Laboratory for Training, Research and Methods, Siegfriedstraße 104, 64646 Heppenheim, Germany
[8]CeSQ, Centro Studi sul Quaternario ONLUS. Via Nuova dell'Ammazzatoio 7, I - 52037 Sansepolcro (Arezzo), Italy
[9]Università degli Studi di Siena, Dipartimento di Scienze Fisiche, della Terra e dell'Ambiente, Unità di Ricerca Preistoria e Antropologia, Via Laterina 8, 53100 Siena, Italy
[10]Earth Sciences, University of New England, Armidale NSW 2351, Australia
[11]Department of Anatomy and Developmental Biology, Monash University, Melbourne VIC 3800, Australia
[12]Senckenberg Research Institute, Senckenberganlage 25, 60325 Frankfurt am Main, Germany

Introduction

Dental caries are a major oral health problem in modern human societies[1], representing one of the most common chronic dental diseases around the world. The need to treat carious teeth was well-known during historical times as well. To improve pain relief, medieval treatments were based on either humoral theory using herbal remedies or anatomical principles[2,3]. Ancient Greeks and mainly Romans were acquainted with caries removal by drilling and cleaning the infected cavity [4,5], and Egyptian texts confirm this practice was established at least in the fifth millennia BP[6].

The most ancient evidence of dentistry dates back to the Neolithic period, probably associated with the increase in carbohydrate-rich diets [some bacteria[7] such as *Streptococcus mutans*, convert fermentable carbohydrates to form acids; an increase in acidity might favour the demineralisation of the dental tissues[1]] typical of agricultural societies[8] when compared with the more varied diet of hunter-gatherers[9,10]. Indeed, beeswax dental filling was discovered in ca. 6,500 calibrated years before present (cal yr BP) human tooth from

Slovenia[11], while tooth perforations from bow drill, presumably to remove decayed tissues, were observed in ca. 9,000 cal yr BP molars from a Neolithic graveyard in Pakistan[12].

Before the Neolithic, primitive forms of oral hygiene were represented by the use of toothpicks (flexible or inflexible probes probably made of bone and/or wood)[13], potentially to remove food particles between teeth, leaving characteristic interproximal grooves (in the mesial and distal surface of the teeth, but not in the occlusal surface) bucco-lingually elongated[14]. This practice is documented from the beginning of the genus *Homo* and is extremely common among Neandertals and Palaeolithic modern humans[13,14]. However, because during the Palaeolithic toothpicking is not associated with carious lesions[15], it is suggested to be an applied measure to alleviate painful gums or simply a habitual idiopathic activity13-15. Though toothpick-use was common, Coppa and colleagues12 emphasized that unambiguous evidence of true dental treatment (i.e., attempts to remove carious lesions) was only known from the Early Neolithic. Indeed, Lukas and Pastor16 categorized toothpicks among the Neolithic individuals at Mehrgarh (Pakistan) as habitual and occupational grooves, and only during the Chalcolithic these grooves can be related to therapeutic purposes.

Here we analyse a lower right third molar (RM3) (Fig. 1) of the Late Upper Palaeolithic specimen known as Villabruna showing clear evidence of dental caries manipulation. The specimen is a young male individual (ca. 25 years old) that was recovered in 1988 from the Epigravettian deposit of Riparo Villabruna (Sovramonte – Belluno, Italy), and was directly dated around 14,160-13,820 cal yr BP[17,18] (Supplementary Information; Supplementary Fig. S1).

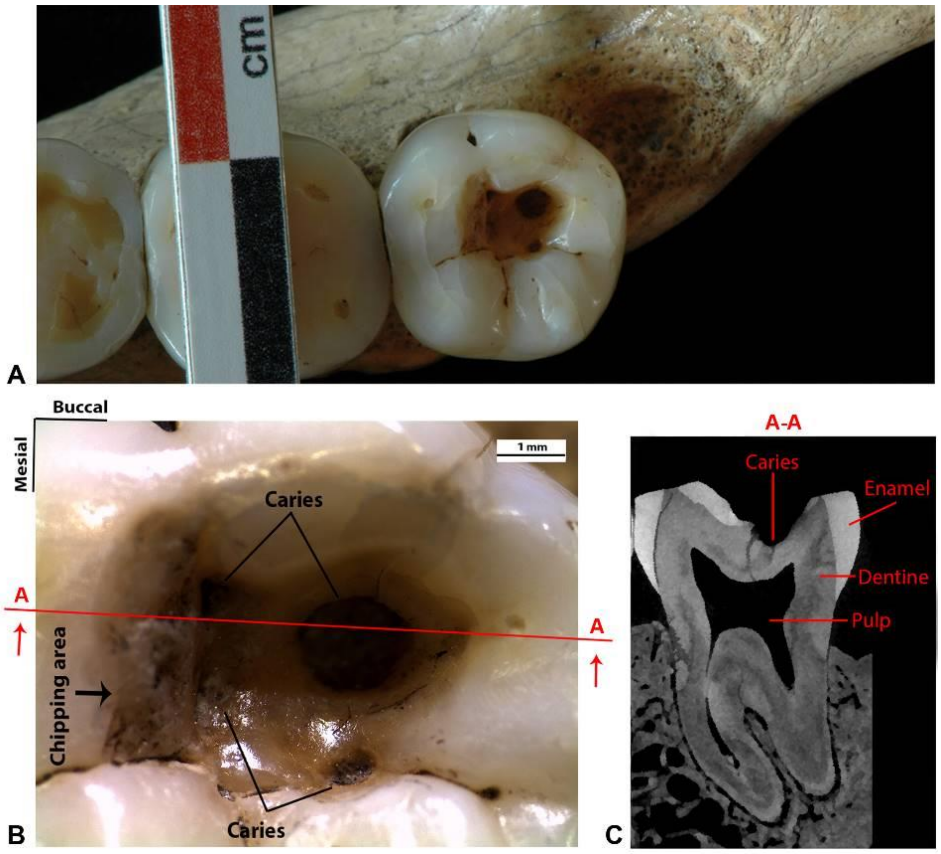

Figure 1. The lower right third molar (RM3) of the Late Upper Palaeolithic specimen known as Villabruna. **(A)** Occlusal view of the RM3. **(B)** Detailed view of the large occlusal cavity with the four carious lesions and the chipping area on the mesial wall. Section A-A is directed mesio-distally, passing through the larger carious lesion. **(C)** MicroCT slice of the Villabruna RM3 in correspondence with section A-A.

Results

The RM_3 retains a large occlusal cavity (mesio-distal=5.84mm; bucco-lingual=3.33mm), with a polished internal surface and extensive enamel chipping traces on the steep mesial wall (Fig. 1A, B) (the other teeth are exempt from caries, except for a tiny hole – incipient caries – in the lingual wall of the RM^3). The cavity, which is located at the level of the hypoconid and

hypoconulid cusps, is sub-squared on the lingual and mesial sides but rounded on the buccal and distal sides. Within the cavity four caries (characterised by demineralised, dark dental tissues) are present[19]. These include three small and shallow pits found in the mesio-buccal and disto-lingual side and a large lesion in the disto-buccal vicinity (mesio-distal=1.8 mm; bucco-lingual=1.6 mm; height=0.96 mm) that penetrates into the dentine producing an empty circular hollow without invading the pulp chamber (Fig. 1C).

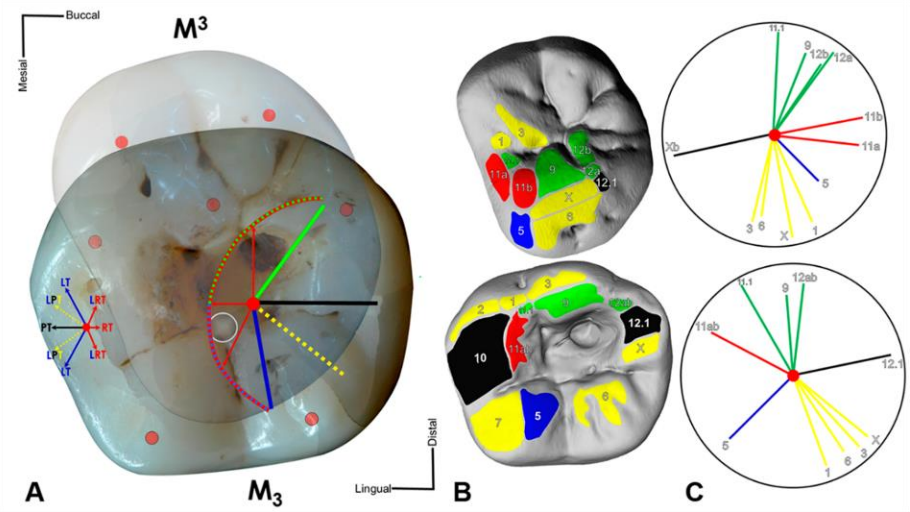

Figure 2. Occlusal relationship between the Villabruna's RM3 and RM3. **(A)** Maximum intercuspation between antagonistic crowns. M3 transparent and mirrored for occlusal view on M3. Red point, cusp tips; grey circle, central fossa center M3. The dental occlusal compass (left) designates general directions of movements in mandibular symphysis out of maximum intercuspation. The dental occlusal compass (right) indicates directions of the M3 protocone tip (red center point). Protrusion (black); lateroprotrusion (yellow); laterotrusion (blue); retrusions (red); mediotrusion (green). **(B)** Wear facet pattern labeled and color-coded. **(C)** Individual occlusal compass results showing spatial orientation of each wear facet.

A functional reconstruction of the dental arches, derived from the information preserved in the dental macrowear pattern (Supplementary Fig. S2), indicates that the main cusp of the antagonistic molar (the protocone of the

RM^3) is responsible for the majority of the wear facets produced on the RM_3 (Fig. 2). Corresponding wear facets on the antagonistic M^3 are located near the cavity, but none of them extend into it. Specifically, the enamel chippings observed in the uppermost mesial margin of the cavity are partially rounded and polished due to wear (facet 11; Fig. 2B), confirming they were produced ante-mortem. A number of chippings deeper in the mesial wall are not encompassed by wear and possess sharp edges. The surface of the unworn chipped area indicates that fracturing has developed through repeated interactions. Occlusal Fingerprint Analysis (OFA) shows that the protocone touches neither the floor nor the deeper mesial wall of the cavity during occlusal movements (Supplementary Information; Supplementary Fig. S3; Supplementary Videos 1, 2), suggesting that the chippings were not produced during masticatory activities.

Scanning Electron Microscopy (SEM) analysis (Quanta Inspect S, FEI Company Hillsboro, USA) of the internal cavity surface reveals characteristic striations (Fig. 3). These are clearly different from typical dental microwear (microscopic scratches), which is produced by attritional contact between lower and upper teeth and by the action of abrasive particles during masticatory activities20. These striations are well documented within the cavity, and occur even on the bottom of the larger disto-buccal carious lesion (Fig. 3). However, they gradually disappear towards the occlusal surface probably as a consequence of tooth wear, thus confirming (along with the wear facet covering the mesial chippings) their ante-mortem formation.

Viewed microscopically and in cross-section, these striations exhibit similar morphological features to cutmarks on bone[21], i.e., Hertzian cones, grooves with a ‘‘V’’ shaped transverse section and microstriation at the bottom, sharply defined, with a high apex, steep sides, narrow cross-sections and well-defined parallel ancillary ridging (Figs. 3, 4; Supplementary Fig. S4).

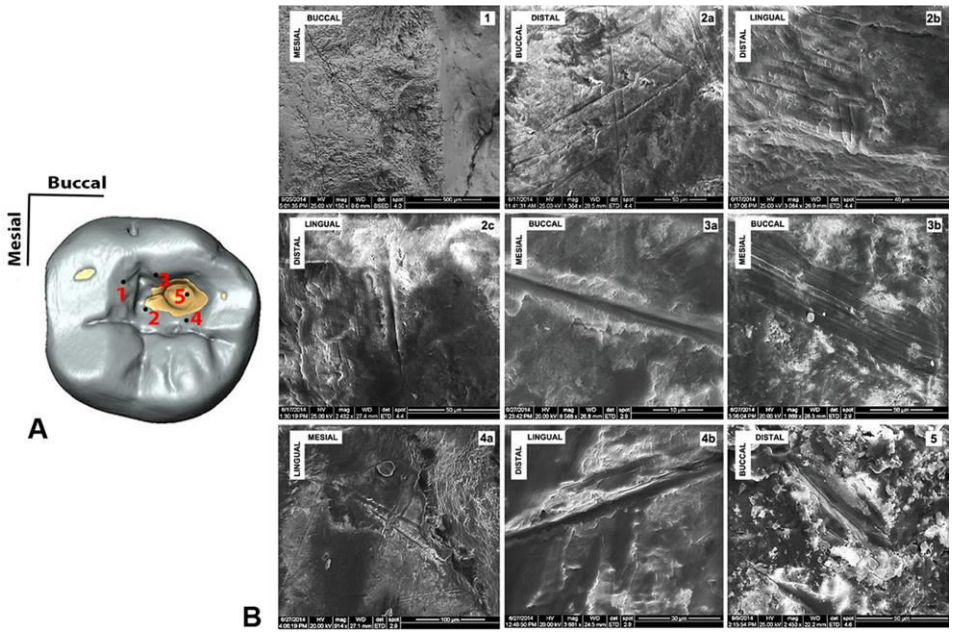

Figure 3. Scanning Electron Microscopy (SEM) images of the striations observed within the carious cavity of the Villabruna RM3. **(A)** Occlusal view of the RM3 digital model, with underlined some of the areas where striations were observed. **(B)** The SEM images: 1, the chipping area; 2a-b-c, the mesial area; 3a-b, the buccal wall of the cavity; 4a-b, the lingual wall of the cavity; 5, inside the large carious lesion.

According to the inferred directionality of the traces, the employed flint tools passed through mesio-buccal > distal, mesial > distal and lingual > disto-buccal axes (Supplementary Fig. S5A, B, C). The study of the orientation of individual traces within the cavity (Supplementary Fig. S5D) indicates a variety of gestures and movements associated with the slicing of the tool edges in different directions. However, it is possible to distinguish two main groupings of lines (i.e., lingual > buccal and mesial > distal; Supplementary Fig. S5D, yellow) potentially produced during back and forward semi-circular levering and scratching movements.

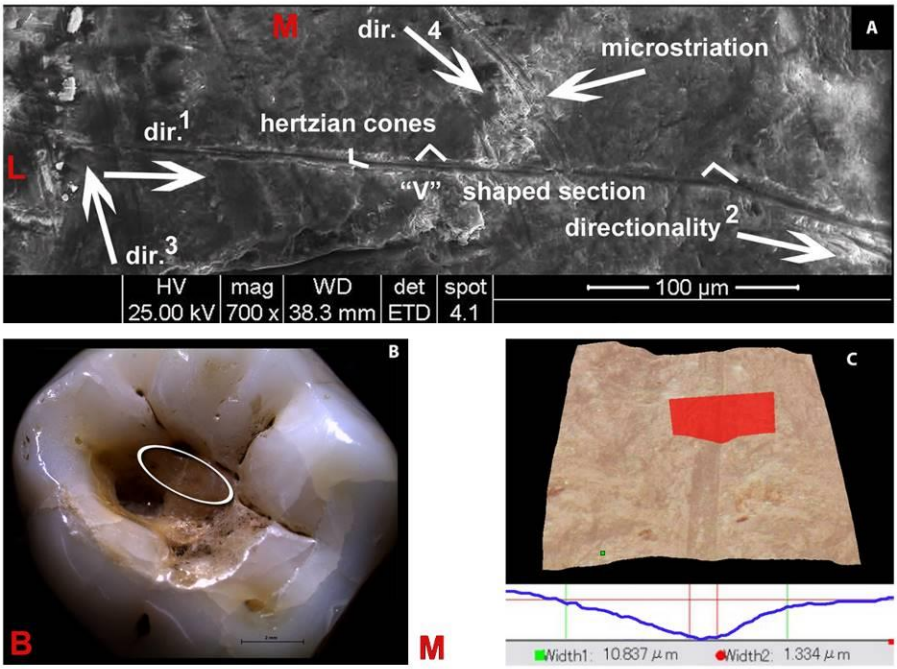

Figure 4. Morphological description of the striations observed in the Villabruna RM3. **(A)** SEM images with morphological and directionality striation features (the numbers indicate the sequence of the gestures). **(B)** Stereo microscopical image of Villabruna RM3 with magnification of the cavity and of the region (ellipse) containing the striations described in this figure (region 2 and 4 in Fig. 3). **(C)** Example of 3D rendering and cross-section of the striation observed in the Villabruna tooth cavity (area 2 in Fig. 3). B, buccal; L, lingual; M, mesial.

Experimental tests carried out on the enamel of three recently extracted M3s using wood, bone and microgravettes Epigravettian experimental microlithic points confirm that the striations observed in the Villabruna specimen were caused by microlithic points (Supplementary Information; Supplementary Table S1). The wood point did not leave any mark on the enamel surface (Supplementary Fig. S6). The bone point produced only extremely faint scratches (Supplementary Fig. S7), whereas the Epigravettian microlithic point produced striations that are identical to those observed in the Villabruna specimen (Supplementary Fig. S8). This was confirmed by further

experiments on six carious human teeth using microlithic points on exposed dentine (Supplementary Information; Supplementary Fig. S9; Supplementary Table S2). The experimental striations also resemble those described by other authors in relation to the action of cutting pieces of meat, held between the anterior teeth, with a stone tool22,23. However, the striations on the Villabruna RM3 appear only within the cavity on the occlusal surface, and would therefore not have been exposed during meat-cutting.

Gas Chromatography-Mass Spectrometry (GC-MS) was used to characterise i) residue adhering to the inner cavity of the RM_3, ii) remnants of what appears to be a mass of organic material integrated within a carbonate concretion buried near the left iliac crest which could possibly be the material used to treat RM_3, and iii) traces of residue adhering to the ilium, potentially originating from the same organic material found in the carbonate concretion (Supplementary Information; Supplementary Fig. S1)[17,18]. A negligible result was obtained for the residue in the inner cavity of the RM_3, as well as from all the samples tested except for one, namely the residue adhering to the ilium (Supplementary Table S3). The profile obtained for this result is suggestive of a natural wax[24] (Supplementary Fig. S10), which could have been locally sourced. A beeswax origin could also be tentatively made, based on the advanced decay of the characteristic alkane profile and the identification of a disaccharide moiety. However, it was not possible to obtain direct evidence for possible therapeutic-palliative medication of the RM_3.

The presence of dental caries in the Villabruna specimen may testify a diet rich in carbohydrate intake. We tested whether there were plant or other micro-remains preserved within the dental cavity, using methods slightly modified from those published previously[25], which were designed to control for potential sources of contamination. The few starches recovered show similar morphology to those found in the control samples from the packing material

(Supplementary Table S4) and are therefore likely to be the result of contamination and cannot be considered indicative of diet.

Discussion

The substantially smaller extension of the demineralised (decayed) tissue when compared with the extensive size of the cavity itself, and the presence of chippings and striations even in the most inaccessible areas of the larger carious pit, strongly suggest intentional (albeit partial) removal of the carious infected/decayed tissue. The Villabruna specimen represents therefore the oldest archaeological evidence of operative manual intervention on a pathological condition (caries), as testified by the striations on the bottom of the carious pit (Fig.3; Supplementary Fig. S4C), potentially to remove the caries and/or to re-establish antagonistic tooth function by removing food particles entrapped within the cavity. This evidence predates the ca. 9,000 cal yr BP Neolithic dental drilling documented in Pakistan[12], as well as the earliest undisputed evidence of cranial surgery, currently represented by the ca. 9,000-7,000 cal yr BP trephination from Vasilevka II, Ukraine[26] and Ensisheim, France[27] [cranial trephination predating the Mesolithic, as the examples suggested by Dastugue[28,29], are highly dubious[26,27]]. Therefore, we suggest that earliest dental caries manipulation entails an adaptation of the toothpicking technique from simple rubbing actions between interproximal teeth using probes made on bone/wood, to scratching/levering activities within the carious lesion using microlithic points.

Recent studies show that dietary changes towards more carbohydrate-rich diet (e.g., large exploitation of grains and starches) may have occurred well before the Neolithic, predating the origin of agriculture by ca. 10,000 years[30,31], if not 20,000 years[32]. Though it is undeniable that the frequency of dental caries increased from the advent of agriculture[9,10], some regions may have experienced a dietary shift during the mid-Late Upper Palaeolithic, as suggested by a greater

incidence of carious lesions (rarely observed in fossil hominins)[33] in some modern human populations[34]. The rise in caries incidence, coupled with appropriate lithic technology during the Late Upper Palaeolithic may have created an optimal context within which to adapt the habitual use of a toothpick (made of wood/bone) towards a rudimentary dental intervention using microlithic tools. Like other Late Upper Palaeolithic cultures, the Epigravettian was characterised by widespread production of backed artifacts made from bladelets, generally used as insets for weaponry[35]. Specifically, the microgravettes were elongated and strong points designed for use as hafted hunting projectiles (Supplementary Fig. S9A), but their small size and hardness were well suited both to enter into small carious cavities and to remove the demineralised but resistant bacterially infected enamel and dentine tissues by levering and scratching (Supplementary Fig. S5A, B, C).

Therefore, the earliest incipient dentistry entails levering and scratching but not drilling practices, as observed later, during the Neolithic and in modern dentistry.

Methods

Micro-CT scan

High-resolution micro-CT images of the Villabruna upper and lower dentition were obtained with a BIR Actis5 microtomographic system (Max Planck Institute for Evolutionary Anthropology, Leipzig, Germany) using the following scan parameters: 130 kV, 100 µA, with 0.50 mm Brass filter. Volume data were reconstructed using isometric voxel length of 30 µm. The micro-CT images of the teeth were virtually segmented using a semiautomatic threshold-based approach in Avizo 7 (Visualization Sciences Group Inc.) both to reconstruct a complete 3D virtual model of the Villabruna dentition and to evaluate the extension of the carious lesion in the RM_3 (Fig. 1C).

Reconstruction of physiological occlusal relationship

The functional reconstruction of the Villabruna dentition follows indications provided by Benazzi at al.[36] and Kullmer et al.[37]. In detail, the upper and lower dentition of the Villabruna specimen was reproduced with high-resolution epoxy and dental stone casts[38]. Moreover, digital surface data of the dentition was acquired with a white light 3D digitisation system (smartSCAN^{3D}, Breuckmann GmbH, Germany), with an average resolutions of ~ 65 µm.

The casts of the upper and lower third molars were used to draw two-dimensional maps of all complementary wear facet pairs on the occlusal surface after their identification with a binocular (Leitz MZ12). In addition, the facets were interactively marked on the virtual models using PolyWorks® 12.0 software (InnovMetric Software Inc., Canada)[39].

The facets were labelled applying the numbering system of Maier and Schneck[39], and colour-coding in the facet maps follows[39-41]. The application of the dental occlusal compass determines relative occlusal movements for each individual wear facet pair. The point of maximum intercuspation (centric

occlusion) marks the start point of directions of movements for the standardised colour-coding in OFA[39]. Blue coloured facets indicate occlusal contacts during latero- and lateroretrusive movements, yellow specifies lateroprotrusion facets, green shows medioretrusive movements, red and black indicate retrusion and protrusion, respectively (Fig. 2). The facet maps are used to identify directions of occlusal movements[41,42], and support setup of the condyle boxes of the dental articulator.

For physiological repositioning of the teeth we aligned casts of each tooth crown in a dental articulator system (PROTAR, KaVo Dental GmbH, Germany). With a dental articulator system it is possible to reproduce natural occlusal movements, while macroscopically observe the contact situations[36,37] . The epoxy cast specimens were positioned in the articulator after taking its lower jaw dimensions (general geometry, condylar axis position, occlusal and the mid-sagittal plane) from a 3D-print of the complete lower jaw (data from micro-CT).

After positioning of the mandibular resin dentition in the articulator, the maxilla epoxy cast was positioned with the best-fit occlusal relationship possible. Once the initial position is setup, the epoxy casts are replaced with dental stone copies on a wax basis. A slight distortion in the original specimen prevents a proper occlusion. Therefore we used dental stone copies, which can be easily cut at the interproximal planes that each crown can be repositioned independently. Both arches were mounted with dental gypsum between duett-plates and montage-plates (Baumann Dental GmbH) in the articulator. All crowns were then removed from the arches bases.

The upper and lower right M3s of the right and left sides were repositioned first. Based on their occlusal fingerprint (wear facet pattern) they provide important occlusal precision for matching the antagonistic pairs. When the third molar pairs are positioned in maximum intercuspation, we set up the articulator condyle boxes to constrain possible articulator movements for the

individual occlusal simulation. Subsequently the antagonistic occlusal pairs can be restored in their dental arches in the same way. The articulator allows testing of the occlusal position of each repositioned tooth pair to ensure consistency of functional movements throughout the tooth rows in accordance with the colour-coded occlusal compass. The anterior dentition of Villabruna was reconstructed last, because it does not show any contact in maximum intercuspation of the dental arches.

Virtual Occlusal Fingerprint Analysis (OFA)

Virtual Occlusal Fingerprint Analysis was applied to evaluate the physiological occlusal movements and crown contacts. The upper and lower jaw digital models were aligned with a virtual model generated from a surface scan from the physical reconstruction of the dental arches in maximum intercuspation (Supplementary Fig. S2), using a best-fit algorithm in IMInspect module of PolyWorks® 12.0.

We verified the kinematics of the occlusal movements (i.e., the pathway of incursive and excursive movements) applying the "Occlusal Fingerprint Analyser" (OFA) software. The OFA software is a virtual tool developed at the Senckenberg Research Institute in Frankfurt (Germany) to detect relief guided dental collisions of antagonistic tooth crowns[43-45]. The OFA software records the occlusal pathways and sequential surface contacts derived from collision detection, deflection and breakfree algorithms (Supplementary Fig. S3; Supplementary Videos 1, 2).

Experimental replication of striations

Test 1

Experimental scratching/levering activities were carried out on the enamel surface of three recently extracted lower M_3s to test three kinds of point tools (Supplementary Table S1): wood point (Supplementary Fig. S6C), bone point (Supplementary Fig. S7C) and microlithic point (Supplementary Fig. S8C). These tools were produced by Matteo Romandini e Rossella Duches (University of Ferrara). The wood point was produced on *Larix decidua*, as coniferous trees dominated the landscape during the period of the burial. The bone point was obtained from the diaphysis of a large size ungulate, and is comparable to bone points found in the burial kit (Supplementary Fig. S1). The microlithic point was made by direct retouching of bladelets extracted from red and grey flint cores, comparable to those exploited by the Epigravettian settlers at Riparo Villabruna.

The same force was applied during the tests. The breakage of the point defined the end of the experiment (Supplementary Table S1).

Test 2

Experimental tests were carried out using microgravette Epigravettian points on six medieval carious human molars (Supplementary Table S2) collected from the Department of Cultural Heritage (University of Bologna, Italy). Different forces were applied in relation to dentine exposure, and several parameters were evaluated, such as the type of tool used (tool shape efficacy), actions, directions, inclinations and duration of treatment (Supplementary Table S2).

Analysis of the cross-sectional geometry

The Villabruna RM_3 and the six archaeological human molars used for the experimental tests were analysed using a Hirox Digital Microscope KH-7700 with an MXG-10C body, OL-140II and OL-700II lenses and an AD-10S

Directional Lighting Adapter. This portable instrument, housed at the University of Siena, provides a 3D composite image through the overlapping of a series of pictures taken at different focus levels. It enables us to observe the cross section of grooves and to collect metrical parameters[46,47], as recently shown for the study of archaeological cutmarks and interproximal grooves on human teeth[13,47,48]. The following metrical parameters were collected: DC (depth of cut), BT (breadth at the top), BF (breadth at the floor) and RTF (ratio between the breadth at the top and the breadth at the floor of cut).

Three striations within the Villabruna RM_3 cavity were analysed. Two are located in the region 2 and one in the region 5 (Fig. 3). The striations are shallow (DC is less than 4 µm) and narrow (BT between 2.5 and 17.5 µm), and cross sections are V-shaped (Supplementary Fig. S4A, B, C). This characteristic is quantified by the high value of ratio between breadth at the top and breadth at the floor of grooves (RTF comprised between 6.3 and 8.3).

Experimental grooves inflicted by the use of Epigravettian points on exposed dentine are V-shaped, with RTF ranging from 5.2 and 13.1 (n=6) (Supplementary Fig. S9), resembling those observed in the Villabruna RM_3.

Gas Chromatography-Mass Spectrometry (GC-MS)

Beeswax has already been identified in ancient therapeutic dental practices[11], and could potentially have been used in the case of the Villabruna individual. Another related possibility which has antibacterial and antifungal properties is propolis, a sticky material that honeybees collect from living plants, mix with wax and use to construct and repair their hives[49]. The chemical composition of both beeswax and propolis are known[49,50], and characterisation can be carried out using organic residue analysis (ORA).

Sampling was carried out by CDS at the Max Planck Institute for Evolutionary Anthropology, Leipzig. Scrapings of the residue adhering to the outer and inner surfaces of the ilium were obtained for testing using a sterilised

scalpel. A sample was taken from the organic material integrated within a carbonate concretion buried in close proximity to the left iliac crest, and the surrounding soil was tested as a control. The material adhered to the cavity in the molar proved difficult to sample. To avoid damaging the inner surface of the tooth, repeated washings with small quantities of an organic solvent (dichloromethane:methanol, 2:1, *v:v*) were taken using a sterilised glass Pasteur pipette to directly dissolve organic compounds present in the residue. Supplementary Table S3 reports the sampling details.

Solvent Extraction

All solvents used were HPLC grade solvents (Roth), and the standard purity was ≥99% (Sigma-Aldrich). Glassware was sterilised before use and a method blank was included to monitor laboratory contamination. Isotopically labelled $C_{18:0}$ was used as an internal standard for quantification purposes.

Prior to extraction, 10µg of isotopically labelled $C_{18:0}$ internal standard were added to all the samples. To each sample, 2mL of dichloromethane:methanol (2:1; *v:v*) solution were added. The samples were shaken and sonicated for 15 minutes, and then centrifuged (3500rpm, 10 minutes, room temperature). The solvent containing the extracted lipid was pipetted into screw capped test tubes and the extraction was repeated twice more, combining the lipid extracts. The solvent was then evaporated to dryness under a gentle stream of nitrogen and mild heating (30°C) to obtain the total lipid extract (TLE). Each sample was rehydrated using 120µL of hexane and then partitioned [1:1]. The solvent was evaporated, and both parts of the samples were stored at -20°C pending further analysis. One part of each sample was derivatised (silylated) and analysed, the other stored.

Saponification

Potential 'unbound' lipid fractions in samples VIL01, VIL02, VIL03 and VIL04 were targeted by saponification. To each sample, 1mL of 0.5M methanolic

sodium hydroxide solution made up in methanol:water (9:1, *v:v*) was added. The samples were shaken and vortexed, and then heated (90 minutes, 70°C). The samples were allowed to cool and centrifuged (4000 rpm, 10 minutes, room temperature). The supernatant was pipetted into screw-capped test tubes. The neutral fraction was extracted three times using 1mL of hexane into small glass vials. The aqueous fraction was acidified to a pH 3 using *c.*0.4mL of 6M hydrochloric acid. The acid fraction was extracted three times into small vials, using 1mL of hexane. Both the acid and neutral fractions were evaporated to dryness using mild heating (30°C) and a gentle stream of nitrogen. The neutral fraction was silylated prior to GC-MS analysis, while the acid fraction was methylated before silylation and GC-MS analysis.

Methylation

200µL of Boron Triflouride (14% Methanol) were added to each of the samples, which were then heated for 1 hour at 70°C. The reaction was quenched with 2 drops of double distilled water, and allowed to cool. Methylated lipids were extracted three times using 2mL hexane. Samples were evaporated to dryness using mild heating (30°C) and a gentle stream of nitrogen, then rehydrate using 120µL of hexane and partitioned [1:1]. The solvent was evaporated and samples store at -20°C pending further analysis. One part of each sample was silylated prior to GC-MS analysis.

Silylation

30µL of pyridine were added to the dried samples at room temperature, followed by 55µL of MSTFA (*N*-Methyl-*N*-trifluoroacetamide). The samples were agitated for 30 minutes at 37°C, then centrifuged to remove any remaining drops on the snap caps, and transferred to autosampler vials containing micro inserts.

Gas-Chromatography Mass-Spectrometry (GC-MS) Analysis

GC-MS analysis was carried out on an Agilent 6890 Gas Chromatograph coupled with a Quadrupole Mass Spectrometer (MS) (Agilent, Germany), equipped with an Agilent 7683 series auto sampler (Agilent, Germany). A Hewlett Packard 5973 Mass Selective Detector (MSD) was used for GC-MS analysis. The GC was fitted with a 30m DB-5MS (5% phenyl methyl siloxane) Agilent column, with a 0.25mm internal diameter and a film thickness of 0.25µm. The samples were injected in splitless mode at 300°C. Helium was used as the carrier gas, with a flow rate of 1mL min^{-1}. The oven was programmed at 50°C for 2 minutes, then ramped at 10°C per minute to 325°C and held for 15 minutes. The MS was operated in Electron Impact mode (EI; 70eV), at a full scan range of *m/z* 50 to 550, with a scan time of 3s per scan. Data acquisition was carried out using Data Analysis Version 3.3 (Bruker Daltonics) data system. Data analysis was performed using MSD ChemStation Version D.00.01.

Plant microremain analysis

The Villabruna remains were brought to the archaeological material laboratory in the Max Planck Institute for Evolutionary Anthropology, where they were sampled by AGH. The caries on the lower molar was sampled for possible plant microremains by adding a small volume of double distilled water (~50µl) to the cavity using an adjustable volume pipet with a plastic disposable tip, agitating the surface by pumping the water in and out of the pipet, and finally transferring all of the water to a microcentrifuge tube. Later 1ml of ddH2O was added, and the tube vortexed for 15sec, and centrifuged for 5min at 3krpm. 950µl of supernatant was removed and the pellet resuspended in the remaining 50µl, 10µl of which was mounted on a slide, with 10µl 25% glycerin.

We also collected several kinds of control samples, including samples of the containers in which the fossil material was stored, to look for

contamination from the post-excavation curation. We took samples from the bubble wrap and stuffing in the box in which the mandible was stored, as well as the stuffing from the skull box and small fragments from the bottom of the skull box. These controls were sampled by holding them with forceps over a 15ml tube, and washing them with a stream of ddH2O which was collected in the tube. The tube then centrifuged, then all but ~50µl removed, and 10µl of this remainder mounted and examined. Finally, when a batch of samples was mounted for a day's worth of microscopy, we prepared a blank slide, which contained only 10µl dH2O and 10µl 25% glycerin.

We perform regular cleaning and testing procedures to assess possible lab contamination. The laminar flow hood and the surrounding bench areas were cleaned once a week with hot tap water and starch-free soap, followed by a wipe with 5% bleach, and a final tap water wipe rinse. Since the results of Crowther and colleagues[51], we now recommend using NaOH instead of bleach. Every two weeks, the laminar flow hood and the bench work area were tested for contaminants by wiping the entire surface with a wet towel, rinsing the towel into a 50ml tube, centrifuging this tube, pipetting off the supernatant and mounting the remainder on a slide. Records were kept of the contaminant load before and after cleaning, with photographs and written descriptions to allow comparison to the archaeological material. All of our reagents and mounting material were changed once a month, and the water and glycerin containers were tested once every two months for contaminants. In addition to the weekly cleaning, the work areas were cleaned immediately prior to sampling with soap and a water rinse.

References

1. Cummins, D. Dental caries: a disease which remains a public health concern in the 21st century--the exploration of a breakthrough technology for caries prevention. *J Clin Dent* **24,** 1-14 (2013).

2. Anderson, T. Dental treatment in Medieval England. *Br Dent J* **197,** 419–425 (2004).

3. Khodadoust, K., Ardalan, M., Pourabbas, R. & Abdolrahimi, M. Dental and oral diseases in Medieval Persia, lessons from Hedayat Akhawayni. *J Med Ethics Hist* **2,** 6-9 (2013).

4. Guerini, V. A. History of Dentistry from The Most Ancient Times until the End of The eighteenth Century. *Lea & Febiger* (1909).

5. Kanner, L. Folklore Of The Teeth: History of Dentistry. Macmillan's dental library (1935).

6. Ring, M.E. Dentistry: An Illustrated History. *Harry N. Abrams* (1985).

7. Adler, C.J. *et al.* Sequencing ancient calcified dental plaque shows changes in oral microbiota with dietary shifts of the Neolithic and Industrial revolutions. *Nat Genet* **45,** 450–455 (2013).

8. Warinner, C. *et al*. Direct evidence of milk consumption from ancient human dental calculus. *Sci Rep* **4,** 7104 (2014).

9. Braidwood, R., Howe, B. & Reed, C. The Iranian Prehistoric Project: new problems arise as more is learned of the first attempts at food production and settled village life. *Science* **133,** 2008–2010 (1961).

10. Oelzea, V. *et al.* Early Neolithic diet and animal husbandry: stable isotope evidence from three Linearbandkeramik (LBK) sites in Central Germany. *J Archaeol Sci* **38,** 270–279 (2011).

11. Bernardini, F. *et al.* Beeswax as Dental Filling on a Neolithic Human Tooth. *PLoS One* **7,** e44904 (2012).
12. Coppa, A. *et al.* Early Neolithic tradition of dentistry. *Nature* **440,** 755-756 (2006).

13. Ricci, S. *et al.* Toothpick use among Epigravettian Humans from Grotta Paglicci (Italy). *Int J Osteoarchaeol* doi: 10.1002/oa.2420 (2014).

14. Lozano, M., Subirà, M., Aparicio, J., Lorenzo, C. & Gómez-Merino, G. Toothpicking and periodontal disease in a Neanderthal specimen from Cova Foradà site (Valencia, Spain). *PLoS One* **8,** e76852 (2013).

15. Lebel, S. *et al.* Comparative morphology and paleobiology of Middle Pleistocene human remains from the Bau de l'Aubesier, Vaucluse, France. *Proc Natl Acad Sci USA* **98,** 11097-102 (2001).

16. Lukas, J.R. & Pastor, R.F. Activity-Induced Patterns of Dental Abrasion in Prehistoric Pakistan: Evidence From Mehrgarh and Harappa. *Am J Phys Anthropol* 76, 377-398 (1988).

17. Aimar, A. *et al*. Les Abris Villabruna dans la Vallèe du Cismon. *Preistoria Alpina* **28,** 227- 254 (1992).

18. Vercellotti, G., Alciati, G., Richards, M. & Formicola, V. The Late Upper Paleolithic skeleton Villabruna 1 (Italy): A source of data on biology and behavior of a 14.000 year-old hunter. *J Anthropol Sci* **86,** 143-163 (2008).

19. Alciati, G., Coppa, A., Macchiarelli, R. & Pertile, F. La dentizione del cacciatore epigravettiano del riparo Villabruna A (valle del Cismon, Belluno). *Quaderni d'Anatomia Pratica* **49,** 73-100 (1993).

20. Kaidonis, J.A. Tooth wear: the view of the anthropologist. *Clin Oral Invest* **12,** 21-26 (2008).

21. Bromage, T. & Boyde, A. Microscopic Criteria for the Determination of Directionality of Cutmarks on Bone. *Am J Phys Anthropol* **65,** 359-366 (1984).

22. Frayer, D.W. *et al.* More than 500,000 years of right-handedness in Europe. *Laterality* **17,** 51-69 (2012).
23. Estalrrich, A. & Rosas, A. Handedness in Neandertals from the El Sidrón (Asturias, Spain): evidence from instrumental striations with ontogenetic inferences. *PLoS One* **8,** e62797 (2013).

24. Jones, J., Higham, T.F.G., Oldfield, R., O'Connor, T. & Buckley, S.A. Evidence for prehistoric origins of Egyptian mummification in Late Neolithic burials. *PLoS One* **9,** e103608 (2014).

25. Henry, A., Brooks, A. & Piperno, D. Plant foods and the dietary ecology of Neanderthals and early modern humans. *J Hum Evol* **69,** 44-54 (2014).

26. Lillie, M. Cranial surgery dates back to Mesolithic. *Nature* **391,** 854 (1998).

27. Alt, K. *et al.* Evidence for stone age cranial surgery. *Nature* **387,** 360 (1997).

28. Dastugue, J. Paléopathologie. La nécropole épipaléolithique de Taforalt, Maroc oriental. (ed. *Ferembach, D.*) 133–158 (Éditions du CNRS, 1962).

29. Dastugue, J. Pathologie des hommes épipaléolithiques d'Afalou-bou-Rhummel, Algérie, *L'Anthropologie* **79,** 483–506 (1975).

30. Piperno, D., Weiss, E., Holst, I. & Nadel, D. Processing of wild cereal grains in the Upper Palaeolithic revealed by starch grain analysis. *Nature* **430,** 670–673 (2004).

31. Liu, L., Bestel, S., Shi, J., Song, Y. & Chen, X. Paleolithic human exploitation of plant foods during the last glacial maximum in North China. *Proc Natl Acad Sci USA* **110,** 5380-5385 (2013).

32. Revedin, A. *et al*. Thirty thousand-year-old evidence of plant food processing. *Proc Natl Acad Sci USA* **107,** 18815–18819 (2010).

33. Grine, F., Gwinnett, A. & Oaks, J. Early hominid dental pathology: interproximal caries in 1.5 million-year-old Paranthropus robustus from Swartkrans. *Arch Oral Biol* **35,** 381-386 (1990).

34. Humphrey, L.T. *et al.* Earliest evidence for caries and exploitation of starchy plant foods in Pleistocene hunter-gatherers from Morocco. *Proc Natl Acad Sci USA* **111,** 954-959 (2014).

35. Palma di Cesnola, A. Le Paléolithique supérieur en Italie (Jérôme Million, 2001).

36. Benazzi, S., Kullmer, O., Schulz, D., Gruppioni, G. & Weber, G.W. Individual tooth macrowear pattern guides the reconstruction of Sts 52 (*Australopithecus africanus*) dental arches. *Am J Phys Anthropol* **150,** 324-329 (2013).

37. Kullmer, O. *et al.* Dental arch restoration using tooth macrowear patterns with application to *Rudapithecus hungaricus*, from the late Miocene of Rudabánya. *J Hum Evol* **64,** 151- 160 (2013).

38. Fiorenza, L., Benazzi, S. & Kullmer, O. Morphology, wear and 3D digital surface models: materials and techniques to create high-resolution replicas of teeth. *J Anthropol Sci* **87**, 211–218 (2009).

39. Kullmer, O. *et al*. Technical Note: Occlusal Fingerprint Analysis: Quantification of Tooth Wear Pattern. *Am J Phys Anthropol* **139,** 600–605 (2009).

40. Maier, W. & Schneck, G. Konstruktionsmorphologische Untersuchungen am Gebiß der hominoiden Primaten. *Z Morph Anthrop* **72,** 127–169 (1981).

41. Schulz, D. NAT – Die Naturgemäße Aufwachstechnik. Teil 1: Der anteriore Bereich. (Fuchstal, Teamwork Media GmbH, 2003).

42. Schulz, D. NAT – Die Naturgemäße Aufwachstechnik. Teil2: Der posteriore Bereich. (Fuchstal, Teamwork Media GmbH, 2008).

43. Benazzi, S., Kullmer, O., Grosse, I.R. & Weber, G.W. Using occlusal wear information and finite element analysis to investigate stress distributions in human molars. *J Anat* **219,** 259–272 (2011).

44. Benazzi, S. *et al.* The Evolutionary Paradox of Tooth Wear: Simply Destruction or Inevitable Adaptation? *PLoS One* **8,** e62263 (2013).

45. Benazzi, S., Nguyen, H.N., Kullmer, O. & Hublin, J.J. Unravelling the functional biomechanics of dental features and tooth wear. *PLoS One* **8,** e69990 (2013).

46. Bello, S.M. & Soligo, C. A new method for the quantitative analysis of cutmark micromorphology. *J Archaeol Sci* **35,** 1542-1552 (2008).

47. Boschin, F. & Crezzini, J. Morphometrical Analysis on Cut Marks Using a 3D Digital Microscope. *Int J Osteoarchaeol* **22,** 549–562 (2012).

48. Crezzini, J., Boschin, F., Boscato, P. & Wierer, U. Wild cats and cut marks: Exploitation of Felis silvestris in the Mesolithic of Galgenbühel/Dos de la Forca (South Tyrol, Italy). *Quatern Int* **330,** 52-60 (2014).

49. Bankova, V.S., De Castro, S.L. & Marcucci, M. Propolis: recent advances in chemistry and plant origin. *Apidologie* **31,** 3-15 (2000).

50. Heron, C., Nemcek, N., Bonfield, K.M., Dixon, D. & Ottaway, B.S. The chemistry of Neolithic beeswax. *Naturwissenschaften* **81,** 266-269 (1994).

51. Crowther, A., Haslam, M., Oakden, N., Walde, D. & Mercader, J. Documenting Contamination in Ancient Starch Laboratories. *J Archaeol Sci* **49,** 90-104 (2014).

Acknowledgments

The fieldwork at the Villabruna Rockshelter was granted by the Ministry of Culture, the Veneto Region and the Sovramonte Village Public Administration and supported by the Belluno Museum Association. Veneto Archaeological Heritage gave permission for non-destructive analyses and the micro-sampling of the Villabruna specimen. We thank M. Rea, P. Sibilla, M. Aimetti, U. Menz, C. Hemm, S. Freidline, F. Fiorillo and H. Temming for technical support. C. Brikemeyer and S. Deshmukh from the AG Massenspedktrometrie, Universität Leipzig, ran the samples submitted for GC-MS analysis. S. Schmidt and T. Büdel assisted with the sample preparation. S.A. Buckley is thanked for helpful comments on the MS data. We are grateful to Mr. Aldo Villabruna for support in fundraising for this specific study and the Laboratory of Archaeozoology and Taphonomy (L.A.T.) for giving access to the Stereomicroscopy. OFA software

programming was financed by the German Science Foundation (DFG). This is publication no XX of the DFG Research Unit 771 “Function and performance enhancement in the mammalian dentition - phylogenetic and ontogenetic impact on the masticatory apparatus”.

Author Contributions

S.B., G.O., M.P. and M.R. initiated and organized the project. G.O. segmented and reconstructed the digital model of the teeth. G.O., L.F., O.K. and S.B. identified and mapped the wear facets on the occlusal surface of the molars. D.S. and O.K. carried out the functional reconstruction of the Villabruna dentition. O.K. carried out the Occlusal Fingerprint Analysis using the OFA software. A.H. analysed the microremains. C.S. performed Mass spectrometry analysis. M.P., M.R. and G.O. carried out the experimental test. G.O. and C.M. identified the striations with SEM. J.C., F.B., P.B. and M.R. analysed the cross-section of the striations. G.O., S.B., M.P., M.R., O.K., D.S., A.H., C.S., L.F. and W.A. analysed the data. G.O., S.B., M.P., M.R., O.K., D.S., A.H., C.S., W.A., J.C., F.B., P.B., L.F., K.J., T.D., A.B., J.M.C., J.J.H. and C.M. discussed the results. S.B., G.O., O.K., M.P., M.R., C.S., A.H., C.M., L.F., K.J., J.C., F.B., P.B., T.D., J.J.H. and J.M.C. wrote and edited the manuscript.

Additional Information

Supplementary information accompanies this paper at
http://www.nature.com/srep

Supplementary Information

The Villabruna burial

The burial of Riparo Villabruna (Supplementary Fig. S1) was discovered in the interiot of the small shelter named Riparo Villabruna A (Sovramonte – Belluno, Italy). The burial was exposed by a cut made for the purpose of widening a road. Within this process both the lower limbs of the burial were severed at the distal femoral shafts1. The subject2 was an adult male, who was buried outstretched within a grave 30-40 cm deep. The skull was facing towards the individuals left hand side, and was in close proximity to the shelter wall. A container, probably a bag, was placed on the left forearm. Within the container were six objects. These included two refitted fragments of a bone point engraved with two series of notches, a backed knife, a blade made on flint, a core made on flint, a siltstone pebble "retoucher" and a lump of unidentified material with attached carbonate concretions. The blade and core, the siltstone pebble as well as part of both the radius and the iliac crest show differential traces of weathering and surface corrosion.

After the body had been placed in the grave, it was covered with large stones collected on the Cismon e Rosna stream beds, few hundred meters from the shelter. The cobbles were further painted with red ocher1.

Following the removal of the stones during archaeological excavation, the skeleton was delicately recovered using aspirators, soft brushes and distilled water to remove the finer sedimentary particles. A thin carbonate concretion lens covered the skull surface, and was manually removed during excavation. The teeth emerged clean and unscathed, and no mechanical intervention was required to clean them.

Radiocarbon dating both on charcoal from the pit sediment (R-2023: 12,040±150 yr BP)1, and directly of the skull (KIA-27004: 12,140±70)2 place the burial in the interval 14,400-13,800 cal yr BP (CalPal Calibration Program).

OFA results

The results show that the protocone of the upper right third molar (RM3) makes contact with the uppermost margin of the mesial wall of the cavity during an orthal incursive movement. . The protocone contact – manifesting in a protrusive movement through the cavity - thereby produced mesio-distally elongated wear facets along the lingual and buccal margins of the cavity (Supplementary Video 1). The movement of the protocone produces a deeply worn and tub-shaped enamel basin along the distal margin of the cavity (Supplementary Fig. S3). An OFA sequence performed with the full dental arch reconstruction produced similar results, which suggests that the cavity was present for a substantial period within the life-time of the individual (Supplementary Video 2).

Experimental replication of striations

First test

Information about the three recently extracted molars, point tool (wood, bone and microgravette Epigravettian point) used, action, direction, inclination and duration of treatment are reported in Supplementary Table S1.

Ind-1 (RM3): After 10 seconds the bone point broke and its length was reduced of ca. 1 mm (Supplementary Fig. S6).

Ind-2 (LM3): After 5 seconds the pressure exerted on the hafted backed point immediately caused the micro-fracture of the tool. After 15 seconds chippings on the enamel were observed; after ca. 1’00’’ minute the tool was still intact (Supplementary Fig. S7).

Ind-3 (LM3): After 5 seconds the point broke, and after 28 seconds the tool was considered inefficient (Supplementary Fig. S8).

Second test

Information about the six (carious) medieval human tooth classes, tool (microgravette Epigravettian points) used, action, direction, inclination and

duration of treatment are reported in Supplementary Table S2 (see also Supplementary Fig. S9).

Vald-1 (RM3): After 5 minutes, part of the enamel was removed reaching and exposing the primary dentine tissue. After almost 9 minutes, the tool was still intact.

Vald-2 (RM3): After 1.26 minutes the first signs of flint breakage appeared. At 2.10 minutes abrasive action of the flint tool produced several striations on the enamel. After 4.00 minutes the enamel was scraped.

Guid-1 (RM2): After 1.12 minutes of mesio-distal movements, fractures on the flint tool were observed. The changing of movements (i.e., helicoidal lever and twisting) was more efficient, producing several small enamel chippings.

Guid-2 (RM3): After a few seconds the flint point broke and was consequently reduced in length (ca. 3mm), probably due to the pressure produced through the hafted backed point.

Guid-3 (RM2): The pressure exerted on the hafted backed point immediately caused the fracture of the tool. Moreover, tiny fragments of flint fell into the carious cavity.

Guid-4 (LM2): The dominant movement recorded (inverse and direct clockwise force) produced several striations on the exposed dentine. After 2 minutes, chippings appeared on the edge of the tool.

Gas-Chromatography Mass-Spectrometry (GC-MS) results

Very small quantities of lipids were obtained for all samples tested. GC-MS characterization was dominated by non-diagnostic fatty acids, precluding a secure interpretation (Supplementary Table S3). Analysis of the organic material integrated within the carbonate concretion, as well as of the soil control sample revealed a very similar profile, suggestive of a similar origin. A negligible lipid profile with no evidence for diagnostic biomarkers was obtained for the residue adhering to the inner walls of the tooth cavity. The lipid profile

obtained for the organic residue deposited on the outer and inner surfaces of the ilium differed from the associated mass of material (Supplementary Fig. S10). It comprised a range of saturated and monounsaturated fatty acids, cholesterol possibly arising from endogenous skeletal lipids (3, and a suite of alkanes with 24 to 35 carbon atoms. The alkane profile showed no odd or even preference, and none of the alkanes identified dominated the series.

References

Aimar, A. *et al*. Les Abris Villabruna dans la Vallèe du Cismon. *Preistoria Alpina* **28**, 227- 254 (1992).

Vercellotti, G., Alciati, G., Richards, M. & Formicola, V. The Late Upper Paleolithic skeleton Villabruna 1 (Italy): A source of data on biology and behavior of a 14.000 year-old hunter. *J Anthropol Sci* **86**, 143-163 (2008).

Evershed, R.P., Turner-Walker, G., Hedges, R.E.M., Tuross, N. & Leyden, A. Preliminary results for the analysis of lipids in ancient bone. *J Archaeol Sci* **22**, 277-290 (1995).

SUPPLEMENTARY FIGURES

Supplementary Figure S1. The Late Upper Palaeolithic burial Villabruna. Above the left radius, the following items are visible, 12 o'clock clockwise: 1, backed knife; 2, siltstone pebble; 3, remnants of the nodule of unidentified material placed near the left iliac crest; 4, blade; 5, the refitted bone point. The red arrow in the left image points towards the area where residues adhering to the ilium were found (photo by A. Broglio).

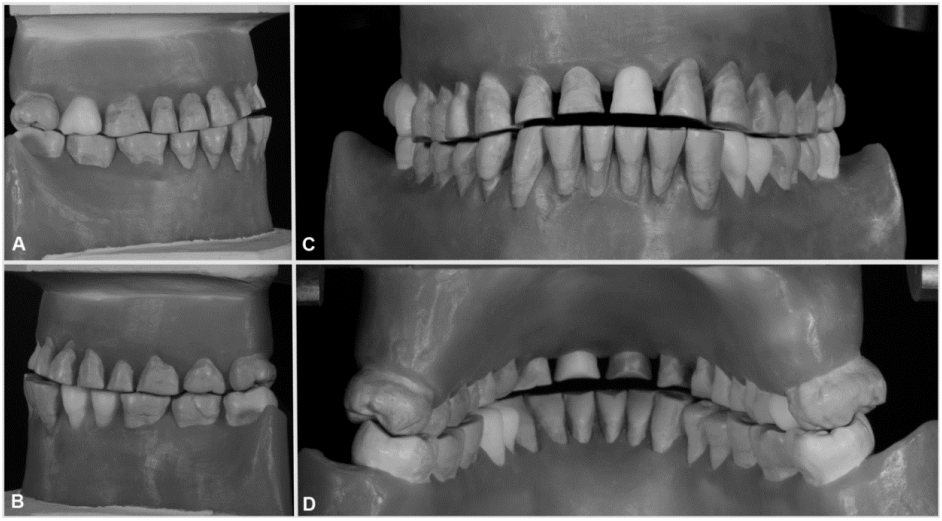

Supplementary Figure S2. Physical reconstruction of the Villabruna dental arches, derived from occlusal wear pattern analysis. (A) Right side. (B) Left side. (C) Frontal (buccal) view. (D) Posterior (lingual) view.

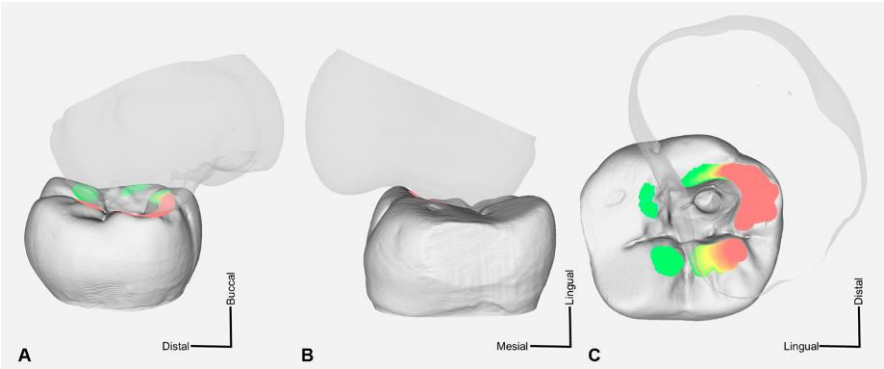

Supplementary Figure S3. OFA results. Snapshots from Occlusal Fingerprint Analyser software (OFA) showing sequential colour gradient of antagonistic occlusal collisions visualized on the M_3 crown from first to last contacts (green to red) during the powerstroke movements. (A) Distal view. (B) Mesial view. (C) Occlusal view. M^3 crown transparent.

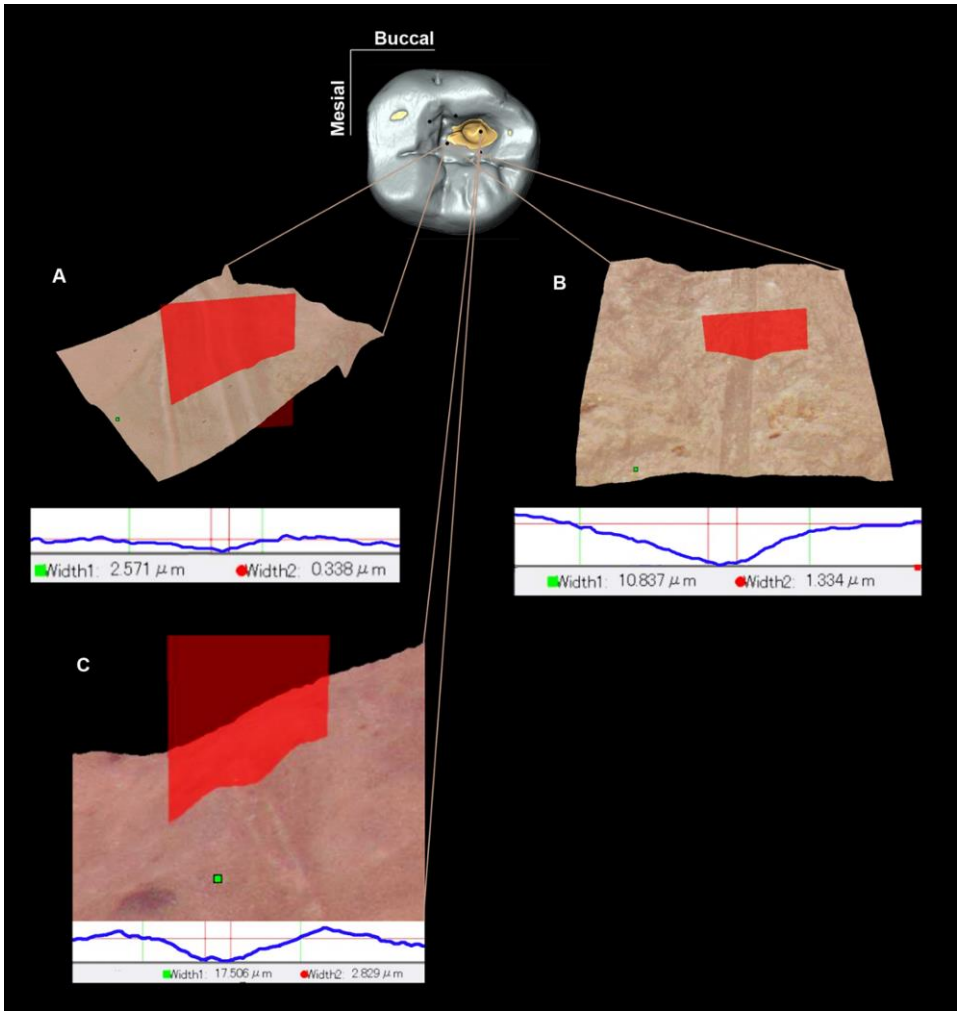

Supplementary Figure S4. 3D rendering and cross-sections of the striations observed in the RM_3 cavity of the Villabruna burial. (A, B) Area 2 in Fig. 3. (C) Area 5 in Fig. 3. The striations are shallow, narrow, and the cross sections are V-shaped. This characteristic is reflected in the high value for the ratio between breadth at the top, and breadth at the floor of the grooves. These data fit very well within the expected variability of marks produced using a flint tool, and resemble experimental flint tool striations represented in Fig. S5.

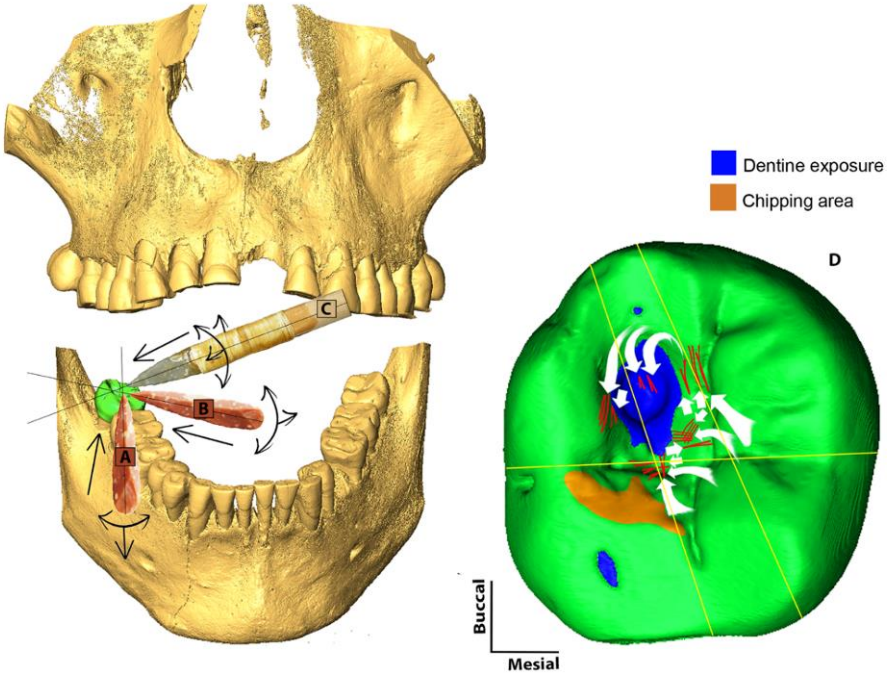

Supplementary Figure S5. Orientation and location of the striations observed in the RM_3 cavity of Villabruna. Direction of flint tool action. (A) Mesio-buccal > distal. (B) Mesial > distal. (C) Lingual > bucco-distal. (D) The RM_3 of Villabruna with highlighted the position and orientation (white arrows) of the striations (in red). The orientation of individual traces within the cavity indicates a great variety of gestures and movements linked to the running of the siliceous edges in different directions. It is possible to distinguish two main groups of direction lines (yellow) in the entrance-exit of the tool employed.

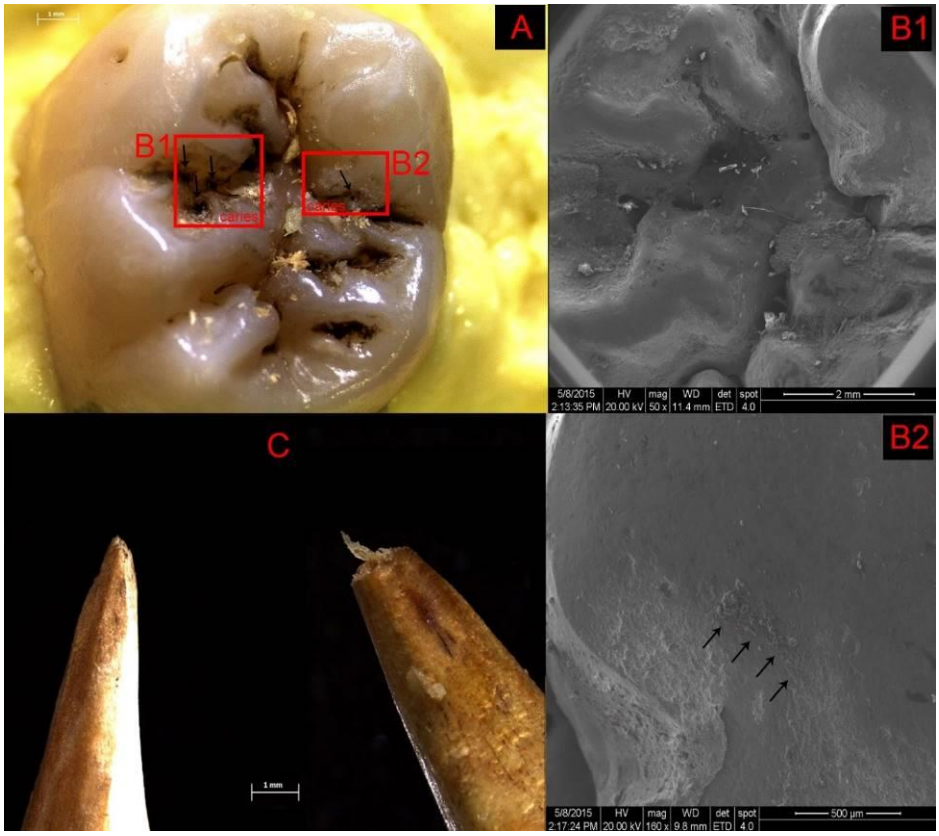

Supplementary Figure S6. Experimental test on the enamel of a recently extracted modern human molar using a wood point tool. (A) Occlusal view of a modern human LM_3 (Ind-3); the squares identified the areas were the wood point was tested. (B1 and B2) SEM images within the areas delimited by the squares shown in A; arrows in B2 point towards wood debris. (C) The wood point before (to the left) and after (to the right) the experimental test.

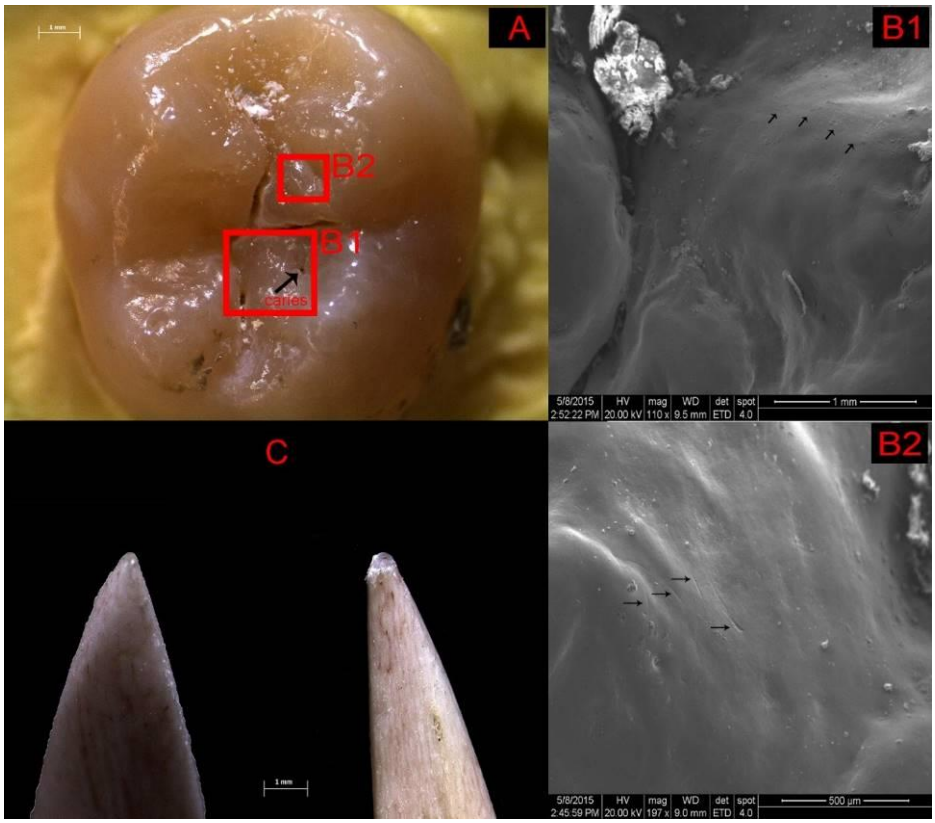

Supplementary Figure S7. Experimental test on the enamel of a recently extracted modern human molar using a bone point tool. (A) Occlusal view of a modern human LM_3 (Ind-1); the squares identified the areas were the bone point was tested. (B1 and B2) SEM images within the areas delimited by the squares shown in A; arrows point towards micro-scratches produced by the bone tool. (C) The bone point before (to the left) and after (to the right) the experimental test.

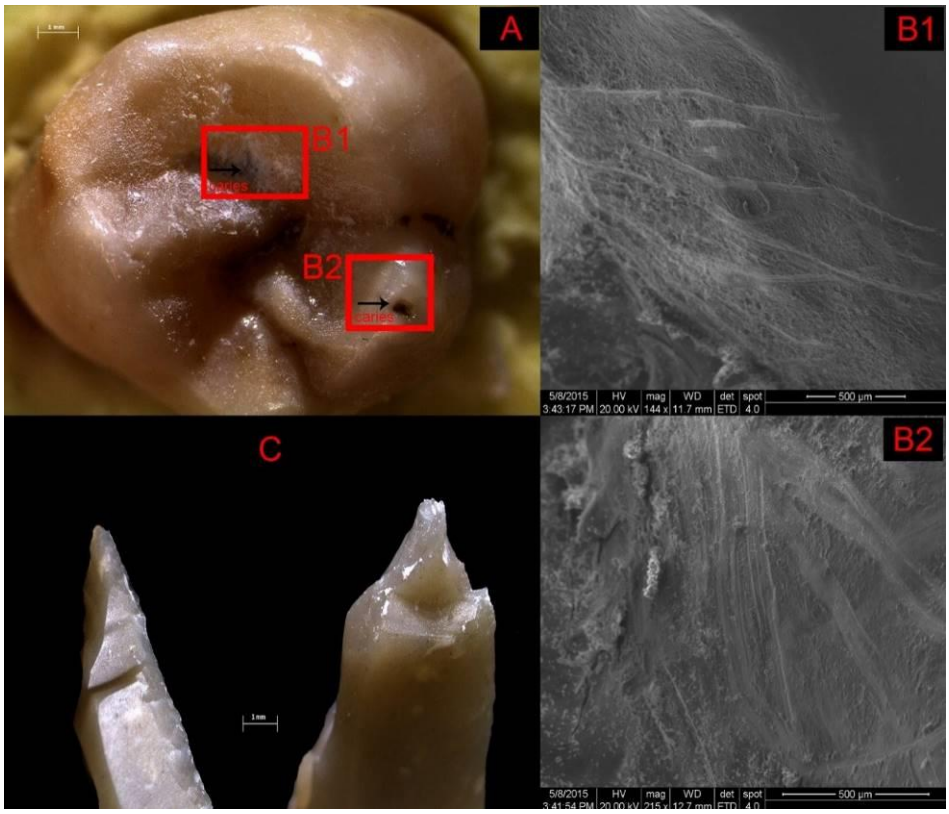

Supplementary Figure S8. Experimental test on the enamel of a recently extracted modern human molar using a microgravette Epigravettian point. (A) Occlusal view of a modern human LM_3 (Ind-2); the squares identified the areas were the microlithic point was tested. (B1 and B2) SEM images within the areas delimited by the squares shown in A; arrows point towards the extensive striations produced by the microlithic point. (C) The microlithic point before (to the left) and after (to the right) the experimental test.

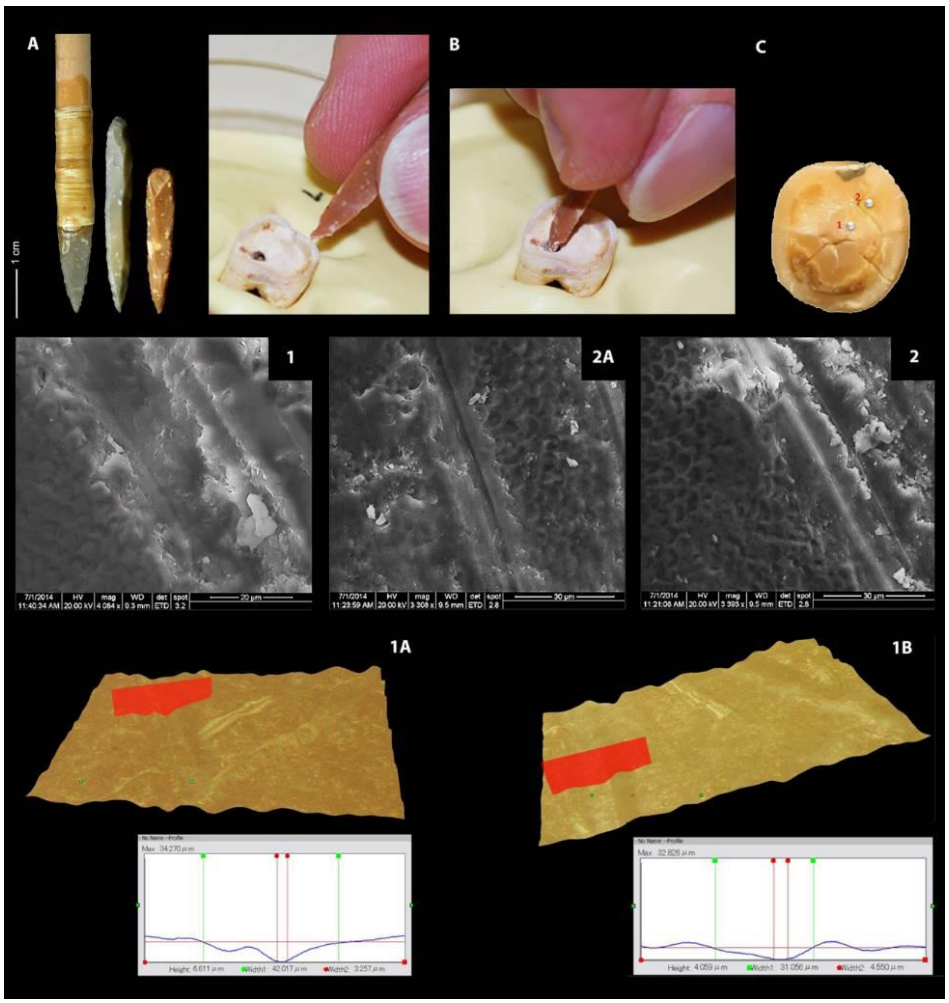

Supplementary Figure S9. Experimental test on modern human molars, SEM and 3D rendering cross-sections analyses. (A) Experimental late Epigravettian backed points made on flint comparable to those used by the Villabruna individual; to the left, hafted backed point used for the lingual > bucco-distal experimental scratching (it corresponds to Supplementary Fig. S4C). (B) Late Epigravettian backed point directly gripped and used on a modern human molar (collected from a bioarchaeological sample at the Department of Cultural Heritage, University of Bologna) which had been set in rubber for this purpose. (C) Occlusal view of a modern human tooth with the location of the main flint tool scratching produced on the exposed dentine (area 1 and 2). For this tooth, 1, 2a, 2 (middle of the figure) show detailed SEM images of the striations related to area 1 and 2, respectively. On the bottom, 1a and 1b represent 3D rendering and cross-sections of the striation observed in area 1: groove 1a is V-

shaped and shows a visible shoulder striation; groove 1b is _/-shaped; its asymmetry can be related to the inclination of the tool.

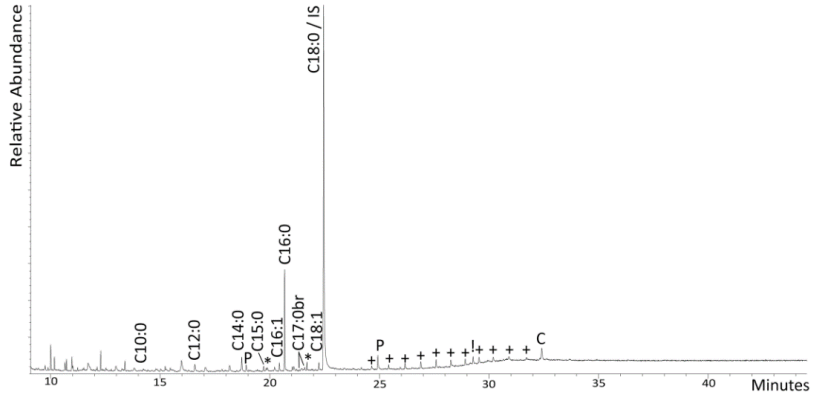

Supplementary Figure S10. Gas Chromatography-Mass Spectrometry results. Total Ion Chromatogram showing the composition of the solvent extracted organic residue adhering to the inner surface of the ilium, run as trimethylsilylated esters. [Cx:y: Fatty acid where x is the carbon number and y is the degree of unsaturation; +: Alkanes (C25-C35); *: Alcohols; !: Cholesterol; P: Phthalate contamination; C: contaminant; IS: Internal standard]

SUPPLEMENTARY TABLES

Supplementary Table S1. Description of the experimental tests on three recently extracted lower third molars (M_3) using point tools made on different material.

Specimen ID	Tools	Action	Direction	Inclination	Time
Ind-1 (RM_3)	bone point	Twisting, clockwise rotation and helicoidal lever	Mesial>distal	50°	45’
Ind-2 (LM_3)	backed point	Helicoidal lever, twisting, clockwise rotation	Mesial>distal	60°	1’30’
Ind-3 (LM_3)	wood point	Helicoidal lever and twisting	Mesial>distal	55°	28’

Supplementary Table S2. Description of the experimental tests on six medieval molars.

Specimen ID	Tools	Action	Direction	Inclination	Time
Vald-1 (RM_3)	Backed point	Clockwise rotation, helicoidal lever and twisting	Mesial>distal	60°	9’25"
Vald-2 (RM_3)	Backed point	Clockwise/Counterclockwise bidirectional rotation	Mesial>distal	60°	8’21’’
Guid-1 (RM_2)	Backed point	Helicoidal lever and twisting	Mesial>distal	60°	3’29’’
Guid-2 (RM_3)	Hafted backed point	Counterclockwise rotation	Lingual>bucco-distal drilling	60°	1’25’’
Guid-3 (RM^2)	Hafted backed point	Counterclockwise rotation	Mesial>buccal	60°	0.47’
Guid-4 (LM_2)	Backed point	Inverse and direct (clockwise)	Mesial>buccal	60°	2’27"

Supplementary Table S3. Gas-Chromatography Mass-Spectrometry (GC-MS) results. Table listing the location from where each of the samples were taken and the quantity tested, the corresponding total lipid extract (TLE, Tr. denotes trace amounts), and the lipids identified after GC-MS analysis of the solvent extracted residue. Saponification yielded saponification yielded insignificant quantities of lipid residues results.

Code	Sample	Weight (mg)	TLE (μg)	Lipids identified by GC-MS
VIL01	Ilium (inner)	1.4	< 10	**Fatty acids:** $C_{10:0}$, $C_{12:0}$, $C_{14:0}$, $C_{15:0}$, $C_{16:1}$, $C_{16:0}$, $C_{17:0br}$, $C_{18:1}$, $C_{18:0;}$ **Alcohols:** C_{16}, $C_{18;}$ **Alkanes:** C_{25}, C_{26}, C_{27}, C_{28}, C_{29}, C_{30}, C_{31}, C_{32}, C_{33}, C_{34}, C_{35}; **Sterols:** Cholesterol; **Phthalate Plasticiser**
VIL02	Ilium (outer)	3.0	Tr.	**Fatty acids:** $C_{12:0}$, $C_{14:0}$, $C_{15:0}$, $C_{16:1}$, $C_{16:0;}$ **Alcohols:** C_{16}, $C_{18;}$ **Alkanes:** C_{24}, C_{25},C_{26}, C_{27}, C_{28}, C_{29}, C_{30}, C_{31}, C_{32}, C_{33}, C_{34}, $C_{35;}$ **Disaccharide; Phthalate Plasticiser**
VIL03	Soil control	159.4	Tr.	**Fatty acids:** $C_{16:0}$, $C_{18:0;}$ **Alcohols:** $C_{18;}$ **Phthalate Plasticiser**
VIL04	Organic material in concretion	27.2	Tr.	**Fatty acids:** $C_{16:0}$, $C_{18:0;}$ **Alcohols:** $C_{18;}$ **Phthalate Plasticiser**
VIL05	Tooth cavity	n/a	Tr.	**Fatty acids:** $C_{14:0}$, $C_{15:0}$, $C_{16:0}$, $C_{18:0;}$ **Alcohols:** C_{18}

Cx:y: Fatty acid where x is the carbon number and y is the degree of unsaturation; Cx: Alcohols where x denotes the carbon number; Br: branched.

Supplementary Table S4. Results of calculus samples and phytolith identification.

Sample	Results
Cavity rinse	**10 starches, all polyhedral with centric fissured hila. Several fibres and chunky material, no phytoliths**
Stuffing from mandible box	**49 starches, all polyhedral with centric fissured hila. Several are damaged (cracked, broken, etc.)**
Bubble wrap from mandible box	**7 starches, polyhedral with centric fissured hila, many fibres, one pollen grain probably from pine**
Fragments from skull box	**Many fibres, particles, and chunks, no starch, no phytoliths**
Stuffing from skull box	**12 starches, polyhedral with centric fissured hila, many fibres, some with starches attached**
Day 1 control slide	**Very clean slide, a few fibres**
Day 2 control slide	**Clean slide, a few fibres, one plant particle with bordered pits**
Day 3 control slide	**Very clean slide, a few fibres**

SUPPLEMENTARY VIDEO LEGENDS

Supplementary Video 1. Results obtained using the Occlusal Fingerprint Analyser (OFA) software for the right M3 pair. Virtual results showing detected sequential antagonistic occlusal contacts covering the wear facet pattern on the right M3s. The dominant horizontal occlusal direction is protrusive. Green highlights previous and red current contacts.

Supplementary Video 2. Results obtained using the Occlusal Fingerprint Analyser (OFA) software for the complete Villabruna dentition. Virtual models of the reconstructed Villabruna specimen dental arches after simulating a bite situation on the right side. Sequential occlusal contacts are visible on the lower arch model. Green highlights previous and red current contacts.

American Journal of Physical Anthropology
(*Am J Phys Anthropol. 2017a; 00:1–16. https://doi.org/10.1002/ajpa.23216.)*

The dawn of dentistry in the Late Upper Paleolithic: An early case of pathological intervention at Riparo Fredian.

Gregorio Oxilia[1,2], Flavia Fiorillo[3], Francesco Boschin[4,5], Elisabetta Boaretto[6], Salvatore A. Apicella[3], Chiara Matteucci[3], Daniele Panetta[7], Rossella Pistocchi[8], Franca Guerrini[8], Cristiana Margherita[2], Massimo Andretta[9], Rita Sorrentino[2,10], Giovanni Boschian[11], Simona Arrighi[4,5], Irene Dori[1], Giuseppe Mancuso[2], Jacopo Crezzini[4,5], Alessandro Riga[1], Maria C. Serrangeli[2], Antonino Vazzana[2], Piero A. Salvadori[7], Mariangela Vandini[3], Carlo Tozzi[12], Adriana Moroni[4,5], Robin N. M. Feeney[13], John C. Willman[14], Jacopo Moggi-Cecchi[1]§ and Stefano Benazzi[2,15]§.

[1]Department of Biology, University of Florence, Via del Proconsolo, 12, 50122 Firenze, Italy

[2]Laboratory of Anthropology, Department of Cultural Heritage, University of Bologna, Via degli Ariani 1, 48121 Ravenna, Italy

[3]Conservation Science Laboratory for Cultural Heritage, Department of Cultural Heritage, University of Bologna, Via degli Ariani 1, 48121 Ravenna, Italy

[4]Study Centre for the Quaternary Period (CeSQ), Via Nuova dell'Ammazzatoio 7, I - 52037 Sansepolcro (Arezzo), Italy

[5]*Department of Physical Sciences*, Earth and Environment, University of Siena, Research Unit in Prehistory and Anthropology, Via Laterina 8, 53100 Siena, Italy

[6]Max Planck-Weizmann Center for Integrative Archaeology and Anthropology, D-REAMS Radiocarbon Laboratory, Weizmann Institute of Science, 7610001 Rehovot, Israel

[7]Institute of Clinical Physiology, IFC-CNR, Via G. Moruzzi 1, 56124 Pisa, Italy

[8]Department of Biological, Geological and Environmental Sciences, University of Bologna. Via Sant'Alberto 163, 48123 Ravenna, Italy

[9] School of Science, University of Bologna, Via dell'Agricoltura 5, 48123 Ravenna, Italy

[10] Department of Biological, Geological and Environmental Sciences – BiGeA University of Bologna Via Selmi 3, 40126, Bologna, Italy

[11] Department of Biology, University of Pisa, via Derna 1, 56125 Pisa, Italy

[12]Department of Civilisations and Forms of Knowledge, University of Pisa, Via Pasquale Paoli, 15, 56126 Pisa, Italy

[13]UCD School of Medicine, Health Science Centre, University College Dublin, Belfield, Dublin 4, Ireland

[14]Department of Anthropology, Campus Box 1114, Washington University, Saint Louis, MO 63130 USA

[15]Department of Human Evolution, Max Planck Institute for Evolutionary Anthropology, Deutscher Platz 6, 04103 Leipzig, Germany

START MANUSCRIPT

To date, the earliest examples of definitive prehistoric dentistry come from Neolithic contexts. A Neolithic graveyard (MR3) at Mehrgarh in Pakistan contained 11 drilled teeth, belonging to nine individuals, of which at least four of the teeth had associated decay (Coppa et al., 2006). It is not possible determinate whether the lack of decay in the remaining seven teeth was due to successful removal of infected dental tissue. An individual from a Danish Neolithic passage grave at Hulbjerg exhibits drilling near the bifurcation of the right M2 roots (Bennike and Alexandersen, 2003; Bennike and Fredebo, 1986). The individual also exhibits periodontal disease and caries suggesting that drilling was related to pathological intervention (Bennike and Alexandersen, 2003). A final example of an early dental intervention concerns a 'beeswax' filling from Neolithic Slovenia, which was probably used to seal an antemortem/perimortem crown fracture for palliative purposes (Bernardini et al., 2012). While many more chronologically-recent cases of pathology-induced dental interventions are well-documented among both food-producers and hunter-gatherers from Old and New World contexts (Bennike and Alexandersen, 2003; Ortiz et al., 2016, Schwartz et al., 1995; Seidel et al., 2005; Turner, 2004, White et al., 1997), there is little evidence for similar pathological interventions preceding the Neolithic.

An exception is a Late Upper Paleolithic specimen from Villabruna (Sovramonte – Belluno, Italy, directly dated to 14,160-13,820 calendar years ago [cal BP]) (Vercellotti et al., 2008). The Villabruna 1 individual exhibits caries on the right M3 that was clearly manipulated with a lithic or osseous tool in vivo in an effort to partially clean decay through scraping and levering actions (Oxilia et al., 2015). However, the location of the caries in the distal-most portion of the mouth would have made it very difficult to fully clean and may explain why this manipulation was less extensive than many of the more

obvious drilling interventions in later prehistoric and historic examples (e.g. Bennike and Alexandersen, 2003; Coppa et al., 2006; Ortiz et al., 2016; Schwartz et al., 1995; Seidel et al., 2005; Turner, 2004; White et al., 1997).

Other evidence for the palliative treatment of inflamed gingiva among Pleistocene hunter-gatherers derives from interproximal grooves caused by dental probing or "toothpicking" (Lozano et al., 2013; Ungar et al., 2001). However, these features are also documented throughout the Holocene and are not always clearly associated with pathology (Brown and Molnar, 1990; Lukacs and Pastor, 1988; Molnar, 2008; Molnar, 1971). By contrast, Late Upper Paleolithic tooth extractions (i.e., avulsion or ablation) that were likely related to cultural modification of the dentition as an expression of social identities (Bocquentin, 2011; De Groote and Humphrey, 2016; Humphrey and Bocaege, 2008; Stojanowski et al., 2014; Willman et al., 2016). While not related to the treatment of pathology, ablation does offer evidence of invasive dental modifications in Late Upper Paleolithic contexts. Thus, toothpicking, caries manipulation, and ablation among Late Pleistocene hunter-gatherers experiencing high rates of dentognathic pathology (e.g., Capasso, 2011; Frayer, 1989; Humphrey et al., 2014; Lacy, 2014, 2015; Willman et al., 2016), suggest that the prerequisite stimuli (i.e., pathological affliction) and cultural practices for developing early dentistry practices may have much greater antiquity than currently documented.

Here we analyze two upper central incisors from a modern human recovered from the Late Upper Paleolithic site of Riparo Fredian (Molazzana, Lucca, Italy) (Boschian et al., 1995). Both I1s exhibit antemortem modification to their pulp chambers in the form of striations and the presence of a composite material (bitumen and organic fibers) on the walls of the pulp cavities and in the pulp canal (Fig. 1). We provide a differential diagnosis for these features, and suggest that the modifications are intentional anthropogenic by-products of a pathology-induced therapeutic dental intervention.

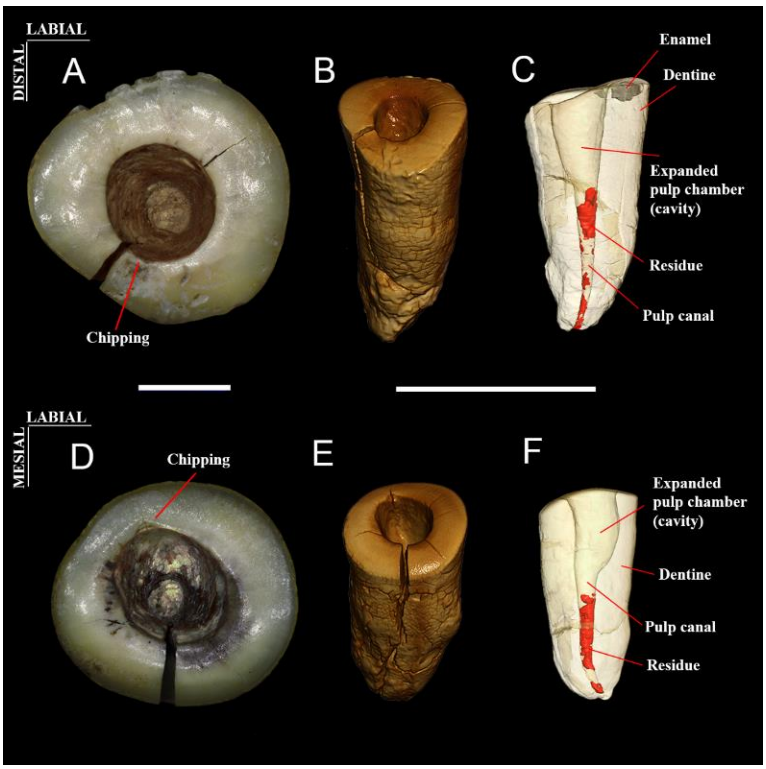

Figure 1. The upper right and left first incisors (RI1, LI1) of Riparo Fredian. (a) The RI1 in occlusal view. (b) Volume rendering of RI1 viewed from the lingual side. (c) Digital reconstruction of the RI1 with transparent dentine to show the residue; mesio-lingual view. (d) The LI1 in occlusal view; note the black patina within the cavity. (e) Volume rendering of LI1 viewed from the lingual side. (f) Digital reconstruction of LI1 with dentine in transparent to show the residue; distal view. Scale bar: a and d) 2 mm; b, c and e, f) 1 cm.

Archaeological context

The Riparo Fredian is a mountainous area in northern Tuscany situated between the Alpi Apuane ridge to the west and the Apennines to the east. The site is located within the valley of the Turrite Secca River (in the territory of Molazzana, near Lucca), a tributary of the Serchio River (Fig. 2).

Thorough archaeological surveys carried out within the area brought to light several prehistoric settlements ascribed to the Late Upper Paleolithic (Late Epigravettian) and Mesolithic (Sauveterrian and Castelnovian) (Biagi et al., 1981; Guidi, 1989; Tozzi, 1995). The results reveal that the area was completely abandoned during the Late Alpine Glacial, when the glacial fronts expanded downward to an elevation of about 700-800 m. The first groups re-entered the area during the Late Glacial Interstadial, and occupied sites at the bottom or on the lower sides of the valleys, whereas sites at higher elevation were not colonized until the Early Holocene. Riparo Fredian was found during these surveys, and systematic excavations were carried out from 1987 to 1990. It is situated on a river terrace about 2-3 m above the bottom of the valley, at about 360 m above sea level, and includes a habitation area of a few square meters.

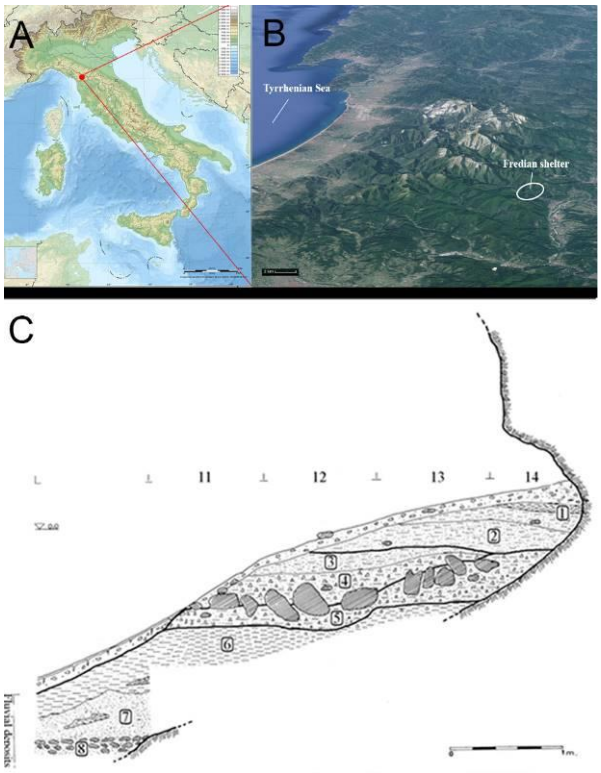

Figure 2. Location of Riparo Fredian (44° 04′ 21” N, 10° 25′ 07” E). (a) Topographic map of Italy, in red: Riparo Fredian. (b) Satellite view of western coast. (c) Section of stratigraphic sequence.

The stratigraphic sequence (Fig. 2) is rather thin (1.60 m). The bottom of the sequence includes sandy river deposits (layers 8, 7 and 6), overlain by an archaeological sequence that includes Late Epigravettian (layer 5) and Mesolithic (layers 4 and 3) lithic industries. The sequence is terminated by thin lenses (layers 2 and 1) containing a few minute fragments of coarse pottery (Boschian et al., 1995). A cobble pavement of limited size was found at the top of layer 5 in the innermost area of the rock shelter (Fig. 3). This pavement included several large river cobbles that were irregularly distributed on a surface of about 2 m2 and slightly protruded upwards into layer 4. Layer 4 also overlies layer 5 in the other areas of the shelter, where the two layers are in direct contact, and lack the cobble pavement. Most of the teeth found in the outer part of the cobble pavement were included in layer 4, whereas those found in the inside of the pavement were included mostly in layer 5. The following processes explaining the stratigraphic position of the human remains can be reconstructed by observing the architecture of the stratigraphic unit and the characteristics of the sediments. An erosion process, subsequent to the formation of layer 5 but preceding the deposition of layer 4, eroded layer 5 on the outer side of the shelter and excavated a shallow trough. The cobbles of the outer part of the pavement slid into the trough and rotated towards the outside of the shelter and were found leaning slightly outwards. Sediments of layer 5, reworked by the erosion, accumulated into the trough together with the cobbles and formed the foundation for the outer part of layer 4. This process operated less intensely inside the rockshelter and reworked only the topmost part of layer 5, leaving the cobbles in situ and originating the inner part of layer 4, which is much thinner than the outer one. Consequently, layer 4 is thicker in the outer

area of the shelter, whereas layer 5 is thicker in the inside area. As a result, layer 4 is largely composed of reworked parts of layer 5. Thus, it appears that the teeth were all originally embedded in layer 5, but those within the outer part of the cobble pavement were incorporated within layer 4 after reworking; conversely, those found in the inner part, where reworking was limited, remained in situ and hence were mostly associated with layer 5. Layer 5 was 14C AMS dated on charcoal to 10,870±119 BP (AA10952, 13040 - 12600 cal BP for ±2σ calibrated range), and layer 4 to 9,458±91 BP (AA10951, 11106 - 10500 cal BP for ±2σ calibrated range).

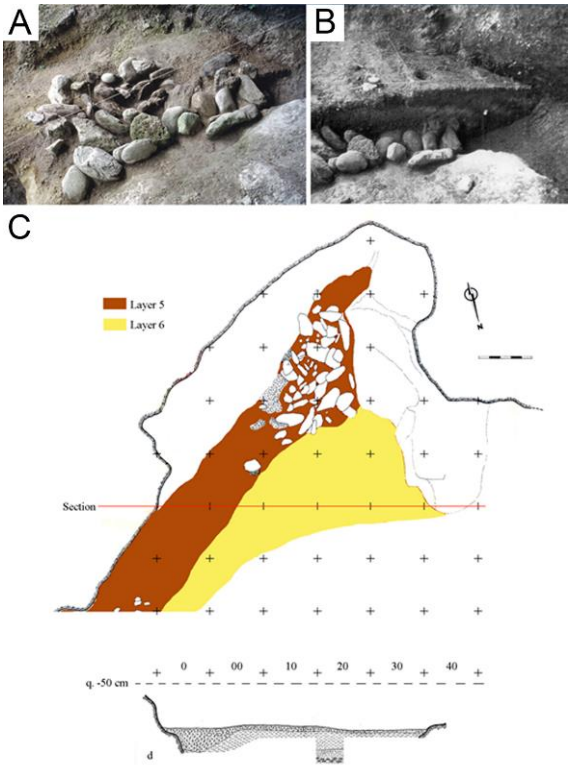

Figure 3. The cobble pavement of Riparo Fredian. (a) Cobblestone of layer 5. (b) Section of the upper stratigraphic sequence. (c, d) Map and section of the rock-shelter.

The human remains from Riparo Fredian mostly consist of isolated teeth and these teeth have been attributed to six individuals (three subadults, three adults) based on dental anatomical features and levels of macroscopic wear (Boschian et al., 1995; Vierin, 2012). All of the teeth attributed to individual Fredian 5 (Fig. 4) were recovered from layer 5 next to an cobblestone artificially placed at its top (Boschian et al., 1995), which is attributed to the Final Epigravettian and dated by 14C on charcoal between 13,040-12,600 cal BP (Boschian et al., 1995; D'Errico et al., 2011).

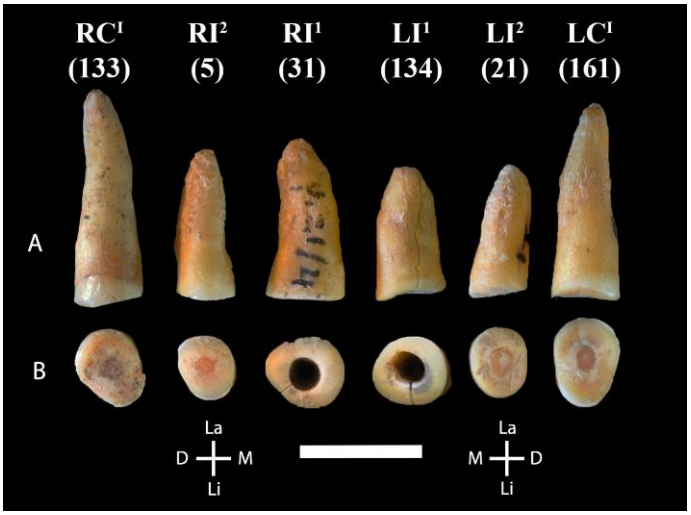

Figure 4. Teeth attributed to Fredian 5. (a) Labial view. (b) Occlusal view. From left to right: upper right canine, upper right second incisor, upper right first incisor, upper left first incisor, upper left second incisor, upper left canine. Scale bar: 1cm.

Materials and Methods

The dental remains of Fredian 5.

Teeth 133 and 161 are right and left maxillary canines (C1s), respectively. The occlusal cross-sections are asymmetrically oval, broad anteriorly, tapered distally, and the roots are long. Both C1s have wear scores of 7 (Smith, 1984), but wear is slightly more advanced on the left C1. Teeth 31 and 134, the subjects of the present study, are right and left maxillary central incisors (I1s), respectively. Siding is based primarily on the distolateral projection of the root apices. The right I1 preserves a hairline rim of enamel on its anterior face (stage 7: Smith, 1984). The left I1 is more circular in cross-section due to its greater degree of occlusal wear (stage 8: Smith, 1984). Both I1 roots are mediolaterally and anteroposteriorly broad, a characteristic of maxillary central incisors that distinguishes them from the heavily worn C1s and the maxillary second incisors (I2s). Teeth 5 and 21 have been identified as right and left I2s, respectively. The occlusal cross-sections are relatively round (compared to the canines and central incisors) and small in size. Siding is based primarily on wear associations between adjacent teeth. Each left tooth (134, 21, and 161) has a total length (root apex to occlusal surface) that is several millimetres less than that of their right-side antimeres.

Further evidence for tooth siding is provided through wear pattern associations. For instance, there is continuity in the wear planes and edge-rounding by side, which suggest that the behaviors resulting in wear differed between right and left sides of the mouth. The differential wear suggests that the left-side anterior teeth were used more extensively for masticatory and paramasticatory behaviors since compensatory hypereruption would have kept the teeth in the same occlusal plane as the right-side anterior teeth despite progressive occlusal wear. However, the cause of differential wear is not immediately apparent. One possibility is that the anterior dental wear asymmetries may relate to the handedness of Fredian 5 during masticatory and

non-masticatory behaviors. Another possibility is related to the timing of pulp exposure, infection, and subsequent antemortem modification of the pulp chambers. These explanations need not be mutually exclusive but are difficult to disentangle.

The subsequent analyses will focus on the pathological nature of the teeth as well as purported antemortem modifications indicative of probable dentistry.

MicroCT and digital reconstruction

High-resolution MicroCT images of the two upper central incisors were obtained with a Xalt MicroCT scanner (Panetta et al., 2012). All teeth were scanned at 50 kVp, 2 mm Al filtration, 960 projections over 360°, 0.9 mAs/projection for a total scan time of 50 minutes per sample. All the tomographic images were reconstructed using a modified Feldkamp algorithm (Feldkamp et al., 1984) with embedded compensation for mechanical misalignments and raw data pre-correction for beam-hardening and reduction of ring artifacts in the digital images. All images were reconstructed on a volume dataset of 600x600x1000 cubic voxels, each with a size of 18.4 μm. The image stacks were segmented using a semiautomatic threshold-based approach in Avizo 7 (Visualization Sciences Group Inc.) to distinguish between the dental tissues and the residue filling the pulp chamber as well as to reconstruct 3D digital models of the teeth.

Scanning electron microscope (SEM) and energy dispersion X-ray spectroscopy (EDS)

Back-scattered electron images and EDS spectra were collected on a low-vacuum ESEM FEI Quanta 200, equipped with an Oxford energy dispersive spectrometer. The analyses were conducted using an acceleration

voltage up to 30 kV and EDS analyses performed at a working distance of 10 mm for 100 seconds. No sample preparation was required.

3D digital microscope

Multifocal images of anthropic cavities (up to 160X) were obtained using a Hirox KH-7700 Digital Microscope equipped with MX(G)-5040Z lens and an AD-5040LOWS adapter. Multifocal images of vegetal fibers as well as 3D images of microstriations (up to 7000X) were captured using a MX(G)-10C lens equipped with a OL-140II and OL-700II adapters and an AD-10S Directional Lighting Adapter. Multifocal and 3D images were created by overlapping a series of 120 photographs taken at different focus levels (Crezzini et al., 2014; Moretti et al., 2015). This procedure enables the observation of analyzed surfaces from different points of view, creation of cross-sections of the microstriations, and allows collection of linear, angular, and areal measurements (Boschin and Crezzini, 2012; Crezzini et al., 2014).

Fourier-Transformed Infrared Spectroscopy (FTIR)

FTIR spectroscopy was chosen because its sensitivity allows information to be gained from the small amount of material extracted from the teeth, which is otherwise insufficient for chromatographic analyses. Moreover, the advantages of FTIR (i.e., speed, economical and permits sample size) are added to the Attenuated Total Reflection (ATR) mode, which does not require sample preparation because the powdered sample is placed directly on the ATR prism. In this way, the impact preparation in KBr pellet and chemical alterations that may occur with chromatography are avoided (Hollund et al., 2013).

Once the incrustation of secondary dentine and matrix adhering at the bottom of the cavity was removed, FTIR-ATR was performed on the black film found inside the pulp cavities of both teeth. The samples were obtained with a scalpel scraping the inner surface subsequent to analysis of surface striae.

Samples were also collected from the soil in which the teeth were embedded to control for possible contamination from exogenous materials.

FTIR analyses were performed in ATR mode with a Tensor 27 FTIR Spectrometer equipped with a diamond crystal. Spectra were recorded in the range of 4000-400 cm-1 at a spectral resolution of 4 cm-1 and 128 scans. Data acquisition was carried out using OPUS 7.2 software, the spectra were baseline corrected, the CO2 was removed and a smooth performed.

Raman microscopy

A small amount of material containing the black patina encrusted on the internal surface of the teeth was investigated by Raman microscopy. The Raman spectra were collected with a Bruker Senterra Microscope interfaced with an Olympus microscope (20x-50x objective lens) fitted with a 785nm laser. The analyses were carried out with a 10mW laser power in the 50-2600 cm-1 spectral region and a resolution of 3 cm-1.

Identification of the fibers

The samples were stained with the fluorochrome Calcofluor White M2R (Fluorescent Brightener 28, Sigma) that readily binds to cellulose and chitin. A working stock solution of 10 mg ml-1 of Calcofluor white M2R was made in distilled water and then filtered through a 0.22 µm filter. The samples, mounted between slides and glass coverslips in distilled water, were treated with one drop of the Calcofluor solution. After removing the excess water, the presence of lignin was analyzed through acid Phloroglucinol staining (Phloroglucinol Sigma). The samples mounted between slides were treated with the stain (1% in ethanol) and then acidified with a drop of concentrated hydrochloric acid. The stained samples were observed under an inverted epifluorescence microscope Zeiss Axiovert 100, equipped with an UV filter (BP 365, FT 395, LP 397). The microscope was equipped with a Nikon color video

camera Digital Sight DS-Fi2 with a DS-U3 control unit for image capture and Nis Elements-3 software was used for image analysis.

Radiocarbon dating

Fourier-Transform Infrared Spectroscopy

Both dentine and enamel from the Fredian 5 canine were analyzed with FTIR analysis to determine the state of preservation. A few dozen micrograms of dentine and enamel were separately powdered and homogenized in an agate mortar and pestle, mixed with a few milligrams of anhydrous KBr (Aldrich), and formed into a pellet. Infrared spectra were obtained at 4 cm-1 resolution Nicolet 380 FT-IR in transmission mode. The infrared splitting factors were calculated from the spectra following the method of Weiner and Bar-Yosef (Weiner and Bar-Yosef, 1990). The splitting factor for the enamel and dentine were 4.0 and 3.1, respectively. These values are in the range of well-preserved enamel and dentine (Asscher et al., 2011a,b). The FTIR spectrum of dentine mineral also showed absorption peaks at 1,651 cm-1 (amide I) and 1,556 cm-1 (amide II), indicating the presence of collagen clearly.

Dentine Collagen Extraction, Purification and Characterization

Some 193 mg of dentine was dissolved in 1N HCl to remove the mineral phase, centrifuged and rinsed three times in deionized water by centrifugation (6000 rpm for 2 min), and resuspension of the pellet. The pre-treatment procedure (Boaretto et al., 2009) for radiocarbon dating uses the acid-alkali- acid (AAA) technique and filtration, after gelatinization, with Eezi filter and ultrafiltration (Yizhaq et al., 2005). Prior to the AMS (Accelerator Mass Spectrometry) target preparation the extracted collagen was analyzed with FTIR (Asscher et al., 2011a) The spectrum showed the three aminoacid peaks of amide I, II and hydroxyproline at 1650, 1550 and 1450 cm-1, respectively. No other minerals were detected.

Target Preparation and AMS Analysis

The extracted collagen sample RTD-8546 was combusted to CO2 in vacuum sealed quartz tubes containing approximately 200 mg of copper oxide (Merck) and heated to 900°C for 200 minutes. The CO2 was divided into 3 aliquots and then each was reduced to graphite using cobalt (Fluka) (approximately 1mg) as a catalyst and hydrogen, and heated to 700°C for 20 hours. The graphite produced was analyzed for 14C content at the D-REAMS Radiocarbon Laboratory at the Weizmann Institute. Calibrated ranges in calendar years have been obtained from calibration tables (Reimer et al. 2013) by means of OxCal v4.2.4 (Bronk Ramsey and Lee, 2013).

Results

Both upper central incisors are heavily worn with occlusal exposure of each pulp chamber (RI1: mesio-distal =2.82 mm; labio-lingual=3.08 mm; LI1: mesio-distal=2.77 mm; labio-lingual=2.84 mm). The pulp chambers show a rounded perforation (hereafter called "cavity") that appear to be circumferentially (albeit unevenly) enlarged (Fig. 1a, d) and extend into the root for 4.82 mm (RI1) and 4.25 mm (LI1), with a sudden transition with the preserved portion of the pulp canal, which is partially filled with organic residue (Fig. 1c, f). Scanning Electron Microscopy (SEM) analysis showed microwear in the form of small scratches on the polished incisal surface and occlusal margins of the cavities (Fig. 5).

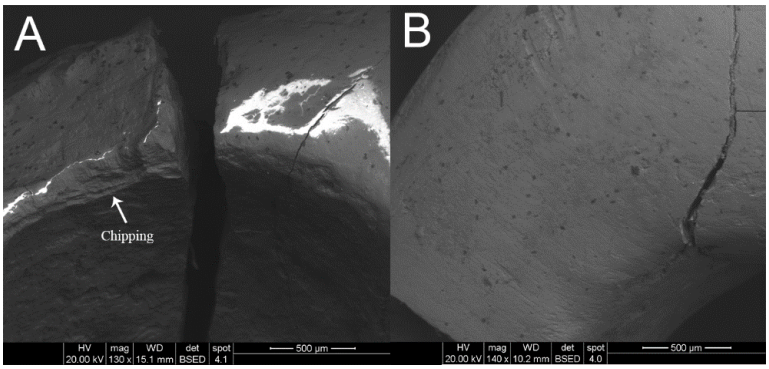

Figure 5. Margin of the cavities related to microwear. (a) Upper right first incisor (ID=31). (b) Upper left first incisor (ID=134).

Additional SEM analysis revealed striations in the internal cavity surface (Fig. 6), which differ from the typical dental microwear pattern, along with two dentine chips on the lingual (RI1) and labial (LI1) margins, respectively (Fig. 1a, d). The margins of the chipped dentine exhibit smooth and rounded edges, similar to antemortem enamel chipping (Bonfiglioli et al., 2004; Scott and Winn, 2011), which indicates some degree of in vivo occlusal wear and tool-use following exposure of the pulp cavity and the chipping of the dentine. Together, the scratches and rounding of the dental chips on the margins of the cavities suggest that Fredian 5 survived initial pulp exposure and continued to use their anterior teeth for daily activities prior to death.

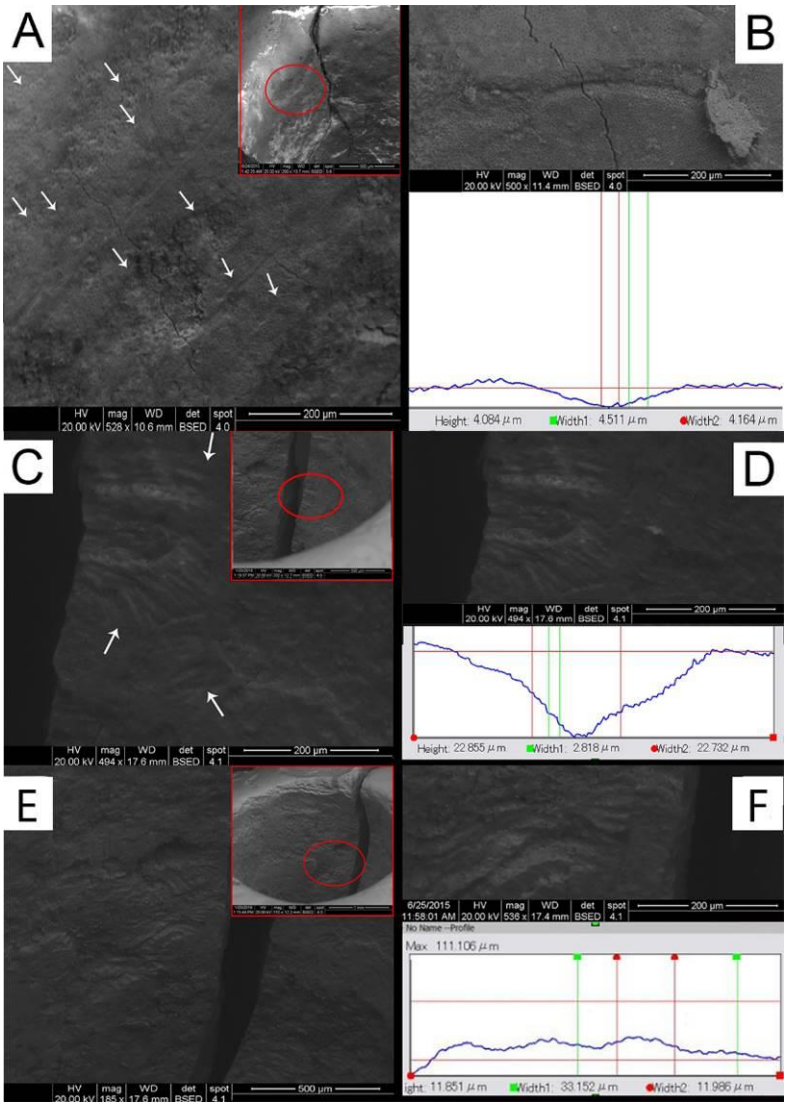

Figure 6. Representative striations observed in the cavity of upper left first incisor (ID=134). (a) SEM image. (b) Cross-section obtained using a Hirox KH-7700 Digital Microscope and the upper right first incisor (ID=31). (c-f) SEM images. (d-f) Cross-sections obtained by Hirox KH-7700.

The striations on the internal surfaces of the pulp cavities are distinguished from the scratches on the occlusal surface by a difference in orientation and by a distinct morphological appearance. The shape and cross-section of the

striations are diagnostic of the instrument used to produce them and the activities involved. Some are “V” shaped in transverse section and have a combination of attributes similar to the recognition criteria of slicing cut marks (Fig. 6d) (morphological categories 2, 4 and 5 [Boschin and Crezzini, 2012]) produced by stone tools, while others are shallower with more rounded cross-sections (Fig. 6b, f). The latter resemble those produced during experimental tests in dentine with a bone tool (Oxilia et al., 2015).

The residue filling the pulp canals was removed and analyzed by SEM and stereomicroscopy. SEM analysis shows the presence of dentinal tubules, suggesting the residue has extensive dentine adhering to it postmortem (Supporting Information Figure S1). Moreover, a number of microscopic materials with a fibrous-like morphology were found; however, only a few could be isolated due to their small dimensions and fragmented state. The fibers were observed using an optical microscope and examined by means of histochemical methods. Two main morphological classes were documented. The Type 1 fiber had a length of 51.56 µm and an irregular width with a mean diameter of 24.4 µm (Fig. 7a). It was flexible with some distinct folds and reacted with the staining specific for cellulose and chitin (Fig. 7b), but not with the one specific for lignin. Due to the size and morphology, this fiber type was more consistent with a plant fiber classification rather than fungi. The Type 2 fiber had a light brown pigmentation, a round morphology with a diameter of approximately 60 µm, and was also flexible but seemingly hollow (Fig. 7c). This fiber did not react with either cellulose (Fig. 7d) or lignin (Fig. 7e) stains. The size, morphology and histochemical results obtained from this fiber suggest it should be classified as hair.

Fourier transform infrared spectroscopy (FTIR) analysis was carried out on the black patina adhering to the inner walls of the cavities and on the soil from the deposit from which the teeth were retrieved. First, it was possible to discard external contamination as the soil analyses showed a composition of

calcite, silicates and quartz (Supporting Information Figure S2). The FTIR spectra obtained on the black patina are similar in both samples (Fig. 8). The peaks at 1022, 600 and 562 cm-1 (stretching and bending modes of PO4) are related to hydroxyapatite, due to the contamination of dentine adhering to the black patina. Furthermore, the sharp and strong peaks at 2922 (CH3 bending bond) and 2850 cm-1 (CH2 bending bond) and the weak peak at 2956 cm-1 show the presence of organic matter with strong absorption of aliphatic CH.

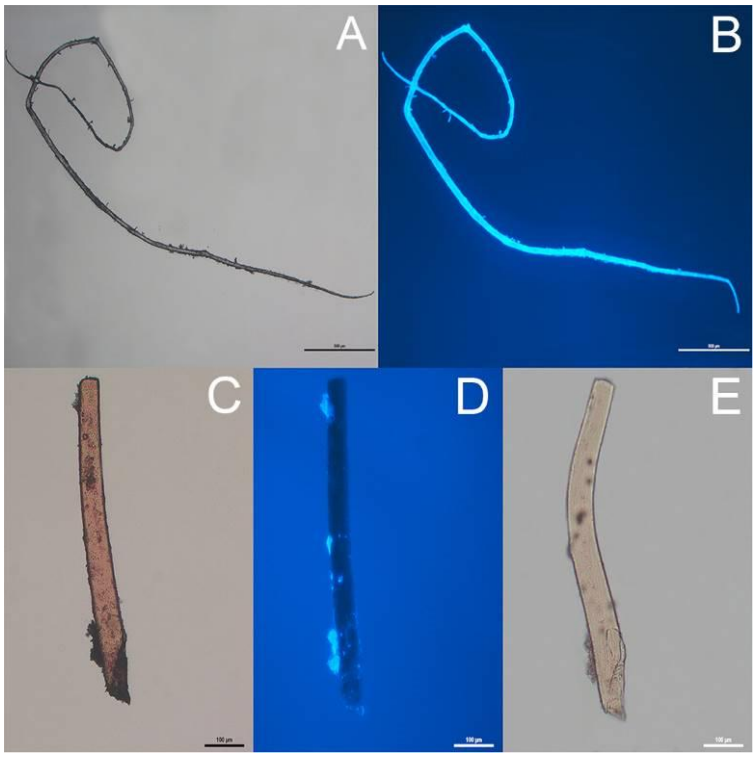

Figure 7. Fibers observed under optical microscope and examined by means of histochemical methods. (a) Type 1 unstained fiber observed under light microscope (50x). (b) Type 1 fiber stained with Calcofluor white and displaying the fluorescence due to the positive reaction with cellulose. (c) Type 2 unstained fiber (light microscope, 100x). (d) Stained with Calcofluor white (lack of

fluorescence = no cellulose). (e) Stained with Phuoroglucinol (lack of red color = no lignin).

The lack of a defined peak in the 1750-1650 cm-1 region suggests the organic material does

not have a carbonyl group, thereby excluding the presence of oil, wax, gums, natural resin or proteinaceous material, such as egg or animal glue (Daher et al., 2010; Derrick et al., 1999). According to previous studies (Cârciumaru et al., 2012; Hassan et al., 2013; Lamontagne et al., 2001), the two characteristic peaks at 1472 and 1382 cm-1 could indicate the presence of CH2 and CH3 bending bonds, respectively. The closest spectral match is with a reference spectrum gained from the IRUG online database (Harvard University Database, 2016) and is ascribable to bitumen.

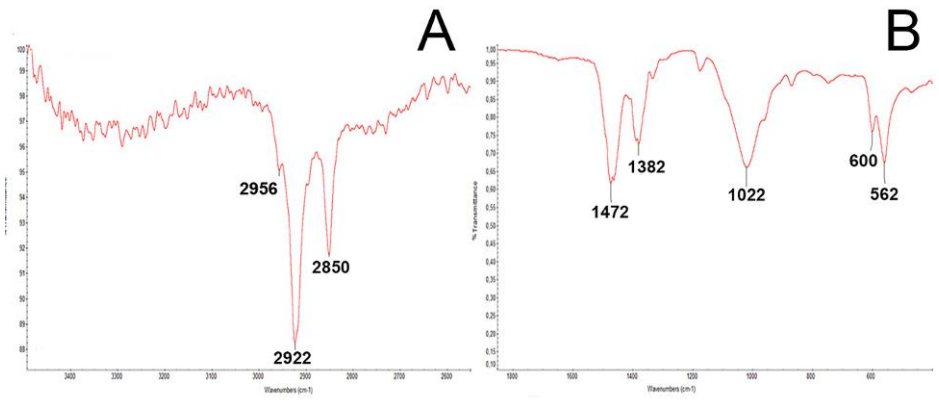

Figure 8. Spectra of the black patina collected by FTIR spectroscopy in Attenuated Total Reflection (ATR) mode. The small amount of material extracted from the cavity was fragile and fragmented causing noise in the spectra registered, which further presents a strong absorption of the inorganic part of the tooth. (a) Spectra showing the presence of organic matter (2956, 2922 and 2850 cm-1). (b) Spectra revealing the peaks related to bitumen (1472, 1382 cm-1).

A Raman spectrum was additionally acquired on the internal surface of the pulp cavities to distinguish the characteristic peaks of hydroxyapatite at 962 cm-1 (Supporting Information Figure S3). The spectrum of interest on the black patina, instead, shows broad peaks around 1305 and 1595 cm-1, which can be associated with amorphous carbon, probably attributable to bitumen.

Bitumen is an organic material with a very complex chemistry (Vandenabeele et al., 2007) because it is a mixture mostly of hydrocarbons with a small number of heterocyclic species and functional groups containing sulphur, nitrogen and oxygen. Accordingly, the energy dispersion X-ray spectroscopy (EDS) spectra were acquired on a small grain of material containing the black patina encrusted on the tooth's inner surface. An increasing degree of carbon (C) and the presence of sulphur (S) and nitrogen (N) were found in addition to the elements related to the chemical composition (Ca, P, O) of the teeth (Supporting Information Figure S4). This result can therefore be explained by the presence of sulphur, nitrogen and oxygen in the bitumen composition as heterocyclic atoms (McNally, 2011).

A direct radiocarbon date for Fredian 5 was obtained from the dentine of the right canine (RTD 8546) (Supporting Information Figure S5; Supporting Information Table S1). The new radiocarbon date, 11,000±40 14C year BP is well in the range of the Epigravettian period with a 95.4% probability calibrated range of 13,000-12,740 cal BP.

Discussion

Fredian 5 exhibits occlusal pulp exposure of both I1s, but this affliction is not an unusual occurrence among Late Upper Paleolithic hunter-gatherers (e.g., Capasso, 2001; Da-Gloria and Larsen, 2014; Lieverse et al., 2007; Lukacs, 1988; Porr and Alt, 2006) that warrants further explanation. However, the internal surface modifications to the pulp cavities, in addition to the presence of bitumen and organic fibers, is an unusual occurrence among Late Upper

Paleolithic hunter-gatherers that begs further explanation. Caries manipulation was previously recorded in the penecontemporaneous (Epipaleolithic) Villabruna 1 individual (Oxilia et al., 2015), suggesting that the presence of the above features could be the result of similar pathology manipulation in Fredian 5. Thus, we offer a differential diagnosis for the suite of characteristics associated with the pulp cavity modifications documented for Fredian 5. We have identified four possible diagnoses: 1) Postmortem/Taphonomic Modifications; 2) Ingestive Behaviors and Teeth-as-Tools; 3) Cultural Modification for Social Expression; and 4) Therapeutic Dentistry. We explore each diagnosis in detail below and discuss potential overlap between them.

1. Postmortem/Taphonomic Modifications

The exposed pulp chambers are undoubtedly antemortem, but the extent to which the markings on the internal surface of the pulp cavities are of antemortem versus postmortem origin must be explored further. Dental drilling tends to produce parallel striations or microgrooves around the circumference of the drilled cavity (e.g., Bennike and Alexandersen, 2003; Coppa et al., 2006; Ortiz et al., 2016; Schwartz et al., 1995; Seidel et al., 2005; Turner, 2004; White et al., 1997). The case of Fredian 5 shows less-intensive markings than documented in chronologically more recent examples of dental drilling and the striations are parallel to the horizontal axis of the tooth. These markings would be consistent with the twisting of a hard implement (e.g., bone or lithic) placed inside the pulp cavities, and are similar to the striations created by the scraping and levering actions during caries manipulation in Villabruna 1 (Oxilia et al., 2015). The same forms of striations are not found on the occlusal external root surfaces of the Fredian 5 anterior teeth. If the markings on the internal surface are the product of postmortem damage caused by cleaning, we would expect to see similar marking on the occlusal surfaces, but there are no such markings. Therefore, we find it difficult to explain how a postmortem process could

preferentially leave marking on internal surfaces while leaving the external surfaces unmarked.

Moreover, bitumen is known to have been used as hafting compound by Pleistocene foragers from Middle and Upper Paleolithic contexts (Boëda et al. 1996, 2008; Cârciumaru et al., 2012). Bitumen, along with other hafting materials (e.g., pitch and resin), have been documented in museum collections derived from decades old excavations (Cârciumaru et al., 2012; Dinnis et al., 2009), which attests to the possibility of long-term preservation of such residues following excavation, repeated handling, and curation. It is difficult to explain how a postmortem processes that would cause an organic substance such as bitumen to be preferentially deposited (and preserved) only inside the two pulp cavities, but be absent on the external surfaces of the teeth and surrounding archaeological matrix from the site (see Results). Consequently, we view a scenario in which postmortem, taphonomic processes caused the modifications to the Fredian 5 pulp cavities as unlikely.

2. Ingestive Behaviors and Teeth-as-Tools

The exposure of pulp chambers through attrition is not uncommon among hunter-gatherers, for it is often found among foragers with extensive anterior tooth wear caused by a combination of ingestive food processing behaviors and non-masticatory uses of the "teeth-as-tools". In the case of Fredian 5 it is evident from the presence of fine occlusal striations and rounding of the dentin chips around the exposed pulp cavities that the I1s continued to be used after pulp exposure for ingestive and/or non-masticatory behaviors.

Given the presence of occlusal wear following antemortem pulp exposure there is a possibility that the striations inside the pulp cavities could have been caused by continued anterior tooth-use. For instance, some hunter-gatherers retouch the working-edge of lithic implements with their anterior teeth (Gould, 1968), a process that could introduce microflakes into exposed pulp

cavities. Grit, bone fragments, and other abrasive materials from food or various materials worked between the anterior teeth (e.g., wood, hide, plant and animal fibers) could also have entered the exposed pulp cavities of Fredian 5 unintentionally. With this scenario, the foreign materials or debris entering the pulp cavities would had to have moved along a horizontal plane to produce the striations documented in the Fredian pulp cavities, but such movements are unlikely to be produced by the vertical motions and compressive forces of the teeth and jaws during ingestive and/or non-masticatory behaviors. Rather, such striations are more likely to have been induced by movements that involved twisting and scraping an implement along a horizontal axis within the pulp cavity. A lack of dietary microwear within the cavities also suggests that mastication was unlikely to have contributed greatly to the expansion of the cavities. The most parsimonious explanation is that Fredian 5, perhaps with the assistance of another individual, intentionally manipulated an object that produced horizontal striations on the internal walls of the cavity.

Support for this interpretation comes from Villabruna 1, which also lacked dietary microwear deep within the manipulated caries but does present distinctive, tool-induced striations within the margins of the caries (Oxilia et al., 2015). Experiments show that striations similar to those occurring in Fredian 5 (in shape, cross-section, and orientation [horizontal]) are produced through levering and twisting actions with osseous and lithic tools (Oxilia, et al., 2015).

If Fredian 5 used their anterior dentition to manipulate implements covered in bitumen (e.g., items waterproofed with bitumen or hafted objects), then it is also likely that the occlusal surfaces of the I1s would be more extensively impregnated with bitumen. Instead, only the edges of the exposed pulp cavities, the internal surfaces, and the deep recesses within the pulp canal are infilled with bitumen. Furthermore, there are no traces of bitumen on the occlusal surfaces of the other four anterior teeth of Fredian 5 despite their similar states of wear. If the bitumen in the pulp cavities entered

unintentionally, we expect that traces of bitumen on the occlusal surfaces to be variably present across all six anterior teeth, not just within the pulp cavities of the I1s. The majority of the residue is found deep in the pulp canal rather than distributed throughout the entire pulp chamber/cavity, and it is notable that no bitumen is found embedded recesses of the antemortem enamel and dentin chips on either tooth. We expect that the accumulation of residue through unintentional causes would not limit the majority of bitumen accumulation to the pulp canals, and that the occlusal recesses caused by chipping would likely retain remnants of bitumen even after continued dietary and non-masticatory tooth-use. Given neither circumstance is observed in Fredian 5, we find the presence, location, and preservation of bitumen in the pulp canals difficult to explain without invoking explicit anthropogenic intentions.

The orientation of the striations inside the pulp cavities suggests intentional movements of an extraneous implement, while the presence of bitumen inside the pulp cavities, but no other surfaces, also suggest intentional placement of the bitumen. However, it is much more difficult to rule out an unintentional origin of the vegetal and hair fibers in the pulp cavities. These materials could have been unintentionally adhered to the bitumen when it was placed in the cavities, regardless of whether bitumen was entered through dietary or non-dietary behaviors, or intentionally placed inside the cavities. Given the degraded characteristics of the fibers, and the low number recovered, we cannot rule out their presence as an unintentional result of dietary and/or non-masticatory behavior. Therefore, we suggest intentional behaviors produced the internal pulp cavity striations and presence of bitumen, but we cannot determine intentionality for the presence of organic fibers in the pulp cavities definitively.

3. Cultural Modification for Social Expression

Regional traditions of intentional dental modification for purposes of cultural expression of social identities are well documented in the Late Upper Paleolithic and are best represented by the practice of dental ablation throughout North Africa, Southwest and Southeast Asia, and Australia during the Late Pleistocene (see review in Willman et al., 2016). However, ablation generally leaves large gaps in the dental arcade due to the tooth removal that disrupt patterns of occlusion and dental wear (Humphrey and Bocaege, 2008). Occlusal wear is relatively even and extensive across all six of the maxillary anterior teeth of Fredian 5, which suggests that the individual's mandibular isomeres were present (i.e., not ablated) and in occlusion. Using the same logic, we can rule out ablation through "tooth-knocking" (i.e., breaking the crown off at the cervix: Pietrusewsky and Douglas, 1993), and add that there are no signs of root resorption (Fig. 4) typical of traumatic fracture (Lukacs, 2007).

The filing of anterior dental crowns into specific shapes to express aspects of social identity is well-documented from prehistory into the ethnographic present (Alt and Pichler, 1998; Fastlicht, 1976; Milner and Larsen, 1991; Stojanowski et al., 2016; Tiesler, 2011), and provides an alternative for the dental modification found in Fredian 5. However, to date there is only one case of abrasive wear from a Late Upper Paleolithic context that resembles filing (Bocquentin et al., 2013). The case concerns flattened and polished labial enamel on the upper central incisors of an Early Natufian individual from Jordan, but the wear cannot be definitively attributed to the use of teeth-as-tools or an intentional marker of social identity (Bocquentin et al., 2013). Filing generally involves shaping of the crown without removal of the entire crown (e.g., Alt and Pichler, 1998; Fastlicht, 1976; Milner and Larsen, 1991; Stojanowski et al., 2016; Tiesler, 2011), which is inconsistent with the complete loss of crowns in Fredian 5.

A last possibility for cultural modification of social expression would be that the pulp chambers were modified, drilled, or otherwise expanded for the

inclusion of a foreign object (e.g., inlays), although this is unlikely for a number of reasons. First, inlays are generally associated with drilling into the labial surfaces of teeth to prepare for the placement of decorative materials (e.g., turquoise and gold) as this would be readily visible to others (Alt and Pichler, 1998; Fastlicht, 1976; Milner and Larsen, 1991; Tiesler, 2011). However, there are no documented cases of decorative inlays being placed in modified pulp chambers/cavities in the archaeological or ethnohistorical literature to our knowledge. Second, while drilling to prepare inlays shares technological attributes with the drilling procedures used for therapeutic purposes (Bennike and Alexandersen, 2003; Coppa et al., 2006; Ortiz et al., 2016; Schwartz et al., 1995; Seidel et al., 2005; Turner, 2004; White et al., 1997), there is no evidence for this form of extensive drilling prior to the Neolithic (Coppa et al., 2006). Moreover, an exposed and modified pulp cavity would have been sensitive to non-therapeutic inclusions such as inlays or other decorative objects, when subjected to any compressive forces during masticatory and/or non-masticatory behaviors. Lastly, the presence of occlusal wear and rounded edges of dentine chips provides evidence for the continued use of the well-worn roots as a functional occlusal surfaces before death. If foreign objects were placed in the pulp cavities for cultural/aesthetic purposes one would not expect to see microwear related to normal tooth-use on the occlusal surfaces. We therefore suggest that an antemortem/cultural expression scenario is unlikely to explain the modifications to the I1 teeth of Fredian 5.

4. Therapeutic Dentistry

A final possibility for the presence of a suite of antemortem modifications of the I1 pulp cavities of Fredian 5 dentition may be through a therapeutic dental intervention. Pulp exposure is commonly associated with severe anterior dental attrition among foragers (Da-Gloria and Larsen, 2014; Lieverse et al., 2007; Lukacs, 1988; Porr and Alt, 2006), and high rates of oral

pathology have recently become well documented among Terminal Pleistocene foragers (e.g., Capasso, 2001; Frayer, 1989; Humphrey et al., 2014; Lacy, 2014, 2015; Willman et al., 2016). These rates of pathology suggest that a precedent for exploring pathology-induced dental interventions was present among Late Upper Paleolithic foraging groups. Similarly, the recent documentation of dental manipulation associated with pathology (caries) in the Late Upper Paleolithic Villabruna 1 fossil (Oxilia et al., 2015) suggests that other early cases of dental intervention may yet be documented.

Villabruna 1 exhibits striations consistent with scraping, levering, and probing an occlusal surface caries on a mandibular third molar – remnants of behaviors that partially removed the caries (Oxilia et al., 2015). Fredian 5 exhibits a degree of intentional modification that is similar to that of Villabruna 1. The Fredian 5 pulp cavities exhibit horizontal striations produced by scraping and twisting actions of an abrasive, hand-held implement that resulted in circumferential enlargement of the cavities (in comparison to recent dental drilling interventions). The similarities between the striations in the two specimens suggests intentional, manually-implemented, behaviors rather than unintentional byproducts of tooth-using behaviors, aesthetic modifications, or taphonomy.

Crediting a motive to the intentional dental modifications in Fredian 5 is made more difficult by the considerable differences in the form of the modifications compared to other documented cases from the Holocene – namely those that involved drilling for probable therapeutic purposes (Bennike and Alexandersen, 2003; Coppa et al., 2006; Ortiz et al., 2016; Schwartz et al., 1995; Seidel et al., 2005; Turner, 2004; White et al., 1997). The use of levering and scraping in Villabruna 1, rather than drilling, can be explained by the distal position of the carious lesion in the oral cavity (of the right M3). This is noteworthy because there are no documented cases of third molar dental drilling in more recent contexts (Bennike and Alexandersen, 2003; Coppa et al., 2006;

Ortiz et al., 2016; Schwartz et al., 1995; Seidel et al., 2005; Turner, 2004; White et al., 1997).

In contrast to Villabruna 1, access to the I1s of Fredian 5 would not preclude a more invasive drilling intervention like those found in many Holocene contexts. Additional concentric striations may be obscured by remnants of bitumen. Indeed, no bitumen was associated with the Villabruna 1 caries and the striations associated with caries manipulated are much clearer (Oxilia et al. 2015).

However, the subtle horizontal striations and circumferential enlargement of the cavities do show clear evidence intentional manipulation.

Numerous other explanations could account for the subtle nature of the horizontal striations in the Fredian 5 pulp cavities (e.g., some striations were erased through later abrasive wear – from removing and reapplying an organic filling, or from food and other debris entering the cavity following the initial use of bitumen). Although it is also probable that the intervention was simple less-invasive than those documented from more recent contexts.

The subtle markings from Fredian 5 (and to some extent, Villabruna 1) are infrequently documented compared to the obvious drill-induced modifications from the Holocene, but this infrequency may be biased due to the ease of identification in the latter cases. Indeed, the subtle modifications to the pulp chambers of Fredian 5 and caries manipulation of Villabruna 1 were difficult to observe macroscopically, and required extensive microscopic, microCT, and residue analyses to completely characterize. Consequently, the subtle manipulation of pathologies in the two cases from the Italian Epigravettian suggest that Holocene case studies of purposeful drilling should not be used as baseline characteristics for all pathology-induced dental interventions. It is probable that additional cases have gone undocumented given no reference for identifying the subtle modifications of Fredian 5 and Villabruna 1 existed until recently.

The presence of bitumen in the pulp cavities of Fredian 5 is an additional unique finding that is most likely explained by a therapeutic diagnosis. The lack of bitumen on any surface other than the inside of the pulp cavities is suggestive of intentional placement. Uses of bitumen are not unknown in the Paleolithic (Boëda et al. 1996, 2008; Cârciumaru et al., 2012), but have not been documented on dental surfaces prior to this study. However, residue and microfossil studies of dental surfaces are relatively recent innovations in paleoanthropology and unique discoveries have been made in most studies to date (Hardy et al., 2012, 2016; Henry et al., 2011; Radini et al., 2016). The presence of bitumen (and horizontal striations) inside the pulp cavity but not on other surfaces of the teeth suggests intentionality in their placement in the cavities. Therefore, the bitumen and pathological exposure of the pulp chambers through attrition may likely have been therapeutic.

While it is speculative in the present study, the use of bitumen could have been used as an antiseptic or to provide an anti-microbial barrier between the body and the environment (Bourée et al., 2011; Connan, 1999). A similar suggestion has been made for a Neolithic beeswax filling (Bernardini et al., 2013). Furthermore, the presence of hair and plant fibers could indicate the use of a composite filling material, but there is no way to be certain that the hair and vegetal fibers were purposefully placed in the cavities like the bitumen likely was. However, the probable use of medicinal plants is not without precedence in the Pleistocene (Hardy et al., 2012) and early Holocene (Aveling and Heron, 1999). There is also ample ethnographic documentation of plants used for the treatment of toothaches, caries, pulpitis, and other ailments (Buckley et al., 2014; Elvin-Lewis, 1982, 1986; Moerman, 1998; Willey and Hofmann, 1994).

Conclusions

Given the evidence for probable dentistry in Fredian 5 it is now possible to suggest that the caries manipulation found in Villabruna (Oxilia et al., 2015)

may be part of a broader trend, or tradition, of pathology-induced dental interventions among Late Upper Paleolithic Italian foragers. Both Fredian 5 and Villabruna 1 represent cases where implements were used to manipulate dental pathologies. The Late Pleistocene is a period of increasingly diverse and broad spectrum socioeconomic activities. The concomitant increase in dentognathic pathology likely called for novel strategies to cope with changing morbidity profiles. Thus, this discovery marks a much earlier instance of pathology-induced therapeutic dental interventions than previously known.

Acknowledgements

We dedicate this paper to Mario Dini, a young researcher of the University of Pisa who died prematurely. Mario devoted most of his research to the study of the Paleolithic and Mesolithic sites in the Serchio river valley. He recovered the human remains from the deposits at Riparo Fredian and entrusted two of the authors (J. M.-C. and A. R.) to carry out a new and detailed study of them. AMS date was funded by the Exilarch's Foundation, the DANGOOR Research Accelerator Mass Spectrometry Laboratory (D-REAMS), and the Max Planck-Weizmann Center for Integrative Archaeology and Anthropology. JCW was funded by the Leakey Foundation. The authors declare no potential conflicts of interest with respect to the authorship and/or publication of this article.

The datasets supporting this article have been uploaded as part of the Supporting Information.

References

Alt, K.W. & Pichler, S.L. (1998). Artificial modifications of human teeth. In K.W. Alt, F.W. Rösing & M. Teschler-Nicola, (Eds.), *Dental Anthropology: Fundamentals, Limits, and Prospects* (pp. 387-415). Wien: Springer Verlag.

Asscher Y., Regev L., Weiner S., Boaretto E. (2011a). Atomic disorder in fossil tooth and bone mineral: an FTIR study using the grinding curve method. *ArcheoSciences.* 35, 135–141.

Asscher Y., Weiner S., Boaretto E. (2011b). Variations in atomic disorder in biogenic carbonate hydroxyapatite using the infrared spectrum grinding curve method. *Adv. Funct. Mater.* 21, 3308–3313.

Aveling E.M., Heron C. (1999). Chewing tar in the early Holocene: an archaeological and ethnographic evaluation. *Antiquity.* 73, 579-584.

Bennike P., Fredebo L. (1986) Dental treatment in the stone age. *Bull. Hist. Dent.* 34. 81-87.

Bennike, P. & Alexandersen, V. (2003). Dental modification in the past. In E. Iregren & L. Larsson (Eds.), *A Tooth for a Tooth* (pp. 85-100). Lund: University of Lund.

Bernardini F., Tuniz C., Coppa A., Manini L., Derossi D., Eichert, D.…, Levchenko V. (2012). Beeswax as Dental Filling on a Neolithic Human Tooth. *PLoS One*. 7, 1–9.

Biagi P., Castelletti L., Cremaschi M., Sala B., Tozzi C. (1981). Popolazione e territorio nell'Appennino tosco-emiliano e nel tratto centrale della pianura del Po tra il IX e il V millennio. *Emilia Preromana*. 8, 13-36.

Bocquentin F. (2011). Avulsions dentaires et identité régionale chez les Natoufiens. *Tüba-Ar*. 14, 261-270.

Bocquentin, F., Crevecoeur, I., Semal, P. (2013). Artificial modification of the central upper incisors of *Homo 4* (Plot XX J burial). In P.C. Edwards (Ed.), *Wadi Hammeh 27, an Early Natufian Settlement at Pella in Jordan* (pp. 383-387). Leiden: Brill.

Boaretto E., Wu X., Yuana J., Bar-Yosef O., Chu V., Pan Y., …, Weiner, S. (2009). Radiocarbon Dating of Charcoal and Bone Collagen Associated with Early Pottery at Yuchanyan Cave, Hunan Province, China. *Proc. Natl. Acad. Sci.* U. S. A. 106, 9595–9600.

Bonfiglioli B., Mariotti V., Facchini F., Belcastro M.G., Condemi S. (2004). Masticatory and non-masticatory dental modifications in the Epipalaeolithic necropolis of Taforalt (Morocco). *Int. J. Osteoarchaeol.* 14. 448-456.

Boschian G., Mallegni F., Tozzi C. (1995). The Epigravettian and Mesolithic site of Fredian Shelter (in Tuscany). *Quaternaria*. V, 45–80.

Boschin F., Crezzini J. (2012). Morphometrical Analysis on Cut Marks Using a 3D Digital Microscope. *Int. J. Osteoarchaeol.* 22, 549–562.

Bourée, P., Blanc-Valleron, M.M., Ensaf, M., Ensaf, A. (2011). Usage du

bitume en médecine au cours des âges. In Ferrandis JJ & Gourevitch D. (Eds.), *Histoire des Sciences Médicales (*pp. 119-125) Paris:Société française d'Histoire de la Médecine.

Bronk Ramsey C., Lee S. (2013). Recent and Planned Developments of the Program OxCal. *Radiocarbon.* 55, 720–730.

Brown T., Molnar S. (1990). Interproximal grooving and task activity in Australia. *Am. J. Phys. Anthropol.* 81, 545–553.

Buckley S., Usai D., Jakob T., Radini A., Hardy K.. (2014). Dental calculus reveals unique insights into food items, cooking and plant processing in prehistoric Central Sudan. *PLoS One*. 9, e100808.

Cârciumaru M., Ion R.M., Nițu E.C., Ştefânescu R. (2012). New evidence of adhesive as hafting material on Middle and Upper Palaeolithic artefacts from Gura Cheii-Râşnov Cave (Romania). *J. Archaeol. Sci.* 39, 1942–1950.

Clement A.F., Hillson S.W., Aiello L.C., (2012). Tooth wear, Neanderthal facial morphology and the anterior dental loading hypothesis. *J. Hum. Evol.* 62, 367-376.

Capasso, L. (2001). Paleopatologia dei Cromagnoniani del Fucino. In U. Grossi, Irti & V. Pagani (Eds.), *Il Fucino e le Aree Limitrofe nell'Antichità* (pp. 42-55). Archeoclub d'Italia: Avezzano.

Coppa A., Bondioli L., Cucina A., Frayer D. W., Jarrige C, Jarrigge J.F., …, Macchiarelli, R. (2006). Early Neolithic tradition of dentistry. *Nature*. 440, 755–756.

Connan J. (1999). Use and trade of bitumen in antiquity and prehistory: molecular archaeology reveals secrets of past civilizations. *Philo. Trans. Royal Soc. London B.* 354, 33-50.

Crezzini J., Boschin F., Boscato P., Wierer U. (2014). Wild cats and cut marks: Exploitation of Felis silvestris in the Mesolithic of Galgenbühel/Dos de la Forca (South Tyrol, Italy). *Quatern. Int.* 330, 52–60.

D'Errico F., Banks W.E., Vanhaeren M., Laroulandie V., Langlais M. (2011). PACEA Geo-Referenced Radiocarbon Database. *PaleoAnthropol.*, doi:10.4207/PA.2011.ART40.

Da-Gloria P., Larsen C.S. (2014). Oral health of the Paleoamericans of Lagoa Santa, central Brazil. *Am. J. Phys. Anthropol.* 154, 11-26.

Daher C., Paris C., Le Hô A.S., Bellot-Gurlet L., Échard J.P. (2010). A joint use of Raman and Infrared spectroscopies for the identification of natural organic media used in ancient varnishes. J. *Raman Spectrosc.* 41, 1494–1499.

De Groote I., Humphrey L.T. (2016). Characterizing evulsion in the Later Stone Age Maghreb: Age, sex and effects on mastication. *Quatern. Intern.* 413, 50-61.

Derrick, M.R., Stulik, D.C., Landry, J.M. (1999). *Infrared Spectroscopy in Conservation Science, Scientific tools for conservation*. Getty Conserv. Institute, Los Angeles.

Deter C.A., (2009). Gradients of occlusal wear in hunter-gatherers and agriculturalists. *Am. J. Phys. Anthropol.* 138, 247-254.

Elvin-Lewis M. (1982). The therapeutic potential of plants used in dental folk medicine. *Odonto-Stomatol. Trop*. 5, 107-117.

Elvin-Lewis, M. (1986). Therapeutic rationale of plants used to treat dental infections. In: Etkin NL, editor. (pp. 48-69). *Plants in Indigenous Medicine and Diet: Biobehavioral Approaches*. Bedford Hills: Redgrave Publishing.

Fastlicht, S. (1976). *Tooth mutilations and dentistry in Pre-Columbian Mexico*. Berlin: Quintessenz Verlags-GmbH.

Feldkamp I.A., Davis L.C., Kress J.W. (1984). Pratical cone-beam algorithm. *J Opt Soc Am A Opt Image Sci Vi.* 1, 612–619.

Frayer, D.W. (1989). Oral pathologies in the European Upper Paleolithic and Mesolithic. In I. Hershkovitz (Ed.), *People and Culture in Change: Proceedings of the Second Symposium on Upper Palaeolithic, Mesolithic and Neolithic Populations of Europe and the Mediterranean Basin* (pp. 255-281). Oxford: BAR International Series.

Guidi, O. (1989). *L'età della pietra in Garfagnana e nella Media Valle del Serchio.* Lucca: Maria Pacini Fazzi.

Hardy K., Buckley S., Collins M.J., Estalrrich A., Brothwell D., Copeland L., …, Lalueza-Fox C. (2012). Neanderthal medics Evidence for food, cooking, and medicinal plants entrapped in dental calculus.

Naturwissenschaften. 99, 617–626.

Hardy K., Radini A., Buckley S., Blasco R., Copeland L., Burjachs F., … Bermúdez de Castro J.M. (2016). Diet and environment 1.2 million years ago revealed through analysis of dental calculus from Europe's oldest hominin at Sima del Elefante, Spain. *Sci. Nature.* 104, 1-5.

Hardy, K. (2016). Plants as raw materials. In: Hardy K & Kubiak-Martens L. (Eds.), *Wild Harvest: Plants in the Hominin and Pre-Agrarian Human Worlds* (pp. 71-90). Oxford: Oxbow Books.

Harvard University Art Museums, Straus Center for Conservation, US. 'INR00109, Asphaltum'. Infrared and Raman Users Group Spectral Database. Web. 10 March 2016. <www.irug.org>.

Hassan A.M., Mazrouaa A.M., Youssif M.A., Shahba R.M.A., Youssif M. (2013). Evaluation of Some Insulated Greases Prepared from Rubber and Bitumen Thickeners. *Int. J. Org. Chem.* 3, 71–80.

Henry A.G., Brooks A.S., Piperno D.R. (2011). Microfossils in calculus demonstrate consumption of plants and cooked foods in Neanderthal diets (Shanidar III, Iraq; Spy I and II, Belgium). *Proc. Nat. Acad. Sci.* 108, 486-491.

Hinton R.J., (1981). Form and patterning of anterior tooth wear among aboriginal human groups. *Am. J. Phys. Anthropol*. 54, 555-564.

Hollund H.I., Ariese F., Fernandes R., Jans M.M.E., Kars H. (2013). Testing an alternative high-throughput tool for investigating bone

diagenesis: FTIR in Attenuated Total Reflection (ATR) mode. *Archaeometry*, 55, 507–532.

Humphrey L.T., Bocaege E. (2008). Tooth evulsion in the Maghreb: Chronological and geographical patterns. *African Archaeol. Rev.* 25, 109–123.

Humphrey L.T., De Groote I., Morale J., Barton N,, Collcutt S., Ramsey C.B., Bouzouggar A. (2014). Earliest evidence for caries and exploitation of starchy plant foods in Pleistocene hunter-gatherers from Morocco. *Proc. Natl. Acad. Sci*. USA 111, 954–959.

Lacy, S,A. (2014). *Oral Health and its Implications in Late Pleistocene Western Eurasian Humans*. Washington University, Saint Louis.

Lacy, S.A. (2015). The dental metrics, morphology, and oral paleopathology of Oberkassel 1 and 2. In L. Giemsch & R. W. Schmitz (Eds.), *The Late Glacial Burial from Oberkassel Revisited* (pp. 1-17). Verlag Phillip von Zabern: Damstadt.

Lamontagne J., Dumas P., Mouillet V., Kister J. (2001). Comparison by Fourier transform infrared (FTIR) spectroscopy of different ageing techniques: Application to road bitumens. *Fuel*, 80, 483-488.

Lieverse A.R., Link D.W., Bazaliiskiy V.I., Goriunova O.I., Weber A.W., (2007). Dental health indicators of hunter–gatherer adaptation and cultural change in Siberia's Cis-Baikal. *Am. J. Phys. Anthropol*. 134, 323-339.

Lozano M., Subirà M., Aparicio J., Lorenzo C., Gómez-Merino G. (2013). Toothpicking and Periodontal Disease in a Neanderthal Specimen from

Cova Foradà Site (Valencia, Spain). *PLoS One*, 8, 6–11.

Lukacs J., Pastor R. (1988). Activity-induced patterns of dental abrasion in prehistoric Pakistan: Evidence from Mehrgarh and Harappa. *Am. J. Phys. Anthropol.* 76, 377–398.

Lukacs J.R. (2007). Dental trauma and antemortem tooth loss in prehistoric Canary Islanders: prevalence and contributing factors. *Int. J. Osteoarchaeol*. 17, 157-173.

Milner, G.R., & Larsen, C.S. (1991). Teeth as artifacts of human behavior: intentional mutilation and accidental modification. In M.A. Kelley & C.S. Larsen (Eds.), *Advances in Dental Anthropology* (pp. 357-378). New York: Wiley-Liss.

McNally, T. (2011). Introduction to polymer modified bitumen (PmB). In T. McNally (Ed.), *Woodhead Publishing Series in Civil and Structural Engineering.* Dublin: Woodhead Publishing.

Moerman, D.E. (1998). *Native American Ethnobotany*. Portland: Timber Press.

Moretti E., Arrighi S., Boschin F., Crezzini J., Aureli D., Ronchitelli A. (2015). Using 3D Microscopy to Analyze Experimental Cut Marks on Animal Bones Produced with Different Stone Tools. *Ethnobiol. Lett.* 6, 267-275.

Molnar P. (2008), Dental wear and oral pathology: Possible evidence and consequences of habitual use of teeth in a Swedish Neolithic sample. *Am. J.*

Phys. Anthropol. 136, 423–431.

Molnar S. (1971), Human tooth wear, tooth function and cultural variability. *Am. J. Phys. Anthropol.* 34, 27–42.

Ortiz A., Torres Pino E.C., Orellana González E. (2016). First evidence of pre-Hispanic dentistry in South America – Insights from Cusco, Peru. *HOMO.* 67, 100-109.

Oxilia G., Peresani M., Romandini M., Matteucci C., Debono Spiteri C., Henry A.G.,…, Benazzi S. (2015). Earliest evidence of dental caries manipulation in the Late Upper Palaeolithic. *Sci. Rep.* 5, 12150.

Panetta D., Belcari N., Del Guerra A., Bartolomei A., Salvadori P.A. (2012). Analysis of image sharpness reproducibility on a novel engineered MicroCT scanner with variable geometry and embedded recalibration software. *Phys. Medica.* 28, 166–173.

Pietrusewsky M., Douglas M.T. (1993). Tooth ablation in old Hawai'i. *J. Polynes. Soc.* 102, 255-272.

Porr M., Alt K.W., (2006). The burial of Bad Dürrenberg, central Germany: Osteopathology and osteoarchaeology of a Late Mesolithic shaman's grave. *Int. J. Osteoarchaeol.* 16, 395-406.

Radini A., Buckley S., Rosas A., Estalrrich A., de la Rasilla M., Hardy K. (2016). Neanderthals, trees and dental calculus: new evidence from El Sidrón. *Antiquity.* 90, 290-301.

Reimer P.J., Bard E., Bayliss A., Beck J.W., Blackwell P.G., Ramsey C.B.,

…, Van der Plicht J. (2013). IntCal13 and Marine13 Radiocarbon Age Calibration Curves 0-50,000 Years cal BP. *Radiocarbon.* 55, 1869–1887.

Scott G.R., Winn J.R. (2011). Dental chipping: Contrasting patterns of microtrauma in Inuit and European populations. *Int. J. Osteoarchaeol.* 21, 723-731.

Seidel J.C., Colten R.H., Thibodeau E.A., Aghajanian J.G. (2005). Iatrogenic molar borings in 18th and early 19th century Native American dentitions. *Am. J. Phys. Anthropol*. 127, 7-12.

Schwartz J.H., Brauer J., Gordon-Larsen P. (1995). Tigaran (Point Hope, Alaska) tooth drilling. *Am. J. Phys. Anthropol.* 97, 77-82.

Smith B. H. (1984). Patterns of molar wear in hunter–gatherers and agriculturalists. *Am. J. Phys. Anthropol*. 63, 39–56.

Stojanowski C.M., Carver C.L., Miller K.A. (2014). Incisor avulsion, social identity and Saharan population history: New data from the Early Holocene southern Sahara. *J. Anthropol. Archaeol.* 35, 79-91.

Stojanowski, C.M., Johnson, K.M., Paul, K.S., Carver, C.L. (2016). Indicators of idiosyncratic behavior in the dentition. In J.D. Irish & G.R. Scott (Eds), *A Companion to Dental Anthropology*. (pp. 377-395). Malden: John Wiley & Sons, Inc.

Tiesler, V. (2011). Decoraciones dentales. In A. Cucina (Ed.). *Manual de Antropología Dental*, (pp. 183-206). Mérida: Universidad Autónoma de Yucatán.

Tozzi C. (1995). Prospezioni sistematiche. In: memoria di Giuliano Cremonesi. *Un ecosistema montano: la valle del Serchio e l'Appennino tosco-emiliano.* (pp. 93-127).

Turner C.G. (2004). A second drilled tooth from prehistoric western North America. *Am. Antiquity.* 69, 356-360.

Ungar P.S., Grine F.E., Teaford M.F., Pérez-Pérez A. (2001). A review of interproximal wear grooves on fossil hominin teeth with new evidence from Olduvai Gorge. *Archives Oral Biol.* 46, 285-292.

Vandenabeele P., Ortega-Avilès M., Castilleros D.T., Moens L. (2007). Raman spectroscopic analysis of Mexican natural artists' materials. *Spectrochimica Acta A.* 68, 1085–1088.

Vercellotti G., Alciati G., Richards M., Formicola V. (2008). The Late Upper Paleolithic skeleton Villabruna 1 (Italy): A source of data on biology and behavior of a 14.000 year-old hunter. *J. Anthropol. Sci.* 86, 143–163.

Vierin, S. (2012). *Revisione dei Reperti Umani Provenienti dal Sito Epigravettiano e Mesolitico 'Riparo Fredian', Molazzana, (LU).* Universita' Degli Studi di Firenze, Firenze.

Weiner S., Bar-Yosef O. (1990). States of preservation of bones from prehistoric sites in the Near East: a survey. *J. Archaeol. Sci.* 17, 187–196.

White T.D., Degusta D., Richards G.D. (1997). Prehistoric Dentistry in the American Southwest: A Drilled Canine From Sky Aerie, Colorado. *Am. J. Phys. Anthropol.* 103, 409–414.

Willey, P., Hofman, J.L. (1994). Interproximal grooves, toothaches, and purple coneflowers. In: Owsley, D.W., Jantz, R.L., (Eds.), *Skeletal Biology in the Great Plains: Migration, Warfare, Health, and Subsistence*. (pp. 147-157). Washington: Smithsonian Institution Press.

Willman J.C., Shackelford L., Demeter F. (2016). Incisor ablation among the late upper paleolithic people of Tam Hang (Northern Laos): Social identity, mortuary practice, and oral health. *Am. J. Phys. Anthropol.* 160, 519-28.

Yizhaq M., Mintz G., Cohen I., Khalaily H., Weiner S., Boaretto E. (2005). Quality controlled radiocarbon dating of bones and charcoal from the Early Pre-Pottery Neolithic B (PPNB) of Motza (Israel). *Radiocarbon*. 47, 193–206.

American Journal of Physical Anthropology
(*Am J Phys Anthropol. 2017b. doi: 10.1002/ajpa.23254)*

Letter to the editor: Reply to Hardy & Buckley: Earliest evidence of bitumen from Homo sp. teeth is from El Sidrón

Gregorio Oxilia[1,2], Flavia Fiorillo[3], Francesco Boschin[4,5], Elisabetta Boaretto[6], Salvatore A. Apicella[3], Chiara Matteucci[3], Daniele Panetta[7], Rossella Pistocchi[8], Franca Guerrini[8], Cristiana Margherita[2], Massimo Andretta[9], Rita Sorrentino[2,10], Giovanni Boschian[11], Simona Arrighi[4,5], Irene Dori[1], Giuseppe Mancuso[2], Jacopo Crezzini[4,5], Alessandro Riga[1], Maria C. Serrangeli[2], Antonino Vazzana[2], Piero A. Salvadori[7], Mariangela Vandini[3], Carlo Tozzi[12], Adriana Moroni[4,5], Robin N. M. Feeney[13], John C. Willman[14], Jacopo Moggi-Cecchi[1]§ and Stefano Benazzi[2,15]§.

[1]Department of Biology, University of Florence, Via del Proconsolo, 12, 50122 Firenze, Italy

[2]Laboratory of Anthropology, Department of Cultural Heritage, University of Bologna, Via degli Ariani 1, 48121 Ravenna, Italy

[3]Conservation Science Laboratory for Cultural Heritage, Department of Cultural Heritage, University of Bologna, Via degli Ariani 1, 48121 Ravenna, Italy

[4]Study Centre for the Quaternary Period (CeSQ), Via Nuova dell'Ammazzatoio 7, I - 52037 Sansepolcro (Arezzo), Italy

[5]*Department of Physical Sciences*, Earth and Environment, University of Siena, Research Unit in Prehistory and Anthropology, Via Laterina 8, 53100 Siena,

Italy
[6]Max Planck-Weizmann Center for Integrative Archaeology and Anthropology, D-REAMS Radiocarbon Laboratory, Weizmann Institute of Science, 7610001 Rehovot, Israel
[7]Institute of Clinical Physiology, IFC-CNR, Via G. Moruzzi 1, 56124 Pisa, Italy
[8]Department of Biological, Geological and Environmental Sciences, University of Bologna. Via Sant'Alberto 163, 48123 Ravenna, Italy
[9] School of Science, University of Bologna, Via dell'Agricoltura 5, 48123 Ravenna, Italy
[10] Department of Biological, Geological and Environmental Sciences – BiGeA University of Bologna Via Selmi 3, 40126, Bologna, Italy
[11] Department of Biology, University of Pisa, via Derna 1, 56125 Pisa, Italy
[12]Department of Civilisations and Forms of Knowledge, University of Pisa, Via Pasquale Paoli, 15, 56126 Pisa, Italy
[13]UCD School of Medicine, Health Science Centre, University College Dublin, Belfield, Dublin 4, Ireland
[14]Department of Anthropology, Campus Box 1114, Washington University, Saint Louis, MO 63130 USA
[15]Department of Human Evolution, Max Planck Institute for Evolutionary Anthropology, Deutscher Platz 6, 04103 Leipzig, Germany

In our recent article (Oxilia et al. 2017), we report of the presence of antemortem modifications to both I^1 pulp chambers from a single individual (Fredian 5) from the Epigravettian context of Riparo Fredian (Tuscany, Italy). The analysis included the direct dating of the Fredian 5 in addition to microscopic, microCT, and residue analyses of the internal and external surfaces of the modified I^1s. After a detailed differential diagnosis, we conclude that our results are "*consistent with tool-assisted manipulation to remove necrotic or infected pulp in vivo and the subsequent use of a composite, organic*

filling. Fredian 5 confirms the practice of dentistry—specifically, a pathology-induced intervention" (Oxilia et al. 2017: 2). In response to our article, Hardy and Buckley (in press) take issue with both the methods used to analyze the residues retrieved from the pulp cavities of Fredian 5 and our interpretation of the residue as "bitumen". Furthermore, they argue that we wrongfully attribute our findings as the earliest instance of bitumen found on Pleistocene human teeth given it was described earlier among the Neandertals from El Sidrón (Hardy et al. 2012; Radini et al. 2016, 2017). We address these concerns below.

In referring to methods, Hardy and Buckley (in press) suggest that gas chromatographic-mass spectrometric (GS-MS) techniques are more successful in identifying the original organic source of the dark patina – a point that we agree with. However, we opted for a combination of Fourier-transformed infrared spectroscopy (FTIR), scanning electron microscope and energy dispersion X-ray spectroscopy (SEM-EDS), and Raman microscopy to analyze the dark patina in the pulp cavities due to the difficulties in sampling a larger quantity of the residue. Minimizing damage to the sampled tooth was our foremost concern as the dark patina was only present inside the pulp cavities and made both visualization and retrieval of residue through mechanical methods difficult. In addition, the residue was concentrated in a hard and thin layer, that was well-adhered to the dentine of the pulp cavities. Lastly, obtaining greater quantities of the residue would have risked damage to the subtle, antemortem microstriations that are present on the internal walls of the pulp cavities. Analysis of the microstriations was a key feature of our analysis and conclusions – thus, damaging the microstriations with more extensive sampling was strictly avoided. We concede that a total weight of the sample was not reported (Hardy and Buckley (in press)), but an accurate assessment was not possible because the weight of the residue would be overestimated by the presence of dentin (which is visible in the FTIR spectrum). Therefore, the three

integrated techniques (FTIR spectroscopy, SEM-EDS and Raman microscopy) were preferred to minimize sample destruction and manipulation.

It was considered appropriate to use FTIR to first obtain a result on the overall composition of the patina since it is simple, fast, repeatable technique that is able to detect organic and inorganic compounds in a single analysis. Given that FTIR is non-destructive, we were then able to use the same small sample for SEM-EDS and Raman microscopy analyses. With reference to the interpretation of the results, SEM-EDS and Raman were used to refine our interpretations, in the case of poorer selectivity of FTIR with respect to GC-MS, thus providing the most complete and conclusive results possible while minimizing damage to Fredian 5.

The FTIR results allowed for the identification of a probable compound with bitumen peaks, as already indicated (Oxilia et al. 2017: 9-10). It cannot be ruled out that it is an oil/fats substance that was subjected to polymerization and decarboxylation, as suggested by Hardy and Buckley (in press), since our hypothesis only "*suggests the organic material does not have a carbonyl group*" (Oxilia et al. 2017: 9). However, the results obtained with SEM-EDS and Raman are consistent with what was obtained by FTIR. The presence of elements such as C, N and the considerable amount of S, detectable by SEM-EDS, may be attributed to a protein, and therefore could indicate a mixture of oil/fats and protein material, or association with bitumen. In FTIR spectra, however, there are no clear protein peaks.

We agree with Hardy and Buckley (in press) that the black color of the patina is not an indication of the origin of the material, nor the presence of amorphous carbon, which can result from other residues. The paper of Vandenabeele (2007) provides two broad Raman features for Mexican bitumen around 1600 and 1400 cm^{-1} probably attributed to the presence of carbon, and therefore our result is "*probably attributable to bitumen*" (Oxilia et al. 2017:

10). In this regard, there is a typographic error with the citation in the wrong line; we, however, intended to cite the paper in the previous sentence and we thank Hardy and Buckley (in press) for pointing out this error.

We further wish to underline that the presence of other materials in the studied patina were not excluded, but that the results of the three aforementioned techniques converge, in favor of bitumen; the closest spectral match with a bitumen standard of the IRUG database leads to the more plausible bitumen hypothesis.

Another factor in our conclusion was the consideration of published papers (such as Hardy 2012, Radini et. al 2016, Boëda et al. 1996 and 2008, Cârciumaru et al. 2012, and Connan 1999), which identified bitumen in prehistoric samples. On account of these studies, it was possible to draw conclusions with greater confidence on the presence of this compound among Paleolithic hunter-gatherers.

In addition, the absence of standardized protocols to be used for analyses of this kind allows for a more flexible methodology. In this case, since it was not possible to isolate the sample from the teeth and that the choice of minimally-destructive techniques was highly desirable, the authors developed the protocol used to study the black patina present within the cavities of the teeth around the use of FTIR spectroscopy, SEM-EDS and Raman microscopy.

Lastly, we agree with Hardy and Buckley (in press) that the earliest evidence of bitumen found on any hominin dentition comes from El Sidrón (Hardy et al. 2012; Radini et al. 2016). Indeed, our statement that "*Uses of bitumen…have not been documented on dental surfaces prior to this study"* (Oxilia et al. 2017: 13) should have been qualified with a statement indicating that bitumen had not been associated with therapeutic dentistry in the Paleolithic prior to this study. However, there is a major difference in conclusion between our study and those focusing on the El Sidrón Neandertals.

We hypothesized that the presence of bitumen in the pulp cavities of Fredian 5 was due to intentional placement of the substance for curative purposes (Oxilia et al. 2017). In contrast, the presence of "*bitumen or oil shale entrapped within the dental calculus*" (Hardy et al. 2012: 618) was more likely present in the El Sidrón calculus because of tooth contact with bitumen-hafted tools (Hardy et al. 2012; Hardy and Buckley in press; Radini et al. 2016, 2017).

Finally, our conclusions are of consequence because *"the internal surface modifications to the pulp cavities, in addition to the presence of bitumen and organic fibers, is an unusual occurrence among Late Upper Paleolithic hunter-gatherers"* (Oxilia et al. 2017: 10). Nonetheless, we are grateful for the criticism put forth by Hardy and Buckley (in press), and the opportunity given to us by the Editor to clarify our results.

References

Cârciumaru M., Ion R.M., Nițu E.C., Ştefânescu R. (2012). New evidence of adhesive as hafting material on Middle and Upper Palaeolithic artefacts from Gura Cheii-Râşnov Cave (Romania). *Journal of Archaeological Science,* 39, 1942–1950.

Boëda, E., Bonilauri, S., Connan, J., Jarvie, D., Mercier, N., Tobey, M., Valladas, H., Al Sakhel, H. & Muhesen, S. (2008). Middle Palaeolithic bitumen use at Umm el Tlel around 70 000 BP. *Antiquity,* 82, 853–861.

Boëda, E., Connan J., Dessort, D., Muhesen, S., Mercier, N., Valladas, H. and Tisnerat, N. (1996). Bitumen as a hafting material on Middle Palaeolithic artefacts. *Nature*, 380, 336–338

Connan J (1999) Use and trade of bitumen in antiquity and prehistory: molecular archaeology reveals secrets of past civilisations. *Philosophical* Transactions *of the* Royal Society *B (Biological Sciences),* 354, 33–50.

Hardy, K., Buckley, S. (in press) Earliest evidence of bitumen from Homo sp. teeth is from El Sidrón. *American Journal of Physical Anthropology*.

Hardy, K., Buckley, S., Collins, M.J., Estalrrich, A., Brothwell, D., Copeland, L., García-Tabernero, A., García-Vargas, S., de la Rasilla, M., Lalueza-Fox, C., Huguet, R., Bastir, M., Santamaría, D., Madella, M., Fernández Cortés, A., Rosas, A. (2012) Neanderthal medics? Evidence for food, cooking and medicinal plants entrapped in dental calculus. *Naturwissenschaften* 99, 617-626. DOI: 10.1007/s00114-012-0942-0.

Oxilia, G., Fiorillo, F., Boschin, F., Boaretto, E., Apicella, S. A., Matteucci, C…… Benazzi, S. (2017) The dawn of dentistry in the late upper Paleolithic: An early case of pathological intervention at Riparo Fredian. *American Journal of Physical Anthropology*, 1-16. DOI: 10.1002/ajpa.23216.

Radini, A. Buckley, S., Rosas, A., Estalrrich, A., de la Rasilla, M., Hardy, K. (2016) Neanderthals and Trees: Non-edible conifer fibres found in Neanderthal dental calculus suggests extra-masticatory activity. *Antiquity*, 90, 290-301.

Radini, A., Buckley, S., Nikita, E., Copeland, L., Hardy, K. (2017) Beyond Food: The rich and varied pathways for inclusion of microscopic remains into ancient dental calculus. 2017. *Yearbook of Physical Anthropology*, 162, 71-83. DOI:10.1002/ajpa.23147.

Vandenabeele, P., Ortega-Avilès, M., Castilleros, D. T., & Moens, L. (2007). Raman spectroscopic analysis of Mexican natural artists' materials. *Spectrochimica Acta A*, 68, 1085–1088.

Journal of Human Evolution
(J Hum Evo. 30; 1e6)

A reassessment of the presumed Torrener Bärenhöhle's Paleolithic human tooth

Cristiana Margherita[1], Sahra Talamo[2], Karin Wiltschke-Schrotta[3], Sascha Senck[4], Gregorio Oxilia[5], Rita Sorrentino[1], Giuseppe Mancuso[1], Giorgio Gruppioni[1], Robert Lindner[6], Jean-Jacques Hublin[2], Stefano Benazzi[1, 2]

[1]Department of Cultural Heritage, University of Bologna, Via degli Ariani 1, 48121 Ravenna, Italy
[2]Department of Human Evolution, Max Planck Institute for Evolutionary Anthropology, Deutscher Platz 6, 04103 Leipzig, Germany
[3]Department of Anthropology, Natural History Museum, Burgring 7, 1010 Wien, Austria
[4]University of Applied Sciences Upper Austria, Stelzhamerstraße 23, 4600 Wels, Austria
[5]Department of Biology, University of Firenze, Via del Proconsolo 12, 50122 Florence, Italy
[6]Haus der Natur - Museum für Natur und Technik, Museumsplatz 5, 5020 Salzburg, Austria

Keywords: *Homo sapiens*; Neandertals; Teeth; Enamel thickness; Micro-CT; Radiocarbon dating

Introduction

Torrener Bärenhöhle's cave is a corridor located about 810 meters near Golling and der Salzach (Salzburg, Austria). The cave was discovered in 1924 by Hermann Gruber, an Austrian alpine guide. After the initial speleological survey (carried out by Fritz and Robert Ödl) the cave was subject of a paleontological excavation commissioned by the newly founded (in 1924) Natural History Museum in Salzburg (now Haus der Natur). The excavation unearthed an enormous amount of animal bones mostly belonging to Ursus spelaeus, for a total of more than 90 individuals. Since then, the cave has been called "Torrener Bärenhöhle", meaning "Bear Cave" (Klappacher, 1979). In 1933 Kurt Ehrenberg identified 5 hollow bones among the cave findings as possible scrapers and awls (Ehrenberg 1933, 1938), and in 1972 Ehrenberg identified even more (artificially) modified bones (Ehrenberg 1972).

Until 1971 the publications about this cave have always mentioned animal bones only, but later on Gaisberger reported the presence of a human molar attributed to 1924 Torrener Bärenhöhle's collection (typescript dated 1971 reporting the finding of the tooth in January 1971, the original was in the archive of the museum Haus der Natur). When Gaisberger identified the tooth among the bones from the "Bärenhöhle" he showed it to the museum geologist, Rudolf Vogeltanz, who verified the identification as human molar.

In contrast with the 1971 report, an inventory started on January 1st 1968 (starting No. 4000) already lists a "left upper 6th molar of a Homo sapiens, leg. H. Gruber" as third entry (No. 4003) (Fig. 1), indicating that the tooth had already been identified as human tooth by that year. This inventory was laid out by Gustave Abel, then president of the Speleology Association of Salzburg ("Salzburger Höhlenverein", today "Landesverein für Höhlenkunde in Salzburg"). Abel consigned the inventory to the archive of the "Landesverein

für Höhlenkunde", nevertheless the museum was not aware of the existence of this document until after Abel's death in 1994, when the list was handed over to the museum. This fact may explain the double "discovery" of the tooth in the museum collection in 1968 and 1971. Anyway, in both cases the finding of the tooth was attributed to the initial discoverer of the cave H. Gruber in 1924. In the museum inventory, and - as an old label suggests - also in the exhibition of the "Haus der Natur" the tooth was always attributed to H. sapiens, with no age given. Moreover, in an old label of the "Haus der Natur" Museum the tooth is classified as upper third molar (Fig. S1).

Between 1965 and 1984 detailed prehistoric excavations were carried out in the so called "Schlenkendurchgangshöhle", a cave approximately 14 km NE of "Torrener Bärenhöhle". The excavations were financed by the Austrian Academy of Sciences and coordinated by Ehrenberg and his student Karl Mais. During these excavations again presumed stone artifacts were identified and dated between 40.000 to 30.000 years B.P. (Klappacher, 1992). These simple "Mousterian-type" stone tools gave rise to the assumption that the region was visited by ice-age hunters. Ehrenberg and Mais (1970) wrote that it is most likely "that the maker [of these tools] was the Neanderthal". Consequently the tooth found in the nearby Torrener Bärenhöhle was also attributed to H. neandertalensis in a review of local prehistoric findings (Urbanek, 1991). Subsequently a copy of the tooth was prepared for the Museum Burg Golling (Gollingan der Salzach) and was there exhibited as a Neandertal molar. Obviously, this last classification sheds doubts about the real taxonomy of the tooth, an issue that is not restricted to the Torrener Bärenhöhle specimen but that affects several human remains discovered decades ago, for which scanty and ambiguous information are available (Benazzi et al., 2011a; 2011b; 2014a; 2015).

In this contribution we investigate the tooth from Torrener Bärenhöhle's cave (here after called T.B.I). This tooth was microCT-scanned to digitally

study its external and internal morphology, and sampled for AMS radiocarbon dating to establish its taxonomy and chronology.

Figure 1. Torrener Bärenhöhle's tooth

Materials and Methods

Morphological description

The evaluation of T.B.I nonmetric traits was done according to standards outlined by the Arizona State University Dental Anthropology System, ASUDAS (Turner et al., 1991).

Morphometric analysis

High-resolution μCT images of T.B.I were obtained with a GE Phoenix Nanotom ® S microtomographic system (University of Applied Sciences, Wels, Austria) using the following scan parameters: 150 kV, 160 μA, 750 ms, 0.5 mm copper filter. Volume data were reconstructed using isometric voxels of 13.167 μm. The image stacks were segmented with a semiautomatic approach in Avizo

7.0 (Visualization Sciences Group Inc.) in order to separate the enamel from the dentine and to reconstruct a 3D digital model of the tooth.

The 3D model was optimized and oriented in Rapidform XOR2 (INUS Technology, Inc., Seoul, Korea) aligning the cervical plane (computed as the best-fit plane at the cervical line) parallel to the xy-plane of the Cartesian coordinate system and rotating the tooth around the z-axis according to indications provided by Benazzi and colleagues (2011c; see also Benazzi et al., 2009).The crown outline was projected onto the cervical plane and inscribed in a bounding box tangential to the most extreme points of the crown to identify the MD and BL diameters (Benazzi et al. 2013). In order to quantify 2D relative cusp area (as a percentage of the total crown base area; see Bailey, 2004), a spline curve was digitized in the fissures that separate the cusps (the digitalization of the hypocone is approximate due to Torrener Bärenhöhle's stage of wear), and then orthogonally projected on the cervical plane. The occlusal polygon was obtained connecting the dentine's horn tips, and then projected onto the cervical plane to measure the cusp angles (identified as A = protocone, B = paracone, C = metacone, D = hypocone) (Bailey, 2002; 2004; Benazzi et al., 2013).

To calculate the 2D and 3D enamel thickness we followed the guidelines provided by Benazzi and colleagues (2014b) for molars. In particular, for the 2D enamel thickness we considered the mesial plane of section, i.e. a plane passing through the mesial cusps and orthogonal to the cervical plane. The measurements recorded from the section were: the area of the enamel cap (mm^2), the area of the coronal dentine that includes the coronal pulp (mm^2), the length of the enamel-dentine junction (EDJ; mm), the 2D average enamel thickness (2D AET, mm) and 2D relative enamel thickness (2D RET, scale-free). To quantify the 3D enamel thickness, the crown was separated by the root using the interpolated surface of the cervical line (Benazzi et al., 2014b). We measured: the enamel volume (mm3), the coronal dentine volume,

which includes the volume of the crown pulp chamber(mm3), and the EDJ surface (mm2). These measurements were used for the computation of both 3D average enamel thickness (3D AET, mm) and the 3D relative enamel thickness (3D RET, scale-free) index (Fig. S2).

Metric comparison

The MD and BL diameters of T.B.I were compared to a Late Pleistocene human sample (Neandertals, N; southwest Asian Middle Paleolithic H. sapiens, MPHS; European Upper Paleolithic H. sapiens, UPHS; and modern H. sapiens, MHS) collected from the literature (Table S1). The comparative dataset for molars' relative cusp areas was collected from Bailey (2002). Comparative data for cusp angles, 2D and 3D enamel thickness were created ex novo and includes N and HS, with different wear stages (Table S2). Since cusp angles have been always measured on the occlusal external surface (Bailey, 2002), we collected new data taking cusp angles from the EDJ (Table S3). Standardized scores (Z-score) of T.B.I values were computed to establish to which group means (for N, MPHS, UPHS, MHS) the values of Torrener Bärenhöle I were closest to.

Radiocarbon dating

The root was sampled for AMS dating at the Max Planck Institute for Evolutionary Anthropology laboratory (Lab Code S-EVA). The extraction of collagen was performed on 500 mg of sample using the method established by Talamo and Richards (2011). Stable isotopic analyses were undertaken also at MPI-EVA, Leipzig, using a Thermo Finnigan Flash EA coupled to a Delta V isotope ratio mass spectrometer. For good quality collagen, the C:N ratio should be between 2.9 and 3.6, and the collagen yield no less than 1% of the sample weight (Ambrose, 1990; Klinken, 1999). The collagen was sent to the Klaus-

Tschira-AMS facility of the Curt-Engelhorn Centre in Mannheim, Germany (Lab Code MAMS), for AMS radiocarbon dating (Kromer et al., 2013).

Results

Morphological description

Torrener Bärenhöle I (T.B.I) is an upper right second molar (RM2) with both crown (MD = 8.22 mm; BL = 11.25 mm) and root (length = 18.62 mm) preserved. The tooth is moderately worn, equal to wear stage 2 based on Smith (1984). In occlusal view the crown outline is sub-square, with three main cusps (protocone, paracone and metacone), and the disto-lingual one (hypocone) markedly reduced (ASUDAS grade 2) and obscured due to tooth wear. Evidence of the hypocone is still visible on the EDJ surface, where it is possible to observe also the crista oblique. A small carious pit is present in the groove between the two buccal cusps. The carious lesion has perforated the enamel producing two cavities in the underlying dentine (Fig. 2; Fig S3) but without reaching the pulp chamber.

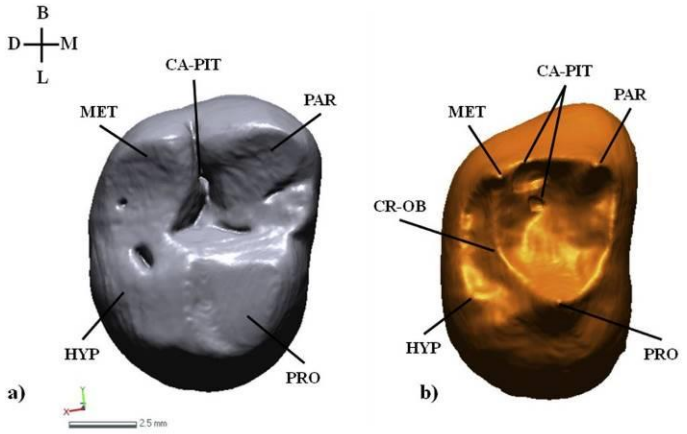

Figure 2. Torrener Bärenhöhle 1: a) 3D digital model of the crown; b) 3D digital model of the enamel-dentine junction (EDJ). PRO = Protocone, PAR =

paracone, MET = metacone, HYP = Hypocone, CR-OB = crista oblique, CA-PIT = carious pit.

An interproximal wear facet is visible only on the distal aspect of the crown (length ¼ 1.98 mm; width ¼ 1.43 mm; Fig. 3a). On both the mesial and distal aspects, at the cervix and just below the enamel, there are interproximal grooves bucco-lingually elongated, with a smooth surface and concave profile (completely different from generally flat interproximal wear facets), probably produced by the use of toothpicks (Fig. 3a, b).

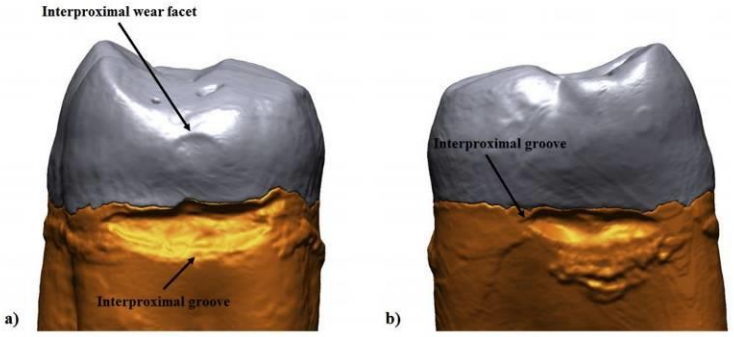

Figure 3. a) Interproximal wear facet and interproximal groove observed on the distal side of the tooth; b) Interproximal groove observed on the mesial side of the tooth.

The tooth is hypotaurodont (Taurodont Index ¼ 30.6; SOM Fig. S4) according to Keene (1966), and shows three roots: two buccal roots, which bifurcate at the cervical third, and a lingual root, which fuses mesially and distally with the buccal ones. The marked hypocone reduction, the lack of Carabelli's trait and a mesial paracone tubercle (among others; see Table 1), and the low expression of taurodontism resemble more H. sapiens than Neandertal M2s. The marked hypocone reduction and the lack of the Carabelli’s trait,

mesial paracone tubercle (among others; see Table 1), and the low expression of taurodontism resemble more H. sapiens than Neandertal M2s.

Table 1. Nonmetric dental traits observed Torrener Bärenhöle I (T.B.I) compared with their frequency (%) in Neandertal(N; n=32) and Upper Paleolithic Homo sapiens (UPHS; n=8).[a]

	Metacone reduction	**Hypocone reduction**	**Cusp 5**	**Carabelli's trait**	**Mesial paracone tubercle**	**Mesial accessory tubercle**	**Protoconule**
T. B. I	N	Y	N	N	N	N	N
N	3.1	3.1	61.9	50	60	70	77.8
UPHS	0	22.2	33.3	0	0	33.3	33.3

[a]Comparative data from Benazzi et al. 2013; Neandertal (N), Upper Paleolithic *Homo sapiens* (UPHS).

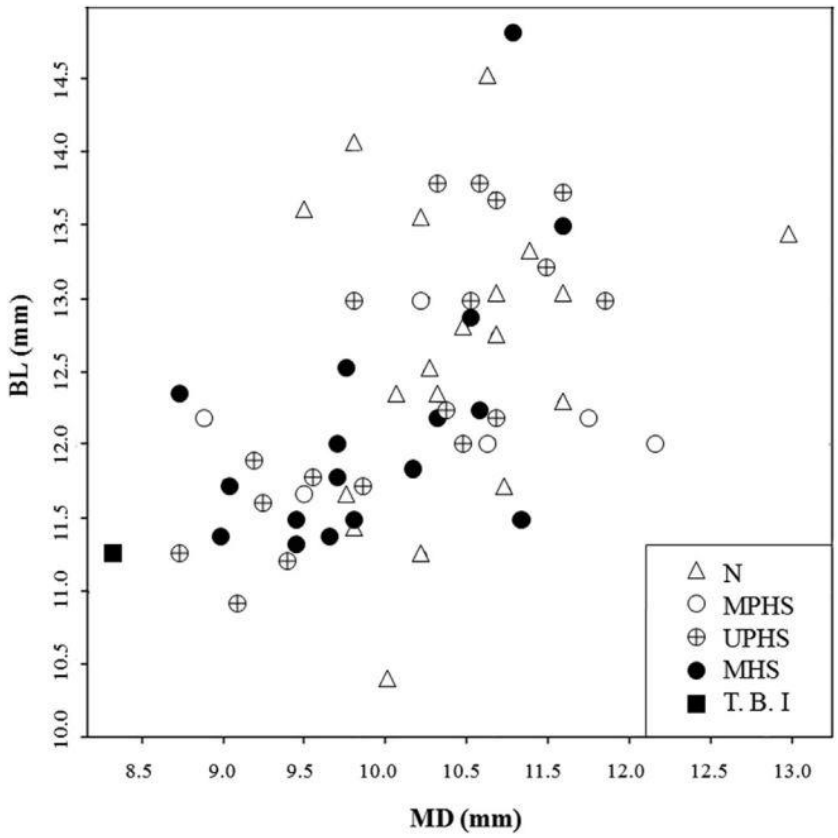

Figure 4. Scatter plot between MD and BL diameters of M2; Neandertal (N), Middle Paleolithic Homo sapiens (MPHS), Upper Paleolithic Homo sapiens (UPHS), modern Homo sapiens (MHS).

Morphometric Analysis

The scatter plot of the crown diameters shows that T.B. I is extremely small, falling in the lower range of the UPHS and MHS variability (for the MD diameter T.B. I is even the smallest tooth of our HS sample) and completely outside the Neandertal range (Fig. 4).

As regards relative cusps areas, T.B.I is closer to MHS values for protocone and metacone, whereas it is near UPHS values for paracone and

hypocone. Concerning cusps angles of the occlusal polygon area, the Z-score computed for T.B. I is near to MHS for all angles (Table 2).

The 2D enamel thickness values show a small enamel area and small coronal dentine area. The Z-score computed for the 2D RET is closer to Neandertals values (wear stage 1, 2). For the 3D relative enamel thickness, which is much more reliable than the 2D RET index (Benazzi et al., 2014b) T.B.I is closer to the HS variability (wear 1, 2) (Table 3).

Table 2. Relative cusps[a] areas and cusp angles of Torrener Bärenhöle I (T.B.I) M^2, standardized to Z-score of the hominin samples used in this study.

		N	**MPHS**	**UPHS**	**MHS**
Trait	**T. B. I**	**Mean (SD/n) Z-score**	**Mean (SD/n) Z-score**	**Mean (SD/n) Z-score**	**Mean (SD/n) Z-score**
Protocone	37,88	31,9 (2,1/11) 2,85	33,8 (2,2/3) 1,85	41,7 (5,4/7) -0,71	35,0 (3,8/79) 0,76
Paracone	31,00	28,4 (2,9/11) 0,90	25,0 (1,7/3) 3,53	30,1 (2,7/7) 0,33	29,3 (2,5/79) 0,68
Metacone	22,50	21,2 (1,7/11) 0,76	18,7 (1,8/3) 2,11	19,8 (3,3/7) 0,82	21,0 (2,5/79) 0,60
Hypocone	8,59	19,0 (3,7/11) -2,81	22,5 (2,1/3) -6,62	8,5 (4,6/7) 0,02	14,7 (5,4/79) -1,13
Cusp angles					
A	95,96	115,95 (4,58/13) -4,36			105,79 (19,00/11) -0,51
B	69,09	61,14 (9,12/13) 0,93			68,41 (9,88/11) 0,12

C	109,51	114,43 (9,14/13) -0,53		104,05 (11,96/11) 0,45
D	85,43	68,46 (5,36/13) 3,15		80,92 (20,71/11) 0,21

[a]Comparative data from Bailey (2002); Neandertal (N), Middle Paleolithic *Homo sapiens* (MPHS), Upper Paleolithic *Homo sapiens* (UPHS), modern *Homo sapiens* (MHS).

Table 3. Two-dimensional (2D) and three-dimensional (3D) relative enamel thickness. Torrener Bärenhöle I (T.B.I) is standardized to Z-scores of the Neandertal and *H. sapiens* (HS) M^2 sample in different wear stages.

Taxon	**Wear stage***	**2D RET Mean (SD/n) Range**	**Z-scores for 2D RET**	**3D RET Mean (SD/n) Range**	**Z-scores for 3D RET**
T.B.I	2	17,38		21,13	
N	1/2	18,03 (2,46/12) 13,64-21,86	-0,26	18.28 (2,54/12) 12,91-22,74	1,12
N	3	13,93 (0,47/2) 13,60-14,26	-7,34	15,32 (0,10/2) 15,25-15,39	58,1
HS	1/2	22,27	-1,16	24,24	-0,87

		(4,18/12)		(3,57/12)	
		16,91-31,41		18,35-30	
HS	3	14,55 (0,55/2)	5,14	17,49	6,38
		14,15-14,94		(0,57/2)	
				17,09-17,90	

Standard deviation is indicated in parenthesis. RET, relative enamel thickness index. * Based on Smith, 1984.

Radiocarbon dating

The isotopic values, C:N ratios and yield of collagen of the tooth were fully within the acceptable range (Table 4). The radiocarbon date of the tooth is listed in Table 4. The date was corrected for a preparation background estimated from 14C free bone samples, kindly provided by the MAMS and pretreated in the same way as the archaeological sample. The radiocarbon date is 221±23 14C BP, was calibrated using Oxcal 4.2 (Ramsey and Lee, 2013) with the IntCal13 curve (Reimer et al. 2013) (Table 4). The Bärenhöhle tooth belongs to a recent modern human dated between 1644-1950 Cal AD (95.3% confidence).

Table 4. AMS radiocarbon dating of the Bärenhöhle tooth, C:N ratios, amount of collagen extracted (%Coll) refer to the >30 kDa fraction. The calibration was performed using Oxcal 4.2 (Ramsey and Lee, 2013) with the IntCal13 curve (Reimer et al. 2013).

% Coll	**δ13 C**	**δ15 N**	**% C**	**% N**	**C: N**	**AMS**	**14 C**	**Er r**	**Calibrated**
17.93	-19.8	8.9	45.1	16.5	3.2	MAMS-24105	221	23	1644-1950 Cal AD

Discussion and conclusions

The morphological features preserved in T.B.I, in particular the presence distally of an interproximal facet and grooves in both the mesial and distal aspect of the tooth (the latter related to toothpickings), clearly support the attribution of T.B.I to an upper right second molar (RM2), and not to an upper left third molar as it held previously on the museum label.

Concerning its taxonomic classification, both non-metric and morphometric traits clearly suggest that the Torrener Bärenhöle tooth belonged to H. sapiens, not to Neandertal, individual. The only ambiguous parameter is related to the 2D enamel thickness, whose value is closer to the Neandertal mean. It is important to highlight, however, that the 2D RET index is less reliable than the 3D RET index. Indeed because the mesial section passes through the cusp tips (i.e., paracone and protocone), which are much more affected by wear than other regions of the crown (e.g., occlusal basin, lateral wall of the crown), the 2D RET index is consequently more negatively influenced by tooth wear than the 3D RET index.

Most importantly, the recent age obtained by a direct 14C dating of the tooth (1644-1950 Cal AD at 95.3% confidence) definitively excludes the possibility that T.B.I was retrieved in the Mousterian levels of Torrener Bärenhöle's cave, as proposed by Döppes and Rabeder (1998).

The Torrener Bärenhöhle is regularly flooded, and the cave bear bones as well as the tooth were found in sedimentary deposits in potholes on the cave floor (Hell 1925) with no paleontological stratification. Although Döppes and Rabeder (1998) in their register of Pliozean and Pleistozean faunal sites of Austria attributed the cave-bear bones to the early Würm, the tooth obviously has a much younger history. The most likely explanation is that the tooth comes from a individual (from around 1800) who died in the Torrenere Bärenhöhle or

a hydrologically connected cave system and was transported by water to its finding place amongst the cave bear bones.

Based on these results, the copy of the Torrener Bärenhöle's tooth was removed from display in the Museum Burg Golling. The results of the dating and the presented investigation have been added to the label and the inventory information in the Museum Haus der Natur, making sure that this tooth is not considered in future for comparative studies of fossil hominins. It is also suggested that the supposedly artificially modified bones from the Torrener Bärenhöle (Ehrenberg 1933, 1938, 1972) should be thoroughly reexamined to clarify their natural or human-made origin. Finally, this study emphasizes the need for a taxonomical/chronological reassessment of human remains discovered and studied decades ago and for which scanty archaeological/anthropological information are available (Benazzi et al., 2014a; Benazzi et al. 2013).

Acknowledgements

We are grateful to Frank Schröder, Erich Urbanek and Sebastian Krutter from the Museum Burg Golling for making us aware of the "Neandertal tooth", and Wolfgang Reichmann (NHMW) for the Photos. We also thank Rosa Conte for proofreading this manuscript.

References

Ambrose, S.H., 1990. Preparation and characterization of bone and tooth collagen for isotopic analysis. J. Archaeol. Sci. 17, 431-451.

Bailey, S.E., 2002. Neandertal dental morphology: implication for modern human origins. Ph.D. Dissertation, Arizona State University.

Bailey, S.E., 2004. A morphometric analysis of maxillary molar crowns of Middle-Late Pleistocene hominins. J. Hum. Evol. 47,183-198.

Benazzi, S., Fantini, M., De Crescenzio, F., Persiani, F., Gruppioni, G., 2009. Improving the spatial orientation of human teeth using a virtual 3D approach. J. Hum. Evol. 56, 286-293.

Benazzi, S., Douka, K., Fornai, C., Bauer, C.C., Kullmer, O., Svoboda, J., Pap, I., Mallegni, F., Bayle, P., Coquerelle, M., Condemi, S., Ronchitelli, A., Harvati, K., Weber, G.W., 2011a. Early dispersal of modern humans in Europe and implications for Neanderthal behaviour. Nature 479, 525-528.

Benazzi, S., Viola, B., Kullmer, O., Fiorenza, L., Harvati, K., Paul, T., Gruppioni, G., Weber, G. W., Mallegni, F., 2011b. A reassessment of the Neandertal teeth from Taddeo Cave (Southern Italy). J. Hum. Evol. 61, 377-387.

Benazzi, S., Coquerelle, M., Fiorenza, L., Bookstein, F., Katina, S., Kullmer, O., 2011c. Comparison of Dental Measurement Systems for

Taxonomic Assignment of First Molars. Am. J. Phys. Anthropol. 144, 342-354.

Benazzi, S., Bailey, S.E., Mallegni, F., 2013. A morphometric analysis of the Neandertal upper second molar Leuca I. Am. J. Phys. Anthropol.152, 300-305.

Benazzi, S., Peresani, M., Talamo, S., Fu, Q., Mannino, M.A., Richards, M.P., Hublin, J.-J., 2014a. A reassessment of the presumed Neandertal remains from San Bernardino Cave, Italy. J. Hum. Evol. 66, 89-94.

Benazzi, S., Panetta, D., Fornai, C., Toussaint, M., Gruppioni, G., Hublin, J.-J., 2014b.Technical Note: Guidelines for the digital computation of 2D and 3D enamel thickness in Hominid teeth. Am. J. Phys. Anthropol. 153, 305-313.

Benazzi, S., Slon, S., Talamo, S., Negrino, F., Peresani, M., Bailey, S.E., Sawyer, S., Panetta, D., Vicino, G., Starnini, E., Mannino, M.A., Salvadori, P.A., Meyer, M., Pääbo, S., Hublin, J.-J., 2015. The Makers of the Protoaurignacian and Implications for Neandertal Extinction. Science 348, 793-796.

Döppes, D., Rabeder, G. (Ed.), 1998. Pliozäne und pleistozäne Faunen Österreichs: ein Katalog der wichtigsten Fossilfundstellen und ihrer Faunen. Band 10. Verlag der Österreichischen Akademie der Wissenschaften, Wien.

Ehrenberg, K., 1933. Über Knochenartefakte aus eiszeitlichen

Höhlenablagerungen. Verhandl. Zoolog.-Botan. Ges. Wien 83.

Ehrenberg, K., 1938. Über einige artefaktverdächtige Knochenfragmente aus der Torrener Bärenhöhle (Salzburg). Wiener Prähistorische Zeitschrift XXV, 20-29.

Ehrenberg, K., Mais, K., 1970. Die Schlenkendurchgangshöhlen-Expedition 1970. Anzeiger math.-naturw. Kl. Österr. Ak. Wiss. Jg. 1971, Nr. 2 1971.

Ehrenberg, K., 1972. Bemerkenswerte Höhlenbärenknochenfunde aus der Bärenhöhle im Torrenerfall. Anzeiger der math-naturw. Klasse der Österreichischen Akademie der Wissenschaften. 10, 1-8.

Gaisberger, K., 1971. Berich. Über den Fund eines Menschenzahnes in Grabungsmaterial der Torrener Bärenhöhle.

Hell, M., 1925. Bärenhöhle am N-Hang des Hagengebirges im Dachsteinkalk. Mitteilungen über Höhlen- und Karstforschung Jahrgang 1925, Heft 3, 100.

Keene, H.J., 1966. A morphologic and biometric study of taurodontism in a contemporary population. Am. J.Phys. Anthropol. 25, 208-209.

Klappacher, W., Knapczyk, H. (Ed.), 1979. Salzburger Höhlenbuch - Band 3. Landesverein für Höhlenkunde in Salzburg. Burgfriedverlag. Salzburg.

Klappacher, W. (Ed.), 1992. Salzburger Höhlenbuch - Band 5. Landesverein für Höhlenkunde in Salzburg, Eigenverlag, Salzburg.

Klinken, G.J.V., 1999. Bone collagen quality indicators for palaeodietary and radiocarbon measurements. J. Archaeol. Sci. 26, 687-695.

Kromer, B., Lindauer, S., Synal, H.-A.,Wacker, L., 2013. MAMS-a new AMS facility at the Curt-Engelhorn-Centre for Achaeometry, Mannheim, Germany. Nucl.Instrum.Meth. B 294, 11-13.

Ramsey, C.B., Lee S., 2013. Recent and planned developments of the program OxCal. Radiocarbon 55,720-730.

Reimer P.J., Bard, E., Bayliss, A., Beck J.W., Blackwell, P.G., Bronk Ramsey, C., Buck, C.E., Cheng, H., Edwards, R.L., Friedrich, M., Grootes, P. M., Guilderson, T.P., Haflidason, H., Hajdas, I., Hatté, H., Heaton, T.J., Hoffmann, D.L., Hogg, A.G., Hughen, K.A., Kaiser, K.F., Kromer, B., Manning, S.W., Niu, M., Reimer, R.W., Richards, D.A., Scott, E.M., Southon, J.R., Staff, R.A., Turney, C.S.M., Plicht, J.V.D., 2013. IntCal13 and Marine13 Radiocarbon Age Calibration Curves 0-50,000 Years cal BP. Radiocarbon 55, 1869-1887.

Smith, B.H., 1984. Patterns of molar wear in hunter-gatherers and agriculturalists. Am. J. Phys. Anthropol. 63, 39-56.

Talamo, S., Richards, M., 2011. A comparison of bone pretreatment methods for AMS

dating of samples >30,000 BP. Radiocarbon 53, 443-449.

Turner, C.G.II, Nichol, C.R., Scott, G.R., 1991. Scoring Procedures for Key Morphological Traits of the Permanent Dentition: The Arizona State University Dental Anthropology System. In: Kelley, M.A., Larsen, C.S. (Eds.), Advances in Dental Anthropology. Wiley-Liss, New York, pp. 13-31.

Urbanek, E., 1991.Wichtige ur- und frühgeschichtliche Fundpunkte. In: Hoffmann, R., Urbanek, E. (Eds.), Golling - Geschichte einer Marktgemeinde. Eigenverlag der Marktgemeinde Golling, pp. 43-70.

Quateranry International
(Quaternary International, 425; 437-444.)

A reassessment of the Middle Paleolithic human remains from Riparo Tagliente, Italy

Julie Arnaud[a*], Carlo Peretto[a], Daniele Panetta[b], Maria Tripodi[b], Federica Fontana[a], Marta Arzarello[a], Ursula Thun Hohenstein[a], Claudio Berto[a], Benedetto Sala[a], Gregorio Oxilia[c,d], Piero A. Salvadori[b], Stefano Benazzi[d,e]

[a]Department of Humanities, Section of Prehistorical and Anthropological Sciences, University of Ferrara, LT, Teknehub, C.so Ercole I d'Este 32, 44121 Ferrara, Italy.
[b]CNR Institute of Clinical Physiology, Via G. Moruzzi 1, 56124, Pisa, Italy.
[c]Department of Biology, University of Florence, Via del Proconsolo, 12, 50122 Firenze, Italy.
[d]Department of Cultural Heritage, University of Bologna, Via degli Ariani 1, 48121, Ravenna, Italy.
[e]Department of Human Evolution, Max Planck Institute for Evolutionary Anthropology, Deutscher Platz 6, 04103, Leipzig, Germany

Introduction

Paleoanthropological research is often biased by the small sample size, which limits our perception of human variability. There is a constant need to update and develop the methods considered fundamental, for the progress of the discipline. The discovery of new fossil remains has an important place in the understanding of taxon variability, but the assessment and reassessment of specimen already present in collection and forgotten by the scientific community constitute further opportunities. For the latter, very limited and sometimes imprecise information is available and most of the time, it is to the international community at large (Benazzi et al., 2015, 2013a, 2013b, 2011b, 2011c).

This is the case for the two teeth discovered in the Mousterian deposits of Riparo Tagliente (Stallavena di Grezzana, Verona) during excavations directed by A. Guerreschi and C. Peretto (Bartolomei et al., 1982; Villa et al., 2001).

Even though Riparo Tagliente is well known through the exhaustive study of its lithic industries and faunal remains, these two human specimens have only been published in the proceeding of a national congress (i.e. XIII Congresso dell'Associazione degli Antropologi italiani, Villa et al., 2001), a paper that is not available easily to the scientific community and which contains only partial description of the human remains. For this reason, among others, Tagliente 3 and Tagliente 4 were never used in reference collections for morphological and morphometric comparison.

In general, Neandertals deciduous teeth are less studied than permanent teeth, from which numerous useful protocol have been (Bailey, 2004; Benazzi et al., 2011a; Gómez-Robles et al., 2008). In the last few years the tendency has gradually changed and useful protocols have been developed for the taxonomical investigation of deciduous dentition (Bailey and Hublin, 2006; Bailey et al., 2016, 2014a, 2014b; Bayle, 2008; Bayle et al., 2010, 2009a,

2009b; Benazzi et al., 2012, 2015, 2014a; Fornai et al., 2014; Grine, 2005; Macchiarelli, 2013; Macchiarelli et al., 2006; Mahoney, 2013, 2010; Toussaint et al., 2010; Zanolli et al., 2010), but still further work is required to understand the morphological and morphometric variability of hominin deciduous teeth.

Therefore, in this contribution we present a reassessment of the Tagliente 3 and Tagliente 4 human deciduous teeth through a detailed morphological and metrical description based on micro-CT imaging.

Results and data generated may be useful for the integration of these deciduous human remains in future comparative samples and show how the reconsideration of forgotten fossils can bring new information on taxonomic variability.

Riparo Tagliente

Riparo Tagliente (Stallavena di Grezzana, Verona, N-E Italy) lies on the west slope of Valpantena, one of the main valley-bottoms of the pre-Alpine massif of Monti Lessini, at an altitude of 250 m AMSL (Fig.1a). The rock-shelter occupies a strategic position at the crossroads of different topographic formations - the plain, the valley-bottom, the rocky slopes and the top of the massif - matching a mosaic of landscapes rich in different faunal and vegetal resources, which have varied in distribution over time. The limestone nature of the massif has led to several karst cavities and brought abundant lithic and mineral resources, namely a variety of cherts, which were extensively exploited by the inhabitants of the Palaeolithic site. Discovered in 1958 by Francesco Tagliente, the site was initially investigated, from 1962 to 1964, by the Museo Civico di Storia Naturale of Verona. In 1967 excavations were resumed by the University of Ferrara and are still in progress. Up to the mid-seventies research focused mostly on the excavation of a long trench running transversally to the rock-shelter and a smaller one located in the most internal area (Southern sector, Fig.1d). A 4.50 m deep stratigraphic series was thus brought to light formed by

two main deposits separated by river erosion: a lower one referred to MIS 4-3 occupation with Mousterian and Aurignacian assemblages and an upper one dated to the Lateglacial attesting a Late Epigravettian occupation (Fig.1a and c). From the late ‘70s onwards extensive excavations were undertaken in the northern area of the site.

The Mousterian sequence, which represents the focus of this paper, begins with colluvial deposits and thermoclastic sediments (levels 52-44). This unit is covered by a massive rockfall and by clasts derived from the degradation of the walls of the rockshelter (levels 43-40). In the upper part (levels 39-31), loess sediments prevail. The teeth Tagliente 3 and Tagliente 4, were recovered in levels 36βI-βII and 37bαII, respectively. At the top of this sequence, and in apparent stratigraphic continuity, level 25 contains an Aurignacian industry with Dufour bladelets.

Small mammals are mostly documented by dental remains (Bartolomei et al., 1982). The assemblage is dominated by Microtus arvalis in the whole sequence (except for level 25), with the presence of cold indicators such as Microtus oeconomus, Microtus gregalis, Ochotona sp. and Sicista sp. These species are replaced by Chionomys nivalis and Apodemus sp. in the upper layers (from 35 to 31) suggesting a less continental condition with an increase in humidity even though low temperatures continue.

The majority of the large mammal remains analyzed from the uppermost Mousterian levels (41-35) consists of teeth, mandible fragments, limb elements, vertebrae, and sesamoids belonging to adults and sub-adults ungulates (Thun Hohenstein and Peretto, 2005). The most represented species is roe deer, followed by red deer, ibex and chamois; among the carnivores, wolf and bear dominate; marmot remains have been identified among the rodents. In the lower levels (44-52), the composition of the faunal assemblage remains unchanged among the artiodactyls, while carnivores increase in the number of faunal remains, along with a greater variety of taxa being represented (wolf,

fox, bear, leopard, mustelids). The abundance of roe deer, and the presence of elk and marmot may suggest a relatively cold-temperate and a rather humid climate. The presence of foetal or neonatal cervid bones indicates that Neandertals occupied the rockshelter mainly during the spring (Thun Hohenstein and Peretto, 2005). Cutmarks and intentional bone fracturing are well documented along the whole sequence, mostly on artiodactyls and on some marmot remains (Alhaique et al., 2004).

The Mousterian sequence is characterized by the use of different reduction methods, all on local raw materials (chert) collected in a secondary position in the surroundings of the site. The most represented method is the opportunistic method (c.f. S.S.D.A, Forestier, 1993). The Levallois method (Boëda, 1994) is also present within the lineal and recurrent modalities represented. In the lower levels, centripetal recurrent Levallois is the most frequent, but in the upper part of the sequence, unipolar recurrent Levallois becomes dominant (Arzarello and Peretto, 2005). The discoid method (Boëda, 1993) is also attested to, and in some cases is used, the final reduction of the Levallois cores. One of the most important peculiarities of the lithic assemblage is the presence of a volumetric laminar debitage starting from level 37 (Arzarello and Peretto, 2005). The retouched assemblage is mainly represented by side-scrapers and denticulates made on opportunistic and more rarely on Levallois flakes.

Up until now, no radiometric dating has been undertaken on the Mousterian stratigraphical sequence. However, the faunal assemblage and the sedimentological analysis suggests a chronology spanning between MIS 3 and MIS 4 (Bartolomei et al., 1982).

The two human teeth were discovered in 1979 (Tagliente 3) and in 1998 (Tagliente 4) in the Mousterian deposits, respectively 36βI-βII and 37bαII.

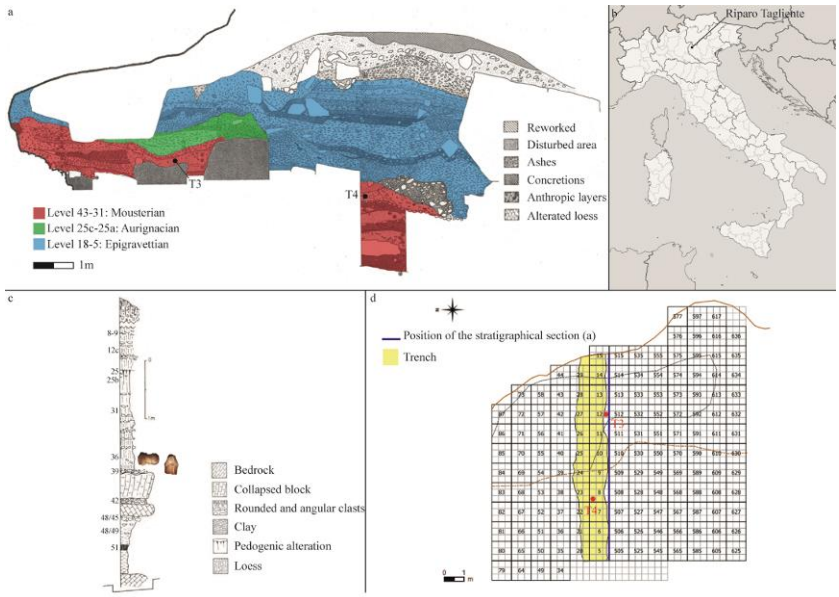

Figure 1: Riparo Tagliente, stratigraphical transversal section of the deposit (a); geographical position of the site (b); simplified stratigraphy of the deposits in the southern area (c); planimetry of the excavation area (d) (modified from Bartolomei et al., 1982, 1984).

1. Material and Methods

1.1. Micro-CT scan

High-resolution micro-CT images of Tagliente 3 and Tagliente 4 were obtained with the Xalt micro-CT scanner (Panetta et al., 2012). All teeth were scanned at 50 kVp, 2 mm Al filtration, 800 projections over 360°, 2.1 mAs/projection for a total scan time of 40 minutes per sample. All the tomographic images were reconstructed using a modified Feldkamp algorithm (Feldkamp et al., 1984) with embedded compensation for mechanical misalignments and raw data pre-correction for beam-hardening and ring artifacts reduction. All images were reconstructed on a volume dataset of 8503 cubic voxels, each with a size of 18.4 μm3. The micro-CT images of the original sample were virtually segmented using Seg3D (http://www.seg3d.org).

The segmented enamel cap and virtually filled dentin were converted to meshes using the Windged-Edge Mesh (WEM) tool of the MeVisLab software (http://www.mevislab.de).

1.2. Morphological description and metric comparison

Metric and non-metric traits were evaluated on the digital models. The assessment of non-metric traits was made based on standards outlined by the Arizona State University Dental Anthropology System, ASUDAS (Turner et al., 1991). Although ASUDAS has been devised for modern human permanent dentition, we applied the protocol to collect non-metric dental traits for the deciduous teeth. Ages at death for the deciduous teeth were assessed using a combination of different observations, such as tooth formation, dental eruption and root resorption through recent modern human references provided by Moorrees et al. (1963), Ubelaker (1978) and AlQahtani (2010).

For metric traits, we measured the mesio-distal (MD) and bucco-lingual (BL) diameters on the digital model. The dimensions obtained were then compared to a sample of Neandertals (N), Upper Paleolithic Homo sapiens (UPHS) and recent Homo sapiens (RHS) collected from Crevecoeur et al. (2010), Tixier and Tillier (1991) and Foster et al. (1969).

In order to compute dental tissue proportions two different approaches were applied to separate the crown dentine from the root dentine. The first method, which was carried out in Avizo v7.1 (Visualization Sciences Group Inc.), entails an average plan situated equidistantly between “The most apical plane of section containing a continuous ring of enamel at the cervix...” and “…the most apical plane that is both parallel to the continuous ring of enamel and which contains the most apical extension of enamel…” (Olejniczak, 2006: 127). The second method, which was carried out in Rapidform XOR (INUS Technology, Seoul, Korea), follows recent indications provided by Benazzi and colleagues (2014): a spline curve was digitized on the cervical line to isolate the

coronal dentine, which was then sealed at the bottom by a smooth surface interpolating the curve itself. The following measurements were collected: Ve = Volume of enamel (in mm3), Vcdp = Volume of dentine and pulp in the crown (in mm3), Vcd = Volume of dentine in the crown (in mm3), Sedj = Surface area of the enamel-dentine junction (in mm2), AET = average of enamel thickness (Ve/Sedj) (mm) and RET = relative enamel thickness (AET/(Vcdp)1/3) (scale-free).

The results were compared to those obtained by Bayle et al. (2009a, 2010) for unworn or slightly worn teeth in a reduced sample of Neandertals, UPHS and RHS. It is worthwhile noting that Bayle and colleagues used the first method which was not developed for anterior teeth. It is for this reason we include enamel thickness data using recent guidelines (Benazzi et al., 2014), even though no comparative data is available (see discussion for more considerations).

Finally, we performed 3D topographic mapping of enamel distribution as the minimum distance between the external enamel surface and the underlying EDJ, and the results were displayed using a chromatic scale (from dark blue to red).

Table 1. Dental dimensions (in mm) of the Tagliente teeth compared to a reference sample composed of Neandertals (N); Upper Paleolithic Homo sapiens (UPHS); RHS = recent H. sapiens (RHS) (m = mean; s = standard deviation; n = number of individuals).

		dm^2	dLc
		BL	BL
		m ± s (n)	m ± s (n)
Tagliente		10.2	6.7
N		10.3 ± 0.4 (13)[a]	6.0 ± 0.5 (23)[b]
UPHS		10.5 ± 0.5 (15)[a]	6.0 ± 0.4 (21)[b]
RHS	European (UK)[c]	9.3 ± 0.7 (100)	5.2 ± 0.6 (100)

[a] Tixier and Tillier, 1991.
[b] Crevecoeur et al., 2010.
[c] Foster et al., 1969.

2. Results

Tagliente 3: Upper right second deciduous molar (Rdm2), represented by an incomplete crown and root almost completely resorbed (Fig. 2). The crown present an advanced stage of occlusal wear (stage 4 based on Molnar, 1971) and is broken disto-lingually, affecting almost the entire hypocone. In the mesio-buccal side, a large flake of enamel is missing, exposing the underlying dentine (Fig. 2). On the occlusal surface, three main cusps are still visible, and a distal enlargement, near the disto-lingual fracture of the crown suggests that a large hypocone was present. When the enamel is digitally removed, the remnants of three principal cusps, as well as a complex pattern of grooves, crests and accessory cusps are visible on the EDJ. The paracone is the larger cusp, probably followed by the hypocone (this inference is based on the trend of the EDJ outline), the protocone and finally the metacone. The size of the protocone is reduced, owing to the large Carabelli's tubercle, corresponding to a grade 7 according to Ortiz et al. (2012) (Fig. 3). This Carabelli's cusp is connected to the apex of the protocone by a "cingulum protocone-crest"(Korenhof, 1960). The protocone is in contact with the metacone by an oblique crest, from which secondary crests are rooted. A C5 cusp appears on the distal ridge, between the metacone and the hypocone (Fig. 3). Moreover, an anterior fovea is bordered distally by a small crest that connects the mesial slopes of the paracone and the protocone (Fig. 3).

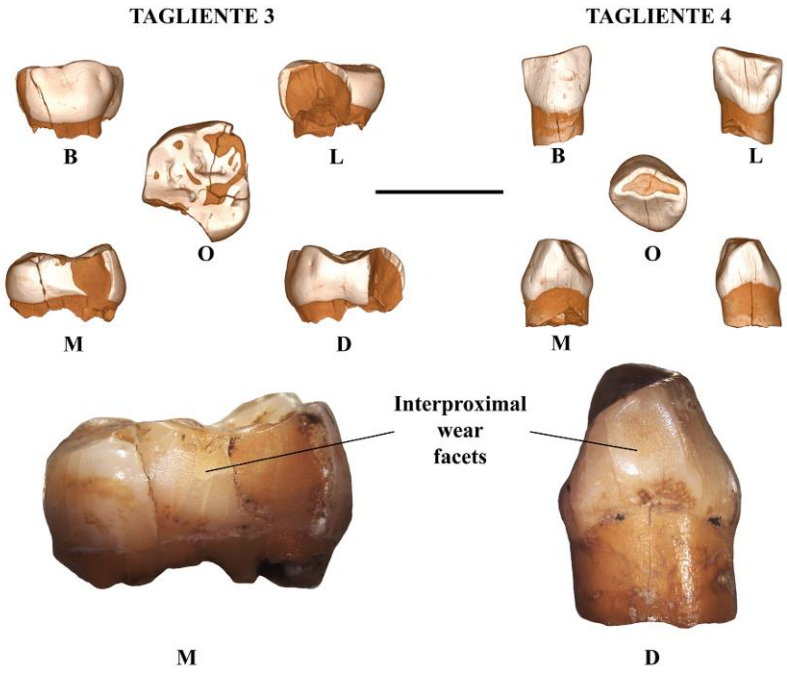

Figure 2: Three-dimensional digital models of Tagliente 3 and Tagliente 4. Binocular microscope images (magnification 25x) of the mesial (Tagliente 3) and distal (Tagliente 4) interproximal wear facets. The black bar is equivalent to 1 cm. B, buccal; D, distal; L, lingual; M, mesial; O, occlusal.

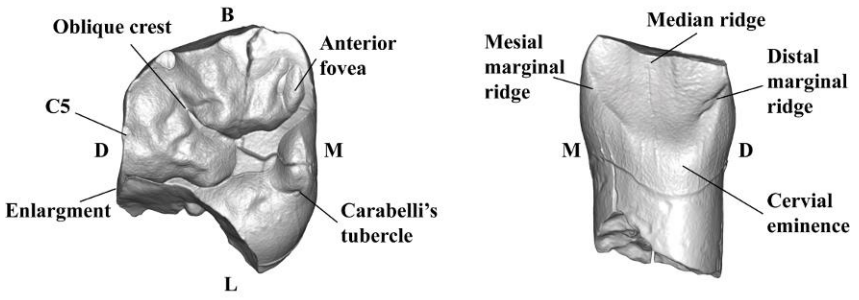

Figure 3: 3D digital model of the mesial. enamel-dentine junction (EDJ) of Tagliente 3 and Tagliente 4. B, buccal; D, distal; L, lingual; M,

Both the mesial and the distal aspects bear interproximal wear facets, which were partially removed by fractures (Fig. 2). The preserved mesial facet (length = 2.5mm; height = 2.3mm) is larger than the distal ones. The latter is split into two facets, a smaller facet displaced buccally (length = 1.5mm; height = 1.3mm), and a larger, but broken, facet displaced lingually (length = 1.4mm; height = 2.4mm).

Root resorption suggests that the tooth had been lost ante-mortem due to the eruption of the permanent fourth premolar. The degree of resorption (stage Res3/4 of Moorrees, 1963) corresponds to an age ranging from about nine to 12 years based on the work of Shackelford et al. (2012). There is no evidence of either caries or enamel hypoplasia.

The tooth crown has a MD diameter of 9.0 mm (minimum estimation due to interproximal wear and crown facture) and a BL diameter of 10.2 mm (minimum estimation due to crown facture) (Table 1). At the cervix, the MD diameter is 6.9 mm (the BL diameter cannot be measured).

Comparative data for the BL diameter is reported in Table 1. The computed Z-score of Tagliente 3 is closer to the Neandertal mean than to the Upper Paleolithic and the recent Homo sapiens ranges of variation.

Table 2. Linear, surface and volumetric dimensions of Tagliente 4 (calculated with both methods) compared to Neandertals (N), Upper Palaeolithic Homo sapiens (UPHS) La Madeleine 4 (LM4) and Lagar Velho 1 (LaVe1) and Recent Homo sapiens (RHS) deciduous lower cani ne (from Bayle et al., 2009a, 2010). (Ve = total volume of enamel; Vcdp = volume of dentine+pulp in the crown; Vcd = Volume of dentine in the crown; Sedj = Surface area of the enamel-dentine junction; AET = Average of Enamel Thickness; RET = Relative Enamel Thickness).

Lc		Ve (mm^3)	Vcdp (mm^3)	Vcd (mm^3)	Sedj (mm^2)	AET (mm)	RET
Tagliente 4 (Olejniczak, 2006)		27.80	85.83	82.67	88.80	0.31	7.40
Tagliente 4 (Benazzi et al., 2014a, b)		27.77	89.96	86.84	86.22	0.32	7.19
N (n = 5)	Mean	32.78	87.67	75.00	91.99	0.36	8.02
	Range	*25.52–37.86*	*76.87–110.91*	*49.79–101.14*	*85.51–104.34*	*0.30–0.39*	*7.02–8.74*
UPHS	LM4	32.87	59.76	56.16	70.76	0.46	11.88
	LaVe1	36.73	68.66	62.72	73.49	0.50	12.21
RHS (n = 4)	Mean	32.49	48.51	44.25	65.23	0.50	13.66
	Range	*29.97–40.22*	*35.03–55.8*	*32.93–48.98*	*49.78–75.42*	*0.41–0.59*	*10.71–15.78*

Italics represent the range of variation (min-max).

Due to the poor integrity of Tagliente 3, volumetric comparison was not performed. Nevertheless, topographic mapping shows a thinner lateral enamel thickness distribution (mainly in the cervical third), similar to the pattern observed for the Roc de Marsal Neandertal children (Fig. S1) (Zanolli et al., 2010).

Tagliente 4: Lower right deciduous canine (LRdc) with a well-preserved crown and about one-fourth of the root preserved (Fig. 2). The enamel shows several longitudinal fractures from the cervix to the incisal surface, which do not affect the underlying dentine. The incisal surface is worn obliquely, mesially to distally, exposing a large area of dentine equivalent to wear stage 4 (Molnar, 1971). From the incisal view the crown appears asymmetrical, mainly due to the distal projection of a moderate lingual cervical eminence (but no tubercle-like structure). The buccal surface exhibits mesio-distal convexity, which is maximum mesially (ASUDAS grade 4) but almost concavely flattened distally, thus contributing to the asymmetry of the tooth. The lingual surface is concave, bordered by a moderate mesial and a more

marked distal marginal ridge, as well as a median ridge (as also clearly shown in the EDJ, Fig. 3), which merge at the cervical eminence giving a semishovel shaped aspect of the crown (ASUDAS grade 4). This general morphology, the moderate buccal bulging of the crown and the reduced flaring of the mesial and distal sides are more consistent with a lower than an upper deciduous canine.

Interproximal wear facets are visible on the mesial and distal sides (Fig. 2), the distal being more extensive (length = 2.6mm; height = 2.6mm) than the mesial (length = 1.3mm; height = 2.8mm).

The preserved root, slightly more elongated labially (midlabial height = 2.9 mm) than lingually (midlingual height = 2.5 mm), is resorbed (stage Res3/4 of Moorrees, 1963), confirming an age of approximately six years on the basis of recent human standards (AlQahtani et al., 2010; Ubelaker, 1978). There is no evidence of either caries or enamel hypoplasia.

The tooth crown has a MD diameter of 6.8 mm (minimum estimation due to wear) and a BL diameter of 6.7 mm (Table 1). At the cervix, the MD diameter is 5.1 mm and BL diameter is 6.1 mm.

The comparative analysis of the BL diameter of Tagliente 4 is reported on Table 1. The computed Z-score is closer to the Neandertal mean but not far from UPHS variability. However, the dimensions of Tagliente 4 are clearly out of the range of variability of RHS. Enamel thickness values obtained using the two protocols (Benazzi et al., 2014b; Olejniczak, 2006) should be considered with caution, as 1) the tooth is heavily worn and 2) the comparative sample size is extremely low (Table 2). Even though there are differences in using the two approaches, in both cases Tagliente 4 falls inside the Neandertal range of variation in terms of crown dentine volume (86.84 – 82.67 mm3), surface area of the EDJ (88.80 – 86.22 mm2), AET (0.31 – 0.32 mm) and RET (7.19 – 7.4) indexes (Table 2, Fig. S2).

3. Discussion

Morphological variability of hominin deciduous teeth has been less explored than the permanent dentition. Moreover, in several cases the information is unknown to the international scientific community (e.g., published in national journals) (Benazzi et al., 2015, 2011b) and, when available, it might be inaccurate, as demonstrated after their reassessment (Benazzi et al., 2013b, 2011b, 2011c). Therefore, it is important to provide a detailed morphological description of these fossil remains using state-of-the art techniques, making the data available to the scientific community for further investigation, and for the development of accurate methodologies for the analysis of deciduous dentition.

3.1. Classification

While we confirm the identification of Tagliente 3 as an upper right second deciduous molar, as proposed by Villa and colleagues (2001) by the pattern of the enamel-dentine junction, the situation for Tagliente 4 is different. This specimen has been previously assigned to an upper left deciduous canine (Villa et al., 2001). The morphological reassessment of this tooth and the investigation of the internal structure configuration (EDJ) has allowed for the reconsideration of Tagliente 4 as a lower right deciduous canine.

3.2. Taxonomic considerations

In the case of Tagliente 3, the investigation of the internal structure (i.e. EDJ) has revealed, and clarified some Neandertal derived features on the configuration of the occlusal surface. For instance, the distribution of enamel thickness fits the configuration of some Neandertals specimens (Fig.S1). Furthermore, the pattern of traits on the EDJ is frequently observed in Neandertal's first permanent molar (Bailey, 2006; Bailey et al., 2014b): presence of a distal enlargement near the disto-lingual fracture (the remnant of a

large hypocone), a Carabelli's tubercle, a C5 and an overall complex EDJ morphology (Fig. 3). Since Bailey et al. (2014a) suggest a strong correlation between M1 and dm2, we can attribute the specimen Tagliente 3 to Neandertals. It is worthwhile noting that the Tagliente 3 EDJ revealed the presence of a direct connection between Carabelli's cusp and the mesial marginal ridge, a configuration that was not observed by Ortiz et al. (2012), suggesting that the variability of expression of the Carabelli's trait is larger than what was previously thought.

The taxonomic attribution of Tagliente 4, based on its morphology, is less obvious because of the lack of discriminative morphological features in deciduous canines. However, based on the BL diameter, the tooth plots in the upper range of the Neandertal variability, and outside the RHS range of variation. Similar affiliation to Neandertal is further suggested by the dentine volume (the minimum volume due to tooth wear) and the RET index within Neandertal range of variation and outside UPHS and RHS, even though the latter should be considered with caution as the heavy occlusal wear has affected and reduced the original index (i.e., the RET index computed for an unworn tooth). Further studies need to 1) increase the deciduous canines sample size and 2) test the influence of tooth wear on the computation of the indexes in the canines, as recently carried out for the lower second deciduous incisor (Benazzi et al., 2015).

We also point out the possibility that Tagliente 3 and Tagliente 4 might belong to the same individual. In fact, in terms of root resorption, occlusal wear and relative dimensions, both teeth present a similar pattern. Furthermore, the level 36βI-βII bearing Tagliente 3 is highly affected by bioturbation, consequently it might be possible that both teeth belong to the same level and the same individual.

3.3. Methodological considerations

For the definition of the crown area we applied two different approaches, one based on the elaboration of an average plane (Olejniczak, 2006) and the other using the cervical line itself to separate the coronal dentine from the root dentine (Benazzi et al., 2014b). We choose to apply both approaches because the data from the reference sample was collected following the first procedure (Bayle et al., 2010). Nevertheless, this protocol has not been conceived for anterior teeth because 1) it does not take into consideration the sinus trend of the cervical lines and 2) it is observer dependent. The second approach, on the other hand, has been specifically developed for anterior dentition. Our results show that the Olejniczak (2006) approach tends to underestimate the "true" volume of the elements (i.e.Ve, Vcdp and Vc, Tab. 2). It appears, then, essential in the future to spread and apply this new protocol in order to build a consistent reference sample.

Conclusions

The reassessment of the two human remains from Riparo Tagliente has revealed its importance by bringing out new data on the variability of Neandertal deciduous dentitions, useful for further investigation. Tagliente 3 has confirmed the complex morphology of the EDJ structure found in Neandertals dm2, while Tagliente 4 has increased the known Neandertal deciduous canine range of variation. Finally, both teeth have shown the importance of using internal structure parameters, in particular dentine volume for taxonomic attribution.

The lack of a precise radiometric date for the teeth makes it difficult to carry out a consistent comparative analysis with coeval specimens and, consequently, a proper integration into the evolutionary context of the Italian peninsula. Although the two specimens can be referred, on a stratigraphical

basis, to the time range included between MIS 4-3, it seems necessary to undertake radiochronological dating for future studies.

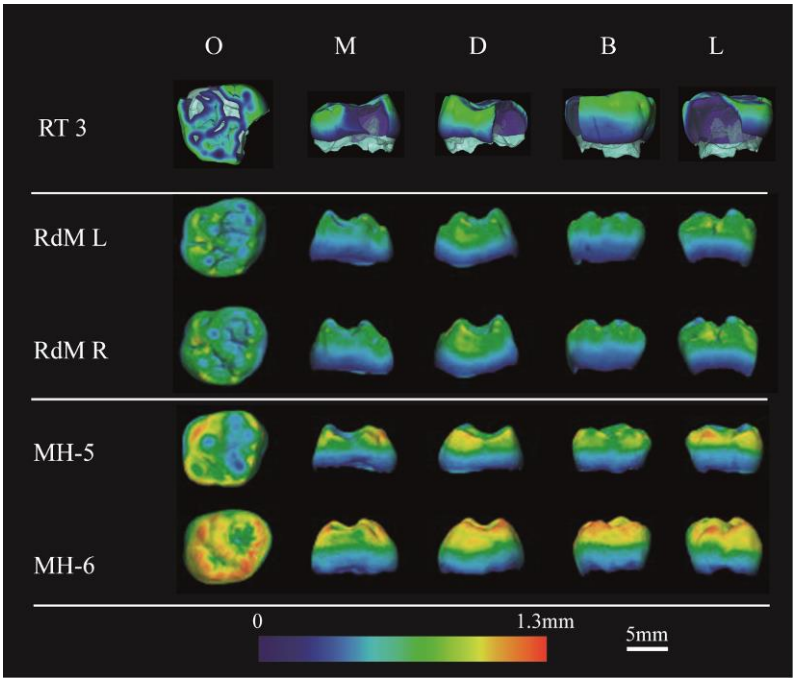

Figure S1 : Topographic maps of enamel thickness distribution of Tagliente 3 compared to right and left deciduous upper second molar from the Roc de Marsal Neandertal children (RdM L and RdMR) and two modern human dm^2 (MH-5 and MH-6) (from Zanolli et al., 2010). Images of Tagliente 3 are mirrored to fit the orientation of the comparative specimens. The chromatic scale range from the thinner (dark-blue) to the thicker (red) enamel. O, occlusal; M, mesial; D, distal; B, buccal; L, lingual.

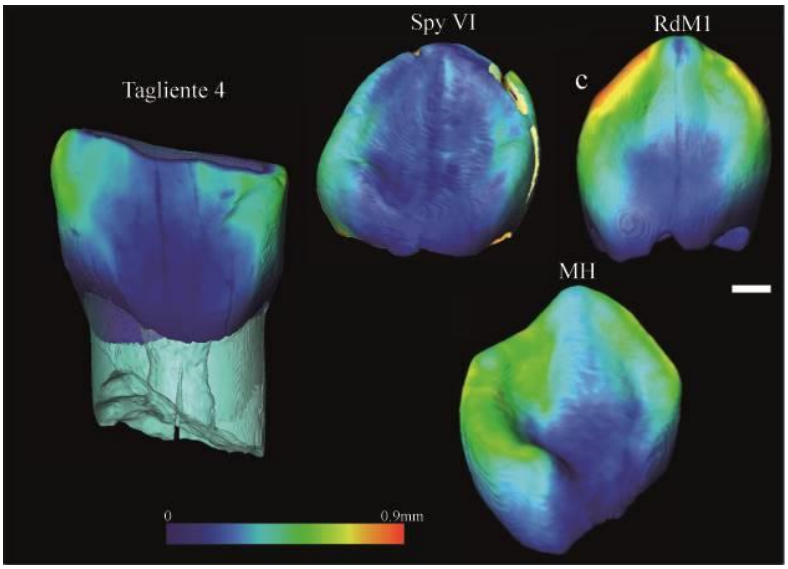

Figure S2: Topographic maps of enamel thickness distribution of Tagliente 4 compared to deciduous lower left canine from the Roc de Marsal and Spy VI Neandertal child (RdM1 and Spy VI) and a modern human (MH) (from Crevecoeur et al., 2010). Images of Tagliente 4 are mirrored to fit the orientation of the comparative specimens. The chromatic scale range from the thinner (dark-blue) to the thicker (red) enamel. O, occlusal; M, mesial; D, distal; B, buccal; L, lingual. The white bar is equivalent to 1 mm.

Bibliographical references

Alhaique, F., Bisconti, M., Bietti, A., Castiglioni, E., Cilli, C., Fasani, L., Giacobini, G., Grifoni, R., Guerreschi, A., Iacopini, A., Malerba, G., Peretto, C., Recchi, A., Rocci Riss, A., Ronchitelli, A., Rottoli, M., Thun Hohenstein, U., Tozzi, C., Visentini, P., Wilkens, B., 2004. Animal resources and subsistence strategies. Coll. Antropol. 28, 23–40.

AlQahtani, S.J., Hector, M.P., Liversidge, H.M., 2010. Brief communication: The London atlas of human tooth development and eruption. Am. J. Phys. Anthropol. 142, 481–90. doi:10.1002/ajpa.21258

Arzarello, M., Peretto, C., 2005. Nouvelles données sur les caractéristiques et l'évolution techno-économique de l'industrie moustérienne du Riparo Tagliente (Verone, Italie), in: Molines, N., Moncel, M.H., Morrier, J.L. (Eds.), Le Premiers Peuplements En Europe. Colloque International : Données Récents Sur Les Modalités de Peuplement et Sur Le Cadre Chronostratigraphique, Géologique et Paléogéographique Des Industries Du Paléolithique Ancien et Moyen En Europe. BAR International Series 1364, Archaeopress, Oxford, pp. 281–289.

Bailey, S.E., 2006. The evolution of non-metric dental variation in Europe. Mitteilungen der Gesellschaft für Urgeschichte 15.

Bailey, S.E., 2004. A morphometric analysis of maxillary molar crowns of Middle-Late Pleistocene hominins. J. Hum. Evol. 47, 183–198.

Bailey, S.E., Benazzi, S., Buti, L., Hublin, J.-J., 2016. Allometry, Merism and tooth shape of the lower second deciduous molar and first permanent molar. Am. J. Phys. Anthropol. 159, 93–105.

Bailey, S.E., Benazzi, S., Hublin, J.-J., 2014a. Allometry, Merism and tooth shape of the upper deciduous M2 and permanent M1. Am. J. Phys. Anthropol. 154, 104–114.

Bailey, S.E., Benazzi, S., Souday, C., Astorino, C., Paul, K., Hublin, J.-J., 2014b. Taxonomic differences in deciduous upper second molar crown outlines of Homo sapiens, Homo neanderthalensis and Homo erectus. J. Hum. Evol. 72, 1–9. doi:10.1016/j.jhevol.2014.02.008

Bailey, S.E., Hublin, J.-J., 2006. Dental remains from the Grotte du Renne at Arcy-sur-Cure (Yonne). J. Hum. Evol. 50, 485–508.

Bartolomei, G., Broglio, A., Cattani, L., Cremaschi, M., Guerreschi, A., Mantovani, E., Peretto, C., Sala, B., 1982. I depositi Wurmiani del Riparo Tagliente. Ann. dell'Università di Ferrara XV, 51–105.

Bartolomei, G., Cattani, L., Cremaschi, M., Favero, V., Paganelli, A., 1984. L'evoluzione dell'ambiente nel Quaternario, in: Verona, B.P. di (Ed.), Il Veneto Nell'antichità, Preistoria E Protostoria. Verona, pp. 43–141.

Bayle, P., 2008. Analyses quantitatives par imagerie à haute résolution des séquences de maturation dentaire et des proportions des tissus des dents déciduales chez les Néanderthaliens et les Hommes modernes. Toulouse 3.

Bayle, P., Braga, J., Mazurier, A., Macchiarelli, R., 2009a. Brief communication: high-resolution assessment of the dental developmental pattern and characterization of tooth tissue proportions in the late Upper Paleolithic child from La Madeleine, France. Am. J. Phys. Anthropol. 138, 493–8. doi:10.1002/ajpa.21000.

Bayle, P., Braga, J., Mazurier, A., Macchiarelli, R., 2009b. Dental developmental pattern of the Neanderthal child from Roc de Marsal: a high-resolution 3D analysis. J. Hum. Evol. 56, 66–75. doi:10.1016/j.jhevol.2008.09.002

Bayle, P., Macchiarelli, R., Trinkaus, E., Duarte, C., Mazurier, A., Zilhão, J., 2010. Dental maturational sequence and dental tissue proportions in the early Upper Paleolithic child from Abrigo do Lagar Velho, Portugal. Proc. Natl. Acad. Sci. U. S. A. 107, 1338–42. doi:10.1073/pnas.0914202107

Benazzi, S., Bailey, S.E., Mallegni, F., 2013a. Brief communication: A morphometric analysis of the neandertal upper second molar Leuca I. Am. J. Phys. Anthropol. 152, 300–5. doi:10.1002/ajpa.22355

Benazzi, S., Bailey, S.E., Peresani, M., Mannino, M.A., Romandini, M., Richards, M.P., Hublin, J.-J., 2014a. Middle Paleolithic and Uluzzian human remains from Fumane Cave, Italy. J. Hum. Evol. doi:10.1016/j.jhevol.2014.03.001

Benazzi, S., Coquerelle, M., Fiorenza, L., Bookstein, F., Katina, S., Kullmer, O., 2011a. Comparison of dental measurement systems for taxonomic assignment of first molars. Am. J. Phys. Anthropol. 144, 342–54. doi:10.1002/ajpa.21409

Benazzi, S., Douka, K., Fornai, C., Bauer, C.C., Kullmer, O., Svoboda, J.J., Pap, I.I., Mallegni, F., Bayle, P., Coquerelle, M., Condemi, S., Ronchitelli, A., Harvati, K., Weber, G.W., 2011b. Early dispersal of modern humans in Europe and implications for Neanderthal behaviour. Nature 479, 525–528. doi:10.1038/nature10617

Benazzi, S., Fornai, C., Buti, L., Toussaint, M., Mallegni, F., Ricci, S., Gruppioni, G., Weber, G.W., Condemi, S., Ronchitelli, A., 2012. Cervical and crown outline analysis of worn Neanderthal and modern

human lower second deciduous molars. Am. J. Phys. Anthropol. 149, 537–546. doi:10.1002/ajpa.22155

Benazzi, S., Panetta, D., Fornai, C., Toussaint, M., Gruppioni, G., Hublin, J.-J., 2014b. Technical Note: Guidelines for the digital computation of 2D and 3D enamel thickness in hominoid teeth. Am. J. Phys. Anthropol. 153, 305–313. doi:10.1002/ajpa.22421

Benazzi, S., Peresani, M., Talamo, S., Fu, Q., Mannino, M.A., Richards, M.P., Hublin, J.-J., 2013b. A reassessment of the presumed Neandertal remains from San Bernardino Cave, Italy. J. Hum. Evol. 66, 89–94. doi:10.1016/j.jhevol.2013.09.009

Benazzi, S., Talamo, V.S.S., Negrino, F., Peresani, M., Sawyer, S., Panetta, D., Vicino, G., Starnini, E., Salvadori, P.A., Meyer, M., Pääbo, S., Hublin, J.-J., Slon, V., Talamo, S., Negrino, F., Peresani, M., Bailey, S.E., Sawyer, S., Panetta, D., Vicino, G., Starnini, E., Mannino, M.A., Salvadori, P.A., Meyer, M., Pääbo, S., Hublin, J.-J., 2015. The makers of the Protoaurignacian and implications for Neandertal extinction. Science (80-.). 348, 793–6. doi:10.1126/science.aaa2773

Benazzi, S., Viola, B., Kullmer, O., Fiorenza, L., Harvati, K., Paul, T., Gruppioni, G., Weber, G.W., Mallegni, F., 2011c. A reassessment of the Neanderthal teeth from Taddeo cave (southern Italy). J. Hum. Evol. 61, 377–87. doi:10.1016/j.jhevol.2011.05.001

Boëda, E., 1994. Le concept Levallois: variabilité des méthodes, Monographie du CRA. Paris.

Boëda, E., 1993. Le débitage discoide et le débitage Levallois récurrent centripète. Bull. la Société Préhistorique Française 90-6, 392–404.

Crevecoeur, I., Bayle, P., Rougier, H., Maureille, B., Higham, T., van der Plicht, J., De Clerck, N., Semal, P., 2010. The Spy VI child: A newly discovered Neandertal infant. J. Hum. Evol. 59, 641–656.

Feldkamp, I.A., Davis, L.C., Kress, J.W., 1984. Pratical cone-beam algorithm. J. Opt. Soc. Am. A Opt. Image Sci. Vis.

Forestier, H., 1993. Le Clactonien: Mise en application d'une nouvelle méthode de débitage s'inscrivant dans la variabilité des systèmes de production lithique du Paléolithique ancien. Paleo 5, 53–82.

Fornai, C., Benazzi, S., Svoboda, J., Pap, I., Harvati, K., Weber, G.W., 2014. Enamel thickness variation of deciduous first and second upper molars in modern humans and Neanderthals. J. Hum. Evol. 76, 83–91.

Foster, T.D., Hamilton, M.C., Lavelle, C.L.B., 1969. Dentition and dental arch dimensions in British children at the age of to 3 years. Arch. Oral Biol. 14, 1031–1040. doi:10.1016/0003-9969(69)90073-9

Gómez-Robles, A., Martinón-Torres, M., Bermúdez de Castro, J.M., Prado, L., Sarmiento, S., Arsuaga, J.L., 2008. Geometric morphometric analysis of the crown morphology of the lower first premolar of hominins, with special attention to Pleistocene Homo. J. Hum. Evol. 55, 627–38. doi:10.1016/j.jhevol.2008.03.011

Grine, F.E., 2005. Enamel thickness of deciduous and permanent

molars in modern Homo sapiens. Am. J. Phys. Anthropol. 126, 14–31.

Korenhof, C.A.W., 1960. Morphological aspects of the human upper molar. Utrecht, Uitgeveramsatschappij Neerl.

Macchiarelli, R., 2013. From outer to inner structural morphology in dental anthropology: integration of the third dimension in the visualization and quantitative analysis of fossil remains, in: Scott, G.R., Irish, J.D. (Eds.), Anthropological Perspectives on Tooth Morphology. Cambridge University Press, pp. 250–277.

Macchiarelli, R., Bondioli, L., Debénath, A., Mazurier, A., Tournepiche, J.F., Birch, W., Dean, C., 2006. How Neanderthal molar teeth grew. Nature 444, 748–751.

Mahoney, P., 2013. Testing functional and morphological interpretations of enamel thickness along the deciduous tooth row in human children. Am. J. Phys. Anthropol. 151, 518–525.

Mahoney, P., 2010. Two-dimensional patterns of human enamel thickness on deciduous (dm1,dm2) and permanent first (M1) mandibular molars. Arch. Oral Biol. 55, 115–126.

Molnar, S., 1971. Human tooth wear, tooth function and cultural variability. Am. J. Phys. Anthropol. 34, 175–190.

Moorrees, C.F.A., 1963. Formation and resorption of three deciduous teeth in children. Am. J. Phys. Anthropol. 21, 205–213.

Olejniczak, A.J., 2006. Micro-computed tomography of primate molars. Stony Brook University.

Ortiz, A., Skinner, M.M., Bailey, S.E., Hublin, J.-J., 2012. Carabelli's trait revisited: an examination of mesiolingual features at the enamel-dentine junction and enamel surface of Pan and Homo sapiens upper molars. J. Hum. Evol. 63, 586–96. doi:10.1016/j.jhevol.2012.06.003

Panetta, D., Belcari, N., Del Guerra, A., Bartolomei, A., Salvadori, P.A., 2012. Analysis of image sharpness reproducibility on a novel engineered micro-CT scanner with variable geometry and embedded recalibration software. Phys. Med. 28, 166–73. doi:10.1016/j.ejmp.2011.03.006

Shackelford, L.L., Stinespring Harris, A.E., Konigsberg, L.W., 2012. Estimating the distribution of probable age-at-death from dental remains of immature human fossils. Am. J. Phys. Anthropol. 147, 227–253. doi:10.1002/ajpa.21639

Thun Hohenstein, U., Peretto, C., 2005. Faunal exploitation in the Middle Palaeolithic: evidences from Riparo Tagliente (Verona, Italy), in: Molines, N., Moncel, M.-H., Monnier, J.-L. (Eds.), Les Premiers Peuplements En Europe. Colloque International: Données Récents Sur Les Modalités de Peuplement et Sur Le Cadre Chronostratigraphique, Géologique et Paleogeographique Des Industries Du Paléolithique Inferieur et Moyen En Europe. BAR International Series 1364, Oxford, pp. 261–268.

Tixier, J., Tillier, A.-M., 1991. Une molaire d'enfant aurignacien a Ksar

'Aqil (Liban) Mt. Carmel, Israël. Paléorient 17, 89–93. doi:10.3406/paleo.1991.4541

Toussaint, M., Olejniczak, A.J., El Zaatari, S., Cattelain, P., Flas, D., Letourneux, C., Pirson, S., 2010. The Neandertal lower right deciduous second molar from Trou de l'Abîme at Couvin, Belgium. J. Hum. Evol. 58, 56–67. doi:10.1016/j.jhevol.2009.09.006

Turner, C.G., Nichol, C.R., Scott, G.R., 1991. Scoring procedures for key morphological traits of the permanent dentition: the Arizona State University Dental Anthropology System, in: Kelley, M., Larsen, C. (Eds.), Advances in Dental Anthropology. Wiley-Liss, New-York, pp. 13–31.

Ubelaker, D.H., 1978. Human Skeletal Remains: Excavation, Analysis, Interpretation. Aldine, Chicago.

Villa, G., Giacobini, G., Peretto, C., Thun Hohenstein, U., 2001. Neandertal teeth from the Mousterian levels of the Riparo Tagliente (Verona, N-E Italy). Atti del XIII Congr. A.A.I.

Zanolli, C., Bayle, P., Macchiarelli, R., 2010. Tissue proportions and enamel thickness distribution in the early Middle Pleistocene human deciduous molars from Tighenif, Algeria. Comptes Rendus Palevol 9, 341–348.

Paper VII: Margherita et al. 2017

Journal of Human Evolution

(J Hum Evol. 113, 83-90)

Morphological description and morphometric analyses of the Upper Palaeolithic human remains from Dzudzuana and Satsurblia caves, western Georgia

Cristiana Margherita[1], Gregorio Oxilia[1,2], Veronica Barbi[1], Daniele Panetta[3], Jean – Jacques Hublin[4], David Lordkipanidze[5], Tengiz Meshveliani[5], Nino Jakeli[5], Zinovi Matskevich[6], Ofer Bar-Yosef[7], Anna Belfer-Cohen[8], Ron Pinhasi[9,10*], Stefano Benazzi[1,4,*]

[1]Department of Cultural Heritage, University of Bologna, Via degli Ariani 1, 48121 Ravenna, Italy

[2]Department of Biology, University of Florence, Via del Proconsolo 12, 50122 Firenze, Italy

[3]Institute of Clinical Physiology – CNR, Pisa, Italy

[4]Department of Human Evolution, Max Planck Institute for Evolutionary Anthropology, Deutscher Platz 6, 04103 Leipzig, Germany

[5]Georgian National Museum, Department of Prehistory, Tbilisi, Georgia

[6]Israel Antiquities Authority, Jerusalem, Israel

[7]Department of Anthropology, Peabody Museum, Harvard University, 11 Divinity Avenue, Cambridge, MA 02138, USA

[8]The Institute of Archaeology, The Hebrew University of Jerusalem, Mount Scopus, Jerusalem 91905, Israel

[9]School of Archaeology and Earth Institute, University College Dublin, Belfield, Dublin 4, Ireland

[10]Department of Anthropology, University of Vienna, Althanstrasse 14, 1090 Vienna, Austria

Introduction

While paleoanthropologists and archaeologists agree that western Georgia was used as a thoroughfare of human movements to and from the Caucasus (Pinhasi et al., 2012; 2014), the paleoanthropological fossil record of the local Middle and Upper Palaeolithic in this key region is currently limited to scanty human remains. For the Late Pleistocene, the Middle Palaeolithic (MP) Georgian human fossil record consists of a partial maxilla from the site of Sakajia and some isolated teeth from the sites of Bronze Cave, Djruchula, Ortvala and Ortvale Klde, which were all classified as Neandertals (Pinhasi et al., 2012). The Upper Palaeolithic (UP) fossil record consists of a modern human tooth from Bondi cave (Tushabramishvili et al., 2012), recently dated between 39,000 and 35,800 cal. BP (Pleurdeau et al., 2016), and cranial fragments from Sakajia, dated between 12,000-10,000 cal. BP (Nioradze and Otte, 2000) (Fig. S1). Therefore, even though some author suggests that Caucasus represents a sort of *cul de sac* for Neandertal survival, and that modern humans arrived in this area much later compared to other regions (Bar-Yosef and Pilbeam 2000), the paucity of human remains prevents any conclusive assessment.

Here we report additional Upper Palaeolithic human remains from the Imereti region, western Georgia (Fig. S1; see SOM): two isolated teeth from Dzudzuana cave (Bar-Yosef et al., 2011), one isolated tooth and a hemi-mandible bearing teeth from Satsurblia cave (Pinhasi et al., 2014). In particular, the human remains from Dzudzuana cave, dated between 27,000–24,000 cal. BP, fill a huge gap in the Upper Palaeolithic Georgian fossil record

and play an important role in the debate about modern human peopling of the Caucasus.

Materials and methods

Micro-CT

High-resolution µCT images of the teeth from Dzudzuana (Dzu 1 and Dzu 2; Fig. 1) and the isolated tooth from Satsurblia (SATP5-2) (Fig. 2) were obtained with a XALT microtomographic system (Institute of Clinical Physiology, Pisa, Italy) (Panetta et al., 2012). The Satsurblia mandible (Fig. 3) was scanned with a Birscan microtomographic system (Max Planck Institute for Evolutionary Anthropology, Leipzig, Germany) (Scan parameters and processing procedures are described in the SOM).

Morphological description

Terminology for the morphological description of the mandible and the teeth follows White et al. (2012) and Scott and Turner (1997), respectively. Nonmetric traits were evaluated according to standards outlined by the Arizona State University Dental Anthropology System, ASUDAS (Turner et al.,1991), Bailey (2002), Bailey et al. (2011) and Martìnez de Pinillos and colleagues (2014). Occlusal wear stage was assessed based on Molnar (1971). For deciduous teeth, the age at death was estimated using the sequences provided by AlQahtani and colleagues (2010).

Morphometric analyses

Height and breadth of the mandibular corpus were measured in the digital model at the level of both the mental foramen (Buikstra and Ubelaker, 1994) and the lower first molar (Rosas and Bermùdez de Castro, 1999).

In addition to MD and BL crown diameters (Benazzi et al., 2011a; 2013a; Margherita et al., 2016) for the deciduous molars we used crown (for Dzu 1,

Dzu 2 and SATP5-5) and cervical outline analyses (for Dzu 2 and SATP5-5), following methods provided by Benazzi et al. (2011b; 2012a; 2014a) and Bailey et al. (2014). For the permanent teeth we have computed the 3D enamel thickness following guidelines provided by Benazzi and colleagues (2014b). Finally, to assess whether Dzu 1 and Dzu 2 belong to the same individual, both teeth were analysed using the Occusal Fingerprint Analyser (OFA) software package (2008-2014 ZiLoX-IT GbR) (see e.g., Benazzi et al., 2012b; 2013b, c; 2015; 2016; Kullmer et al., 2013; Fiorenza et al., 2015) (for more details about methods see SOM).

Metric comparison

Whereas no metric comparison was undertaken for the mandibular corpus owing to its subadult age, the BL diameters of the deciduous teeth were compared with a sample of Neandertal (N), Upper Palaeolithic *H. sapiens* (UPHS) and recent *H. sapiens* (RHS) teeth collected from the scientific literature (Hillson and Trinkaus, 2002; Henry-Gambier et al., 2004; Hershkovitz et al., 2011). The MD diameter was not considered owing to the interproximal wear. For the permanent dentition, comparative dataset for MD and BL diameters were created *ex novo* and include N, Early *H. sapiens* (EHS) and RHS (Table S1).

The shape variables (Dzu 1 crown outline; Dzu 2 and SATP5-5 crown and cervical outlines) were projected into the shape-space obtained from a principal component analysis (PCA) of the comparative sample used by Bailey et al. (2014) and Benazzi et al. (2012a), respectively. We used cross-validation linear discriminant analysis (LDA) of the Principal Components that account for about 90% of the total variability to assess the closest taxa affiliated with the Dzu 1, Dzu 2 and SATP5-5 specimens.

Comparative data for 3D enamel thickness were created *ex novo* and include N, EHS and RHS with different wear stages (Table S1). The only UPHS

specimen available for enamel thickness analysis (Villabruna, lower left first molar; Vercellotti et al., 2008; Oxilia et al. 2015) was included in the RHS sample. To discern differences in enamel thickness between N and RHS, 3D AET and 3D RET indices were tested using the Mann-Whitney *U* test (α = 0.05; two-tailed) with a Monte Carlo permutation. Standardized scores (Z-score) were computed to establish the group means closest to the values of Dzudzuana and Satsurblia specimens. The data were processed and analysed using R v. 2.15.1 (R Development Core Team, 2012).

Results

Dzudzuana – morphological description

Dzu 1 is an upper right second deciduous molar (Rdm^2), with a complete crown and a cervical quarter of the root (Fig. 1A). The tooth has several visible fractures on the enamel-dentine junction (EDJ; Fig. S3A). While it is heavily worn (wear stage 5) (Fig. 1A), the remnants of four principal cusps, a weak Cusp 5 (ASUDAS grade 1), accessory crests and a small Carabelli's trait are still visible on the EDJ (Fig. S3A). The hypocone is small, giving to the crown a sub-square shape. Dzu 1 has a distal interproximal facet larger (length=5 mm; height=1.6 mm) than the mesial one (length=3.7 mm; height=1 mm). On the buccal wall of the crown there is a large wear facet with dentine exposure, probably related to para-masticatory activities. Root resorption at the R¾ stage suggests that the tooth had been lost ante-mortem and corresponds to an age ranging from nine to 12 years old. The tooth crown has a MD diameter of 9.9 mm and a BL diameter of 10.5 mm (Table 1). At the cervix, the MD diameter is 7.4 mm and BL diameter is 9.9 mm.

Dzu 2 is a worn (wear stage 4) lower right second deciduous molar (Rdm_2) with a complete crown and a cervical quarter of the root (Fig. 1B). The tooth

has several visible fractures, the main one is oriented bucco-lingually and divides the tooth into two parts (see Fig. S2 for the virtual restoration). It is worn (wear stage 4). From the occlusal view the crown outline shows a bucco-distal reduction and a straighter lingual side (Fig. 1B). On the EDJ, five principal cusps, a weak anterior fovea bordered distally by a weak mesial trigonid crest (MeTC), and potentially the remnant of a distal trigonid crest (DTC), almost entirely removed by tooth wear, can be observed (Fig. S3B). Interproximal facets are evident both mesially (length=3.7 mm; height=1.7 mm) and distally (length=5.1 mm; height=2.5 mm). Root resorption is at a Res ¾ grade suggesting that the tooth had been lost ante-mortem, at an age ranging from nine to 12 years old. The tooth crown has a MD diameter of 10.3 mm and a BL diameter of 9.5 mm (Table 1). At the cervix, the MD diameter is 8.6 mm and BL diameter is 7.9 mm.

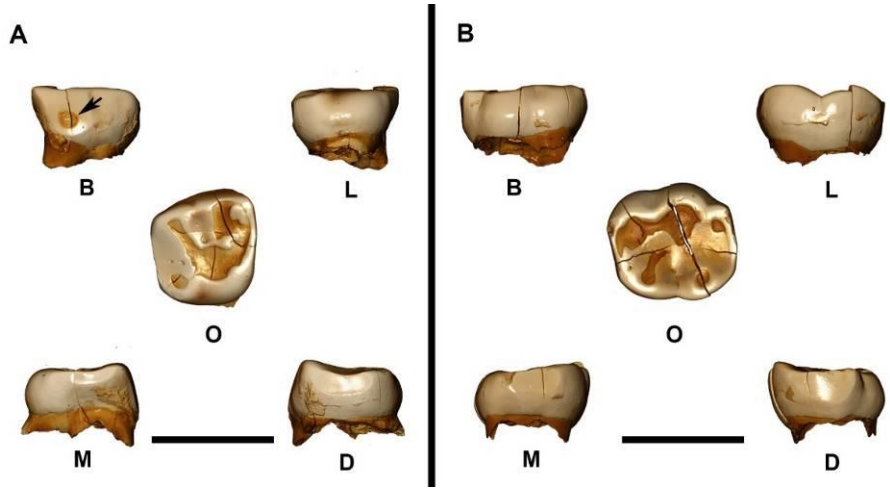

Figure 1. A) Three-dimensional digital models of Dzu 1 (upper right second deciduous molar, Rdm2); B) Three-dimensional digital model of Dzu 2 (lower right second deciduous molar, Rdm2). The black bar is equivalent to 1 cm. B, buccal; D, distal; L, lingual; M, mesial; O, occlusal.

Testing occlusal contacts between Dzu 1 and Dzu 2

Only three occlusal contacts are detected during maximum intercuspation in the OFA software, this suggests that the teeth do not belong to the same individual (Fig. S4; see SOM).

Satsurblia – morphological description

SATP5-2 is an upper right central deciduous incisor (Rdi^1), worn (wear stage 4), with the enamel on the mesial side chipped off and the cervical quarter of the root preserved. A longitudinal fracture, bucco-lingually directed, separates a distal portion of the tooth. (Fig. 2). From the labial view, the crown has moderate labial convexity (ASUDAS grade 3), that becomes less pronounced distally. The lingual surface is concave, and shows a distal marginal ridge (the mesial one is not visible, maybe removed by wear) and a faint median ridge, which disappears as it reaches the cervical eminence (Fig. 2). The stage of resorption is at Res ½ (the preserved portion is 3.5 mm) and suggests that the tooth had been lost ante-mortem through dental development, at an age estimated to be between six and seven years. The tooth crown has a MD diameter of 6.8 mm (minimum estimation due to wear) and a BL diameter of 5.6 mm (Table 1). At the cervix, the MD diameter is 5.5 mm and BL diameter is 4.9 mm.

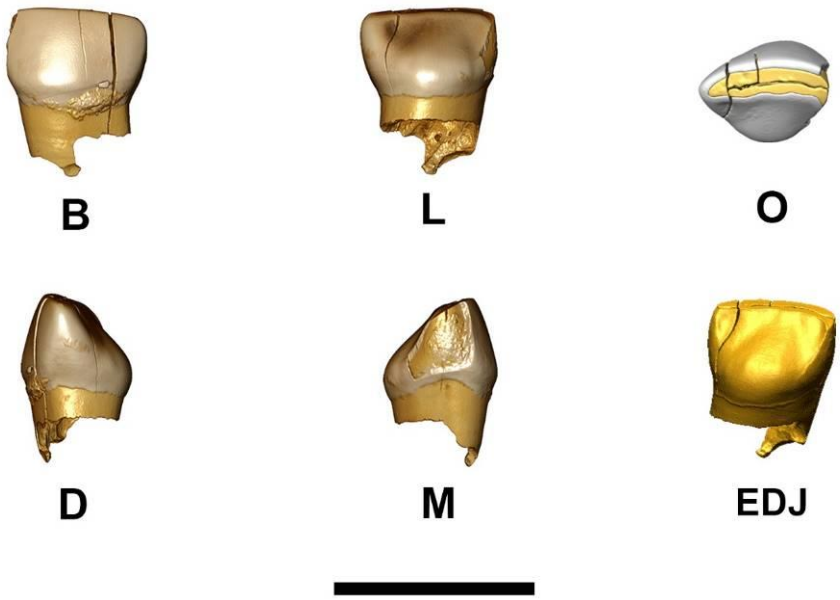

Figure 2. Three-dimensional digital model of SATP5-2 (upper right central deciduous incisor, Rdi1). The black bar is equivalent to 1 cm. B, buccal; D, distal; L, lingual; M, mesial; O, occlusal; EDJ, enamel-dentine junction.

Mandible

SATP5 is an incomplete left hemi-mandible with part of the body and the ramus preserved (Fig. 3A-C). In detail, the gonial region and the condyle process are missing, as well as the portion of the mandibular body in front of an imaginary line that connects the mental foramen and the alveolus of the left first incisor.

In SATP5, only the second deciduous molar (dm_2; SATP5-5) and the first molar (M_1; SATP5-6) are visible, while premolars (P_3 and P_4, respectively SATP5-3and SATP5-4) and second molar (M_2; SATP5-7) are unerupted (Table 1). The teeth are well-preserved, except for a small fracture in the P_3. The P_4 is turned upside down, probably from post-depositional repositioning that occurred within the tooth socket. Since the degree of mineralization of

teeth, dental development and eruption stages correspond to an age ranging from six to seven years. On the lingual side of the hemi-mandible (Fig. 3A), the mylohyoid line runs from the unerupted M_2 till the anterior fracture. On the buccal side (Fig. 3C), the mental foramen is positioned between the interalveolar septa of the deciduous canine and the first deciduous molar.

The maximal height of the corpus is 45.7 mm and its maximal length is 69.8 mm. The height of the corpus at the level of the mental foramen is 21.4 mm, with a thickness of 5.3 mm. At the level of the M_1, the corpus height is 19 mm, with a thickness of 4.8 mm.

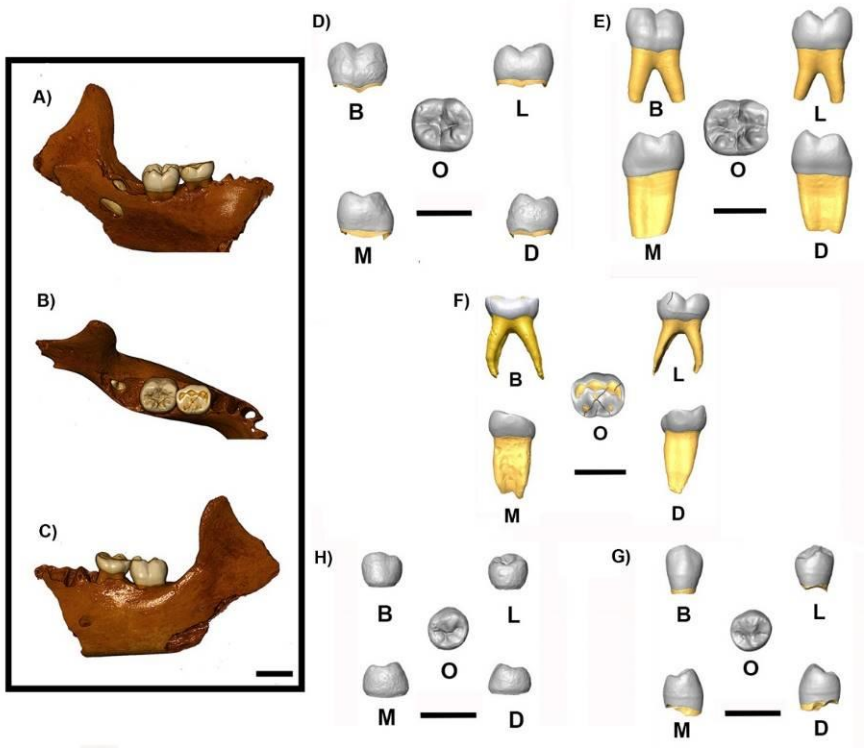

Figure 3. On the left three-dimensional digital model of Satsurblia mandible (SATP5): A) Lingual side; B) Occlusal side; C) Buccal side. On the right three-dimensional digital models of: D) SATP5-7 (lower left second molar, LM2); E) SATP5-6 (lower left first molar, LM1); F) SATP5-5 (left second

deciduous molar, Ldm2); G) SATP5-3 (lower left third premolar, LP3); H) SATP5-4 (lower left fourth premolar, LP4). The black bar is equivalent to 1 cm. B, buccal; D, distal; L, lingual; M, mesial; O, occlusal.

SATP5-3 is a lower left third premolar (LP_3) with a complete, unerupted crown and root in earliest formation, at the Ri developmental stage (Fig. 3G). The crown is sub-circular and shows two main cusps, the protoconid larger than the metaconid, separated by a mesio-distal groove. On the EDJ, two further small dentine horns (hypoconid and entoconid) and a moderate transverse crest connecting the protoconid and metaconid (grade 2, Bailey, 2002) are visible (Fig. S5A).
The tooth crown has a MD diameter of 6.9 mm and a BL diameter of 7.5 mm (Table 1). At the cervix, the MD diameter is 4.7 mm and BL diameter is 6.5 mm.

SATP5-4 is a lower left fourth premolar (LP_4) with a complete, unerupted crown but without the root, at the Crc developmental stages (Fig. 3H). The crown has a circular occlusal outline and shows four cusps, with the metaconid equal in size to the entoconid (ASUDAS grade 4). The mesio-distal groove separates the main cusps. On the EDJ a mesial accessory ridge (MAR) borders an anterior fovea distally (Fig. S5B). The tooth crown has a MD diameter of 7.2 mm and a BL diameter of 7.9 mm (Table 1). At the cervix, the MD diameter is 4.5 mm and the BL diameter is 6.4 mm.

SATP5-5 is a lower left second deciduous molar (Ldm_2) with both crown and root preserved (Fig. 3F). The tooth shows several fractures (see SOM). While it is very worn (wear stage 4), the five principal cusps forming a Y groove pattern can be recognized, as confirmed by the EDJ. A moderate shoulder on the distal side of the metaconid (Fig. S5C) is identified as C7 (ASUDAS grade

1A). The mesial interproximal wear facets are smaller (length=1.5 mm; height=1.1 mm) than the distal one (length=1.9 mm, height=2.1 mm). On the lingual side, traces of calculus are present (Fig. 3F). The tooth crown has a MD diameter of 10 mm and a BL diameter of 8.7 mm (Table 1). At the cervix, the MD diameter is 8.3 mm and BL diameter is 7 mm. Root morphology suggests cynodontism, with root bifurcation placed at 2.7 mm from the cervix. The distal root, longer than the mesial one, measures 11.8 mm.

SATP5-6 is a lower left first molar (LM_1) with crown and root well-preserved (Fig. 3E), at the R ½ developmental stage. The tooth is slightly worn (category 2), with a weak interproximal facet on the mesial side (length=1.8 mm; height=3.4). In occlusal view, the crown has a rectangular outline and has four main well-developed cusps, an entoconulid (C6) and a faint C7 (ASUDAS grade 1A), also visible on the EDJ (Fig. S5D). The metaconid is in contact with the hypoconid, confirming the classic 4-Y groove pattern. The tooth crown has a MD diameter of 10.8 mm and a BL diameter of 10.3 mm (Table 1). At the cervix, the MD diameter is 8.3 mm and the BL diameter is 8.4 mm. The root length measures 9.5 mm on the mesial side, while 8.81 mm on the distal side.

SATP5-7 is an unerupted lower left second molar (LM_2) with a well-preserved crown and cervical quarter of the root, at the Ri development stage (Fig. 3D). The tooth has four well-developed main cusps arranged in an + pattern, and a faint shoulder identified as a C7 (ASUDAS grade 1A). From this latter develops a weak (grade 1 of Bailey et al., 2011) and continuous DTC (Type 3 following Martìnez de Pinillos et al., 2014), visible on the EDJ (Fig. S5E). The tooth crown has a MD diameter of 10.4 mm and a BL diameter of 9.7 mm (Table 1). At the cervix, the MD diameter is 8.7 mm and the BL diameter is 7.8 mm.

Table 1. Inventory of the human remains from Dzudzuana (Dzu) and Satsurblia (SATP5) caves.

Inventory no	Tooth class	MD	BL	Wear stage[a]	Estimated age (years)[b]	Stratigraph Unit	Culture
Dzu 1	Rdm^2	9.9	10.5	5	9-12	Layer C3	Upper Palaeolithic
Dzu 2	Rdm_2	10.3	9.5	4	9-12	Layer C4	Upper Palaeolithic
SATP5-2	Rdi^1	6.8	5.6	4	6-7	Area B	Upper Palaeolithic
Mandible SATP5					6-7	Area B	Upper Palaeolithic
SATP5-3	LP_3	6.9	7.5	1			
SATP5-4	LP_4	7.2	7.9	1			
SATP5-5	Ldm_2	10.0	8.7	4			
SATP5-6	LM_1	10.8	10.3	2			
SATP5-7	LM_2	10.4	9.7	1			

[a] Molnar, 1971.

[b] AlQahtani et al., 2010.

Metric comparison

The Z score computed for the BL diameter of Dzu 1 is closer to the UPHS mean, while for Dzu 2 the Z-score is equally close to Neandertals and UPHS. The BL diameter of SATP5-2 is closer to UPHS mean while the BL diameter of SATP5-5 is closer to the RHS variability (Table 2). The permanent teeth of Satsurblia are small, falling in the range of modern humans (Fig. S6).
254

Table 2. BL diameters (in mm) of Dzudzuana and Satsurblia's deciduous teeth standardized to Z-scores of the hominin samples used in this study. N, Neandertal; UPHS, Upper Palaeolithic H. sapiens; RHS, recent H. sapiens.

	Dzu 1 (Rdm^2)		**Dzu 2 (Rdm_2)**		**SATP5-2 (Rdi^1)**		**SATP5-5 (Ldm_2)**	
	BL Mean (SD/*n*)	Z-score	BL Mean (SD/*n*)	Z-score	BL Mean (SD/*n*)	Z-score	BL Mean (SD/*n*)	Z-score
	10.54		9.53		5.62		8,70	
N	10.2 (0.7/13) [a]	0.48	9.4 (0.5/34) [b]	0.26	6.13 (0.35/23) [b]	-1.45	9.4 (0.5/34) [b]	-1.4
UPHS	10.4 (0.7/11) [a]	0.2	9.44 (0.35/8) [c]	0.26	5.42 (0.35/18) [b]	0.57	9.44 (0.35/8) [c]	-2.11
RHS	9.5 (0.5) [a]	2.08	8.3 (0.6/57) [b]	2.05	4.87 (0.35/47) [b]	2.14	8.3 (0.6/57) [b]	0.67

[a] Hillson and Trinkaus, 2002.

[b] Hershkovitz et al., 2011.

[c] Henry-Gambier et al., 2004.

Dzu 1 crown outline was projected into the shape-space PCA computed by Bailey and colleagues (2014) and is positioned in PCA space (first two

components) within recent and the UPHS variability (Fig. 4A, B). The cross-validation LDA of the first four PCs attributes the tooth to modern human with a Ppost=0.99. Dzu 2 and SATP5-5 crown and cervical outlines were projected in the shape-space computed by Benazzi and colleagues (2014a). Both outlines of SATP5-5 plots within H. sapiens variability (Fig. 4C, D). Whereas, Dzu 2 crown outline falls within H. sapiens (Fig. 4C), but falls within the Neandertals variability for the cervical outline due to its bucco-distal enlargement (Fig. 4D). The cross-validation LDA of the first five PCs shows that SATP5-5 is attributed to modern human with a Ppost=1, while Dzu2 is attributed to modern human based on its crown outline (Ppost=1), but to Neandertals based on its cervical outline (Ppost=0.99). For the 3D RET of Satsurblia permanent posterior teeth the Z-scores computed are always closer to the H. sapiens mean than to Neandertal ones (Table 3 and Table S2).

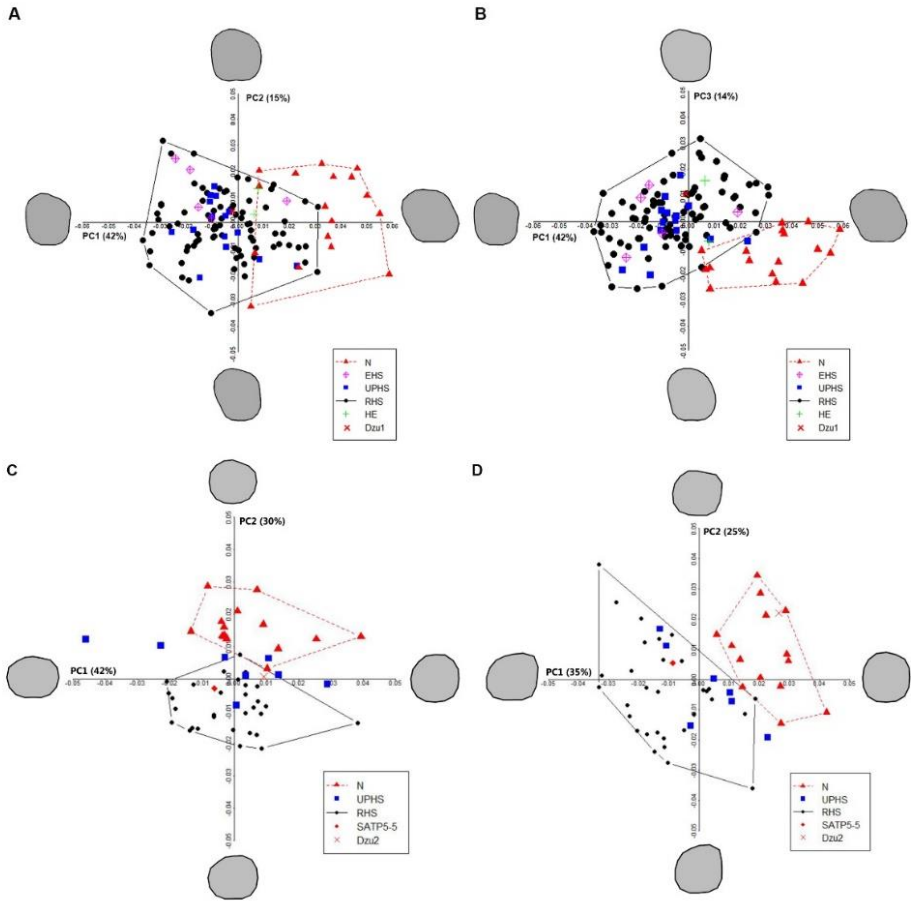

Figure 4. A, B) Shape-space PCA plots of *Homo erectus*, Neandertal and *H. sapiens* (EHS; UPHS; RHS) dms2 crown outlines. A) PC1 plotted against PC2; B) PC1 plotted against PC3. The deformed mean outlines in the four directions of the PCs are drawn at the extremity of each axis. HE, *H. erectus*; N, Neandertal; EHS, Early *H. sapiens*; UPHS, UP *H. sapiens*; RHS, recent *H. sapiens*; C, D) Shape-space PCA plots of Neandertal and *H. sapiens* (RHS and UPHS) dm2 crown outlines (C), and cervical outlines (D). The deformed mean outlines in the four directions of the PCs are drawn at the extremity of each axis. N, Neandertal; UPHS, UP *H. sapiens*; RHS, recent *H. sapiens*.

Table 3. Three-dimensional (3D) relative enamel thickness (RET). Satsurblia specimens are standardized to Z-scores of the Neandertals (N)and Recent H. sapiens (RHS) sample in different wear stages.

Taxon (n)	n	Wear[a]	3D RET Mean (SD)	Z-score
SATP5-3 (LP_3)		1	26.75	
N	8	1-2	18.55 (1.60)	5.12
RHS	11	1-2	24.39 (2.38)	0.99
RHS	4	3	19.60 (0.93)	7.69
SATP5-4 (LP_4)		1	41.46	
N	11	1-2	20.62 (2.37)	8.79
RHS	8	1-2	25.69 (2.22)	7.10
RHS	4	3	25.01 (4.46)	3.69
SATP5-6 (LM_1)		2	20.47	
N	8	1-2	18,61 (1.59)	1.17
N	6	3	15,86 (1.33)	3.47
N	9	4	12,21 (1.66)	4.97
RHS	8	1-2	20.17 (3.50)	0.29
RHS	8	3	16.16 (1.98)	2.18
RHS	5	4	14.30 (2.34)	2.64
SATP5-7 (LM_2)		1	23.7	
N	9	1-2	17.42 (2.60)	2.41
RHS	9	1-2	21.61 (1.73)	1.20

[a] Molnar, 1971.

Discussion and Conclusion

Morphological features and morphometric analyses support the attribution of the human remains from Satsurblia cave and the dm2 from Dzudzuana cave

(Dzu 1) to modern humans. Dzu 2 is more ambiguous, because though the general crown morphology aligns with modern human, the cervical outline plots within the Neandertals variability. Moreover, the evaluation of the occlusal contacts (i.e., OFA software) excludes the attribution of Dzu 1 and Dzu 2 to the same individual. Although it is more likely that Dzu 2 belongs to a modern human, further work is needed (e.g. ancient DNA) to assess the combination of modern human and Neandertal traits, probably a case of interbreeding, reported based on morphometric analysis for this specimen. It is important to note that there is no indication in the relevant archaeological contexts to suggest any 'transitional' (MP-UP) techno-cultural elements. Starting with the earliest remains uncovered in Dzudzuana, Unit D (dated to ca. 33,000 cal. BP, see SOM), there are no traces of any attributes of MP cultures. Moreover, the lithic assemblages of Unit C can be considered as a variant of the "Eastern Gravettian" and "Epi-Gravettian" complexes as the lithic industry from the Area B layers, Satsurblia, from which the human remains described here were recovered (Bar-Yosef et al., 2011; Pinhasi et al. 2014).

This particular case study has provided the opportunity to emphasize the potential of the OFA software to associate isolated teeth. In a previous contribution, two isolated teeth from Taddeo Cave (Italy) were attributed to the same individual by matching the interproximal facets in the OFA software (Benazzi et al., 2011c). This is the first study to use the OFA software for matching isolated antagonistic teeth, even though recent studies suggest that antagonists show close correspondence in macrowear pattern (Kullmer et al., 2012).

Our results also show that even though both SATP5-2 and SATP5 derive from the same layer and share the same age estimate, they should be attributed to different individuals.

In sum, the analyses of the modern human remains from Dzudzuana and Satsurblia caves provide a major addition to the UP human fossil record of Georgia and indicate the unequivocal presence of modern humans in Georgia during the Upper Palaeolithic, supporting the idea that modern humans reached the Caucasus earlier than previously thought, an assumption that until now was supported only by the tooth from the Bondi Cave (Pleurdeau et al., 2016). Even though this region is characterized by several Palaeolithic sites, only two other cave sites (Bondi cave and Sakajia) have yielded human remains from UP deposits. It is important to note that the chronological age of the teeth from Dzudzuana cave (27,000–24,000 cal. BP) falls between the currently oldest modern human tooth Bondi I (Pleurdeau et al., 2016) and the most recent human remains from Sakajia (Nioradze and Otte, 2000), filling the huge gap of more than 20,000 years.

Finally, we provide new information on the 3D enamel thickness of Neandertal and modern human lower molars and premolars at different wear stages following recent guidelines (Benazzi et al., 2014b) taking into consideration the current lack of comparative data for lower (and upper) premolars. Our results confirm that Neandertal M2s have significantly lower RET indices than modern humans (Olejniczak et al., 2008; Smith et al., 2012). However, contrary to our expectations and previous contributions (Macchiarelli et al., 2006; Olejniczak et al., 2008; Bayle et al., 2010; Smith et al., 2012), the results do not support the same discriminatory power for the M1, as differences between the two groups did not reach the significant level. Differences between the two groups appear pronounced in the premolars, ultimately suggesting that P3s and P4s represent valuable tooth classes to discriminate between Neandertals and modern humans. Interestingly, even though the small sample size prevents statistical tests, differences seem to persist at least in wear stage 3, rendering the lower post-canine dentition, and

particularly the premolars, useful tooth classes even when affected by moderate dental wear.

Acknowledgements

The authors are grateful to Heiko Temming for technical support for the metric comparison sample provided by the Department of Human Evolution, Max Planck Institute for Evolutionary Anthropology (Leipzig). We also thank Tommaso Saccone for the elaboration of the general map that showing the location of Dzudzuana, Satsurblia caves and the other georgian sites. Finally, thanks to Rosa Conte for proofreading this manuscript.

References

AlQahtani, S.J., Hector, M.P., Liversidge, H.M., 2010. Brief communication: The London atlas of human tooth development and eruption. American Journal of Physical Anthropology. 142, 481–490.

Bailey, S.E., 2002. A Closer Look at Neanderthal Postcanine Dental Morphology: The Mandibular Dentition. Anatomical Record. 269, 148–156.

Bailey, S.E., Skinner, M.M., Hublin, J.J., 2011. What lies beneath? An evaluation of lower molar trigonid crest patterns based on both dentine and enamel expression. American Journal of Physical Anthropology. 145, 505–518.

Bailey, S.E., Benazzi, S., Souday, C., Astorino, C., Paul, K., Hublin, J.J., 2014. Taxonomic differences in deciduous upper second molar crown outlines of *Homo sapiens*, *Homo neanderthalensis* and *Homo erectus*. Journal of Human Evolution. 72, 1–9.

Bar-Yosef, O., Pilbeam D., (Ed.), 2000. The Geography of Neandertals and Modern Humans in Europe and the Greater Mediterranean. Volume Bulletin No. 8. Peabody Museum Press, Harvard University, Cambridge.

Bar-Yosef, O., Belfer-Cohen, A., Mesheviliani, T., Jakeli, N., Bar-Oz, G., Boaretto, E., Goldberg, P., Kvavadze, E., Matskevich, Z., 2011. Dzudzuana: an Upper Palaeolithic cave site in the Caucasus foothills (Georgia). Antiquity. 85, 331–349.

Bayle, P., Macchiarelli, R., Trinkaus, E., Duarte, C., Mazuriere, A., Zilhão, J., 2010. Dental maturational sequence and dental tissue proportions in the early Upper Paleolithic child from
Abrigo do Lagar Velho, Portugal. PNAS. Vol. 107, no. 4, 1338-1342.

Benazzi, S., Coquerelle, M., Fiorenza, L., Bookstein, F., Katina, S., Kullmer, O., 2011a. Comparison of Dental Measurement Systems for Taxonomic Assignment of First Molars. American Journal of Physical Anthropology. 144, 342-354.

Benazzi, S., Douka, K., Fornai, C., Bauer, C.C., Kullmer, O., Svoboda, J.J., Pap, I.I., Mallegni, F., Bayle, P., Coquerelle, M., Condemi, S., Ronchitelli, A., Harvati, K., Weber, G.W., 2011b. Early dispersal of modern humans in Europe and implications for Neanderthal behaviour. Nature. 479, 525-528.

Benazzi, S., Viola, B., Kullmer, O., Fiorenza, L., Harvati, K., Paul, T., Gruppioni, G., Weber, G.W., Mallegni, F., 2011c. A reassessment of the Neanderthal teeth from Taddeo cave (southern Italy). Journal of Human

Evolution. 61, 377-387.

Benazzi, S., Fornai, C., Buti, L., Toussaint, M., Mallegni, F., Ricci, S., Gruppioni, G., Weber, G.W., Condemi, S., Ronchitelli, A., 2012a. Cervical and crown outline analysis of worn Neanderthal and modern human lower second deciduous molars. American Journal of Physical Anthropology. 149, 537–546.

Benazzi, S., Kullmer, O., Grosse, I., Weber, G., 2012b. Brief communication: comparing loading scenarios in lower first molar supporting bone structure using 3D Finite Element Analysis. American Journal of Physical Anthropology. 147, 128-134.

Benazzi, S., Bailey, S.E., Mallegni, F., 2013a. Brief communication: A morphometric analysis of the Neandertal upper second molar Leuca I. American Journal of Physical Anthropology. 152, 300-305.

Benazzi, S., Nguyen, H.N., Schulz, D., Grosse, I.R., Gruppioni, G., Hublin, J.J., Kullmer, O., 2013b. The Evolutionary Paradox of Tooth Wear: Simply Destruction or Inevitable Adaptation? PLoS One 8, e62263.

Benazzi, S., Nguyen, H.N., Kullmer, O., Hublin, J.J., 2013c. Unravelling the functional biomechanics of dental features and tooth wear. PLoS One 8, e69990.

Benazzi, S., Bailey, S.E., Peresani, M., Mannino, M.A., Romandini, M., Richards, M.P., Hublin, J.J., 2014a. Middle Paleolithic and Uluzzian human remains from Fumane cave, Italy. Journal of Human Evolution. 70,

61-68.

Benazzi, S., Panetta, D., Fornai, C., Toussaint, M., Gruppioni, G., Hublin, J.J., 2014b. Technical Note: Guidelines for the digital computation of 2D and 3D enamel thickness in hominoid teeth. American Journal of Physical Anthropology. 153, 305-313.

Benazzi, S., Nguyen, H.N., Kullmer, O., Hublin, J.J., 2015. Exploring the biomechanics of taurodontism. Journal of Anatomy. 226, 180-8.

Benazzi, S., Nguyen, H.N., Kullmer, O., Kupczik, K., 2016. Dynamic Modelling of Tooth Deformation Using Occlusal Kinematics and Finite Element Analysis. PLoS One 11, e0152663.

Buikstra, J.E., Ubelaker, D.H., (Ed.), 1994. Standards for data collection from human skeletal remains: procedings of a seminar at the field Museum of Natural History. Arkansas Archeological Survey Research Series No. 44.

Fiorenza, L., Nguyen, H.N., Benazzi, S., 2015. Stress Distribution and Molar Macrowear in *Pongo pygmaeus*: A New Approach through Finite Element and Occlusal Fingerprint Analyses. Human Evolution. 30, 215-226.

Henry-Gambier, D., Maureille, B., White, R., 2004. Vestiges Humains Des Niveaux De L ' Aurignacien Ancien Du Site De Brassempouy (Landes). Bulletins et mémemoires de la Société d'Anthropologie de Paris. 16, 49-87.

Hershkovitz, I., Smith, P., Sarig, R., Quam, R., Rodríguez, L., García, R., Arsuaga, J.L., Barkai, R., Gopher, A., 2011. Middle Pleistocene dental remains from Qesem Cave (Israel). American Journal of Physical Anthropology. 144, 575-592.

Hillson, S.W., Trinkaus, E., 2002. Comparative Dental Crown Metrics. In: Zilhão, J.,Trinkaus, E. (Eds.), Portrait of the Artist as a Child. The Gravettian Human Skeleton from the Abrigo do Lagar Velho and its Archeological Context. Trabalhos de Arqueologia Vol. 22, Instituto Português de Arqueologia, Lisboa, pp. 356-364.

Kullmer, O., Schulz, D., Benazzi, S., 2012. An experimental approach to evaluate the correspondence between wear facet position and occlusal movements. Anatomical Record. 295, 846-852.

Kullmer, O., Benazzi, S., Schulz, D., Gunz, P., Kordos, L., Begun, D.R., 2013. Dental arch restoration using tooth macrowear patterns with application to *Rudapithecus hungaricus*, from the late Miocene of Rudabánya, Hungary. Journal of Human Evolution. 64, 151-160.

Macchiarelli, R., Bondioli, L., Debenath, A., Mazurier, A., Tournepiche, J.F., Birch, W., Dean, M.C., 2006. How Neanderthal molar teeth grew. Nature. 444, 748-751.

Margherita, C., Talamo, S., Wiltschke-Schrotta, K., Senck, S., Oxilia, G., Sorrentino, R., Mancuso, G., Gruppioni, G., Lindner, R., Hublin, J.J., Benazzi, S., 2016. A reassessment of the presumed Torrener Bärenhöhle's Paleolithic human tooth. Journal of Human Evolution. 93, 120-125.

Martìnez de Pinillos, M., Martinón-Torres, M., Skinner, M.M., Arsuaga, J.L., Gracia-Téllez, A., Martínez, I., Martín-Francés, L., Bermùdez de Castro, J.M., 2014. Trigonid crests expression in Atapuerca-Sima de los Huesos lower molars: Internal and external morphological expression and evolutionary inferences. Comptes Rendus - Palevol. 13, 205-221.

Molnar, S., 1971. Human tooth wear, tooth function and cultural variability. American Journal of Physical Anthropology. 34, 175-189.

Nioradze, M.G., Otte, M., 2000. Paleolithique superieur de Georgie. Anthropologie. 104, 265-300.

Olejniczak, A.J., Smith, T.M., Feeney, R.N.M., Macchiarelli, R., Mazurier, A., Bondioli, L., Rosas, A., Fortea, J., de la Rasilla, M., Garcia-Tabernero, A., Radovčic, J., Skinner, M.M.,Toussaint, M., Hublin, J.J., 2008. Dental tissue proportions and enamel thickness in Neandertal and modern human molars. Journal of Human Evolution. 55, 12-23.

Oxilia, G., Peresani, M., Romandini, M., Matteucci, C., Debono Spiteri, C., Henry, A.G., Schulz, D., Archer, W., Crezzini, J., Boschin, F., Boscato, P., Jaouen, K., Dogandzic, T., Broglio, A., Moggi-Cecchi, J., Fiorenza, L., Hublin, J.J., Kullmer, O., Benazzi, S., 2015. Earliest evidence of dental caries manipulation in the Late Upper Palaeolithic. Scientific Reports. 5, 12150.

Panetta, D., Belcari, N., Del Guerra, A., Bartolomei, A., Salvadori, P.A., 2012. Analysis of image sharpness reproducibility on a novel engineered micro-CT scanner with variable geometry and embedded recalibration

software. Physica Medica. 28, 166-173.

Pinhasi, R., Nioradze, M., Tushabramishvili, N., Lordkipanidze, D., Pleurdeau, D., Moncel, M.-H., Adler, D.S., Stringer, C., Higham, T.F.G., 2012. New chronology for the Middle Palaeolithic of the southern Caucasus suggests early demise of Neanderthals in this region. Journal of Human Evolution. 63, 770-780.

Pinhasi, R., Meshveliani, T., Matskevich, Z., Bar-Oz, G., Weissbrod, L., Miller, C.E., Wilkinson, K., Lordkipanidze, D., Jakeli, N., Kvavadze, E., Higham, T.F.G., Belfer-Cohen, A., 2014. Satsurblia: New insights of human response and survival across the last glacial maximum in the southern caucasus. PLoS ONE. 9, e111271.

Pleurdeau, D., Moncel, M.-H., Pinhasi, R., Yeshurun, R., Higham, T., Agapishvili, T., Bokeria, M., Muskhelishvili, A., Le Bourdonnec, F.-X., Nomade, S., Poupeau, G., Bocherens, H., Frouin, M., Genty, D., Pierre, M., Pons-Branchu, E., Lordkipanidze, D., Tushabramishvili , N., 2016. Bondi Cave and the Middle-Upper Palaeolithic transition in western Georgia (south Caucasus). Quaternary Science Reviews. 146, 77-98.

Rosas, A., Bermùdez de Castro, J.M., 1999. The ATD6-5 mandibular specimen from Gran Dolina (Atapuerca , Spain). Morphological study and phylogenetic implications. Journal of Human Evolution. 37, 567-590.

Scott, R.G., Turner, C.I., 1997. The anthropology of modern human teeth. Dental morphology and its variation in recent human population. Cambridge University Press, Cambridge.

Smith, T.M., Olejniczak, A.J., Zermeno, J.P., Tafforeau, P., Skinner, M.M., Hoffmann, A., Radovcic, J., Toussaint, M., Kruszynski, R., Menter, C., Moggi-Cecchi, J., Glasmacher, U.A., Kullmer, O., Schrenk, F., Stringer, C., Hublin, J.J., 2012. Variation in enamel thickness within the genus *Homo*. Journal of Human Evolution. 62, 395-411.

Turner II, C.G., Nichol, C.R., Scott, G.R., 1991. Scoring Procedures for Key Morphological Traits of the Permanent Dentition: The Arizona State University Dental Anthropology System. In: Kelley, M.A., Larsen, C.S. (Eds.), Advances in Dental Anthropology. Wiley-Liss, New York, pp. 13-31.

Tushabramishvili, N., Pleurdeau, D., Moncel, M.H., Agapishvili, T., Vekua, A., Bukhsianidze, M., Maureille, B., Muskhelishvili, A., Mshvildadze, M., Kapanadze, N., Lordkipanidze, D., 2012. Human remains from a new Upper Pleistocene sequence in Bondi Cave (Western Georgia). Journal of Human Evolution. 62, 179-185.

Vercellotti, G., Alciati, G., Richards, M., Formicola, V., 2008. The Late Upper Paleolithic skeleton Villabruna 1 (Italy): A source of data on biology and behavior of a 14.000 year-old hunter. Journal of Anthropological Sciences. 86, 143–163.

White, T.D., Black, M.T., Folkens, P.A., (Ed.), 2012. Human Osteology, Third. ed. Elsevier. London.

Supplementary Online Material (SOM)

Index

1. Archaeological contexts

1.1 Dzudzuana cave

The cave of Dzudzuana (Western Georgia [Fig. S1]) was the first to provide a well-dated Upper Palaeolithic (UP) chronostratigraphic sequence for human occupation in the southern Caucasus (Bar-Yosef et al., 2011, their Fig. 2). This sequence comprises three occupational episodes separated by millennia long hiatuses: the lowermost UP phase, Unit D, is dated to 34,500–32,200 calendar years (cal. BP [calibrated years before present]); the following Unit C, is dated to 27,000–24,000 cal. BP (the human teeth studied were retrieved from the lower part of this Unit, in a distinct anthropogenic layer, mixed with chipped stone artefacts and fauna remains); and the latest UP phase, Unit B - dated to 16,500–13,200 cal. BP (Bar-Yosef et al., 2011, their Fig. 3).

Figure S1. Georgia - A general map showing the location of Dzudzuana, Satsurblia caves and the other sites mentioned in the paper (Google Earth).

The chipped stone assemblage of Unit C (which comprises the main material culture remains) is dominated by small blades and bladelets detached predominantly from narrow carinated cores. Besides retouched bladelets, there are the Sakajia points (arched/curved pointed blades with abrupt retouch along the straight edge and a proximal retouched truncation). It is of interest to note the decorative items recovered in this Unit. There were pendants made of stone, bone and teeth (of goats and deer) (Bar-Yosef et al., 2011, their Fig. 6). Other decorated items include incised bone pieces, sometimes with elaborate patterns, of either long bone splinters or ribs. Quite a number of bone tools (and see detailed discussion in Bar-Yosef et al., 2011) were recovered, mostly awls/points made on splinters, shaped by shaving and polishing. Besides those there were also decorated items, polishers, and a single bone needle with an 'eye', according well with the findings in all UP Units of wild flax fibers (Kvavadze et al., 2009).

1.2 Satsurblia cave

The human occupation layers at Satsurblia cave yielded a series of living surfaces dated to (a) prior to the Last Glacial Maximum (LGM) at 25,500–24,400 cal. BP and (b) after the LGM at 17,900–16,200 cal. BP. Excavations were conducted in two main areas: Area A and Area B (Pinhasi et al., 2014, Fig. 2).

Area A is situated in the northwestern part of the cave, near the entrance and Area B is in the rear of the cave adjacent to a trench excavated in the early 1990s. Both areas revealed stratigraphic sequences comprising Pleistocene (UP) and Holocene (Eneolithic and later) deposits. In both areas, the in situ UP layers were extremely rich in anthropogenic remains (e.g., a circular fireplace, large quantities of charcoal and burnt bones, lithics, bone tools, shell ornaments, yellow ochre). The UP sequence of Area A was divided into two main units: A/I and A/II. A/II contained a sequence of living surfaces which

were dated (surface II and III) to 17,000–18,000 cal. BP and as such are the first well-dated evidence for human occupation in the southern Caucasus at the end of the LGM. This fills in a gap in the local UP sequence, namely that between Unit C and Unit B in Dzudzuana cave (western Georgia), dated to 27,000–24,000 cal. BP and 16,000 cal. BP – 13,200 cal. BP, respectively (Pinhasi et al., 2014, Fig. 3). The stratigraphic sequence of Area B includes so far four main archaeological layers (B/I, B/II, B/III, B/IV) and reaches a thickness of >2 m (6.5 m below the datum). Layer B/III is dated to 25,220–24,440 cal. BP (with dates pending for the underlying layer B/IV) (Pinhasi et al., 2014, their Fig. 6). An isolated tooth (SATP5-2) and a hemi-mandible (SATP5) with teeth (LP_3 = SATP5-3, LP_4 = SATP5-4, Ldm_2 = SATP5-5, LM_1 = SATP5-6, LM_2 = SATP5-7) have been recovered from a poorly provenienced UP context in Area B (excavated in the 1990s). The hemi-mandible was directly dated to 11,250 ± 50 BP (OxA-26862) (the specimen was analyzed at Oxford Radiocarbon Laboratory for AMS 14C dating). The obtained radiometric date provides a calibrated range of 13,031-13,225 cal. BP, using Oxcal 4.2 with IntCal 13 calibration curve. The specimen was well preserved, and yielded 13.32% collagen by weight (in modern unadulterated bone, ~20% by weight is collagen) and the C:N atomic ratio was 3.2 (in modern bone, this measure is around 3.21). Its direct date indicates that it is from the late UP occupation phase in Satsurblia. In general, the UP lithic assemblages in Satsurblia differ from those of Dzudzuana Unit C. Though they also represent mostly a bladelet industry, the dominant tool types are obliquely truncated retouched/backed bladelets with some microgravettes and rare Gravette points (Pinhasi et al., 2014).

2. Materials and methods

2.1 Micro-CT

High-resolution micro-CT images of the teeth from Dzudzuana (Dzu 1 and Dzu 2; main text Fig. 1) and the isolated tooth from Satsurblia (SATP5-2) (Fig. 2) were obtained with a XALT microtomographic system (Institute of Clinical Physiology, Pisa, Italy) (Panetta et al., 2012) using the following scan parameters: 50 kV, 0.7 mA, with a 2mm Aluminium filter. The Satsurblia mandible (Fig. 3) was scanned with a Birscan microtomographic system (Max Planck Institute for Evolutionary Anthropology, Leipzig, Germany) using the following scan parameters: 130 kV, 0.1 mA, with a 0.50 mm Brass filter. Volume data were reconstructed using isometric voxels of 18.4 µm for the isolated teeth and 30.15 µm for the mandible.

The image stacks were segmented with a semiautomatic approach in Avizo 7.0 (Visualization Sciences Group Inc.) in order to separate the tissues and to reconstruct three-dimensional (3D) digital models of the teeth and of the mandible, which were then used to support the morphological description and to collect morphometric data (SOM Fig. S2, S3).

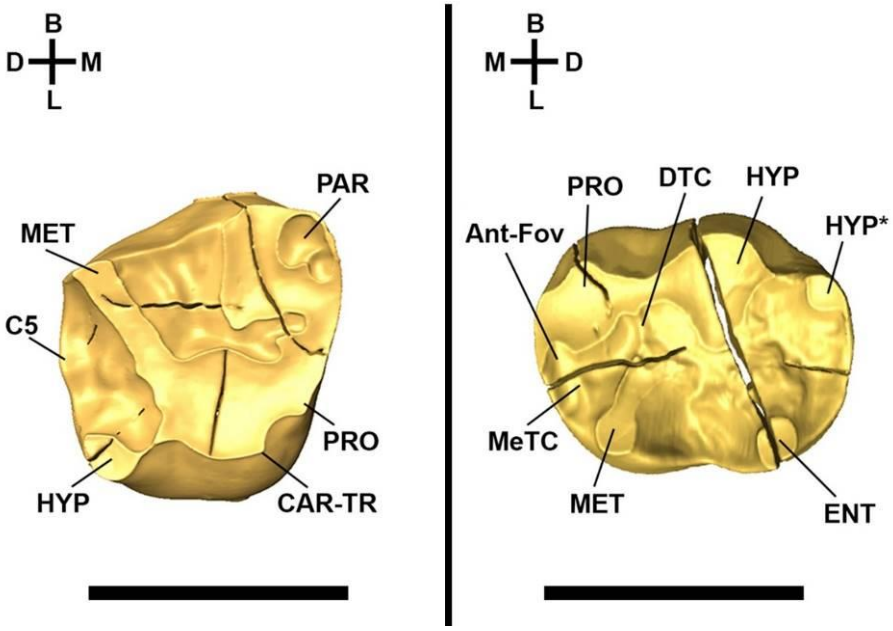

Figure S2. A) Three-dimensional digital models of the enamel-dentine junction (EDJ) of Dzu 1. PRO = protocone; PAR = paracone; MET = metacone; HYP = hypocone; C5 = fifth cusp; CAR-TR = Carabelli's trait. B) Three-dimensional digital model of the EDJ of Dzu 2. PRO = protoconid; MET = metaconid; HYP = hypoconid; HYP* = hypoconulid; ENT = Entoconid; MeTC = mesial trigonid crest; DTC = distal trigonid crest; Ant-Fov = anterior fovea. The black bar is equivalent to 1 cm. B, buccal; D, distal; L, lingual; M, mesial; O, occlusal.

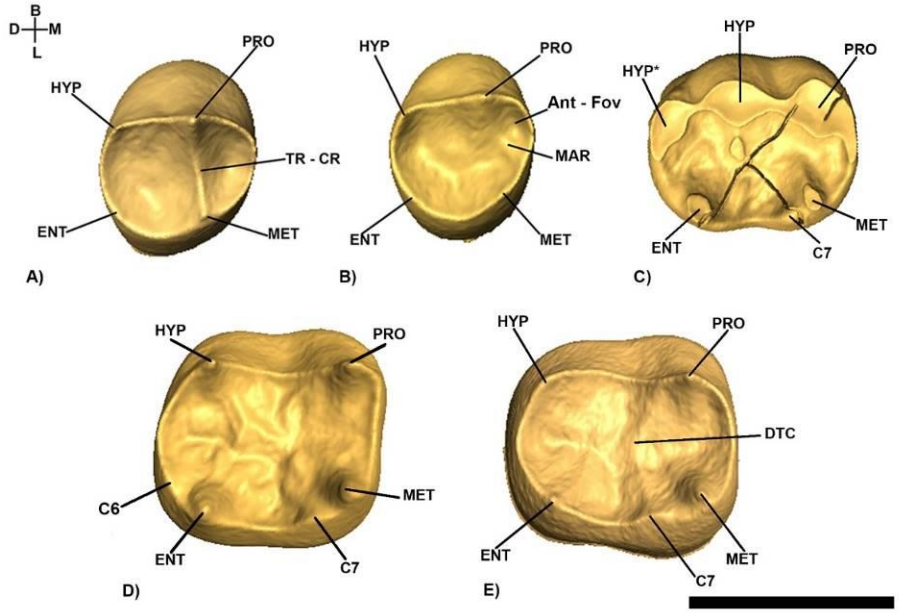

Figure S3. A) Three-dimensional digital models of the EDJ of: A) SATP5-3 (lower left third premolar, LP_3), B) SATP5-4 (lower left fourth premolar, LP_4), C) SATP5-5 (left second deciduous molar, Ldm_2), D) SATP5-6 (lower left first molar, LM_1), E) SATP5-7 (lower left second molar, LM_2). PRO = protoconid; MET = metaconid; HYP = hypoconid; ENT = entoconid; HYP* = hypoconulid; C6 = sixth cusp or entoconulid; C7 = seventh cusp or metoconulid; TR – CR = transverse crest; MAR = mesial accesory ridge; Ant-

Fov = anterior fovea; DTC = distal trigonid crest. The black bar is equivalent to 1 cm. B, buccal; D, distal; L, lingual; M, mesial; O, occlusal.

2.2 Morphometric analyses

Height of the mandibular corpus was measured perpendicular to the alveolar plane, and its breadth was taken at the maximum width of the mandibular corpus (Buikstra and Ubelaker, 1994; Rosas and Bermùdez de Castro, 1999).

The digital models of all the teeth, including the comparison sample, were optimized (e.g., healing defects) and oriented in Rapidform XOR2 (INUS Technology, Inc., Seoul, Korea) before the morphometric analyses. For Dzu 2, a virtual restoration was required before the analyses. This was carried out by moving the distal portion of the tooth until continuity in the cervical line, occlusal and lateral surface of the crown was restored (SOM Fig. S4). Each tooth was oriented by aligning the cervical plane (computed as the best-fit plane at the cervical line) parallel to the xy-plane of the Cartesian coordinate system and rotating the teeth around the z-axis so that the lingual side was parallel to the x-axis (e.g., Benazzi et al., 2012a). The crown outlines were projected onto the cervical plane, while the cervical outlines were represented by the contour of the section identified by the cervical plane itself. Both outlines (i.e., crown and cervical) were inscribed in a bounding box tangential to the most extreme points of the crowns to identify the mesio-distal (MD) and bucco-lingual (BL) diameters (Benazzi et al., 2011a; 2013a; Margherita et al., 2016).

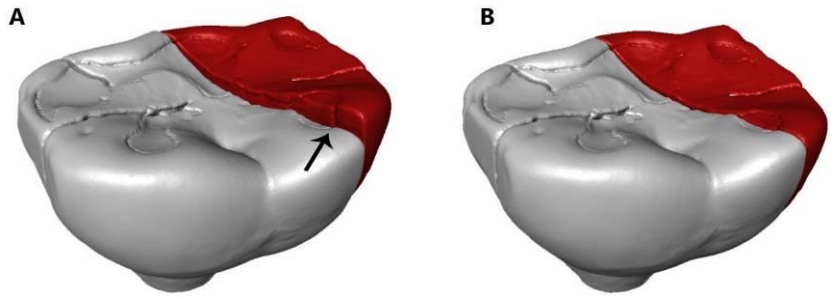

Figure S4. A) Original state of Dzu 2 (the arrow indicates the main crack); B) Virtual restoration of Dzu 2.

Moreover, for the deciduous molars we used crown (for Dzu 1, Dzu 2 and SATP5-5) and cervical outline analyses (for Dzu 2 and SATP5-5), following procedures in Benazzi et al. (2011b; 2012a) and Bailey et al. (2014). The outlines were imported in Rhino 4.0 Beta CAD environment (Robert McNeel and Associates, Seattle, WA), centered superimposing the centroids of their area, represented by 16 pseudolandmarks for Dzu 2 and SATP5-5 (Benazzi et al., 2012a; 2014a) and by 24 pseudolandmarks for Dzu1 (Bailey et al., 2014) obtained by equiangularly spaced radial vectors out of the centroid, and scaled to unit centroid size (Benazzi et al., 2011b; 2012a; Bailey et al., 2014).

For the permanent teeth, we computed 3D enamel thickness following guidelines provided by Benazzi and colleagues (2014b). To quantify the 3D enamel thickness of the permanent teeth, the crown was separated from the root using the interpolated surface of the cervical line. We measured: the enamel volume (mm3); the coronal dentine volume, which includes the volume of the crown pulp chamber (mm3); and the enamel-dentine junction (EDJ) surface (mm2). These measurements were used for the computation of both 3D average enamel thickness (3D AET = volume of enamel divided by the EDJ surface; in mm) and the 3D relative enamel thickness (3D RET = AET divided by the cubic root of dentine volume; scale-free) index.

Finally, in order to assess whether Dzu 1 and Dzu 2 belong to the same individual, both teeth were loaded in the Occusal Fingerprint Analyser (OFA) software (2008-2014 ZiLoX-IT GbR; www.for771.uni-bonn.de/for771-en/ofa). The software allows one model (i.e., Dzu 2) to be moved towards the antagonist (i.e., Dzu 1) along a defined pathway in order to analyse the collision of crown contacts. OFA software prevents the penetration of the models into one another and detects the occlusal contacts through collision detection, deflection and break free algorithms (for more details, see e.g., Benazzi et al., 2012b, 2013b, c, 2015, 2016; Kullmer et al., 2013; Fiorenza et al., 2015). Therefore, the colliding triangles of Dzu 1 and Dzu 2 during maximum intercuspation were detected and visualized to verify that they indeed belong to the same individual.

3. Results

3.1 Testing occlusal contacts between Dzu 1 and Dzu 2

Since Dzu 1 and Dzu 2 were retrieved from the same deposit, share a similar wear stage and root resorption, and represent antagonistic tooth classes (Rdm^2 and Rdm_2, respectively), they might belong to the same individual. However, only three occlusal contacts were detected during maximum intercuspation in the OFA software (SOM Fig. S5). Alternative solutions (e.g., moving Dzu 2 in slightly different positions), made the results even worse (results not shown). Overall, the few contact areas and the large gaps between the occlusal surfaces (Fig. S5) suggest the teeth do not belong to the same individual.

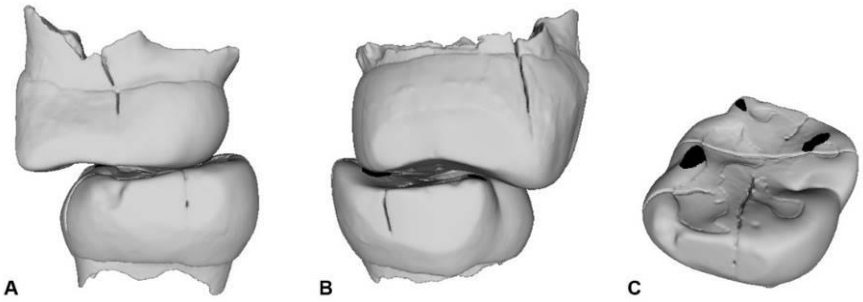

Figure S5. Collision detection for Dzu 1 (Rdm^2) and Dzu 2 (Rdm_2) in the Occlusal Fingerprint Analyser (OFA) software during maximum intercuspation (contact areas in black). A) mesial view; B) distal view; C) occlusal surface of Dzu 2 from mesio-lingual perspective.

3.2 Mandible

SATP5-5 shows several fractures. A fracture directed mesio-buccaly/disto-lingually interesects the occlusal surface, from which a second fracture departs directed mesio-lingually. Another small fracture is visible in the protoconid cusp.

3.3 Metric comparison

The main metric dimensions of the SATP5 mandible are shown in SOM Table S1. The scatter plots between MD and BL diameters of the permanent teeth (see SOM Table S2 for the comparative sample used) are shown in SOM Figure S6.

Table S1. Main metric dimensions of the SATP5 mandible.

Specimen/Sample	**Age at death (years)**	**Corpus height at mental foramen (mm)**	**Corpus thickness at mental foramen (mm)**	**Robusticity Index at mental foramen**[a]	**Source**
SATP5	~ 6.0-7.0	21.4	10.5	49.0	Present study
Neandertals					
Gegant-5	~4.5-5.0	22.6	12.8	56.6	Quam et al., 2015
Palomas 49	~ 2.0	19.2	11.4	59.4	Walker et al., 2010
Barakai	~3.0	20.1	14.2	70.6	Mallegni and Trinkaus, 1997
Archi 1	~3.0	20.0	12.0	60.0	Mallegni and Trinkaus, 1997
Roc de Marsal	~3.0	17.0	12.7	74.7	Madre-Dupouy, 1992
Il Molare 1	~3.5	20.9	12.2	58.4	Mallegni and Trinkaus, 1997
Palomas 7	~4.0	21.3	12.7	59.6	Walker et al., 2010
La Chaise 13	~4.0	20.5	12.5	61.0	Mallegni and Trinkaus, 1997

Devil's Tower	~4.0	22.8	13.6	59.6	Mallegni and Trinkaus, 1997
Cova Negra (CN 7755)	~5.0	20.0	13.3	66.5	Arsuaga et al., 1989
Combe Grenal 1	~7.0	27.4	13.6	49.6	Garralda and Vandermeersch, 2000
Modern Humans					
Le Figuier	~3.0	18.0	10.7	59.4	Billy, 1979
La Madeleine 4	~3.0	19.0	9.4	49.5	Heim, 1991
Lagar Velho	~4.5	20.5	11.5	56.1	Trinkaus, 2002
Skhul 1	~4.5	16.4	11.0	67.1	Mallegni and Trinkaus, 1997
Qafzeh 4	~6.0	26.3	14.2	54.0	Quam et al., 2015
Qafzeh 10	~6.0	24.2	13.3	55.0	Quam et al., 2015
Recent children (n=20)	2.0-5.0	17.2 ± 1.8	10.3 ± 1.0	60.4 ± 6.9	Madre-Dupouy, 1992

[a] Calculated as (corpus thickness/corpus height) X 100.

Table S2. Comparative sample (X indicates inclusion) of the P_3, P_4, M_1 and M_2 used for dental crown diameters (MD and BL) and three-dimensional (3D) enamel thickness analyses.

TAXON	Specimens	Tooth Class	Wear Stage	Diameters	Enamel Thickness
N	ABRISUARD_14_7	LM1	1	X	X
N	ABRISUARD_49	LM1	1	X	X
N	BDJ4C9	LM1	1	X	X
N	Engis	LM1	1	X	X
N	Krapina 52	LM1	1	X	X
N	Krapina 80	LM1	1	X	X
N	La Ferrasie 8	LM1	1	X	
N	Roc_de_Marsal	LM1	1	X	X
N	Taddeo 4[a]	LM1	2	X	X
N	BD1	LM1	4	X	X
N	Krapina 53	LM1	3	X	X
N	Krapina 54	LM1	3	X	X
N	Krapina 55	LM1	3	X	X
N	Krapina 57	LM1	4	X	X
N	Krapina 58	LM1	4	X	X
N	Krapina 59	LM1	4	X	X
N	Le Moustier	LM1	4	X	X
N	Regourdou	LM1	4	X	X
N	St. Cesaire	LM1	4	X	X
N	Vindija_11_39	LM1	4	X	X

N	Weimer_Ehringsdorf	LM1	3	X	X
N	Scla_4A_1[b]	LM1	3		X
N	Scla_4A_9[b]	LM1	3		X
N	Kebara 2	LM1	5	X	X
EHS	AP_6242	LM1	2	X	X
EHS	AP_6277	LM1	1	X	X
EHS	Dar_Es_Sultane 2_H4	LM1	4	X	X
EHS	Temara	LM1	4	X	X
UPHS	Villabruna	LM1	4		X
RHS	167_175_	LM1	2	X	X
RHS	213	LM1	2	X	X
RHS	M5	LM1	2	X	X
RHS	M6	LM1	2	X	X
RHS	R123	LM1	1	X	X
RHS	R488_274	LM1	2	X	X
RHS	R1160_440	LM1	2	X	X
RHS	R2602_1673	LM1	2	X	X
RHS	ULAC_1	LM1	3	X	X
RHS	ULAC_58	LM1	3	X	X
RHS	ULAC_74	LM1	4	X	X
RHS	ULAC_151	LM1	4	X	X
RHS	ULAC_536	LM1	4	X	X
RHS	ULAC_607	LM1	4	X	X
RHS	ULAC_790	LM1	4	X	X
RHS	ULAC_797	LM1	3	X	X
RHS	ULAC_801	LM1	3	X	X

N	Krapina 57	LM2	2	X	X
N	KRP_D1	LM2	2	X	X
N	LeMoustier	LM2	1	X	X
N	Krapina 54	LM2	1	X	X
N	Krapina_55	LM2	1	X	X
N	S36	LM2	2	X	X
N	SD540	LM2	1	X	X
N	Scladina 4A-1[b]	LM2	2		X
N	Scladina 4A-9[b]	LM2	1		X
N	Regourdou	LM2	3	X	X
N	Krapina_58	LM2	4	X	X
N	Krapina_59	LM2	3	X	X
N	St_Cesaire	LM2	4	X	X
EHS	AP_6282	LM2	2	X	X
EHS	Temara	LM2	2	X	X
EHS	Dar_Es_Sultane _H4	LM2	1	X	X
EHS	ElHarhoura	LM2	3	X	X
RHS	M145	LM2	3	X	X
RHS	167_I75	LM2	2	X	X
RHS	Belgian76a	LM2	2	X	X
RHS	M19_	LM2	2	X	X
RHS	M181	LM2	2	X	X
RHS	M190	LM2	2	X	X
RHS	M232	LM2	2	X	X
RHS	R115	LM2	2	X	X
RHS	R123	LM2	1	X	X
RHS	R258	LM2	2	X	X

N	Krapina_D34	LP3	2	X	X
N	Krapina_D111	LP3	1	X	X
N	Krapina_D114	LP3	1	X	X
N	Le_Moustier	LP3	1	X	X
N	Krapina_54	LP3	1	X	X
N	Krapina_52	LP3	1	X	X
N	Krapina_55	LP3	1	X	X
N	Scla_4A_6[b]	LP3	1		X
N	KRAPINA_58	LP3	3	X	X
N	VI_11_45	LP3	3	X	X
EHS	Qafzeh_9	LP3	1	X	X
RHS	M14	LP3	2	X	X
RHS	M35	LP3	1	X	X
RHS	M36	LP3	1	X	X
RHS	ULAC_1	LP3	2	X	X
RHS	ULAC_13	LP3	1	X	X
RHS	ULAC_58	LP3	2	X	X
RHS	ULAC_151	LP3	1	X	X
RHS	ULAC_536	LP3	2	X	X
RHS	ULAC_790	LP3	2	X	X
RHS	ULAC_801	LP3	1	X	X
RHS	ULAC_806	LP3	1	X	X
RHS	ULAC_66	LP3	3	X	X
RHS	ULAC_74	LP3	3	X	X
RHS	ULAC_171	LP3	3	X	X
RHS	ULAC_522	LP3	3	X	X
N	KRP_D35	LP4	2	X	X
N	KRP_D50	LP4	1	X	X

N	KRP_D113	LP4	1	X	X
N	SD_763	LP4	1	X	X
N	CG_29	LP4	1	X	X
N	KRP_D118	LP4	1	X	X
N	Krapina_54	LP4	2	X	X
N	Krapina_52	LP4	1	X	X
N	Le_Moustier	LP4	1	X	X
N	Krapina_58	LP4	3	X	X
N	CG_VIII	LP4	4	X	X
N	Scla 4A-1[b]	LP4	1		X
N	Scla 4A-9[b]	LP4	1		X
EHS	Irhoud_3	LP4	1	X	X
EHS	Qafzeh_9	LP4	1	X	X
EHS	El_Harhoura	LP4	3	X	X
EHS	Temara	LP4	3	X	X
RHS	M7	LP4	1	X	X
RHS	M39	LP4	1	X	X
RHS	ULAC_1	LP4	2	X	X
RHS	ULAC_13	LP4	1	X	X
RHS	ULAC_74	LP4	2	X	X
RHS	ULAC_151	LP4	2	X	X
RHS	ULAC_790	LP4	2	X	X
RHS	ULAC_806	LP4	1	X	X
RHS	ULAC_171	LP4	3	X	X
RHS	ULAC_522	LP4	3	X	X
RHS	ULAC_799	LP4	3	X	X
RHS	ULAC_536	LP4	3	X	X

[a] Benazzi et al., 2011c.

[b] Benazzi et al., 2014c.

The values of the component of the 3D enamel thickness for the Satsurblia permanent posterior teeth and the comparative sample are shown in Tables 3 and S3. For premolars and second molar at wear stage 1–2, Neandertals show significantly lower RET indices than RHS ($p<0.01$; Table 3). In particular, the premolars show the largest differences between the two groups (i.e., Neandertals and H. sapiens). No significant differences were observed for the M1 ($p=0.507$). Even though the small EHS sample size prevents statistical analysis, the EHS means computed for all tooth classes are always closer to RHS than Neandertal.

When the 3D enamel thickness of Satsurblia permanent teeth was compared with the RET mean values computed for Neandertals, EHS and RHS, the computed Z-scores are always closer to the H. sapiens means than to the Neandertal ones (Table 3).

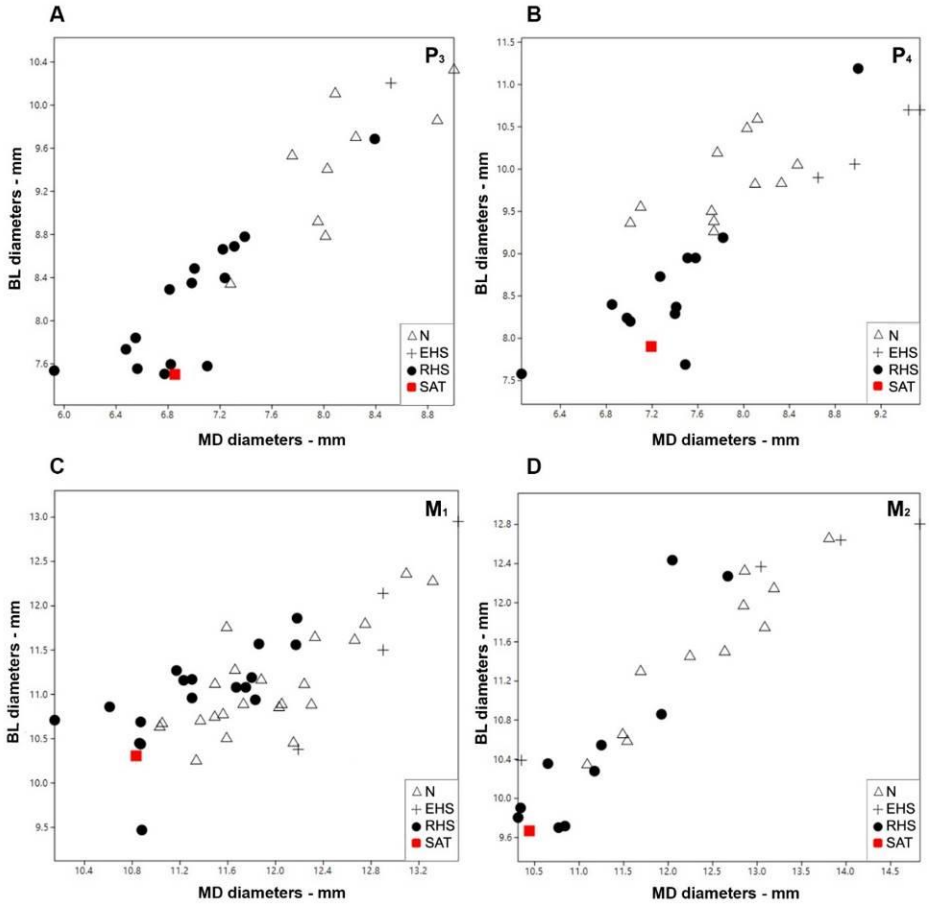

Figure S6. Scatter plot between MD and BL diameters of permanent teeth from Satsurblia cave. N = Neadertals; EHS = early *Homo sapiens*; RHS = recent *Homo sapiens*.

Table S3. Three-dimensional (3D) average enamel thickness (AET) and relative enamel thickness (RET).

Sample [a]	**Wear**[b]	**3D AET Mean (SD/*n*)**	**Z-score**	**3D RET Mean (SD/*n*)**	**Z-score**
SATP5-3 (LP_3)		1.17		26.75	
N	1-2	0.97 (0.08/8)	0.21	18.55 (1.60/8)	5.12
N	3	0.72 (0.09/2)		13.43 (2.14/2)	
EHS	1-2	1.3		24.76	
RHS	1-2	1.10 (0.13/11)	0.54	24.39 (2.38/11)	0.99
RHS	3	0.86 (0.06/4)	5.16	19.60 (0.93/4)	7.69
SATP5-4 (LP_4)		1.61		41.46	
N	1-2	1.08 (0.09/11)	5.89	20.62 (2.37/11)	8.79
N	3	0.86 (0.02/2)		16.49 (0.19/2)	
EHS	1-2	1.39 (0.02/2)		25.23 (1.86/2)	
EHS	3	1.25 (0.07/2)		22.83 (8.37/2)	
RHS	1-2	1.20 (0.12/8)	3.42	25.69	7.10

				(2.22/8)	
RHS	3	1.16 (0.16/4)	2.81	25.01 (4.46/4)	3.69
SATP5-6 (LM_1)		1.26		20.47	
N	1-2	1.22 (0.12/8)	0.33	18.61 (1.59/8)	1.17
N	3	1.08 (0.11/6)	1.64	15,86 (1.33/6)	3.47
N	4	0.81 (0.12/9)	3.75	12,21 (1.66/9)	4.97
EHS	1-2	1.23 (0.31/2)		19.64 (6.30/2)	
EHS	4	1.08 (0,14/2)		14.9 (1.66/2)	
RHS	1-2	1.23 (0,17/8)	0.18	20.17 (3.50/8)	0.29
RHS	3	1.04 (0.11/5)	2	16.16 (1.98/8)	2.18
RHS	4	0.90 (0.12/5)	3	14.30 (2.34/5)	2.64
SATP5-7 (LM_2)		1.37		23.7	
N	1-2	1.18 (0.14/9)	1.36	17.42 (2.60/9)	2.41
N	3	0.94 (0.09/2)		13.88 (0.37/2)	
N	4	0.75 (0.19/2)		11.43 (3.78/2)	

EHS	1-2	1.41 (0.15/3)		22.10 (2.33/3)	
EHS	3	1.07 (0.15/2)		15.53 (0.97/2)	
RHS	1-2	1.34 (0.16/9)	0.19	21.61 (1.73/9)	1.20

[a]Satsurblia specimens are standardized to Z-scores of the Neandertal (N), early *H. sapiens* (EHS) and recent *Homo sapiens* (RHS) samples for different wear stages.

[b] Molnar, 1971.

4. References

Arsuaga, J.L., Gracia, A., Martínez, I., Bermúdez de Castro, J.M., Rosas, A., Villaverde, V., Fumanal, M.P., 1989. The human remains from Cova Negra (Valencia, Spain) and their place in European Pleistocene human evolution. J. Hum. Evol. 18, 55-92.

Bailey, S.E., Benazzi, S., Souday, C., Astorino, C., Paul, K., Hublin, J.J., 2014. Taxonomic differences in deciduous upper second molar crown outlines of *Homo sapiens*, *Homo neanderthalensis* and *Homo erectus*. J. Hum. Evol. 72, 1–9.

Bar-Yosef, O., Belfer-Cohen, A., Mesheviliani, T., Jakeli, N., Bar-Oz, G., Boaretto, E., Goldberg, P., Kvavadze, E., Matskevich, Z., 2011. Dzudzuana: an Upper Palaeolithic cave site in the Caucasus foothills (Georgia). Antiquity 85, 331–349.

Benazzi, S., Coquerelle, M., Fiorenza, L., Bookstein, F., Katina, S., Kullmer, O., 2011a. Comparison of dental measurement systems for taxonomic

assignment of first molars. Am. J. Phys. Anthropol. 144, 342-354.

Benazzi, S., Douka, K., Fornai, C., Bauer, C.C., Kullmer, O., Svoboda, J.J., Pap, I.I., Mallegni, F., Bayle, P., Coquerelle, M., Condemi, S., Ronchitelli, A., Harvati, K., Weber, G.W., 2011b. Early dispersal of modern humans in Europe and implications for Neanderthal behaviour. Nature 479, 525-528.

Benazzi, S., Viola, B., Kullmer, O., Fiorenza, L., Harvati, K., Paul, T., Gruppioni, G., Weber, G.W., Mallegni, F., 2011c. A reassessment of the Neanderthal teeth from Taddeo cave (southern Italy). J. Hum. Evol. 61, 377–387.

Benazzi, S., Fornai, C., Buti, L., Toussaint, M., Mallegni, F., Ricci, S., Gruppioni, G., Weber, G.W., Condemi, S., Ronchitelli, A., 2012a. Cervical and crown outline analysis of worn Neanderthal and modern human lower second deciduous molars. Am. J. Phys. Anthropol. 149, 537–546.

Benazzi, S., Kullmer, O., Grosse, I., Weber, G., 2012b. Brief communication: comparing loading scenarios in lower first molar supporting bone structure using 3D finite element analysis. Am. J. Phys. Anthropol. 147, 128-134.

Benazzi, S., Bailey, S.E., Mallegni, F., 2013a. Brief communication: A morphometric analysis of the Neandertal upper second molar Leuca I. Am. J. Phys. Anthropol. 152, 300-305.

Benazzi, S., Nguyen, H.N., Schulz, D., Grosse, I.R., Gruppioni, G., Hublin, J.J., Kullmer, O., 2013b. The evolutionary paradox of tooth wear: simply destruction or inevitable adaptation? PLOS ONE 8, e62263.

Benazzi, S., Nguyen, H.N., Kullmer, O., Hublin, J.J., 2013c. Unravelling the functional biomechanics of dental features and tooth wear. PLOS ONE 8, e69990.

Benazzi, S., Bailey, S.E., Peresani, M., Mannino, M.A., Romandini, M., Richards, M.P., Hublin, J.J., 2014a. Middle Paleolithic and Uluzzian human remains from Fumane cave, Italy. J. Hum. Evol. 70, 61-68.

Benazzi, S., Panetta, D., Fornai, C., Toussaint, M., Gruppioni, G., Hublin, J.J., 2014b. Technical Note: Guidelines for the digital computation of 2D and 3D enamel thickness in hominoid teeth. Am. J. Phys. Anthropol. 153, 305-313.

Benazzi, S., Toussaint, M., Hublin, J-J., 2014c. Enamel thickness in the Scladina Neandertal teeth. In: Toussaint, M., Bonjean, D. (Eds.), The Scladina I-4A Juvenile Neandertal. Liège: ERAUL, pp. 307 – 314.

Benazzi, S., Nguyen, H.N., Kullmer, O., Hublin, J.J., 2015. Exploring the biomechanics of taurodontism. J. Anat. 226, 180-188.

Benazzi, S., Nguyen, H.N., Kullmer, O., Kupczik, K., 2016. Dynamic modelling of tooth deformation using occlusal kinematics and finite element analysis. PLOS ONE 11, e0152663.

Billy, G., 1979. L'enfant Madgalénien de la Grotte du Figuier (Ardéche). L'Anthropologie
83, 223-252.

Buikstra, J.E., Ubelaker, D.H. (Eds.), 1994. Standards for data collection from human skeletal remains: procedings of a seminar at the Field Museum of Natural History. Arkansas Archeological Survey Research Series No. 44.

Fiorenza, L., Nguyen, H.N., Benazzi, S., 2015. Stress distribution and molar macrowear in *Pongo pygmaeus*: A new approach through finite element and occlusal fingerprint analyses. Hum. Evol. 30, 215-226.

Garralda, M., Vandermeersch, B., 2000. Les Néandertaliens de la Grotte de Combe-Grenal (Domme, France). Paleo 12, 213-259.

Heim, J.L., 1991. L'enfant Magdalénien de la Madeleine. L'Anthropologie 95, 611-638.

Kullmer, O., Benazzi, S., Schulz, D., Gunz, P., Kordos, L., Begun, D.R., 2013. Dental arch restoration using tooth macrowear patterns with application to *Rudapithecus hungaricus*, from the late Miocene of Rudabánya, Hungary. J. Hum. Evol. 64, 151-160.

Kvavadze, E., Bar-Yosef, O., Belfer-Cohen, A., Boaretto, E., Jakeli, N., Matskevich, Z., Meshveliani, T., 2009. 30 000-year-old wild flax fibers. Science 325, 1359.

Madre-Dupouy, M., 1992. L'enfant du Roc de Marsal: Etude Analytique et Comparative. CNRS, Paris.

Mallegni, F., Trinkaus, E., 1997. A reconsideration of the Archi 1 Neandertal mandible. J. Hum. Evol. 33, 651-668.

Margherita, C., Talamo, S., Wiltschke-Schrotta, K., Senck, S., Oxilia, G., Sorrentino, R., Mancuso, G., Gruppioni, G., Lindner, R., Hublin, J.J., Benazzi, S., 2016. A reassessment of the presumed Torrener Bärenhöhle's Paleolithic human tooth. J. Hum. Evol. 93, 120-125.

Molnar, S., 1971. Human tooth wear, tooth function and cultural variability. Am. J. Phys. Anthropol. 34, 175-189.

Panetta, D., Belcari, N., Del Guerra, A., Bartolomei, A., Salvadori, P.A., 2012. Analysis of image sharpness reproducibility on a novel engineered micro-CT scanner with variable geometry and embedded recalibration software. Phys. Medica 28, 166-173.

Pinhasi, R., Meshveliani, T., Matskevich, Z., Bar-Oz, G., Weissbrod, L., Miller, C.E., Wilkinson, K., Lordkipanidze, D., Jakeli, N., Kvavadze, E., Higham, T.F.G., Belfer-Cohen, A., 2014. Satsurblia: New insights of human response and survival across the Last Glacial Maximum in the southern Caucasus. PLOS ONE 9, e111271.

Quam, R., Sanz, M., Daura, J., Robson Brown, K., García-González, R., Rodríguez, L., Dawson, H., Rodríguez, R.F., Gómez, S., Villaescusa, L., Rubio, A., Yagüe, A., Ortega Martínez, M.C., Fullola, J.M., Zilhão, J., Arsuaga, J.L., 2015. The Neandertals of northeastern Iberia: New remains from the Cova del Gegant (Sitges, Barcelona). J. Hum. Evol. 81, 13-28.

Rosas, A., Bermùdez de Castro, J.M., 1999. The ATD6-5 mandibular specimen from Gran Dolina (Atapuerca , Spain). Morphological study and phylogenetic implications. J. Hum. Evol. 37, 567-590.

Trinkaus, E., Ruff, C., Esteves, F., Santos-Coelho, J., Silva, M., Mendonça, M., 2002. The upper limb remains. In: Zilhao, J., Trinkaus, E. (Eds.), Portrait of the Artist as a Child: The Gravettian Human Skeleton from the Abrigo do

Lagar Velho and its Archeological Context. Instituto Português de Arqueología, Lisboa, pp. 466-488.

Walker, M.J., Lombardi, A.V., Zapata, J., Trinkaus, E., 2010. Neandertal mandibles from the Sima de las Palomas del Cabezo Gordo, Murcia, southeastern Spain. Am. J. Phys. Anthropol. 142, 261-272.

Scientific Reports - Nature

(Sci. Rep. 2017, 7 - 2958 doi:10.1038/s41598-017-03025-z)

The first Neanderthal remains from an open-air Middle Palaeolithic site in the Levant

Ella Been[1,2], Erella Hovers[3,4], Ravid Ekshtain[3], Ariel Malinski-Buller[5], Nuha Agha[6], Alon Barash[7], Daniella E. Bar-Yosef Mayer[8,9], Stefano Benazzi[10,11], Jean-Jacques Hublin[11], Lihi Levin[2], Noam Greenbaum[12], Netta Mitki[3], Gregorio Oxilia[13,10,] Naomi Porat [14], Joel Roskin [15,16], Michalle Soudack[17,18], ReuvenYeshurun[19], Ruth Shahack-Gross[15], Nadav Nir[3], Mareike C. Stahlschmidt[20], Yoel Rak[2] & Omry Barzilai[6]

[1] Department of Physical Therapy, Faculty of Health Professions, Ono Academic College, Kiryat Ono 55107, Israel

[2] Department of Anatomy and Anthropology, Sackler Faculty of Medicine, Tel Aviv University, Tel Aviv 69978, Israel

[3] Institute of Archaeology, the Hebrew University of Jerusalem, Jerusalem 91905, Israel

[4] MONREPOS Archaeological Research Centre and Museum for Human Behavioural Evolution, Schloss Monrepos, D - 56567 Neuwied, Germany

[5] Israel Antiquities Authority, P.O. Box 586, Jerusalem 91004, Israel

[6] Faculty of Medicine in the Galilee, Bar Ilan University, Zefat 13115, Israel

[7] Steinhardt Museum of Natural History, Tel Aviv University, Tel Aviv 69978, Israel

[8] Peabody Museum of Archaeology and Ethnology, Harvard University, 11 Divinity Avenue, Cambridge, MA 02138

[9] Department of Cultural Heritage, University of Bologna, Via degli Ariani 1, 48121 Ravenna, Italy

[10] Department of Human Evolution, Max Planck Institute for Evolutionary Anthropology, Deutscher Platz 6, 04103 Leipzig, Germany

[11] Department of Geography & Environmental Studies, University of Haifa, Haifa 34988, Israel

[12] Department of Biology, University of Florence, Via del Proconsolo, 12, 50122 Firenze, Italy

[13] Luminescence Dating Lab, Geological Survey of Israel, Jerusalem 95156, Israel

[14] Department of Maritime Civilizations, University of Haifa, Haifa 34988, Israel

[15] Department of Diagnostic Imaging, Chaim Sheba Medical Center, Tel Hashomer 52621, Israel

[16] Sackler Faculty of Medicine, Tel Aviv University, Tel Aviv 69978, Israel

[17] Zinman Institute of Archaeology, University of Haifa, Haifa 34988, Israel

[18] School of Archaeology, University College Dublin, Belfield, Dublin 4, Ireland

Introduction

The Middle Palaeolithic (MP) of the southern Levant is a significant period for the study of human evolution because two types of hominins, Neandertals and *Homo sapiens*, occupied the region at that time (see, for example, 1, 2). Diagnostic fossil remains of the two species have been found in the Mediterranean woodland region, but until recently, they were discovered only at cave sites (Fig. 1). The absolute chronology of the Levantine MP fossils indicates that *H. sapiens* existed between 120 and 90 ka and again from 55 ka on; Neandertals existed in that region between ca. 80 and ca. 55 ka (3–16). The genomic evidence suggests gene flow from early *H. sapiens* to the eastern Altai Neandertals ca. 100 ka (17) and flow from Neandertals to *H. sapiens* between ca. 60 and 50 ka (18). In the Levant, the archaeological record cannot distinguish between these two MP populations. The lithic variability observed in the Levantine MP is not clearly taxonomy related (19; for a different view see [20]). The two populations left similar material culture remains—in particular, lithic industries that include the Levallois technology. In addition, the populations seem to have had similar settlement and mobility patterns in respect to the use of caves for habitation and burials; at Tabun, these populations used the same cave diachronically (12, 13, 21, 22).

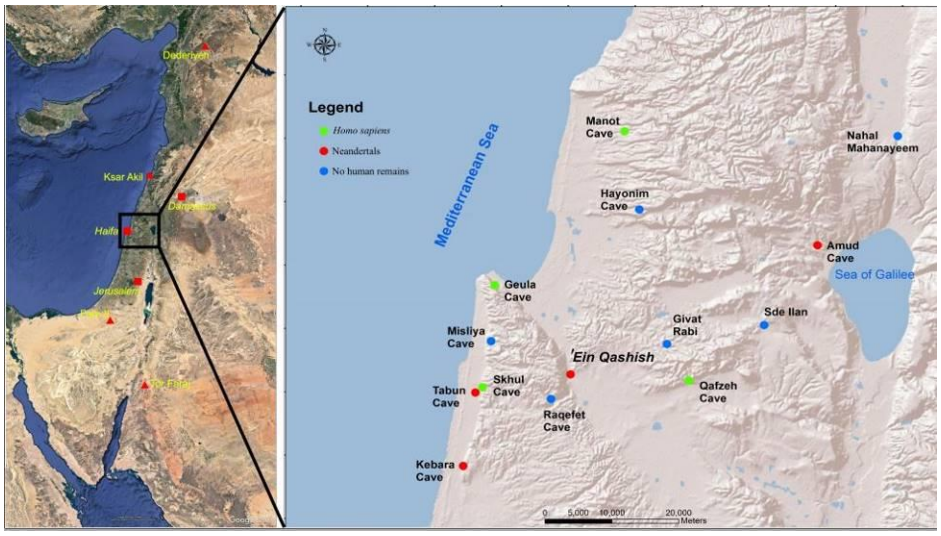

Figure 1. Left Major Middle Palaeolithic sites (triangles) and modern cities (squares) in the Near East. Right: Location of 'Ein Qashish and other Middle Palaeolithic sites in northern Israel. Th map was generated using ESRI ArcInfo v10.4.

The discovery of several previously unknown MP open-air sites in the Mediterranean woodland region in the last decade diverted much of the research focus to MP behaviors associated with the open landscape (e.g., 23). In the absence of taxonomically informative fossil remains, it was impossible to attribute these (as well as previously reported) open-air sites to either Neandertals or *H. sapiens*. Therefore, it was also difficult to determine these species' settlement patterns and territorial behavior within the Levant. The new discovery of Neandertal remains at the late MP open-air site of 'Ein Qashish provides a window into the settlement and mobility patterns of the Neandertals of northern Israel.

The Site

‘Ein Qashish is located on the south bank of the Qishon stream in the Jezreel Valley, facing the eastern slopes of Mount Carmel, Israel (Fig. 1). Excavations at the site in 2009– 2011 exposed remains of a Late Mousterian occupation on the Qishon floodplain (24–28). In 2013, the site was subjected to an extensive salvage excavation during which an area of ca. 650 m2 was dug to a maximum depth of 4.5 m (29; SI 1). The stratigraphy consists of six sedimentary layers comprising four occupational horizons (Fig. 2). The 2013 excavation is laterally and stratigraphically contiguous to the original excavation, with a similar depositional context. The sediments are composed mainly of black heavy clays representing the flood plain of the palaeo-Qishon stream and coarse cobbles transported by short, steep, fast-flowing streams off the eastern flanks of Mount Carmel (25, 26; SI 1). The site sequence was dated through optically stimulated luminescence (OSL), which puts the time range of all the examined archaeological horizons at ca. 70–60 ka (SI 2 Table 1), similar to the range of dates of the stratigraphic sequence of the 2009–2011 excavation, established through the same dating techniques (26).

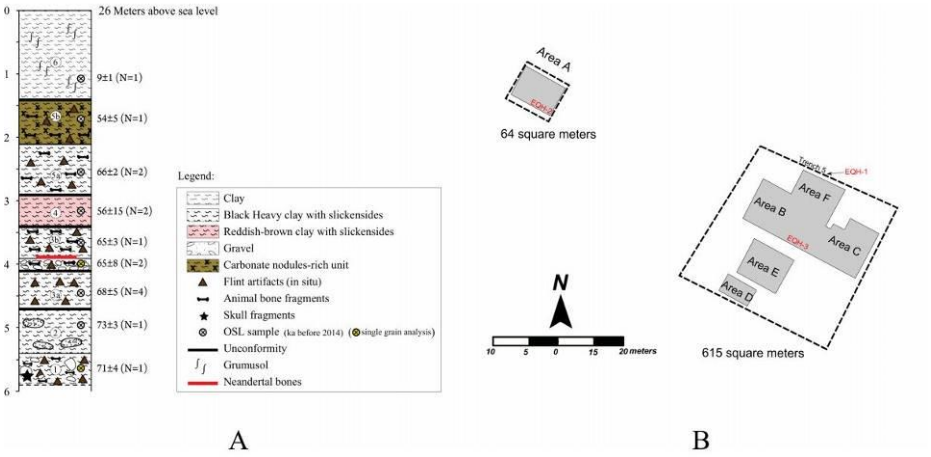

Figure 2. Schematic plan of ‘Ein Qashish. (**A**) Compiled stratigraphic section with vertical locations of OSL dates, in thousands of years, and hominin fossils. (**B**) Plan of excavation areas with spatial locations of hominin fossils.

The Context of the Hominin Remains

The hominin remains from ‘Ein Qashish represent three individuals that were found in three distinct layers (Fig. 2). Specimen EQH1 is a nondiagnostic skull fragment that was discovered in a mechanically dug geological trench prior to the 2013 excavation (29; SI 1). The stratigraphic position of the fossil corresponds to Layer 1, the lowest in the documented sections in the site’s vicinity. Layer 1 is absent from the sequence in the archaeological excavation itself (N.Greenbaum, pers. obs.). Contextual data for the layer are poor. The second fossil, EQH2, is an upper third molar (Fig. 3) from Layer 5a, in Area A. The fossil was found associated with flint artefacts and faunal remains in a horizon with refitted lithic items (51 refitted items in 21 aggregates) (SI 1), indicating a moderately disturbed *in situ* context.

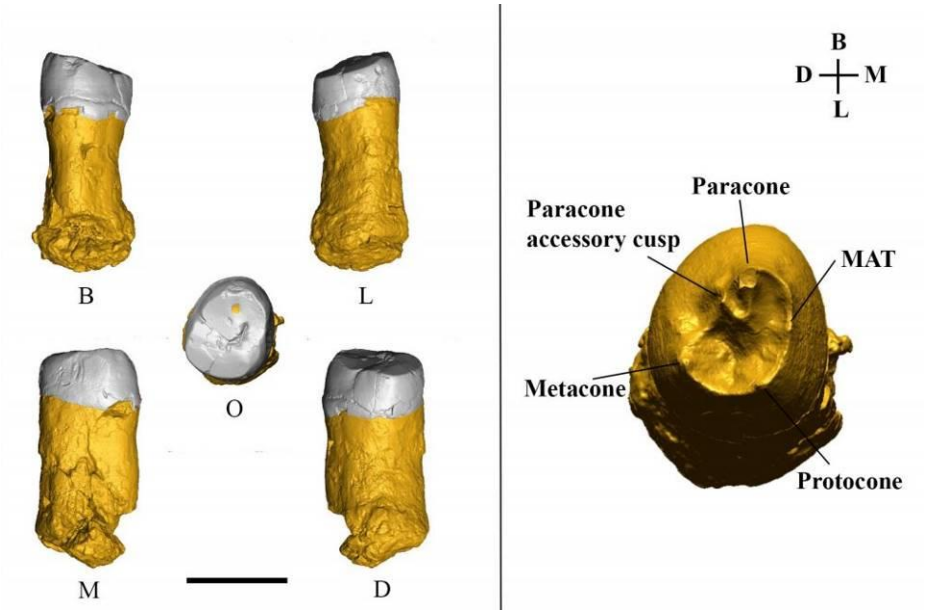

Figure 3. 3D digital model of specimen EQH2, an upper right third molar. Left Various views—B, buccal; L, lingual; M, mesial; D, distal; O, occlusal. Th black bar represents 1 cm. Right: Th enamel-dentine junction (EDJ) surface of EQH2.

The best-preserved specimen is EQH3, consisting of five lower limb bones—a femur, two tibiae, and two fibulae (Fig. 4)—associated with an occupational horizon in stratigraphic Layer 3b, Area B (for details of the archaeological context, see SI 1). The femur and the left tibia of EQH3 were found articulated. The bones were aligned along the same axis, with the right tibia parallel to the left (Fig. 4*A*, *B*). One of the two fibulae (B1880) was discovered ca. 50 cm north of the femur-tibia cluster, and the other fibula (B12255), ca. 70 cm south of the cluster (Fig. 4*A*). Finds other than human remains in this particular horizon comprise fresh flint artefacts (with 21 refitted items from four aggregates); fragmented animal bones; limestone clasts, including potential manuports (possibly anvils); ochre; a roe deer antler; and a seashell, *Hexaplex*

trunculus (Linnaeus, 1758) (SI 1). OSL dating of sediments directly above and below EQH3 puts the fossil at 65 ± 8 ka (SI 2).

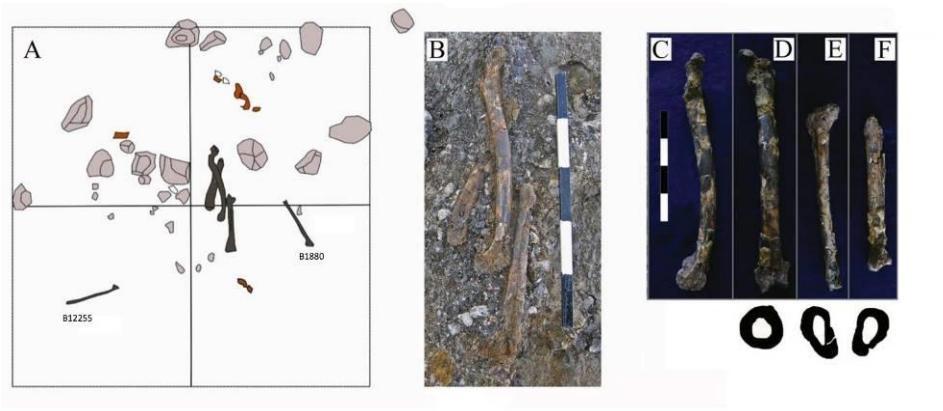

Figure 4. Specimen EQH3. (**A**) Th spatial location of the fie lower limb bones of EQH3 (dark brown); specimens B1880 and B12255 are fiulae. Pink: stones; reddish-brown: faunal remains. (**B**) Th bones *in situ*. Note the partial articulation of the lef femur and lef tibia. (**C**) Lef femur, medial view. (**D**) Lef femur, anterior view; midshaf cross section (underneath). (**E**) Lef tibia, anterior view; midshaf cross section (underneath). (**F**) Right tibia, anterior view; midshaf cross section (underneath).

EQH2

EQH2 is an upper right third molar (RM3) on which both the crown (with a mesiodistal [MD] length of 8.3 mm and buccolingual [BL] length of 9.7 mm) and the root (with a length of 14.3 mm) are preserved. The moderate wear of the tooth, with the dentine exposed on the paracone cusp, corresponds to wear stage (category) 3 of Molnar's dental attrition classification (30). In an occlusal view, the crown outline is oval, and although tooth wear has removed most of the occlusal features, three main cusps (the protocone, paracone, and metacone) can be identified (Fig. 3, right). At the enamel-dentine junction (EDJ) (Fig. 3, right;

SI 3 Table 1), two accessory cusps (the mesial accessory tubercle [MAT] and paracone accessory cusp) are present, but there is no trace of the distolingual cusp (the hypocone) or Carabelli's cusp. An interproximal wear facet (length, 3.81 mm; width, 4.19 mm) is visible only on the mesial side of the tooth (Fig. 3, left). The tooth is hypertaurodontic and does not show root bifurcation. We compared the MD and BL crown diameters of EQH2 to the diameters in tooth samples from Neandertals, early *H. sapiens*, Upper Palaeolithic *H. sapiens*, and recent *H. sapiens* (SI 3 Table 2; SI 3 Fig. 1). There is a large overlap in the distribution of the MD and BL diameters in our comparative sample. The values obtained for EQH2 are the lowest among the fossils and are the closest to the values obtained for the Neandertal specimens Saccopastore 1, Amud 1, and Tabun 1 and the Upper Palaeolithic *H. sapiens* specimen Kostenki XIV (SI 3 Fig. 1). With regard to the relative enamel thickness (RET) index, the z score computed for the EQH2 RET value (18.9) is closer to the Neandertal mean than to the means of early, Upper Palaeolithic, and recent *H. sapiens* (SI 3 Tables 3, 4). Dental tissue volumes and root measurements of EQH2 and the comparative sample (SI 3 Fig. 2; SI 3 Tables 4, 5) show that the root of EQH2 is somewhat larger than in the comparative sample. The computed z score for EQH2's root length, total root volume, pulp volume, and root pulp volume is closer to that of the Neandertals, whereas the coronal pulp volume is closer to that of Upper Palaeolithic *H. sapiens* and the cervical plane area is closer to that of recent *H. sapiens*. The cross-validation linear discriminant analysis of four root variables (root length, root volume, pulp volume, and cervical plane area) shows that 23 modern humans (92% of our sample) and all Neandertals in our sample were correctly classified and attributes EQH2 to *H. neanderthalensis* with a *P*post of 70%. Note that if we remove the cervical plane area from the analysis, EQH2 is attributed to *H. neanderthalensis* with a *P*post value of 81%.

EQH3

The lower limb bones of EQH3 consist of a left femur, two tibiae, and two fibulae. Out of the five lower limb bones, only the femur and two tibiae are preserved enough for analysis (Fig. 4*C–F*). The femur is essentially complete (Fig. 4). The femoral shaft is highly curved on the sagittal plane (i.e., anteroposteriorly), with the apex of the curvature located distal to the midshaft. The midshaft shape ratio (with a pilastric index of 99.1) indicates a rounded cross section (the anteroposterior diameter and mediolateral diameter are nearly equal) (Fig. 4; SI 4 Table 3). The midshaft robusticity index (14.9) indicates a highly robust femur. The midshaft cross-sectional area is large, with a relatively high percentage of cortical bone. All of these features are well-documented Neandertal characteristics that differ considerably from the more gracile femur of early and recent *H. sapiens*. There, the midshaft has a drop-shaped cross section and is straight compared to that of the Neandertals (31–36) (SI 4). The distal epiphysis of the EQH3 femur is relatively small, and the intercondylar fossa is extremely narrow, a feature that is not usually seen in either *H. sapiens* or Neandertals (SI 4). The remains of the right tibia include the diaphysis distal to the soleal line and the distal epiphyses; the proximal part of the tibia is missing (Fig. 4). Nearly complete, the left tibia is missing only its medial malleolus. The tibial plateau is flat, with a robust intercondylar tubercle (the medial part of the intercondylar eminence). Both tibiae exhibit fragmented and slightly distorted shafts, which are robust and narrow mediolaterally (platycnemic), similar to the tibia of Amud 1 (37). The anterior crest of the right and left tibial shafts and the interosseous borders are smooth and rounded. At 81.5, the crural index indicates that the tibia is short relative to the femoral length. Again, most of the striking features of the tibiae are associated with Neandertal morphology: the robust shaft, the rounded anterior crest and interosseous border, and the low crural index. The morphology of these tibiae

contrasts with that of the more gracile *H. sapiens* tibiae, which are characterized by generally angular anterior and interosseous crests and a high crural index (38, 39). The lower limb bones of EQH3 were found close together, with some in articulation. All belong to a male Neandertal, and no duplicate bones were found, suggesting that these bones represent a single individual (SI 4). The estimated height of the individual is 163.6 cm, which is close to the mean height for male Neandertals (166.7 ± 5.9 cm) and significantly less than the considerable height of the *H. sapiens* specimens from Qafzeh and Skhul (185.1 ± 7.1 cm) (SI 4; 40). Computed tomography (CT) reveals the presence of the epiphyseal line at the distal end of the femur and the proximal and distal ends of the tibiae, indicating ossification stage three out of four (41, 42). Thus, the individual's age at death can be estimated at 15–22 y (young adult) (SI 4). The combination of a narrow intercondylar notch and a robust intercondylar tubercle is not often seen in the knee joints of hominins (SI 4). This unique morphology is associated with an avulsion fracture of the anterior cruciate ligament (ACL). Such a traumatic injury occurs most commonly in skeletally immature individuals, between the ages of 8 and 14 years (43). If this pathology was present in the knee of EQH3, the individual might have suffered from instability of the left knee joint and therefore would probably have attempted to minimize the weight borne by the left leg. The small articular surface of the distal femur might be the result of the pathology, given that articular surface area is directly related to the amount of axial pressure exerted on the joint (SI 4; 44).

Discussion

The absolute dating of contexts associated with the Neandertal fossils from Tabun, Dederiyeh, Kebara, and Amud Caves suggests that Neandertals occupied the southern Levant between ca. 80 and ca. 55 ka (3, 6, 10, 12, 13, 45). Because diagnostic hominin remains from open-air sites dated to this period were not available until now (e.g., 46, 47), attributing the occupation of open-air

sites to Neandertal settlement systems called for caution. However, the fossils EQH2 and EQH3 derive from two distinct stratigraphic horizons, and their associated OSL ages suggest that the open-air site of ‘Ein Qashish was used repeatedly by Neandertals from 70 to 60 ka, a period contemporary with the occupation of the Kebara and Amud Caves. The discovery of diagnostic Neandertal remains at the open-air site of ‘Ein Qashish is unusual not only for the Levant but also for Europe, where only two sites, both of which are earlier, have yielded such diagnostic fossils: the French Tourvillel a Rivière and Biache Saint Vaast 2 sites, both dated to marine isotope stage 7 (48, 49). The recovery of the two Neandertal fossils from ‘Ein Qashish raises questions as to the nature of their depositional histories and the inhabitants’ behavioral patterns. Whereas the tooth (EQH2) does not constitute a compelling indication of death at the site, the preservation of bones of two legs, as well as their partial articulation, suggests that the individual represented by EQH3 is likely to have died at the site or nearby. Given the bone state of preservation and articulation, the body remains must have been buried rather fast, either anthropogenically or naturally. The presence of Neandertal fossil remains at MP sites can be interpreted as the result of intentional burial or non anthropogenic deposition (e.g., 50–56). To determine which of the scenarios applies to the ‘Ein Qashish fossils, we evaluated several parameters that may distinguish between the two scenarios: articulation, flexed position, evidence of an excavated pit, intentional coverage of the bones, and the presence of grave goods. Given the available evidence, we cannot determine whether EQH3 is a burial or not. The partial articulation of the left femur and tibia, which attests to a flexed position of the knee (Fig. 4), may support a hypothesis of intentional burial. On the other hand, there are no other body parts of the individual, no visible indication of a pit or the intentional covering of a corpse, and no grave markers. A number of uncommon finds (a seashell, roe deer antler, and ochre) that were unearthed in the same archaeological horizon are not directly associated with the bones of EQH3.

The most informative aspect of the discovery of EQH3 is that it is a Neandertal. The stratigraphic association with a diverse set of material culture remains indicates a habitation context, and the stratigraphic sequence suggests that the locality was used repeatedly. The identification of EQH2 and EQH3 enables us, for the first time, to confidently attribute to Neandertals a set of assemblages from an open-air site in the southern Levant. This discovery in the flat topography of the palaeo-Qishon flood plain demonstrates that locomotor traits did not necessarily constrain Neandertals from exploiting landscapes other than the rugged mountainous terrain (contra (57); see also 58) and, by extension, the ecological mosaic of topographically diverse environments. Hypotheses regarding the demise of the Levantine Neandertals implicate competitive exclusion, direct competition (1, 59), and the inability of the Neandertals to adapt to climate variability and deterioration (e.g., 60). Recent studies focusing on various proxies from Kebara and Amud Caves show that climate change in the Mediterranean zone during the MIS 4 to early MIS 3 time span may not have been as drastic as suggested (61) and that behavioral strategies enabled the Neandertals to cope with ecological change (62, 63). Combined with the dates of the Kebara and Amud Neandertals, the repeated occupation of ‘Ein Qashish in the open landscape during the Levantine late MP reinforces the view that despite possible early interbreeding events (17), Neandertals constituted a resilient population in the Mediterranean ecological zone of the southern Levant shortly before the region was populated by Upper Palaeolithic *H. sapiens* (12-14, 16, 21, 64).

Materials and Methods

EQH-2

High-resolution micro-CT images of EQH2 were obtained with a SkyScan1173 microtomographic system (at the Max Planck Institute for Evolutionary

Anthropology, Leipzig, Germany) using the following scan parameters: 100 kV, 62 uA, with an aluminum- copper filter (1.0 mm thick). Volume data were reconstructed using isometric voxels of 12.90 µm. We segmented the image stack with a semiautomatic threshold-based approach in Avizo 8 (Visualization Sciences Group Inc.) to separate the enamel, the dentine, and the pulp chamber and to reconstruct a 3D digital model of the tooth (Fig. 3). Before beginning the analysis, we oriented the tooth in Rapidform XOR2 software (INUS Technology, Inc., Seoul, Korea): using a spline curve, we manually digitized the cervical line and computed a best-fit plane (the cervical plane; SI 3 Fig. 2) through the points of the curve. The tooth was then rotated until the cervical plane was parallel to the *xy*-plane of the Cartesian coordinate system. The mesiodistal (MD) and buccolingual (BL) crown diameters of EQH2 were measured directly on the digital model and compared with those of Neandertals, early *H. sapiens*, Upper Palaeolithic *H. sapiens*, and recent *H. sapiens* (SI 3 Table 2; SI 3 Fig. 1). Enamel thickness and dental tissue data were analyzed according to guidelines set by Benazzi et al. (65). We measured the enamel volume (in mm3), dentine volume (in mm3, including the volume of the crown pulp chamber), and enamel-dentine junction (EDJ) surface (in mm2) to compute both the average enamel thickness (AET) index (the volume of enamel divided by the EDJ surface; index in millimeters) and the relative enamel thickness (RET) index (the AET index divided by the cubic root of dentine volume; a scale-free index). For root analysis, we followed procedures provided by Kupczik and Hublin (66). Six measurements were taken (SI 3 Fig. 2): root length (from the cervical plane to the apex of the root); total root volume (the volume of the root below the cervical plane, including dentine and pulp); pulp volume; coronal pulp volume (the portion of the pulp above the cervical plane); root pulp volume (the portion of the pulp below the cervical plane); and cervical plane area (the area of the tooth section obtained by sectioning the cervical plane). Dental tissue data and root metrics computed for EQH2 were compared

to a hominin sample that underwent microCT scanning at the Max Planck Institute for Evolutionary Anthropology, at a resolution ranging from 12.58 to 30.19 µm. The hominin sample consisted of M3 teeth from *H. heidelbergensis*, Neandertals, early *H. sapiens*, Upper Palaeolithic *H. sapiens*, and recent *H. sapiens* (SI 3 Table 3). Standardized scores (z scores) were computed to establish which group's mean (Neandertals, early and Upper Palaeolithic *H. sapiens*, or recent *H. sapiens*) the RET index and root metrics of EQH2 were closest to (SI 3 Table 4). Finally, we used a leave-one-out cross-validation linear discriminant analysis (LDA) of root metrics to assign the specimen to the group with the highest posterior probability. For data processing and analyses, we used R software v. 2.15.1 (67).

EQH3

Femoral and tibial length dimensions were obtained with a sliding caliper and osteometric board. For angular measurements, we used a goniometer (SI 4 Tables 1, 2; SI 4 Figs. 1, 2). Osteological measurements follow those defined by Martin (68) and other scholars (36, 69, 70). The bones were scanned on a medical CT scanner at standard medical calibration (120 kV; 0.5 mm thick layers) at the Sheba Medical Center in Israel. The total cross-sectional area and total cross-sectional area of the cortical bone were measured at the reformatted horizontal plane of the femoral midshaft. The illustrations of the midshaft cross sections that appear in Figure 4*D*, *E*, *F* (below the photographs) are based on the horizontal reformatted cross sections of the three bones. A specialist in pediatric radiology (MS) identified the epiphyseal line on the CT scans and noted the presence and absence of pathologies. The results for EQH3 were compared to those for recent *H. sapiens*, early *H. sapiens*, and *H. neanderthalensis*, taken from published data (for example, 36, 70; see SI 4 Tables 3, 4). Well-established morphological differences between the femur and tibia of Neandertals and *H. sapiens* enabled us to identify EQH3 as a Neandertal (SI 4).

Age estimation was based on the stage of epiphyseal union, bone length, and age-related pathology (osteoarthritis) (SI 4). We determined gender on the basis of morphological differences between male and female Neandertals (SI 4 Table 5) (33, 69). The stature estimation was based on 11 formulas: three formulas use femur length, four use tibial length, and four use femoral and tibial length (SI 4 Table 6). EQH3's stature was compared to that of recent *H. sapiens*, early *H. sapiens*, *H. neanderthalensis*, and the Sima de los Huesos hominins (SI 4 Table 7).

References

1. Shea, J.J. The Middle Paleolithic of the East Mediterranean Levant. *J. World Prehist*. **17**,313–394. (2003).

2. Hovers, E. Neandertals and modern humans in the Middle Paleolithic of the Levant: What kind of interaction? *When Neandertals and Moderns Met*, (ed. Conard, N.) 65– 86 (Kerns Verlag, Tübingen, 2006).

3. Valladas, H., et al. Thermoluminescence dates for the Neanderthal burial site at Kebara in Israel. *Nature* **330**, 150–160 (1987).

4. Valladas, H., et al. Thermoluminescence dating of Mousterian 'Proto-Cro-Magnon' remains from Israel and the origin of Modern Man. *Nature* **331**, 614–616 (1988).

5. Valladas, H., Mercier, N., Joron, J.L., & Reyss, J.L. GIF Laboratory dates for Middle Paleolithic Levant. *Neandertals and Modern Humans in*

Western Asia, (eds. Akazawa, T., Aoki, K., Bar-Yosef, O.) 69–76 (Plenum Press, New York, 1998).

6. Valladas, H., et al. TL Dates for the Neandertal site of Amud Cave, Israel. *J. Archaeol. Sci*. **26**, 259–268 (1999).

7. Bar-Yosef, O., & Callander, J. The woman from Tabun: Garrod's doubts in historical perspective. *J. Hum. Evol.* **37**, 879–885 (1999).

8. Grün, R., & Stringer, C.B. Tabun Revisited: Revised ESR Chronology and New ESR and U-series Analyses of Dental Material from Tabun C1. *J. Hum. Evol*. **39**, 601–612 (2000).

9. Stringer, C.B., Grün, R., Schwarcz, H.P., & Goldberg, P. ESR dates for the hominid burial site of Es Skhul in Israel. *Nature* **338**, 756–758 (1989).

10. Mercier, N., et al. Thermoluminescence date for the Mousterian burial site of Es- Skhul, Mt. Carmel. *J. Archaeol. Sci.* **20**, 169–174 (1993).

11. Mercier, N., & Valladas, H. Reassessment of TL age estimates of burnt flints from the Paleolithic site of Tabun Cave, Israel. *J. Hum. Evol*. **45**, 401–409 (2003).

12. Coppa, A., Grün, R., Stringer, C., Eggins, S., & Vargiu, R. Newly recognized Pleistocene human teeth from Tabun Cave, Israel. *J. Hum. Evol*. **49**, 301–315 (2005).

13. Coppa, A., Manni, F., Stringer, C., Vargiu, R., & Vecchi, F. Evidence for new Neanderthal teeth in Tabun Cave (Israel) by the application of self-organizing maps (SOMs). *J. Hum. Evol*. **52**, 601-613 (2007).

14. Bosch, M.D., et al. New chronology for Ksâr 'Akil (Lebanon) supports Levantine route of modern human dispersal into Europe. *Proc. Natl. Acad. Sci. USA* **112**, 7683-7688 (2015).

15. Hovers, E. *The Lithic Assemblages of Qafzeh Cave*. (Oxford University Press, Oxford, 2009).

16. Hershkovitz, I., et al. Levantine cranium from Manot Cave (Israel) foreshadows the first European modern humans. *Nature* **520**, 216–219 (2015).

17. Kuhlwilm, M., et al. Ancient gene flow from early modern humans into Eastern Neanderthals. *Nature*, **530**, 429–433 (2016).

18. Fu, Q., et al. Genome sequence of a 45,000-year-old modern human from western Siberia. *Nature* **524**, 216–219 (2014).

19. Hovers, E., & Belfer-Cohen, A. On variability and complexity: lessons from the Levantine Middle Paleolithic record. *Curr. Anthropol*. **54(S8)**, S337–S357 (2013).

20. Groucutt, H.S., et al. Stone tool assemblages and models for the dispersal of Homo sapiens out of Africa. *Quat. Int.* **382**, 8-30 (2015).

21. McCown, T.D., & Keith, A. *The Stone Age of Mount Carmel II*. (Clarendon Press, Oxford, 1939).

22. Rak, Y. Does any Mousterian cave present evidence of two hominid species? *Neandertals and Modern Humans in Western Asia*, (eds. Akazawa, T., Aoki, K., Bar- Yosef, O.) 353–366 (Plenum Press, New York, 1998).

23. Sharon, G., Zaidner, Y., & Hovers, E. Opportunities, problems and future directions in the study of open air Middle Paleolithic sites. *Quat. Intern*. **331**, 1–5 (2014).

24. Hovers, E., Malinsky-Buller, A., Ekshtain, R., Oron, M., & Yeshurun, R. 'Ein Qashish—a new open air Middle Paleolithic site in northern Israel. *J. Israel. Prehist. Soc*. **38**, 7–40 (2008).

25. Hovers, E., et al. Islands in a stream? Reconstructing site formation processes in the late Middle Paleolithic site of 'Ein Qashish, northern Israel. *Quat. Intern*. **331**, 216– 233 (2014).

26. Greenbaum, N., Ekshtain, R., Malinsky-Buller, A., Porat, N., & Hovers, E. The stratigraphy and paleogeography of the Middle Paleolithic open air site of ‘Ein Qashish, Northern Israel. *Quat. Intern*. **331**, 203–215 (2014).

27. Ekshtain, R., Malinsky-Buller, A., Ilani, S., Segal, I., Hovers, E. Raw material exploitation around the Middle Paleolithic site of ‘Ein Qashish. *Quat. Intern*. **331**, 248–266 (2014).

28. Malinsky-Buller, A., Ekshtain, R., & Hovers, E. Organization of lithic technology at ‘Ein Qashish, a late Middle Paleolithic open air site in Israel. *Quat. Intern*. **331**, 234– 247 (2014).

29. Barzilai, O., Ekshtain, R., Malinsky-Buller, A., & Hovers, E. ‘En Qashish (‘Ein Qashish). *Hadashot Arkheologiot* **127** (2015) http://www.hadashot-esi.org.il.

30. Molnar, S. Human tooth wear, tooth function and cultural variability. *Am. J. Phys. Anthropol.* **34**, 175–190 (1971).

31. Boule, M. *L'homme fossile de La Chapelle-aux-Saints* (Vol. 6) (Masson,1913).

32. Trinkaus, E. The evolution of the hominid femoral diaphysis during the Upper Pleistocene in Europe and the Near East. *Zeitschrift für Morphologie und Anthropologie* 291–319 (1976).

33. Trinkaus, E. *The Shanidar Neandertals* (Academic Press, New York, 1983).

34. Heim, J.L. Les Hommes Fossiles de La Ferrassie. Tome II. Les Squelettes adultes (squelette de membres). *Arch. Inst. Paléontol. Humaine*. **38** (1982).
35. Shackelford, L.L., & Trinkaus, E. Late Pleistocene human femoral diaphyseal curvature. *Am. J. Phys. Anthropol*. **118**, 359–370 (2002).

36. De Groote, I. Femoral curvature in Neanderthals and modern humans: a 3D geometric morphometric analysis. *J. Hum. Evol*. **60**, 540–548 (2011).

37. Lovejoy, C.O., & Trinkaus, E. Strength and robusticity of the Neandertal tibia. *Am. J. Phys. Anthropol*. **53**, 465–470 (1980).

38. Stringer, C.B., Trinkaus, E., Roberts, M.B., Parfitt, S.A., & Macphail, R.I. The middle Pleistocene human tibia from Boxgrove. *J. Hum. Evol*. **34**, 509–547 (1998).

39. Trinkaus, E., & Ruff, C.B. Diaphyseal cross-sectional geometry of Near Eastern Middle Palaeolithic humans: the femur. *J. Archaeol. Sci*. **26**, 409–424 (1999).

40. Carretero, J. M., et al. Stature estimation from complete long bones in the Middle

Pleistocene humans from the Sima de los Huesos, Sierra de Atapuerca (Spain). *J. Hum. Evol*. **62**, 242–255 (2012).

41. O'Connor, J.E., Bogue, C., Spence, L.D., & Last, J. A method to establish the relationship between chronological age and stage of union from radiographic assessment of epiphyseal fusion at the knee: an Irish population study. *J. Anatom*. **212**, 198–209 (2008).

42. Dogaroiu, C., & Avramoiu, M. Correlation between chronological age and the stage of union of the distal femur and proximal tibia epiphyses in a Romanian sample population. *Rom. J. Leg. Med*. **23**, 171–176 (2015).

43. Zionts, L.E. Fractures and dislocations about the knee. *Skeletal Trauma in Children* 3*rd ed*. 439–471 (Philadelphia, PA: Saunders, 2003).

44. Swartz, S.M. The functional morphology of weight bearing: limb joint surface area allometry in anthropoid primates. *J. Zool*. **218**, 441–460 (1989).

45. Kadowaki, S. Issues of Chronological and Geographical Distributions of Middle and Upper Palaeolithic Cultural Variability in the Levant and Implications for the Learning Behavior of Neanderthals and Homo sapiens. *Dynamics of Learning in Neanderthals and Modern Humans Volume 1: Cultural Perspectives, Replacement of Neanderthals by Modern Humans Series* (eds. Akazawa, T., et al.) 59–91 (Springer Japan, 2013) DOI 10.1007/978-4-431-54511-8_4.

46. Sharon, G., & Oron, M. The lithic tool arsenal of a Mousterian hunter, *Quarter. Intern.* **331**, 167–185 (2014).

47. Ziaei, M., Schwarcz, H.P., Hall, C.M., & Grün, R. Radiometric dating of the Mousterian site at Quneitra. *Quneitra: A Mousterian Site on the Golan Heights.* 232– 235 (The Hebrew University, Jerusalem, 1990).

48. Guipert, G., de Lumley, M.A., Tuffreau, A., & Mafart, B. A late Middle Pleistocene hominid: Biache-Saint-Vaast 2, north France. *CR Palevol*. **10**, 21–33 (2010).

49. Faivre, J.P., et al. Middle Pleistocene Human Remains from Tourville la Rivière (Normandy, France) and Their Archaeological Context. *PLoS ONE* **9**(10), e104111. doi:10.1371/journal.pone.0104111 (2014).

50. Belfer-Cohen, A., & Hovers, E. In the eye of the beholder: Mousterian and Natufian burials in the Levant. *Curr. Anthropol*. **33**, 463–467 (1992).

51. Gargett, R.H. Grave shortcomings: the evidence for neandertal burial. *Curr. Anthropol*. **30**, 157–190 (1989).

52. Gargett, R. Middle Palaeolithic burial is not a dead issue: The view from Qafzeh, Saint-Césaire, Kebara, Amud, and Dederiyeh. *J. Hum. Evol*. **37**, 27– 90 (1999).

53. Hovers, E., Kimbel, W.H., & Rak, Y. Amud 7—still a burial. Response to Gargett. *J. Hum. Evol.* **39**, 253–260 (2000).

54. Zilhão, J. Lower and Middle Palaeolithic mortuary behaviours and the origins of ritual burial. *Death Rituals, Social Order and the Archaeology of Immortality in the Ancient World. 'Death Shall Have No Dominion'* (eds. Renfrew, C., Boyd, M.J., Morley, I.) 27–44 (Cambridge University Press, 2015).

55. Rendu, W., et al. Evidence supporting an intentional Neandertal burial at La Chapelle- aux-Saints. *Proc. Natl. Acad. Sci. USA* **111**, 80–86 (2014).

56. Dibble, H.L., et al. A critical look at evidence from La Chapelle-aux-Saints supporting an intentional Neandertal burial. *J. Archaeol. Sci*. **53**, 649–657 (2015).

57. Henry, D.O., et al. The effect of terrain on Neanderthal ecology in the Levant. *Quat. Int* . http://dx.doi.org/10.1016/j.quaint.2015.10.023 (2016).

58. Higgins, R.W., & Ruff, C.B. The effects of distal limb segment shortening on locomotor efficiency in sloped terrain: implications for Neandertal locomotor behavior. *Am. J. Phys. Anthropol*. **146**, 336–345 (2011).

59. Rak, Y. Morphological variation in Homo neanderthalensis and Homo sapiens in the Levant: a biogeographical model. *Species, Species*

Concept and Primate Evolution, (eds. Kimbel, W.H., and Martin, L.B.) 523–536 (Plenum Press, New York, 1993).

60. Shea, J.J. Transitions or turnovers? Climatically-forced extinctions of Homo sapiens and Neanderthals in the east Mediterranean Levant. *Quat. Sci. Rev*. **27**, 2253–2270 4 (2008).

61. Belmaker, M., & Hovers, E. Ecological change and the extinction of the Levantine Neanderthals: implications from a diachronic study of micromammals from Amud Cave, Israel. *Quat. Sci. Rev.* **30**, 3196–3209 (2011).

62. Speth, J.D., & Clark, J. Hunting and overhunting in the Levantine Late Middle Palaeolithic. *Before Farming* **3**, Article 1 (2006).

63. Hartman, G., et al. Isotopic evidence for Last Glacial climatic impacts on Neanderthal gazelle hunting territories at Amud Cave, Israel. *J. Hum. Evol*. **84**, 71-82 (2015).

64. Hublin, J.J. The modern human colonization of western Eurasia: when and where? *Quat. Sci. Rev*. **118**, 194–210 (2015).

65. Benazzi, S., et al. Technical Note: Guidelines for the Digital Computation of 2D and 3D Enamel Thickness in Hominoid Teeth. *Am. J. Phys. Anthropol*. **153**, 305–313 (2014).

66. Kupczik, K., & Hublin, J.J. Mandibular molar root morphology in Neanderthals and Late Pleistocene and recent Homo sapiens. *J. Hum. Evol.* **59**, 525–541 (2010).

67. R Development Core Team. R: a language and environment for statistical computing.R Foundation for Statistical Computing, Vienna, Austria. http://www.r-project.org. (2012).
68. Martin, R. *Lehrbuch der Anthropologie in Systematischer Darstellung mit BesondererBerücksichtigung der Anthropologischen Methoden für Studierende, Ärtze und Forschungsreisende* (Zweiter Band: Kraniologie,Osteologie, 2nd ed. Jena, Gustav Fischer, 1928).

69. Trinkaus, E. Sexual differences in Neanderthal limb bones. *J. Hum. Evol*. **9**, 377–397 (1980).

70. Shackelford, L.L., & Trinkaus, E. Late Pleistocene human femoral diaphyseal curvature. *Am. J. Phys. Anthropol*. **118**, 359–370 (2002).

Information

SI 1. ‘Ein Qashish: Site Background

The site complex of ‘Ein Qashish is located in the Jezreel Valley, ca. 100 m south of the Qishon stream and south of Tel Qashish (SI 1 Fig.1). The site was discovered in a 2004 survey by the Israel Antiquities Authority (IAA). It was excavated during 2005 (24), and again during 2009, 2010 and 2011, by the Hebrew University of Jerusalem (HUJ) (25). The excavations revealed remains of a late Mousterian campsite dated to 70,000–60,000 years ago (26–28). A nearly complete horned skull of an auroch (*Bos primigenius*) was found associated with flint tools during this excavation. Deposition of artefacts and bones was partially secondary, and the original position of the site was hypothesized, on the basis of lithic taphonomy and geomorphological considerations, to be 40–50 m south-southwest of the excavation area (25).

In preparation for the extension of a major highway in the region, archaeological prospection was carried out by the IAA in the site’s vicinity to determine its potential and decide on excavation plans. Mechanical test trenches were dug in 2012 to estimate the size of the site (29). The trenches revealed that the Middle Palaeolithic site extended over an area of more than 1400 m^2 (SI 1 Fig. 1). Notably, a nondiagnostic fragment of a human skull was recovered from the base of Trench 5 in waterlogged sediments corresponding to geological Layer 1 (SI 1 Fig. 1).

Accidental damage to the site led to a large-scale salvage excavation in the summer of 2013. The excavation, a collaboration between the HUJ and the IAA, was conducted in six Areas (A–F), totaling ~650 m^2 (SI 1 Fig. 2). All the areas were excavated according to a single grid system and aligned to the Israel Grid System coordinates.

All artefacts larger than 20 mm were measured three-dimensionally using Total Station instruments (Sokkia 630 and FTD 05). Other artefacts were

collected and bagged according to 50 × 50 cm subsquares and 5 cm spits. All the sediments were dry-sieved and 10–15% were wet-sieved.

Stratigraphy and Sedimentology

The sedimentary sequence exposed in the 2013 excavation was tentatively correlated to a sedimentary sequence documented in geological trenches dug in 2012 (Greenbaum, pers. obs.), which included six layers (Fig. 2). The two lowermost layers were not exposed in the current excavation; thus, the site's sequence begins with Layer 3.

In general, sediments in all layers are dominated by clay but contain also silt and fine sand, rich in quartz. Layer 3 is very rich in stone and bone artefacts, including the remains of EQH-3 in Layer 3b. The layer is composed of dark black, clay-rich sediment (Layer 3a) that grades vertically into gray-black, clay-rich sediment (Layer 3b). The sedimentary layer has abundant slickensides and metallic gley along cracks. This field appearance indicates hydromorphic reducing conditions. In addition, this layer includes fossilized roots and rootlets (rhizoliths), gypsum crystals, occasional calcite veins along cracks, and cobbles from local geological formations. These indicate that the sediments were previously exposed long enough to allow for plant growth (rhizoliths) and evaporation (gypsum), i.e., a habitat conducive to human activity.

Infrared, x-ray fluorescence (XRF), and inductively coupled plasma (ICP) mass spectrometry analyses of minerals and elements in animal bones from this unit show an abundance of iron and manganese oxides. These often appear as dark or reddish-orange coats on and within the bones. Bone mineral crystallinity was evaluated using the infrared splitting factor method. Values measured in 84 samples of animal bones average 3.4+/_0.2, indicating moderately well preserved bone mineral. The human femur bone mineral

crystallinity falls within the same range. All the bones are devoid of collagen (70).

Layer 3 grades into the overlying Layer 4, a reddish brown, clay-rich unit up to ca. 50 cm thick that contains rhizoliths and gypsum crystals. The spatial extent of this unit is more confined than that of the underlying and overlying layers, and Middle Palaeolithic (MP) artefacts are fewer.

The Archaeological Context of the Hominin Finds

Area A, where specimen EQH-2 was found, is situated ca. 30 m west of the area of the excavations carried out during the years 2009, 2010, and 2011, and it may represent the original locality from where the finds were fluvially transported (25). Forty-two m^2 were excavated in this area, exposing two Middle Palaeolithic layers: Layer 5a, 60–90 cm thick, and Layer 5b, 50–70 cm thick. Both layers were cut at the northeastern corner of the area by a Holocene fluvial channel (29). The finds from Layer 5b are abundant and consist of fresh, sharp flint items in a variety of sizes, as well as fragments of animal bones and teeth belonging to large herbivores, mainly auroch. The flint assemblage from this layer is characterized by large primary items showing the initial stages of the knapping sequences. Twenty-one aggregates containing 51 artefacts have been identified so far (work in progress), showing several reduction sequences (SI 1 Fig. 3). Refits from one aggregate were found at maximum vertical distances of 50 cm and maximum horizontal distances of 4 m, suggesting limited postdepositional vertical dispersion. EQH-2 was found in Layer 5a, which yielded fewer finds than its overlying layer, 5b. Lithic production technology was the same as in Layer 5b.

Area B is situated at the northwestern part of the excavation plot. Ca. 45 m^2 were excavated, exposing a well-preserved horizon ca. 20–40 cm thick (Layer 3b). Specimen EQH-3 was found in this layer (SI 1 Fig. 4), which also contained many flint items (mostly in fresh condition with only a few abraded

or patinated), fragmented animal bones, ochre, a complete antler of a roe deer, and a marine mollusk from the Mediterranean Sea, *Hexaplex trunculus* (Linnaeus, 1758) (SI 1 Fig. 5a). Among the large angular cobbles found embedded in the clay were three modified stones that might have functioned as anvils (detailed analysis and residue analysis are in progress) (SI 1 Fig. 5b). These items were found at 22.25–22.20 m above mean sea level, at the same elevation as the EQH-3 bones but several meters from them.

Preliminary refitting efforts in Area B have so far resulted in 4 aggregates composed of 21 flint pieces. Of these, 8 aggregates derive from an artefact concentration in squares L44–L45, at an elevation of 21.96–22.08 m (ca. 3 m north of the remains of EQH-3), with little horizontal (up to 1 m) or vertical (up to 12 cm) movement. The additional aggregate of 2 pieces in squares I41–J41, 21.83–21.86 also shows little horizontal (1 m) or vertical movement (3 cm).

Lithics

All the lithic artefacts from the 2013 excavation were assigned to the Middle Palaeolithic. The densities of lithic artefacts in the various excavation areas differ and may correspond to differences in depositional and postdepositional conditions. The technological makeup of the lithic assemblages is similar, including the Levallois component (SI 1 Fig. 6). The frequencies of Levallois flaking are similarly low in all the excavated areas, a pattern known in many Levantine open-air sites (15 and references therein).

Fauna

A preliminary count and analysis of specimens identifiable to the genus or species level (n = 87) yielded a medium-sized faunal assemblage completely dominated by ungulates; additionally, more than 200 faunal specimens were identified to the level of anatomical part and body-size class. No small game or carnivore skeletal elements were found. The most frequent species is the auroch

(*Bos primigenius*), followed by the mountain gazelle (*Gazella gazella*), Mesopotamian fallow deer (*Dama mesopotamica*), equid (*Equus* sp.), wild boar (*Sus scrofa*), and roe deer (*Capreolus capreolus*). The excavations of 2009, 2010, and 2011 yielded a similar faunal spectrum, dominated by auroch, Mesopotamian fallow deer, and mountain gazelle (25).

Differences were noted in the density of the faunal remains and in their degree of breakage and abrasion within the excavation areas. Most notable were the differences in the density, breakage, and abrasion of remains in Area C, which yielded only a handful of small, weathered fragments, and Areas B and F, which included hundreds of well-preserved, identifiable bones. Some between-area differences were noted in the taxonomic spectrum, specifically the dominance of auroch in Area A and the more even representation of the three major ungulate species in Area B.

Skeletal parts rich in meat, such as upper limb bones, were found in all the excavation areas. Virtually all the limb bones are fragmented, and some show cut marks, typical of meat filleting, as well as hammerstone percussion marks (SI 1 Fig. 7). This indicates that human agents were responsible for the deposition of the animal remains, most probably the result of hunting.

SI 1 Figures

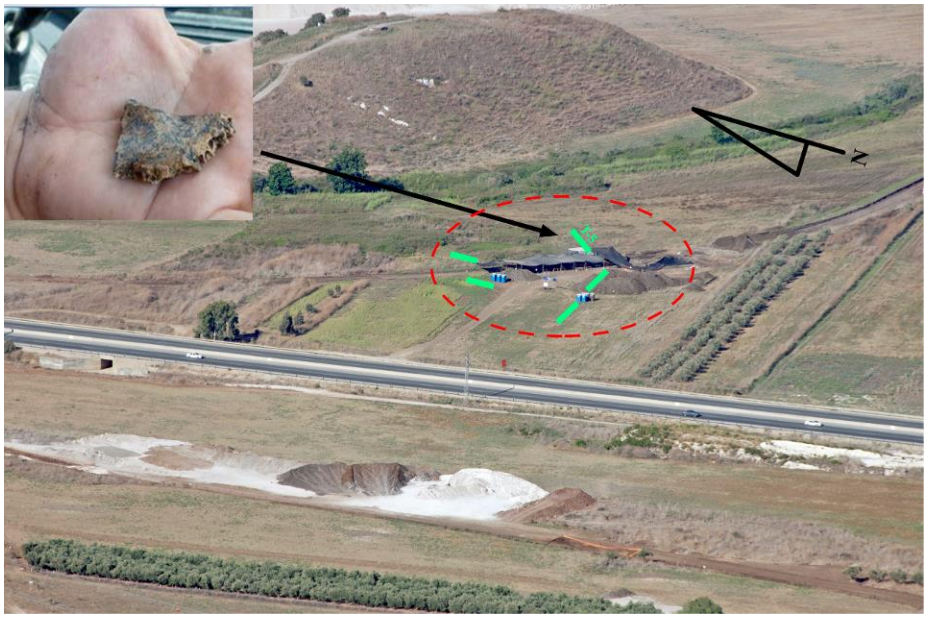

SI 1 Fig. 1. The 2013 excavation at 'Ein Qashish (area under the shade cloth). Locations of the 2009–2011 excavations, and of the 2012 mechanical trenches (in green). The estimated area of the site (dotted red circle) and the location of EQH-1 are indicated.

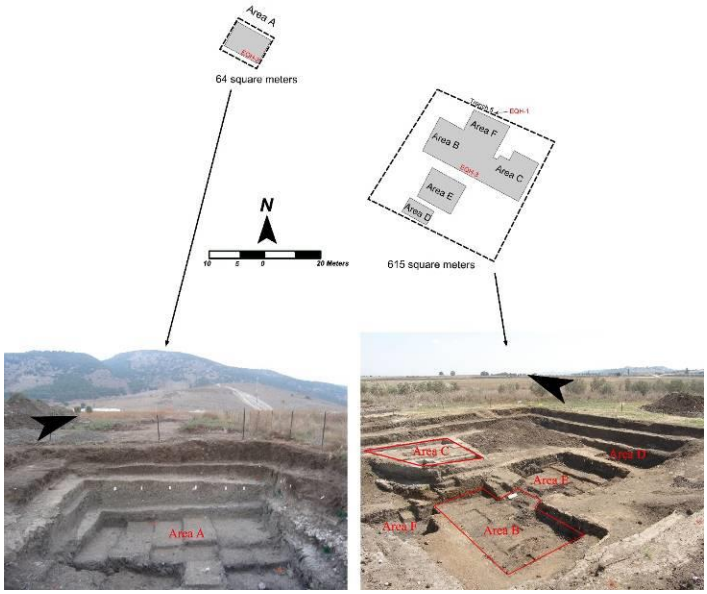

SI 1 Fig. 2. The excavation areas in ‘Ein Qashish (2013).

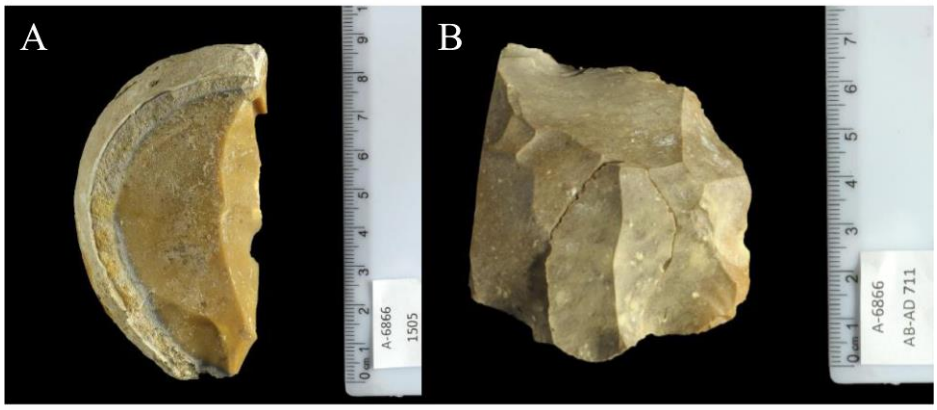

SI 1 Fig. 3. Flint artefacts from Area A. (A) A large flake with cortex. (B) A refitted flint aggregate.

Photo Clara Amit, Courtesy of the Israel Antiquities Authority

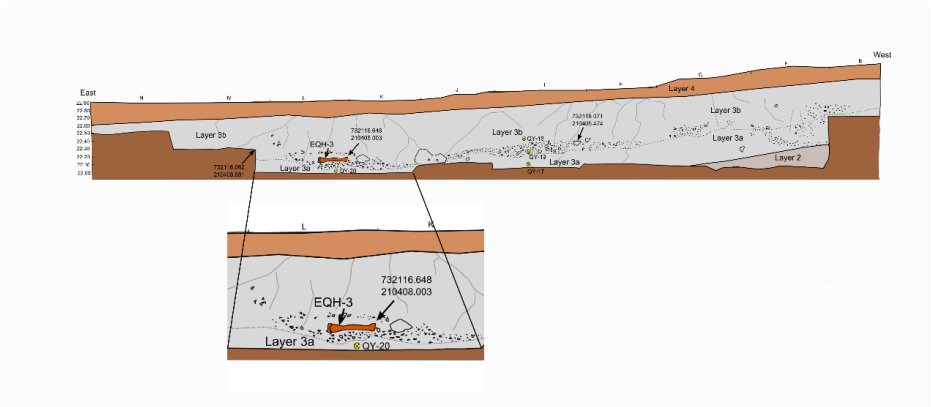

SI 1 Fig. 4. A section showing the sedimentological context of EQH-3 (top), and a close-up of its stratigraphic position (inset at bottom).

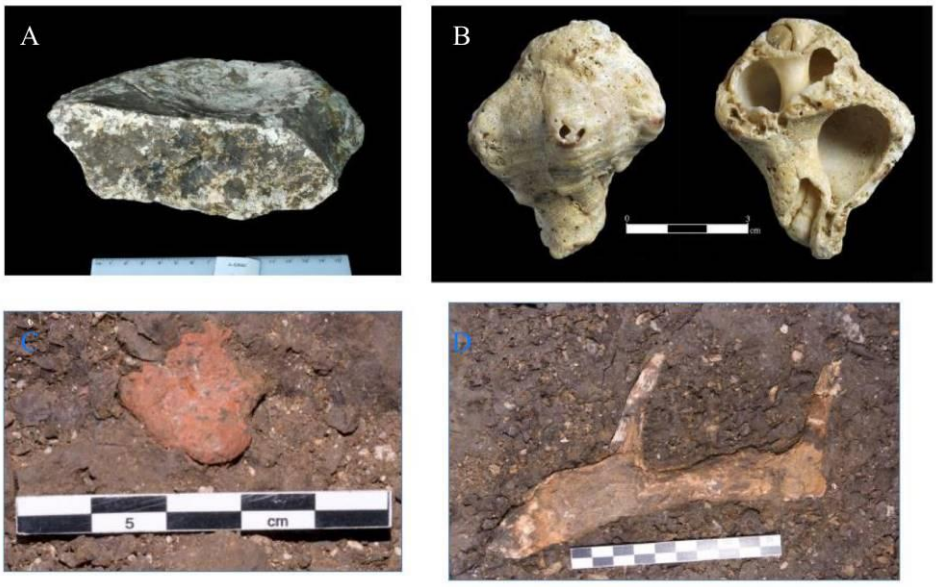

SI 1 Fig. 5. Finds from Layer 3b in Area B. (A) Stone manuport. (B) ***Hexaplex trunculus*** **(Linnaeus, 1758) shell. (C) Ochre. (D) An antler of a roe deer.**

Photo (A, B) Clara Amit, Courtesy of the Israel Antiquities Authority

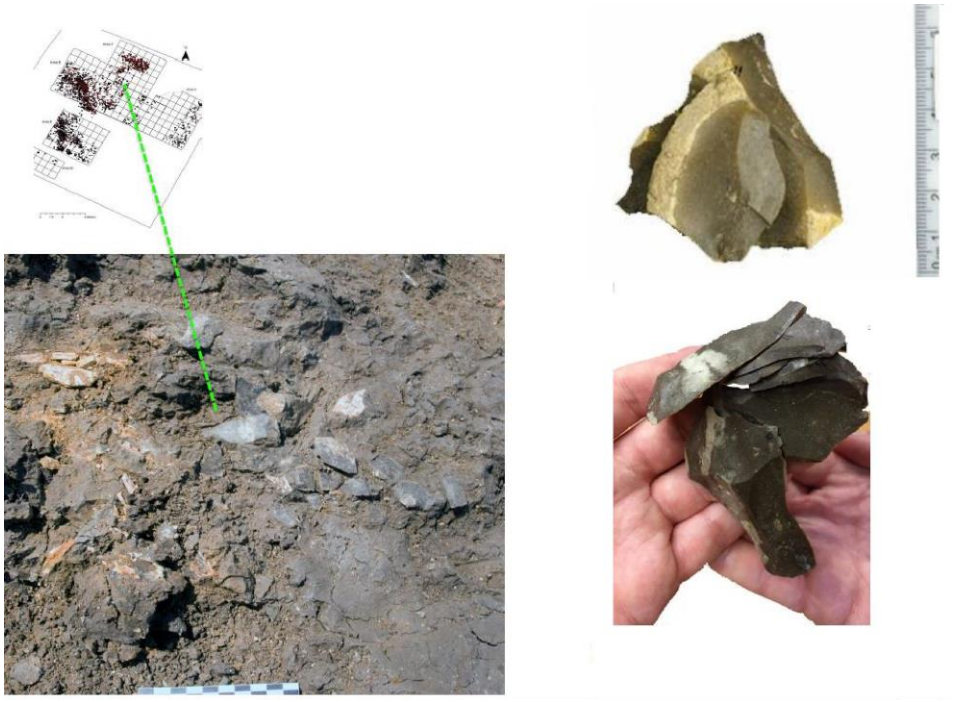

SI 1 Fig. 6. Refitted aggregates from Area B. Refits are laterally and vertically clustered (lower right).

Photo (Top right) Clara Amit, Courtesy of the Israel Antiquities Authority

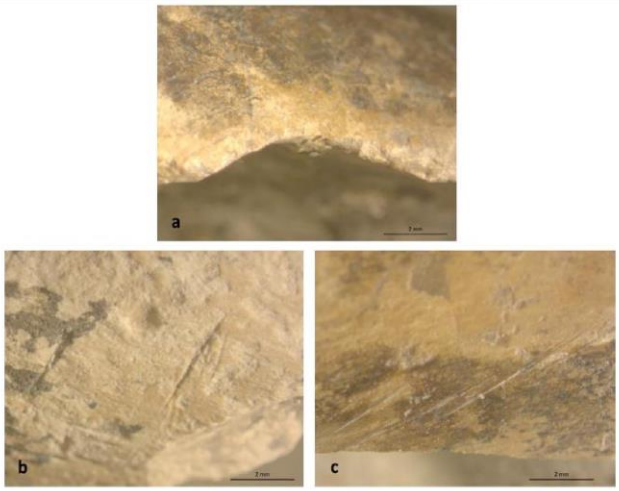

SI 1 Fig. 7. Examples of butchery at ‘Ein Qashish. (a) Medium ungulate (*Dama mesopotamica*) humerus (#2309) bearing hammerstone percussion signs (the conchoidal notch). (b) Large ungulate (*Bos primigenius*) radius (#1063) bearing filleting marks. (c) Medium ungulate (*Dama mesopotamica*) tibia (#1731) bearing filleting marks.

SI 2. Optically Stimulated Luminescence (OSL) Dating

The site sequence of the 2013 excavation was dated through optically stimulated luminescence. After site stratigraphy was established, samples were collected from freshly cleaned sections in the different excavation areas. We collected the samples under cover to prevent any exposure to sunlight and then stored them immediately in black, light-tight bags. We took a complementary sample from the same location for dose rate measurements. Several samples were collected from each of the stratigraphic layers exposed in the different sections.

Quartz in the range of 88-125 μm was extracted and measured under suitable dim orange light using routine laboratory procedures (71). After the sediment sample was sieved to the selected grain size, carbonates were dissolved by soaking in 8% HCl followed by rinsing and drying. Heavy minerals and most feldspars were removed using the Frantz magnetic separator, and HF (40%) etching for 40 min was used to dissolve the remaining feldspars and etch the quartz. The samples were then rinsed in 16% HCl overnight to dissolve any fluorides that may have precipitated.

We measured equivalent doses (D_e) for each sample on 17 to 23 aliquots prepared with 1 or 2 mm masks, using a modified single aliquot regenerative (SAR) protocol (72), and we calculated averages and errors using the central age model (CAM) (73). Measurements were carried out on Risø TL/OSL readers (models DA-12 or DA-15). Dose recovery tests over a range of preheats showed that a dose recovery of 100% can be obtained using a preheat of 10 s at 260°C, a test dose of ~9.3 Gy, and a test dose preheat of 5 s at 240°C. These measurement conditions were used throughout.

Alpha, beta, and gamma dose rates were calculated from the concentrations of the radioactive elements measured by inductively coupled plasma (ICP mass spectrometry (U and Th) or ICP atomic emission

spectroscopy (K), using attenuation factors from (74). Cosmic dose rates were estimated from current burial depths, and water content was measured immediately after sampling (SI 2 Table 1).

To identify the most dominant age components in samples with scattered D_e values, we measured single grains from several samples. The data was processed and reliable grains were selected using criteria as in (75). The main age component was isolated using the finite mixture model (FMM) (74).

All samples show good performance with respect to OSL properties and D_e measurements: the OSL signal was bright and decayed rapidly to background levels, indicating a dominant fast component. Recycling ratios were within 8% of unity, indicating that the SAR protocol corrects appropriately for sensitivity changes, and IR signals were negligible. Dose distributions were mostly normal, with overdispersion values (an indication of scatter beyond that expected from the physical measurements) usually less than 25%.

The ages ranged from 9 ka at the top of the sequence to 70–75 ka at the base of the exposed layers (SI 2 Table 1; Fig. 2*A*). Once preliminary ages were available, it became apparent that samples EQHD-42, EQHD-44, EQHD-46, and EQHD-47 did not conform to the stratigraphic order. (These samples are indicated in SI 2 Fig. 1 as open squares and highlighted in gray in SI 2 Table 1.) Repeated analysis was carried out to ascertain that the D_e values and dose rates were measured correctly. While the D_e values resembled those of nearby samples (from the same unit or section; SI 2 Table 1), the dose rates for three of the four outlier samples were either much higher (sample EQHD-42) or much lower (samples EQHD-44 and EQHD-46) than the mean dose rate calculated from all samples, 1.55 ± 0.32 Gy/ka.

The lower dose rates could have been caused by dilution with a low-dose-rate mineral, such as calcium carbonate ($CaCO_3$). The higher dose rates

could have resulted from high concentrations of clay or heavy minerals. The carbonate contents were thus measured for these outliers, and for 8 additional samples collected for OSL dating from several sections (SI 2 Table 1). The carbonate content for most samples turned out to be in the range of 1–5%, whereas for one of the outlier samples (EQHD-44) it was 43.8%. Thus, the high carbonate content could explain the low dose rate of that particular sample. Since the resulting age is overestimated, dose rates might have been lowered in more recent times by the deposition of carbonates, and current dose rates do not represent the time-averaged dose rate for this sample over its geological history. However, the deposition of carbonates could not be the reason for the low dose rate in two additional samples, as their carbonate content is not high.

We also wanted to check whether the ages calculated for these samples using the site-averaged dose rate are more concordant and agree better with the stratigraphy. SI 2 Table 2 lists these outlying samples, showing their OSL age against the age expected from nearby samples (either from the same unit in other sections, or from the over- and underlying samples). The ages for these samples were recalculated using the averaged dose rates for the entire site (1.55 Gy/ka). For all four samples, the recalculated ages agree much better with the expected ages, further indicating perturbation in the dose rates of individual samples in rather recent times. However, we did not find satisfactory clues for changes in dose rates over time for samples other than EQHD-44, and they were not included in further analyses.

SI 2 Fig. 1 shows the ages with their associated errors by stratigraphic layer. Aside from the outliers, the ages fall within range of 74 ka to 59 ka (solid squares). The stars indicate the stratigraphic locations of EQH-2 (a tooth) and EQH-3 (lower limb bones).

To obtain robust ages for individual layers and obtain a chronological framework for the site, ages from each layer across the sections were averaged, excluding the outliers; these averages are presented in Fig. 2*A*. SI 2 Table 3 lists the samples used to calculate the average for each layer, and its averaged age. Only one sample was collected from Layer 5b: sample EQHD-44 (marked with an asterisk), which turned out to be one of the outliers. As this was the only sample whose low dose rate could clearly be explained by a substantial addition of carbonates at a late stage in the sample's history, here we used the age calculated from the site-averaged dose rate (SI 2 Table 2).

Note the robust ages calculated for Layer 3a, for Layer 3b (where the hominin remains of EQH-3 were found), and for Layer 5a (where the tooth specimen EQH-2 was found). These ages bracket the time of the human remains to 66–68 ka. Note also that OSL dating cannot distinguish clearly between the ages of the lowermost and uppermost Middle Palaeolithic layers (1–5), and it appears that the sediments were deposited rapidly.

SI 2 Tables and Figures

SI 2 Table 1. Field and laboratory data for OSL samples with ages.

See published version

340

SI 2 Table 2. Samples that were not in stratigraphic order and their recalculated ages using a site-averaged dose rate of 1.55 Gy/ka. (See text for details.)

Sample	D_e (Gy)	Dose rate (Gy/ka)	Age (ka)	Expected Age (ka)	Recalculated Age (ka)	$CaCO_3$ (%)
EQHD-42	101	2.26	45±2	<~60-65	65	0.3
EQHD-44	85	0.99	83±5	<~60-65	54	43.8
EQHD-46	105	0.96	109±6	<~70	68	4.1
EQHD-47	124	1.47	84±6	<~70	80	0.6

SI 2 Table 3. Averaged ages for each unit. The ages for Layer 3b are shown from above and below the femur; an average for the entire unit is also shown.

Layer	Sample lab codes (EQHD)	N	Average (ka)
1	16	1	71±4
2	15	1	76±3
3a	14,40,48,51	4	68±5
3b (below femur)	41,50	2	65±8
3b (above femur)	49	1	65±3
3b (average)	41,49,50	3	65±6
4, 4a	13, 52	2	69±3
5a	12,43	2	66±1
5b	44	1	54±5*
6	45	1	9±1

342

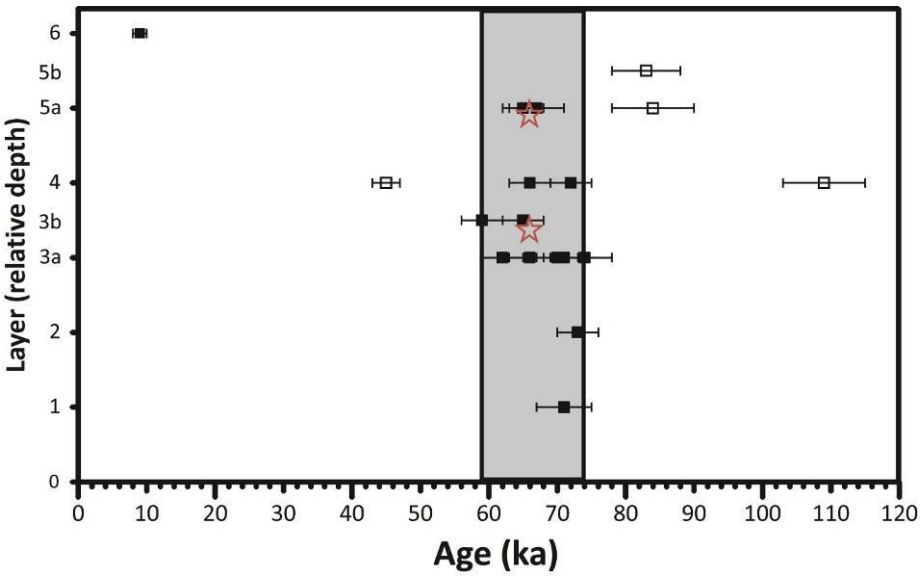

SI 2 Fig. 1. Ages of the stratigraphic layers (black rectangles) with their associated errors (bars). Red stars indicate human remains. Open squares indicate the outliers.

SI 3. EQH-2 (Upper Third Molar)

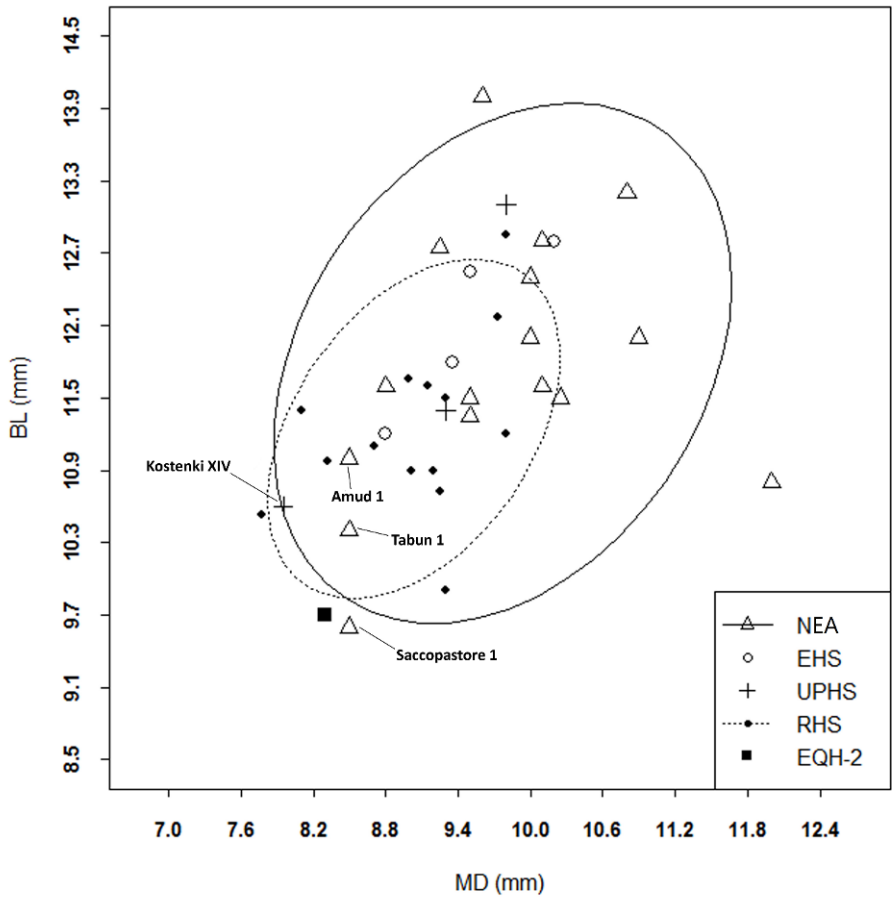

SI 3 Fig.1. Scatterplot of MD diameter vs. BL diameter of M^3. NEA, Neandertal; EHS, early *H. sapiens*; UPHS, Upper Palaeolithic *H. sapiens*; RHS, recent *H. sapiens*. In the scatterplot, the 95% confidence ellipses are reported for NEA and RHS.

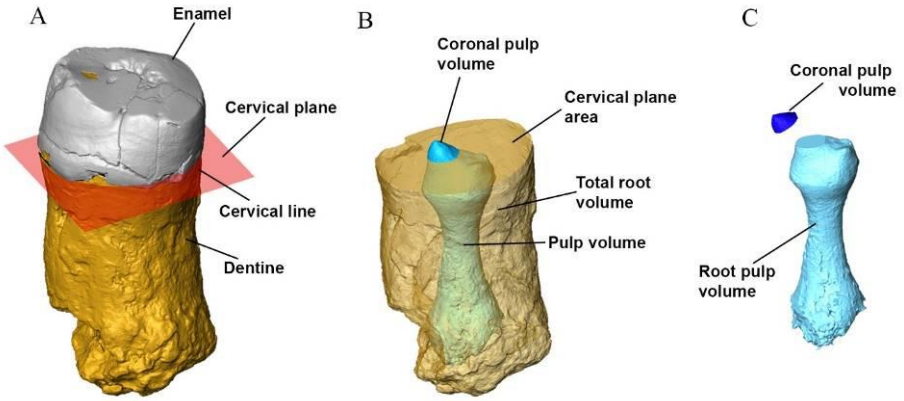

SI 3 Fig. 2. Root metric analysis. (A) The root of EQH-2 (RM^3**)** was separated from the crown along the best-fit plane computed at the cervical line (cervical plane). (B) The root was separated in two parts: total root volume and pulp volume. (C) The pulp volume was divided by the cervical plane into coronal pulp volume and root pulp volume.

SI 3 Table 1. Nonmetric dental traits observed in the enamel-dentine junction of EQH-2 (RM^3) vs. the frequency of these traits (%) in Neandertals (NEA), early and Upper Palaeolithic *H. sapiens* (EHS and UPHS), and recent *H. sapiens* (RHS).

Specimen/Taxon	*n*	Hypocone	Carabelli's trait	Distal accessory tubercle	Mesial accessory tubercle	Paracone accessory cusp
EQH-2	1	Absent	Absent	Absent	Present	Present
NEA	16	100	56.6	31.25	50	100
EHS and UPHS	12	83.3	41.5	16.6	50	41.6
RHS	18	83.3	61.1	11.1	11.1	38.8

SI 3 Table 2. Dental crown diameters (MD and BL), in mm, of M^3 in EQH-2 and the comparative sample.

		MD				BL			
Specimen/Taxon	*n*	Mean	SD	Min.	Max.	Mean	SD	Min.	Max.
EQH-2	1	8.3				9.7			
NEA	16	9.76	0.96	8.5	12	11.78	1.10	9.6	13.2
EHS	4	9.46	0.57	8.8	10.2	12.08	0.72	11.2	12.8
UPHS	3	9.01	0.95	7.95	9.8	11.7	1.27	10.6	13.1
RHS	14	9.03	0.61	7.77	9.8	11.24	0.71	9.9	12.85

NEA, Neandertal; EHS, early *H. sapiens*; UPHS, Upper Palaeolithic *H. sapiens*; RHS, recent *H. sapiens*. Neandertals: Jersey 1, La Quina 5, Le Moustier 1, Saccopastore 2, Spy 1, Spy 2, Tabun 1, Vergisson 1, Vergisson 2, La Croze del Dua 3, La Croze del Dua 4 (76), Amud 1 (77), Shanidar 1, Shanidar 2, Shanidar 4 (33), Krapina 58 (78). EHS: Skhul 4, Skhul 5, Skhul 7 (76), Qafzeh 9 (79). UPHS: Dolni Věstonice 3 (76), Kostenki XIV, Sungir 2 (provided by Bence Viola, Institute of Anthropology, Russian Academy of Sciences, Saint Petersburg). RHS: Vasilyevka III-55 Sloi IV 12, Vasilyevka III-55 N 33, NHMW Breitinger Nr. 87, NHMW Breitinger Nr. 85, NHMW 811, NHMW 9687, Bruckneudorf G905/1, Bruckneudorf G899, NHMW 6034, Bystrovka 3 K7 N 30, NHMW 6031, NHMW 15358, NHMW 15357, Ushauz Cave Sk 1 (provided by Bence Viola, Institute of Anthropology, Russian Academy of Sciences, Saint Petersburg).

SI 3 Table 3. List of fossil and extant human upper third molars (M3) used for enamel thickness and root analysis.

Taxon	Specimen	Wear stage[1]	Enamel thickness	Root
NEA	BD8	2	X	
	El Sidron SD332	2	X	
	El Sidron SD621	1	X	X
	El Sidron SD741	2	X	
	Kebara KMH24	2	X	
	Krp D162	3	X	X
	Krp D163	2	X	X
	Krp D170	2	X	
	Krp D173	3		X
	Krp D178	2	X	X
	Krp D180	2	X	
	Krp D58	2	X	X
	Krp D99	2	X	
	Le Moustier 1	1	X	
	Marillac	1	X	X
	St-Cesaire	2	X	X
EHS	Qafzeh 11	1	X	
	Qafzeh 26	2	X	X
	Skhul 4	4	X	
UPHS	Combe Capelle	2	X	X
	Equus Cave EQ-H12	4	X	X
	Hayonim 19	1	X	
	Hayonim 25	3	X	X
	Hayonim 8	3	X	X
	Les Rois	4		X
	Nahal Oren 24	1	X	X

348

Taxon	Specimen	Wear stage[1]	Enamel thickness	Root
	Nahal Oren 16	2		X
	Oberkassel D999	2	X	X
	Ohalo H2	2	X	
	Villabruna 1	1	X	X
RHS	565	2	X	X
	FJRI r2064-1420	1	X	
	FJRI r2643-1941	1	X	
	FJRI r605-1185	2	X	X
	M072	2	X	X
	M091	2	X	X
	M152	2	X	X
	M157	2	X	X
	M160	2	X	
	M194 30	2	X	X
	M197	2	X	X
	M199	2	X	X
	M20	2	X	X
	M246	2	X	X
	M249	2	X	X
	M65 0385	2	X	X
	Ulac 536	2	X	X
	Wittenberg 2192-39-a	2	X	X

NEA, Neandertal; EHS, early *H. sapiens*; UPHS, Upper Palaeolithic *H. sapiens*; RHS, recent *H. sapiens.*

[1]Based on Molnar (30).

SI 3 Table 4. Three-dimensional enamel thickness of EQH-2 (RM^3) standardized to z scores (for RET index) of the *H. heidelbergensis* (HH), Neandertal (NEA), early and Upper Palaeolithic *H. sapiens* (EHS and UPHS), and recent *H. sapiens* (RHS) M^3 sample for different wear stages. (Standard deviation is indicated in brackets.)

			AET (mm)		RET (scale free)		z scores for RET index
Specimen/Taxon	Wear stage[1]	*n*	Mean	Range	Mean	Range	
EQH-2 HH	3 2	1	0.95 1.2		18.9 23.5		
NEA	1–3	16	1.22 (0.13)	0.95–1.45	19.66 (2.25)	15.42–28.36	-0.33
EHS and UPHS	1–3	10	1.39 (0.17)	1.05–1.58	25.01 (3.85)	19.42–32.37	-1.58
EHS and UPHS	4	2	0.88 (0.02)	0.87–0.90	15.49 (1.28)	14.58–16.40	1.01
RHS	1/2	18	1.45 (0.14)	1.23–1.70	26.48 (4.20)	20.19–35.92	1.81

AET, average enamel thickness index; RET, relative enamel thickness index.

[1]Based on Molnar (30).

SI 3 Table 5. Three-dimensional root analysis of EQH-2 (RM^3) standardized to z scores of the *H. heidelbergensis* (HH), Neandertal (NEA), early *H. sapiens (*EHS), Upper Palaeolithic *H. sapiens (*UPHS), and recent *H. sapiens* (RHS) M^3 sample.

See plubished version

SI 4. Description of the EQH-3 Bones

The EQH-3 specimen consists of five lower limb bones: left femur, right and left tibia, and right and left fibulae. Only the femur and tibiae are the subject of this research.

The femur (Figure 4)

Nearly complete from the articular condyles up to the head, the femur is eroded at the epiphyses and fragmented at the diaphysis. It is robust and highly curved in the sagittal plane, with the apex of the curvature distal to the midshaft. The bicondylar length of the femur is 438 mm and its biomechanical length is 407 mm, both within the range reported for *H. sapiens* and slightly higher than the mean for Neandertals. Note that the bicondylar length might have been slightly longer if the bone were complete (SI 4 Tables 1 and 3). Broken parts of the bone were reconstructed by Yoel Rak.

The proximal femur: The femoral head is partially broken and eroded. The neck is eroded, and its remaining part is distorted, probably due to taphonomic changes. There are remains of the greater and lesser trochanters, but they do not suffice for a full description. The neck shaft angle (119°) indicates coxa vara. The angle of torsion (19°) indicates a high degree of anteversion (SI 4 Tables 1 and 3).

The femoral shaft: The shaft is complete but fragmented. Its overall shape is robust and highly curved, with a smooth anterior surface, while the posterior surface is roughened by the linea aspera. The femoral pilaster (linea aspera pilaster) on the posterior surface of the shaft is missing. The popliteal surface on the posteroinferior part of the femoral shaft is flat and mediolaterally broad. The midshaft shape ratio (with a pilastric index of 99.1) indicates a rounded cross section (the anteroposterior diameter and the mediolateral diameter are nearly equal). The midshaft robusticity index (14.9) is very high in comparison with that of *H. sapiens* (early and recent) and Neandertals,

indicating a very robust femur (SI 4 Table 3). The subpilastric index of the femur (85.6%) reflects the widening of the femoral shaft toward its distal end (at 25% of the femur length).

The distal femur: Both the medial and the lateral condyles of the femur are preserved, but the medial condyle is eroded on its medial side. The medial articular surface is nearly complete; its surface is smooth and wide. The medial epicondyle is eroded, but the adductor tubercle projects medially from the proximal end of the medial condyle. The lateral condyle is longer (along the anteroposterior axis) and narrower (along the mediolateral axis) than the medial condyle. A shallow pit (3 cm in diameter) can be seen on the lateral surface of the lateral condyle, probably due to postmortem pressure exerted on the bone. The intercondylar fossa, located between the two distal articular condyles, is extremely narrow. Its unique shape is not usually seen in the distal femora of *H. sapiens* or Neandertals. The maximum mediolateral condylar breadth and the epiphyseal breadth ratio are small compared with those of Neandertals and *H. sapiens* (SI 4 Tables 1 and 3). This is the result of the narrow lateral condyle and the very narrow intercondylar notch.

Computed tomography (CT) scanning of the bone reveals that the total cross-sectional area of the midshaft is large and the cortical bone is relatively thick (SI 4 Table 3). The CT scan also shows the presence of an epiphyseal line at the distal femur, in accordance with ossification stage 3 out of 4, where the fourth stage implies full ossification (41, 42).

The right tibia (Fig. 4*F*)

The right tibia is missing its proximal part: the remains include the diaphysis, distal to the soleal line, and the distal epiphyses. The proximal end of the tibial shaft is eroded, and the shaft itself is fragmented and slightly distorted. The anterior crest of the tibial shaft is rounded. The interosseous border is

smooth and rounded, resulting in a continuation between the posterior, the medial, and the lateral surface of the tibial shaft. The medial surface of the tibia is wide, with a fracture line running along its long axis. Just proximal to the talar facet is a marked groove running from the medial to the lateral surface, on the anterior side. This groove was caused by tools used in the excavation.

The distal end of the right tibia is remarkably complete. The fibular notch, on its lateral side, is flat and wide. The talar facet has a trapezoid shape; its lateral side is wider than its medial one. The prominent medial malleolus is nearly complete. A squatting facet is seen on the anteroinferior edge of the tibia (SI 4 Tables 2 and 4).

The left tibia (Fig. 4*E*):

The left tibia is nearly complete; it extends from the tibial plateau to the talar facet, but it is missing the medial malleolus. The tibial plateau is flat, and its peripheral edges are eroded. A robust intercondylar tubercle (the medial part of the intercondylar eminence) is clearly visible between the two condyles. The lateral part of the intercondylar eminence is missing. Three centimeters distal to the tibial plateau, on the anterior surface, there is a prominent tibial tuberosity. The superior fibular articular facet is clearly visible on the posterolateral side of the lateral condyle. When viewed laterally, the shaft of the left tibia is fragmented and slightly curved. The shaft is noticeably flattened mediolaterally (i.e., platycnemic). As in the right tibia, the anterior crest of the tibial shaft is rounded, and the interosseous border is smooth and rounded, forming a continuation between the posterior and the lateral surface of the tibial shaft. (Similar morphology is seen in the tibiae of Palomas 96, Shanidar 1, and Shanidar 2 (80)). The medial surface of the EQH-3 tibia is wide, with a fracture line running along the middle of the surface from the proximal to the distal end. Between the proximal and middle thirds of the posterior surface, the soleal line can be seen (SI 4 Tables 2 and 4).

CT scanning of the tibiae reveals the presence of an epiphyseal line at the proximal and distal tibia. This implies ossification stage 3 out of 4 (where stage 4 indicates complete ossification) (41, 42).

Discussion

Neandertal vs. early *H. sapiens*

We attributed EQH-3 to a Neandertal on the basis of femoral and tibial characteristics. Two hominin species are known to have lived in the area (northern Israel) at the MP: early *H. sapiens* and Neandertals. It has been well established that the Neandertal femora have a suite of characteristic features that include a thick, rounded shaft with a very little or no femoral pilaster, a small angle between the neck and the shaft (coxa vara), and a highly robust femoral shaft (31–34). Researchers have also recently emphasized the high curvature of the femoral shaft of Neandertals as compared to that of *H. sapiens*, and the high cortical bone percentage in the femoral midshaft (35, 36, 81). A number of reasons were suggested for this characteristic morphology, including elevated activity level, adaptation to cold, and locomotion (58, 82–84). The characteristic features documented for the femora of early *H. sapiens* include a gracile and straight femoral shaft, with a small articulation area relative to shaft length. The neck shaft angle is high (coxa valga) (21, 36, 79). The midshaft shows a drop-like cross section (long anteroposterior diameter and short mediolateral diameter), with a well-defined femoral pilaster.

The EQH-3 femur is very robust, and the midshaft robusticity index (14.9) is much higher than that of *H. sapiens* (early and recent) and Neandertals; the index is similar to that of the highly robust femora from Shanidar (33). The midshaft cross section (pilastric index, 99.1%) is rounded (the anteroposterior diameter and the mediolateral diameter are nearly equal), a well-documented Neandertal characteristic that contrasts with the more oval shape of the midshaft in *H. sapiens*, due to a more elongated anteroposterior diameter in *H. sapiens*

(33, 36). The femoral shaft of EQH-3 lacks a pilaster and shows a high degree of curvature; both are well-documented Neandertal features. The neck shaft angle (119°, coxa vara) is close to the Neandertal mean and smaller than in *H. sapiens* (124°–130°). The midshaft cross section of EQH-3 reveals a large cross-sectional area with a relatively high percentage of cortical bone. All of the above characteristics suggest that the femur of EQH-3 belonged to a Neandertal rather than to early or recent *H. sapiens*. It should be noted, however, that Neandertals are characterized by a large articular area in relation to femur length, while in *H. sapiens*, the articular area is smaller (84). The relatively small articular area of the EQH-3 femur (epiphyseal breadth ratio = 16.9) is at the lower end known for Neandertals (16.8 for Tabun C1) and below the Neandertal mean (18.9 ± 1.4) (21, 36). The epiphyseal breadth ratio of EQH-3 is close to that of *H. sapiens* (17.1 ± 1.2).

The Neandertal tibia is robust and characterized by an almond-shape cross section with a relatively rounded anterior crest, almost no prominence of the lateral interosseus crest, and a rounded posterior margin (38). The tibia thus contrasts with the more gracile tibiae of early and recent *H. sapiens*, and their generally angular anterior and interosseous crests (38, 86). The Neandertal tibial diaphysis has been described (33, 86, 87) as mesocnemic or euricnemic (average or wide mediolaterally) while that of *H. sapiens* has been described as platycnemic (narrow mediolaterally), mesocnemic, or euricnemic. It is worth noting that the tibia of early *H. sapiens* is very wide mediolaterally. The tibial tuberosity of Neandertals projects more anteriorly than in *H. sapiens*, and the tibial condyles are in a posterior position. The tibiae of EQH-3 are morphologically similar to Neandertal tibiae in the former's distinctive, rounded anterior crest and interosseous crest. The robusticity index of the EQH-3 tibia is higher than that of *H. sapiens* and similar to that of Neandertals (SI 4 Table 4). However, the tibial diaphysis is mediolaterally narrow (platycnemic) in comparison to its anteroposterior length, a feature known to occur in recent *H.*

sapiens and not common in Neandertals or in early *H. sapiens*. It is worth noting that the tibia of another Neandertal from Israel, Amud 1, is also platycnemic, with a cnemic index of 16.5, similar to that of EQH-3.

The crural index in Neandertals is smaller than that of *H. sapiens*, indicating that the distal segment (tibia) is short in relation to the proximal segment (femur). The crural index of EQH-3 is lower than the *H. sapiens* mean and higher than the Neandertal mean. The combination of the femoral and tibial features, together with the low crural index, indicates that the bones belonged to a Neandertal.

Age estimation

We used three long-bone indicators to estimate the age of EQH-3: stage of epiphyseal union, bone length, and age-related pathology (osteoarthritis).

Stage of epiphyseal union: We used the five stages of epiphyseal union described by O'Connor (41) for long bones: non-union (0); beginning union (1), when the epiphyseal and diaphyseal surfaces closely approximate each other; active union (2), when the epiphysis and diaphysis cap each other; recent union (3), when the epiphysis and diaphysis have united to form a single unit of bone, the position of the former epiphysis and diaphysis can still be distinguished, and a fine line of fusion of greater density may remain between the epiphysis and diaphysis; and complete union (4), when the epiphysis and diaphysis are united as a single unit of bone. The distal epiphysis of the femur of EQH-3 and the proximal and distal epiphysis of the tibiae can be assigned to stage 3. A fine line of fusion of greater density (epiphyseal line) is clearly visible in the CT scan between the epiphysis and diaphysis. Stage 3 can be seen in young adults between the ages of 15 and 22 in modern human populations.

Long bone length: We compared the length of the bones of EQH-3 to the femoral and tibial lengths of other Neandertals. The comparison indicates that the long bones of EQH-3 reached full or nearly full adult length.

Age-related pathology: No age-related pathology was identified on any of the bones. We can conclude from these three indicators that the bones of EQH-3 belonged to a young adult (15–22 y) (41, 42).

Male vs. female

The pattern of sexual dimorphism in European and Near Eastern Neandertals is virtually indistinguishable from that of recent *H. sapiens.* Male and female Neandertals are distinguished by their limb bone lengths and articular dimensions. The degrees of size dimorphism found in single-site samples and in the total sexable Neandertal sample are within the expected ranges of variation for the recent *H. sapiens* samples. Furthermore, no differences exist between the Neandertal and recent *H. sapiens* samples with respect to postcranial robusticity as an indicator of sexual dimorphism. In both the fossil and recent samples, the males tend to be slightly more robust than the females, and there is extensive overlap between the sexes (69).

In terms of length and robusticity, the femur of EQH-3 falls within or above the mean for Neandertal males. The tibia presents a somewhat more complex picture. The tibial length falls above the mean for Neandertal males and significantly above the length of Neandertal females. Tibial robusticity, however, falls closer to the mean for Neandertal females than Neandertal males (SI 4 Table 5). Neandertal males also show a lower cnemic index than Neandertal females (SI 4 Table 5); the platycnemic tibia of EQH-3 is at the lower range known for Neandertal males (similar to that of Amud 1) and significantly below the range for Neandertal females (33, 69).

We conclude from this analysis that the bones of EQH-3 belonged to a Neandertal male.

Estimated stature

Stature estimation is used in the reconstruction of the individual's physique during life and provides an indication of size and body mass (40). In fossil hominins, stature is estimated using correlations from recent *H. sapiens* populations. Many formulas for using long bones to calculate stature are found in the literature (88-91, to name a few). We used three types of formulas: formulas based on femur length, formulas based on tibial length, and formulas based on femoral and tibial length (SI 4 Table 6). Using these formulas, we estimated the stature of EQH-3 to be between 159. 9 and 168.6 cm, and we estimated the mean calculated height of EQH-3 to be 163.6 cm (SI 4 Table 6).

The stature of EQH-3 is within the normal range for modern humans, and the specimen would be classified as being of below medium height. The height of EQH-3 is significantly below the estimated height for early *H. sapiens* (males and females), close to the mean for Neandertal males, and above the mean for Neandertal females. A comparison with the hominin specimens from Sima de los Huesos shows that the stature of EQH-3 falls right in the middle between the males and the females (40) (SI 4 Table 7).

Discrepancy between shaft robustness and small articular area

The surprising combination of the very robust diaphysis and the slender epiphysis in the femur of EQH-3 gives rise to some intriguing hypotheses.

The morphology of articular surfaces reflects their weight-bearing properties as well as the stability and mobility of the joints to which they contribute. Osteogenic responses to mechanical loading are known for compact bone in the diaphysis cross section and for trabecular bone in the epiphysis (92). Lieberman (92) claims that the articular surface area is ontogenetically constrained and related to locomotor behavior at the species level and to body mass at the individual level. At the same time, diaphysis cross-sectional geometry is related to individual variations in activity level. This would suggest that EQH-3 was

relatively lightweight or avoided bearing weight on his left knee while still maintaining a high activity level.

Knee pathology

The distal femur and proximal adjacent tibia (left) exhibit some morphological peculiarities. These include the very narrow intercondylar notch, the small lateral articular facet of the distal femur, and the prominent tibial intercondylar eminence between the two tibial plateaus. These features are different from the femur and tibia of Neandertals and *H. sapiens* (SI 4 Tables 3 and 4). In an attempt to understand the nature of these features, we tested three hypotheses:

(1) This is a pleisiomorphic characteristic that can be found in the femur or tibia of other hominins.

(2) This morphology is the result of taphonomy.

(3) The combination of these morphologies represents knee pathology.

After examining the literature and casts of the distal femur and proximal tibia of both *H. erectus* specimens and australopithecines, we concluded that the unique morphology of the knee joint of EQH-3 is different from the morphology of the knee joints of *H. erectus* and australopithecine specimens. We therefore rejected our first hypothesis.

The narrow intercondylar notch might indeed be a result of taphonomical changes, but these cannot be the cause of the small articular condyles and the protruding intercondylar eminence. We therefore partially rejected our second hypothesis.

The medial intercondylar eminence is the attachment area for the anterior cruciate ligament (ACL), one of the four major ligaments that stabilize the knee joint (93). This ligament prevents the knee from going into hyperextension. A narrow intercondylar notch together with a very prominent intercondylar eminence is associated with a well-known knee pathology—a

bony avulsion of the ACL (94–96). These injuries occur most commonly in skeletally immature individuals between the ages of 8 and 14 (43). The mechanism for ACL tearing with or without avulsion is usually traumatic: an unexpected knee hyperextension or a blow to the lateral side of the knee. Patients with ACL avulsion fractures will develop knee hemarthrosis within 12–16 hours, and an inability to walk and run in the days or weeks after the injury. In order to survive, EQH-3 would have had to rely on help from members of his group shortly after the injury occurred. After the acute stage is over, in the months and years after the injury, individuals with ACL avulsion fractures can walk and run but might suffer from knee instability when trying to bear weight (94, 96). If such a pathology did occur in the knee of EQH-3, he might have suffered from instability of the left knee joint and thus tried to bear less weight on his left leg than on his right leg. The small articular surface of the distal femur might be the result of that pathology, as articular surface area is directly related to the amount of axial pressure exerted on the joint. We therefore determined that the third hypothesis is most likely the correct one.

SI 4 Table 1. Description of femur measurements. The numbering of the measurements corresponds to the numbers in SI 4 Fig. 1; note that the measurements in brackets are not depicted in the figure. Unless otherwise specified, measurements are in millimeters.

Measurement	Description
1. Femur bicondylar length (Martin* #2)	Maximum length between the femoral head and the distal condyles
2. Femur biomechanical length	The distance between the most inferior point of the superior femoral neck and the distal condyles
3. Neck shaft angle (degrees) (Martin #29)	The angle between the shaft and the neck
[4. Torsion angle (degrees) (Martin #28)]	The angle between the axis of the femoral neck and the tangent of the posterior surface of the femoral condyles
[5. Femoral AP midshaft diameter (Martin #6)]	The anteroposterior length of the femoral midshaft
6. Femoral ML midshaft diameter (Martin #7)	The mediolateral breadth of the femoral midshaft
[7. Midshaft shape ratio (pilastric index)]	(Anteroposterior midshaft diameter/mediolateral midshaft diameter) ×100
[8. Midshaft circumference (Martin #8)]	The minimum circumference of the femoral midshaft
[9. Subpilastric index]	(Anteroposterior diameter/mediolateral diameter) × 100, at the inferior quarter of the femoral shaft (75% of femur length)

Measurement	Description
[10. Robusticity index†]	(Mediolateral midshaft diameter/bicondylar breadth) × 100
[11. Robusticity index‡]	(Mediolateral midshaft diameter + anteroposterior midshaft diameter) × 100/femur bicondylar length
12. Maximum ML condylar breadth (Martin #21)	The maximum mediolateral breadth of the distal femur
13. ML breadth of lateral condyle	The maximum mediolateral breadth of the lateral condyle
[14. AP length of lateral condyle]	The maximum anteroposterior length of the lateral condyle
15. ML breadth of medial condyle	The maximum breadth of the medial condyle
16. AP length of medial condyle	The maximum anteroposterior length of the medial condyle
[17. Epiphyseal breadth ratio]	(Maximum condylar breadth/biomechanical length) × 100
18. Intercondylar fossa breadth	The distance between the medial wall of the lateral condyle and the lateral wall of the medial condyle at the midcondyle anteroposterior length
19. Intercondylar fossa depth	The horizontal distance between the most anterior point of the inferior border of the intercondylar notch and the tangent to the posterior surface of the femoral condyles

Measurement	Description
20. Chord	In a medial view, the distance between the deepest (most dorsal) point of the anterior femoral contour (just distal to the greater trochanter) and the maximum concavity on the anterior distal shaft (just proximal to the patellar surface)
21. Subtense (Martin #27)	The perpendicular distance from the chord line to the anterior shaft at maximum curvature
22. Point of maximum curvature	The position of the point of the femur's maximum curvature
[23. Total cross-sectional area (mm^2)]	The total cross-sectional area of the midshaft
[24. Cortical cross-sectional area (mm^2)]	The cortical area of the midshaft's cross section
[25. Cortical area ratio]	(Cortical area/total area) × 100

*All citations of Martin in this table refer to Martin (68).

†Trinkaus (32)

‡De Groote (36)

SI 4 Table 2: Description of tibia measurements. The numbering of the measurements corresponds to the numbers in SI 4 Fig. 2; note that the measurements in brackets are not depicted in the figure. Unless otherwise specified, measurements are in millimeters

Measurement	Description
[1. Actual length]	The distance between the most proximal point and the most distal point of the tibia
2. Tibia biomechanical length	The distance between the talar facet and the articular condyle facet
3. Maximum tibial length	For 'Ein Qashish, a composite consisting of the actual length of the left tibia and the medial malleolus length of the right tibia
4. Proximal epiphyseal breadth	The distance between the most lateral end and the most medial end of the proximal tibia
[5. AP diameter at ⅓ of total tibial length]	The anteroposterior diameter of the tibial shaft at one-third of its length, at the nutrient foramen
[6. Mediolateral diameter at ⅓ of total tibial length]	The mediolateral diameter of the tibial shaft at ⅓ of its length
[7. Cnemic index at ⅓ of total tibial length]	(Mediolateral diameter at ⅓ tibial length/anteroposterior diameter at ⅓ tibial length) × 100
[8. Midshaft AP diameter]	The anteroposterior diameter of the tibial shaft at 50% of its length
[9. Midshaft ML diameter]	The mediolateral diameter of the tibial shaft at 50% of its length
[10. Cnemic index at midshaft]	(Midshaft mediolateral diameter/midshaft anteroposterior diameter) × 100

Measurement	Description
[11. Midshaft circumference]	The circumference at the midshaft
[12. Robusticity index]	The square root of the product of the anteroposterior diameter and the mediolateral diameter at the midshaft, divided by the maximum tibial length, times 100
13. Distal tibia maximum ML breadth	The maximum mediolateral breadth of the distal tibia
14. Distal tibia maximum AP length	The maximum anteroposterior length of the distal tibia
15. Distal articular facet maximum ML breadth	The maximum mediolateral breadth of the distal articular facet
16. Distal articular facet, medial end, maximum AP length	The maximum anteroposterior length of the distal articular facet, at the medial end
17. Distal articular facet, lateral end, maximum AP length	The maximum anteroposterior length of the distal articular facet, at the lateral end
18. Medial malleolus length	The vertical distance between the distal end of the articular facet and the tip of the malleolus

SI 4 Table 3: Femur measurements of EQH-3, recent *H. sapiens*, *early H. sapiens*, and Neandertals.

Measurement	**EQH-3**	**Recent *H. sapiens*** $X \pm$ sd	**Early *H. sapiens*** $X \pm$ sd	**Neandertals** $X \pm$ sd
Femur bicondylar length (mm)	438	443.4 ± 26.3[*] (Europeans); 426.5 ± 34.2[†]	492 ± 20.4[*] (Skhul hominids); 460.5 ± 36.7[‡] 456.1 ± 34.2[†]	430.6 ± 27.9[*] 434.8 ± 26.2[‡] 430.3 ± 32.1[†]
Femur biomechanical length (mm)	407	N/A	454.3[§] (Skhul hominids)	409.6[§]
Neck shaft angle (degrees)	119	128.5 ± 4.7[*] 127.4 ± 5.7[†]	130 ± 7.0[*] 124.3 ± 7.6[†]	120 ± 5.3[*] 118.7 ± 5.2[†]
Torsion angle (degrees)	19	16.7 ± 6.9[†]	11.2 ± 9.9[†]	10.4 ± 14.9[†]
Femoral AP midshaft diameter (mm)	32.4	29.5 ± 2.8[*]	33.8 ± 3.7[*]	29.2 ± 3.9[*]
Femoral ML midshaft diameter (mm)	32.7	27.6 ± 2.2[*]	27.3 ± 2.0[*]	29.4 ± 2.1[*]

Measurement	**EQH-3**	**Recent *H. sapiens*** *X* ± sd	**Early *H. sapiens*** *X* ± sd	**Neandertals** *X* ± sd
Midshaft shape ratio (pilastric index)	99	107–119[*] (range of means of various human populations); 114.2 ± 19.1[†]	120 ± 14.9[§] (Skhul hominids); 128.4 ± 20.9[†] 117 ± 10.4[¶]	99.3[*] 103.0 ± 14.5[†] 102 ± 9.3[¶]
Midshaft circumference (mm)	98.17	84.0 ± 4.4 (males)[‖] 74.8 ± 4.0 (females)[‖]	N/A	89–108 (Shanidar 4–6)[#]
Subpilastric index	85.6	88.1 ± 15.7[†]	102.1 ± 18.8[†]	87.6 ± 9.8[†]
Robusticity index[*]	7.4	6.13–6.39[*] (range of means of various human populations)	6.19[*]	6.92 ± 0.16[*]
Robusticity index[†]	14.9	12.4 ± 1.1[†]	13.4 ± 0.9[†]	13.7 ± 1.0[†]
Maximum ML condylar breadth (mm)	73.9	76.2 ± 2.3 (male)[‖] 69.8 ± 2.1 (female)[‖] 88.6 ± 4.2 (male)[**] 78.5 ± 3.0 (female)[**]	81.6 ± 6.7 (Qafzeh & Skhul hominids)[††]	84.3 ± 8.0[††]

Measurement	**EQH-3**	**Recent *H. sapiens*** $X \pm$ sd	**Early *H. sapiens*** $X \pm$ sd	**Neandertals** $X \pm$ sd
ML breadth of lateral condyle (mm)	22.7	25.3 ± 2.6[‡‡]	N/A	N/A
AP length of lateral condyle (mm)	62.5	63.7 ± 5.1[‡‡] 61.1 ± 3.3 (male)[**] 55.4 ± 2.1 (female)[**]	68.8 ± 5.9 (Skhul hominids)[§§]	66.4 ± 6.4[¶¶] (*N* = 7)
ML breadth of medial condyle (mm)	31.0	26.7 ± 2.7[‡‡]	N/A	N/A
AP length of medial condyle (mm)	61.6	61.1 ± 3.4 (male)[**] 55.9 ± 2.9 (female)[**]	61.3 ± 7.2 (Skhul hominids)[§§]	63.3 ± 8.7[¶¶] (*N* = 7)
Epiphyseal breadth ratio	16.9	17.1 ± 1.3[†]	17.1 ± 1.2[†]	18.9 ± 1.4[†]
Intercondylar fossa breadth (mm)	10.7	22 ± 1.8 (male)[**] 18.7 ± 1.0 (female)[**]	N/A	N/A
Intercondylar fossa depth (mm)	24.8	27.8 ± 1.6 (male)[**] 23.7 ± 2.0 (female)[**]	N/A	N/A

Measurement	**EQH-3**	**Recent *H. sapiens*** $X \pm$ sd	**Early *H. sapiens*** $X \pm$ sd	**Neandertals** $X \pm$ sd
Chord (mm)	357	254–343[##] (range of means of various human populations)	334.8 ± 31.0[##]	317.6 ± 28.3[##]
Subtense (mm)	26.6	6.2–11.7[##] (range of means of various human populations)	14.3 ± 3.0[##]	15.5 ± 3.4[##]
Point of maximum curvature (mm)	228	N/A	151.2 ± 21.1[##]	190.5 ± 37.0[##]
Total cross-sectional area (mm^2)	749	456 ± 62 (African-American females) 440 ± 58 (Caucasian females)[‖‖]	606.8 ± 95.4[***]	661.0 ± 54.3[***]
Cortical cross-sectional area (mm^2)	595	N/A	459.5 ± 89.3[***]	523.5 ± 53.6[***]
Cortical area percentage	79.4	N/A	75.6 ± 7.3[***]	79.1 ± 2.7[***]

*Trinkaus (32) †De Groote (36) ‡Walker, et al. (80) §Trinkaus & Ruff (39) ¶Garralda, et al. (97) #Trinkaus (33) ‖Gaikwad & Nikam (98) **Terzidis, et al. (99) ††Adapted from Vandermeersch (79) ‡‡Ho, et al. (100) §§Adapted from McCown & Keith (21) ¶¶Adapted from Heim (34) ##Shackelford & Trinkaus (35) ‖‖Nelson, et al. (101) ***Beauval, et al. (81)

SI 4 Table 4. Tibia measurements of EQH-3, recent *H. sapiens*, early *H. sapiens*, and Neandertals.

Measurement	**EQH-3**		**Recent *H. sapiens***	**Early *H. sapiens***	**Neandertals**
	Left tibia	**Right tibia**			
Actual length (mm)	338.5	290.7	N/A	N/A	N/A
Tibia biomechanical length (mm)	332	N/A	373[*]	409 (Skhul 4); 362 (Cro-Magnon)[*]	305 (Spy); 298 (Tabun 1)[*]
Maximum tibial length (mm)	338.5 +18.5 = 357.0	N/A	(349–376) ± 26[†]	387 ± 29[‡] 391 ± 27[†]	340 ± 26[‡] 337 ± 23[†]
Proximal epiphyseal breadth (mm)	77	N/A	70.6 ± 5.5 [§]	N/A	80 (Shanidar 2)
AP diameter at ⅓ of total tibial length (mm)	38	N/A	33.6 ± 4.0 [§]	N/A	38.4[‡]

Measurement	**EQH-3**		**Recent *H. sapiens***	**Early *H. sapiens***	**Neandertals**
	Left tibia	**Right tibia**			
ML diameter at ⅓ of total tibial length (mm)	23	N/A	22.6 ± 1.5[§]	N/A	26.6[‡]
Cnemic index at ⅓ of total tibial length	60	N/A	64–72 ± 6[‡] (range of means of various human populations)	64 ± 6[‡]	69 ± 6[‡]
Midshaft AP diameter (mm)	36.9	35.32	N/A	35 ± 2.1[¶] (Skhul & Qafzeh hominids)	33.1 ± 3.5[#]
Midshaft ML diameter (mm)	21.5	21.21	N/A	24.8 ± 1.5[¶] (Skhul &Qafzeh hominids)	23.1 ± 2.3[#]

Measurement	EQH-3		Recent *H. sapiens*	Early *H. sapiens*	Neandertals
	Left tibia	Right tibia			
Cnemic index at midshaft	58	60	59.6–74.8[#] (range of means of various human populations)	78.8 ± 2.3 (Skhul & Qafzeh hominids)[#]	68.9 ± 6.6 (males)[#] 74.8 ± 0.5 (females)[#] 69 ± 6[‡] (pooled sample)
Midshaft circumference (mm)	103	96	N/A	84–96 ± 10[¶]	86 ± 8[¶]
Robusticity index	8.0	7.7	6.2–7.1 ± 0.5[‡] (range of means of various human populations)	6.7 ± 0.4[‡]	8.1 ± 0.5[‡]
Distal tibia maximum ML breadth (mm)	N/A	51.14	N/A	N/A	54 (Shanidar)[‖]

Measurement	EQH-3		Recent *H. sapiens*	Early *H. sapiens*	Neandertals
	Left tibia	Right tibia			
Distal tibia maximum AP length (mm)	N/A	36.9	N/A	N/A	39.3 (Shanidar)[‖]
Distal articular facet maximum ML breadth (mm)	N/A	29.53	N/A	N/A	31.3–32 (Shanidar)[‖]
Distal articular facet, medial end, maximum AP length (mm)	N/A	25.73	N/A	N/A	N/A
Distal articular facet, lateral end, maximum AP length (mm)	N/A	33.5	N/A	N/A	28.6–33.0 (Shanidar)[‖]
Medial malleolus length (mm)	N/A	18.5	N/A	N/A	N/A

Measurement	EQH-3		Recent *H. sapiens*	Early *H. sapiens*	Neandertals
	Left tibia	Right tibia			
Crural index: (tibial length/femoral length) × 100		81.5	84–90 ± 4.3** (range of means of various human populations)	85.1 ± 2.8** (*N* = 25)	78.8 ± 1.7** (*N* = 9)

*McCown & Keith (21) †Walker, et al. (80) ‡Lovejoy & Trinkaus (37) §González-Reimers, et al. (102) ¶Stringer, et al. (38) #Trinkaus (69) ‖Trinkaus (33) **Porter (103)

SI 4 Table 5. The femur and tibiae of Neandertal males and females compared to the EQH-3 femur and tibiae.

Measurement	**Male**	**Female**	**EQH-3**
	$X \pm$ sd (N)	$X \pm$ sd (N)	
Femoral bicondylar length	442.8 ± 20.4 (9)*	400.3 ± 14.3 (3)*	438
Tibial length	354.4 ± 19.3 (8)*	310.0 ± 9.5 (3)*	357
Femur robusticity index	7.19 ± 0.59 (8)*	6.91 ± 0.62 (3)*	7.4
Tibial robusticity index	8.24 ± 0.4 (7)*	7.78 ± 0.49 (3)*	7.7–8.0
Tibial cnemic index	68.9 ± 6.6†	74.8 ± 0.5†	61

*Trinkaus (69)

†Trinkaus (33)

SI 4 Table 6. Estimated stature of EQH-3.

Estimation Method	Reference	Population	Formula	Stature estimation for EQH-3
Femur length (FEL)	Sjøvold (104)	All races	2.71 × FEL + 45.86	164.6 (± 4.49)
Femur length	Trotter & Gleser (89)	European-American males	2.38 × FEL + 61.41	165.6 (± 3.27)
Femur length	Trotter & Gleser (89)	African-American males	2.11 × FEL + 70.35	162.8 (± 3.94)
Tibia length (TL)	Sjøvold (104)	All races	3.29 × TL + 47.34	165 (± 4.15)
Tibia length	Trotter & Gleser (89)	European-American males	2.52 × TL + 78.62	168.6 (± 3.37)
Tibia length	Trotter & Gleser (89)	African-American males	2.19 × TL + 86.02	164.2 (± 3.78)
Tibia length	Auerbach & Ruff (91)	North American Arctic males	2.55 × TL + 69.51	160.5 (± 2.99)
(Femur and tibia) length	Trotter & Gleser (89)	European-American males	1.39 × (FEL + TL) + 53.2	163.7 (± 3.55)

Estimation Method	Reference	Population	Formula	Stature estimation for EQH-3
(Femur and tibia) length	Trotter & Gleser (89)	African-American males	1.26 × (FEL + TL) + 59.72	159.9 (± 3.28)
Femur length and tibia length	Auerbach & Ruff (91)	North American Arctic males	(1.28 × FEL) + (1.26 × TL) + 59.86	160.9 (± 2.62)
Femur length and tibia length	Auerbach & Ruff (91)	North American Great Plains males	(1.88 × FEL) + (0.76 × TL) + 54.13	163.6 (± 1.94)
Mean of stature values for EQH-3				163.6

SI 4 Table 7. Comparison of stature estimation for EQH-3, recent *H. sapiens*, early *H. sapiens*, Neandertals, and Sima de los Huesos hominins.

Population	EQH-3	Recent *H. sapiens*[*]	Early *H. sapiens*[*]	Neandertals[*]	Sima de los Huesos hominins[*]
Males & females	163.6	N/A	177.45	160.6	163.6
Males	N/A	Range of means for 124 human populations: 144.1–184.9	185.1 ± 7.1	166.7 ± 5.9	169.5 ± 4.0
Females	N/A	Range of means for 124 human populations: 137.0–167.7	169.8 ± 6.5	154.5 ± 4.6	157.7 ± 2.0

[*]Data from Carretero, et al. (40)

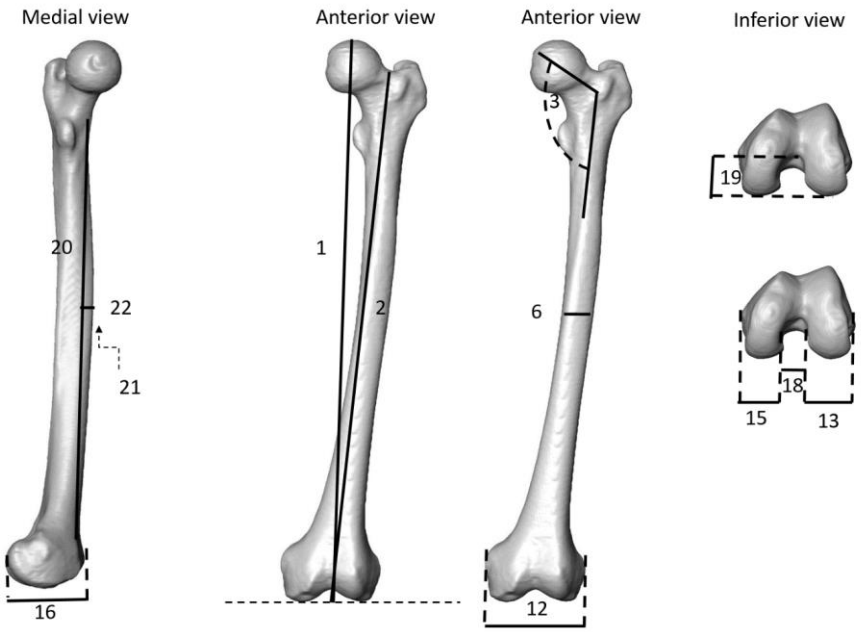

SI 4 Fig. 1. Femoral measurements. The numbers correspond to the measurement numbers in SI 4 Table 1.

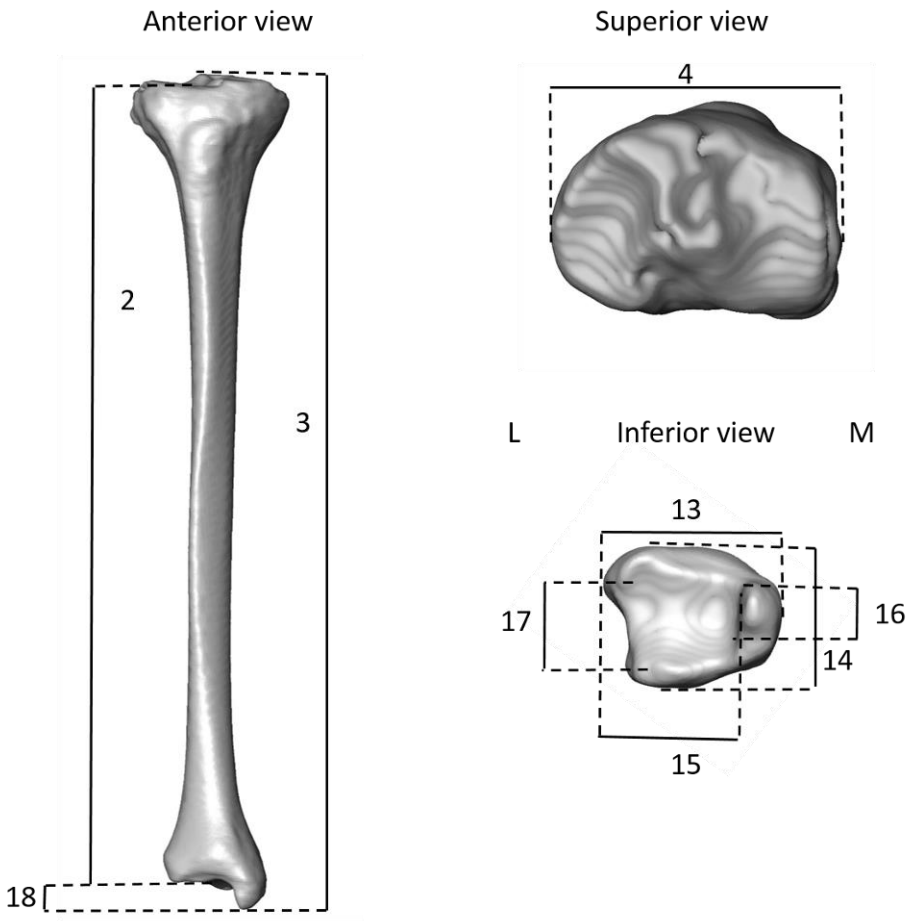

SI 4 Fig. 2. Tibial measurements. The numbers correspond to the measurement numbers in SI 4 Table 2.

382

References

70. Nir. N. Bones and formation processes in the open-air Middle Paleolithic site of Ein Qashish. *MA thesis, Institute of Archaeology*. (The Hebrew University of Jerusalem, 2016).
71. Davidovich. U., Porat, N., Gadot, Y., Avni, Y., & Lipschits, O. Archaeological investigations and OSL dating of terraces at Ramat Rahel, Israel. *J. Field. Archaeol*. **37**, 192–208 (2012).
72. Murray, A.S., & Wintle, A.G. Luminescence dating of quartz using an improved single aliquot regenerative-dose protocol. *Radiat. Meas*. **32**, 57–73 (2000).
73. Galbraith, R.F., & Roberts, R.G. Statistical aspects of equivalent dose and error calculation and display in OSL dating: an overview and some recommendations. *Quat. Geochronol*. **11**, 1–27 (2012).
74. Nambi, K.S.V., & Aitken, M.J. Annual dose conversion factors for TL and ESR dating. *Archaeometry* **28**, 202–205 (1986).
75. Faershtein, G., Porat, N., Avni, Y., & Matmon, A. Aggradation-incision transition in arid environments at the end of the Pleistocene: an example from the Negev Highlands, southern Israel. *Geomorphology* **253**, 289–304 (2016).
76. Frayer, D.W. *Evolution of the Dentition in Upper Paleolithic and Mesolithic Europe.* University of Kansas Publications in Anthropology (vol. 10), (Lawrence, Kansas, 1978).
77. Suzuki, H., & Takai, F., Eds. *The Amud Man and His Cave site* (Academic Press of Japan, 1970).
78. Wolpoff, M.H. The Krapina dental remains. *Am. J. Phys. Anthropol*. **50**, 67-113 (1979).
79. Vandermeersch, B. *Les Hommes Fossiles de Qafzeh (Israël)* (Centre National de la Recherche Scientifique, Paris,1981).

80. Walker, M.J., Ortega, J., Parmová, K., López, M.V., & Trinkaus, E. Morphology, body proportions, and postcranial hypertrophy of a female Neandertal from the Sima de las Palomas, southeastern Spain. *Proc. Natl. Acad. Sci*. **108**, 10087–10091(2011).
81. Beauval, C., et al. A late Neandertal femur from les Rochers-de-Villeneuve, France. *Proc. Natl. Acad. Sci. USA* **102**, 7085–7090 (2005).
82. Stringer, C., & Gamble, C. *In Search of the Neanderthals: Solving the Puzzle of Human Origins* (Thames and Hudson,1993).
83. Ruff, C.B. Climatic adaptation and hominid evolution: the thermoregulatory imperative. *Evol. Anthropol*. 2, 53–60 (1993).
84. Weaver, T.D. The shape of the Neandertal femur is primarily the consequence of a hyperpolar body form. *Proc. Natl. Acad. Sci*. **100**, 6926–6929 (2003).
85. Trinkaus, E., & Ruff, C.B. Diaphyseal cross-sectional geometry of Near Eastern Middle Palaeolithic humans: The Tibia. *J. Archaeol. Sci*. **26**, 1289–1300 (1999).
86. Patte, E. *Les Néanderthaliens*. (Paris, Masson et Cie, 1955).
87. Taylor, J.V. *The Neanderthal Tibia*. PhD thesis. Columbia University (Ann Arbor, University Microfilms, 1968).
88. Trotter, M. Estimation of stature from intact long limb bones. *Personal Identification in Mass Disasters.* (ed. T.D. Stewart) 71-84 (Smithsonian Institution, National Museum of Natural History, Washington, DC, 1970).
89. Trotter, M., & Gleser, G.C. Estimation of stature from long bones of American Whites and Negroes. *Am. J. Phys. Anthropol*. **10**, 463–514 (1952).

90. Feldesman, M.R., & Lundy, J.K. Stature estimates for some African Plio-Pleistocene fossil hominids. *J. Hum. Evol*. **17**, 583–596 (1988).

91. Auerbach, B.M., & Ruff, C.B. Stature estimation formulae for indigenous North American populations. *Am. J. Phys. Anthropol.* **141**, 190–207 (2010).

92. Lieberman, D.E., Devlin, M.J., & Pearson, O.M. Articular area responses to mechanical loading: effects of exercise, age, and skeletal location. *Am. J. Phys. Anthropol.* **116**, 266–277 (2001).

93. Stäubli, H.U., & Rauschning, W. Tibial attachment area of the anterior cruciate ligament in the extended knee position. *Knee Surg. Sport. Tr. A.* **2**, 138–146 (1994).

94. Perugia, D., Basiglini, L., Vadala, A., & Ferretti, A. Clinical and radiological results of arthroscopically treated tibial spine fractures in childhood. *Int. Orthop.* **33**, 243–248 (2009).

95. Furlan, D., Pogorelić, Z., Biočić, M., Jurić, I., & Meštrović, J. Pediatric tibial eminence fractures: arthroscopic treatment using K-wire. *Scand. J. Surgery* **99**, 38–44 (2010).

96. Anderson, A.F., & Anderson, C.N. Correlation of meniscal and articular cartilage injuries in children and adolescents with timing of anterior cruciate ligament reconstruction. *Am. J. Sports Med*. **43**, 275–281 (2015).

97. Garralda, M.D., Galván, B., Hernández, C.M., Mallol, C., Gómez, J.A., & Maureille, B. Neanderthals from El Salt (Alcoy, Spain) in the context of the latest Middle Palaeolithic populations from the southeast of the Iberian Peninsula. *J. Hum. Evol*. **75**, 1–15 (2014).

98. Gaikwad, K.R., & Nikam, V.R. Sexual Dimorphism in Femur. IOSR *J. Dental. Medic. Sci*. **13**, 4–9 (2014).

99. Terzidis, I., et al. Gender and side-to-side differences of femoral condyles morphology: osteometric data from 360 Caucasian dried femori. *Anat. Res. Int*. doi:10.1155/2012/679658 (2012).

100. Ho, W.P., Cheng, C.K., & Liau, J.J. Morphometrical measurements of resected surface of femurs in Chinese knees: correlation to the sizing of current femoral implants. *The Knee* **13**, 12–14 (2006).

101. Nelson, D.A., Barondess, D.A., Hendrix, S.L., & Beck, T.J. Cross-Sectional Geometry, Bone Strength, and Bone Mass in the Proximal Femur in Black and White Postmenopausal Women. *J. Bone. Miner. Res*. **15**, 1992–1997 (2000).

102. González-Reimers, E., et al. Bending and torsional strengths of the tibia vs. simple anthropometric variables among the prehispanic population of El Hierro (Canary Islands). *Eur. J. Anat*. **18**, 8–15 (2014).

103. Porter, A.M.W. Modern human, early modern human and Neanderthal limb proportions. *Int. J. Osteoarchaeol.* **9**, 54–67 (1999).

104. Sjøvold, T. Estimation of stature from long bones utilizing the line of organic correlation. *Hum. Evol*. **5**, 431–447 (1990).

Journal of Anthropological Sciences

Human deciduous teeth from the Middle Stone Age layers of Sibudu Cave (South Africa).

Alessandro Riga [1], Gregorio Oxilia [1,2], Daniele Panetta [3], Piero A. Salvadori [3], Stefano Benazzi [2,4], Lyn Wadley [5], Jacopo Moggi-Cecchi [1].

[1] Department of Biology, University of Florence, Via del Proconsolo, 12, Firenze 50122, Italy

[2] Department of Cultural Heritage, Laboratory of Anthropology, University of Bologna, Via degli Ariani 1, Ravenna 48121, Italy

[3] Institute of Clinical Physiology, IFC-CNR, Via G. Moruzzi 1, Pisa 56124, Italy

[4] Department of Human Evolution, Max Planck Institute for Evolutionary Anthropology, Deutscher Platz 6, Leipzig 04103, Germany

[5] Evolutionary Studies Institute, University of the Witwatersrand, PO WITS 2050, South Africa

Introduction

In the African Pleistocene, the fossil evidence of early *Homo sapiens* populations is still relatively limited, with 52 sites from 12 countries from which mostly isolated specimens, covering a long time span, have been recovered so far (see Grine, 2016 for a systematic review). In this scenario, South Africa contributes with a fairly good record, with human fossils deriving from 15 sites. In most cases, however, the evidence is represented by single specimens – although sites exist where the fossil record is more abundant and/or particularly significant. As such, any new discovery represents an important addition towards the description of the anatomy of these populations and of their variability. Among the South African sites at Sibudu Cave, near the east coast of South Africa, a few human fossils were recorded years ago from the uppermost Middle Stone Age (MSA) layers (Plug, 2004). More recent excavations led to the recovery of two additional specimens – two deciduous teeth. Here, these two teeth (a lower dm1 and a lower di1), recovered from the MSA deposits of the site, are described, and their significance towards the interpretation of the temporal and geographical variability of early *Homo sapiens* populations is discussed.

Sibudu Cave

Sibudu Cave (29°31'S, 31°05'E) is a site located in the province of KwaZulu-Natal (South Africa), about 40 km north of Durban and 15 km inland from the Indian Ocean coast (Figure 1). It is a rock shelter above the uThongathi River with a deep sequence of sediments with traces of occupation from the Iron Age and also the MSA (Wadley and Jacobs, 2004). In the MSA Sibudu was occupied discontinuously, due to environmental conditions or as a result of small populations paying infrequent visits to the area (Jacobs et al., 2008 a; Chase, 2010; Wadley, 2012; Wadley, 2015); yet the MSA deposits include many technocomplexes: pre-Still Bay, Still Bay, Howiesons Poort, post-

Howiesons Poort, late and final MSA assemblages from about 77,000 years (77 ka) ago to 38 ka ago (Jacobs et al., 2008 a,b; Wadley, 2012). On the one hand, the pre-Still Bay lithic assemblage at the base of the sequence is rather difficult to define typologically for it lacks bifacial points and there are only rare retouched tools. The Howiesons Poort Industry, on the other hand, is blade-rich, has many backed tools, like segments and other geometric pieces. The backed tools were hafted and probably used in innovative ways as hunting weapons.

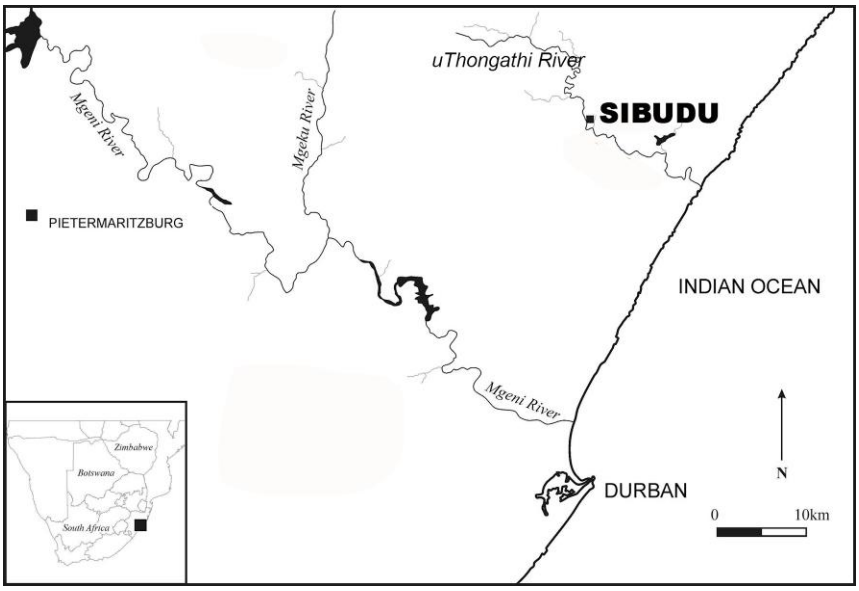

Figure 1. Location of the MSA site Sibudu Cave (KwaZulu-Natal, South Africa).

The MSA layers offer a spectacular archaeological record, documenting a variety of innovation typical of the African MSA, among which is possibly the earliest use of bow and arrow and the use of bone needles (Backwell et al., 2008; Lombard and Phillipson, 2010; Lombard, 2011); the placement of medicinal plants in bedding construction (Wadley et al., 2011); the use of ornaments in the form of perforated shells beads (d'Errico et al., 2008); and the

widespread use of ochre (over 9000 pieces recovered) for a variety of different tasks (Lombard, 2007; Hodgskiss, 2012; Hodgskiss, 2013; Wadley and Langejans, 2014; Soriano et al., 2009; Wadley, 2015).

Sibudu was excavated by Lyn Wadley and a University of the Witwatersrand team between 1998 and 2011; since 2011 the site has been excavated by a team from the University of Tübingen under the direction of Nicholas Conard.

Stratigraphy

Two layers and industries excavated by Wadley are in the spotlight in this paper. These layers are from the basal Brown Sand (BS) member and layer Pinkish-Grey Sand (PGS) from the Howiesons Poort suite of layers. BS is loose, brown sand (7.5YR 4/3 brown) with rock spalls and many encroaching rocks. The member, which has a fairly homogeneous colour and texture has been subdivided into layers BS1 to BS16 based on superimposed 'pavements' of lithics, and the relevant layer here is BS5. PGS is loose, pinkish-grey sand (5 YR 5/2 pinkish grey), with few rock spalls. Layers BS5 and PGS are separated by at least 50 cm of intervening sediment (Figure 2) and the ages for each layer imply that the occupations were about 12 ka apart. This observation is important for the interpretation of the relationship between the human teeth described here.

Age

Sediment samples were collected from the site and quartz grains taken from these were processed in the University of Wollongong laboratory for single grain optically stimulated luminescence (OSL) dating. Extraction, processing and statistical calculation are described elsewhere (Jacobs et al., 2008a, Jacobs and Roberts, 2017). OSL sample SIB 23 (77.3 ± 2.7 ka) is from BS; OSL sample SIB 19 (64.7 ± 2.3 ka) is from PGS (Jacobs et al., 2008a). Jacobs and

Roberts (2017) take the statistical model used in the 2008 study and apply it under three different scenarios to update the dataset.

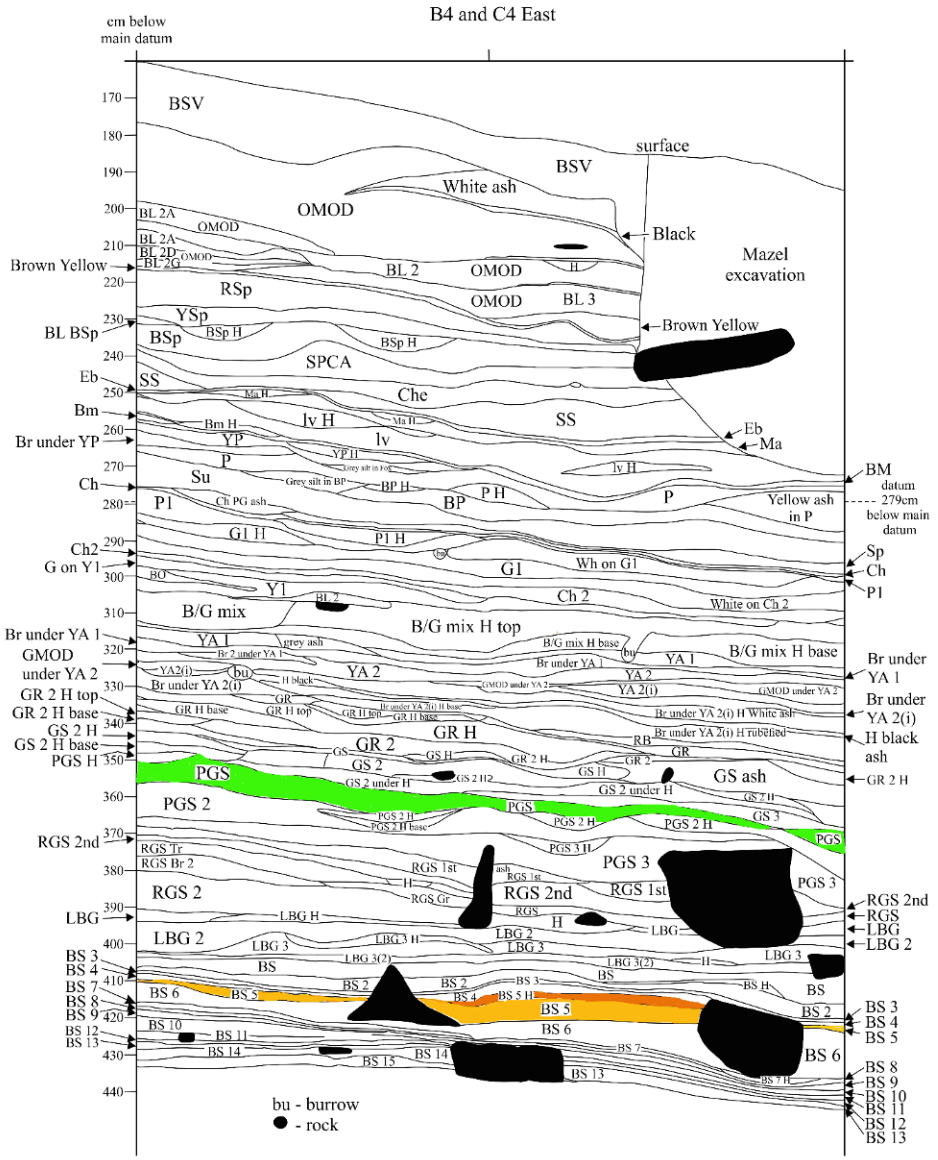

Figure 2. Stratigraphy of the MSA site Sibudu Cave (KwaZulu-Natal, South Africa). PGS and BS5 layers are in colour.

Human fossils

In 2004 Plug (2004) in her faunal analysis of Sibudu Cave materials excavated in the first few years of the Wadley excavation reported two human remains (a lateral malleolus of a fibula and the 3rd phalanx of an adult hand) from the final MSA sediments noting however that they may not belong to the final MSA; a toe bone from slightly earlier MSA sediments and a putative human remain (a fragment of a sternum) from the deeper MSA levels (Plug, 2004) (below Black Lens). Plug recorded that the human bone looked fresher than animal bones in the same layers and she thought they may have derived from the overlying Iron Age occupation. Wadley acknowledges this possibility, but has not discounted the likelihood that the remains may be of MSA origin (Grine, 2016) because the Iron Age pits into the final MSA layers were carefully excavated before taking out MSA material. In the absence of chemical tests, the issue cannot be resolved.

Subsequently, during continued excavations, the two deciduous human teeth presented here were recovered from older MSA layers. The first (catalogue number 2931CA 15 HUM. TO 1, hereafter HUM. TO 1) is a lower left first molar (Ldm_1), deriving from the pre-Still Bay BS member (Square B4b, layer Brown Sand 5 base), with an age of 77.2 ± 2.2 ka; the other (catalogue number 2931CA 15 HUM. TO 2 hereafter HUM. TO 2) is a lower right central incisor (Rdi_1), from the Howiesons Poort PGS layer (Square C4a, layer Pinkish Grey Sand), with an estimated age of 64.7 ± 2.3 ka (Wadley, 2015).

Methods

Acquisition of virtual images

High-resolution micro-CT images of all the teeth were obtained with the Xalt micro-CT scanner (Panetta et al., 2012). The most relevant scanning parameters were 50 kVp, 2 mm Al filtration, 960 projections over 360°, 0.9 mAs/projection for a total scan time of 50 minutes per sample. All the tomographic images were

reconstructed using a modified Feldkamp algorithm with embedded correction for geometric misalignment (Feldkamp et al., 1984; Panetta et al., 2008) and raw data pre-correction for beam-hardening and ring artefacts reduction. All images were reconstructed on a volume dataset of 600x600x1000 cubic voxels, each with a size of 18.4 μm^3.

Measurements

Mesio-Distal (MD) and Bucco-Lingual (BL) crown diameters of both teeth were measured using a digital caliper. Whereas the Ldm_1 is heavily worn, for the Rdi_1 it has been possible to compute enamel thickness following the guidelines provided by Benazzi *et al.* (2014). We measured enamel volume, dentine volume (including also the volume of the crown pulp chamber), and Enamel-Dentine Junction (EDJ) surface; then, we computed both the Average Enamel Thickness index (AET = volume of enamel divided by the EDJ surface) and the Relative Enamel Thickness index (RET = AET divided by the cubic root of dentine volume).

Comparisons and statistical analyses

Crown diameters of the Sibudu teeth have been compared with those of other Pleistocene fossil specimens and extant *Homo sapiens* (EHS) (table 1, table 2 and Appendix A).

The RET value obtained for the Rdi_1 was compared with those of Neandertals, Pleistocene *Homo sapiens* and EHS published by Fabbri et al. (2016), also accounting for the wear stage assessed following Molnar (1971).

The significance of the differences among groups was tested through multivariate analysis of variance (MANOVA), using the Pillai-Bartlett statistic (as suggested by Hand and Taylor, 1987). For the RET comparisons we calculated the standard score (Z score) of the Rdi_1 with respect to the other

samples and used that score to assess the similarities. All statistical analyses were performed using R (R Core Team 2017).

Table 1. Mean mesiodistal (MD) and buccolingual (BL) diameters (in mm) deciduous first mandibular molars in Pleistocene *Homo sapiens* fossil specimens and extant samples. The left dm_1 from Sibudu (2931CA 15 HUM. TO 1, MD=8.9, BL=7.2) is included in the MSA sample. See Appendix 1 for the list of the fossil specimens with individual values and references.

Sample							
	MD	**n**	**sd**		**BL**	**n**	**sd**
Middle Stone Age (MSA)	8.75	4	0.44		7.17	4	0.52
Middle Paleolithic (MP)	9.23	7	0.27		7.50	7	0.58
Iberomaurusian (IBM)	8.38	4	0.53		7.72	4	0.41
Early Upper Paleolithic (EUP)	8.77	10	0.37		7.11	11	0.43
Late Upper Paleolithic (LUP)	8.20	5	0.58		7.10	5	0.35
American Whites	7.80	133	0.42		7.34	133	0.46
Australian Aboriginals	8.19	179	0.53		7.71	185	0.51
South Africans	8.22	35	0.50		7.13	38	0.39
San	8.13	90	0.48		6.89	97	0.34

Table 2. Mesiodistal and buccolingual diameters (in mm) of the Rdi_1 from Sibudu (2931CA 15 HUM. TO 2) and of deciduous first mandibular incisors in Pleistocene *Homo sapiens* fossil specimens and extant samples.

Fossil specimens	Site	Specimen	side	MD	BL	Reference
Middle Stone Age (MSA)	Sibudu cave	2931CA 15 HUM. TO 2	R	4.9	4.3	This paper
	Die Kelders	AP 6290	L	5.1	4.8	Grine, 2000
Middle Paleolithic (MP)	Qafzeh	Qafzeh 10	R	4.2	4.4	Tillier, 1999
Iberomaurusian (IBM)	Afalou-bou-Rhummel	Afalou 4	L	4.6	4	Voisin et al. 2017
	Afalou-bou-Rhummel	Afalou 16	L	4.6	4.6	Voisin et al. 2017
Early Upper Paleolithic (EUP). Gravettain	Lagar Velho	Lagar Velho 1	L	4.7	4.3	Hillson and Trinkaus, 2002
Late Upper Paleolithic (LUP), Magdalenian	Le Figuier	Le Figuier 1	R	4.2	4.3	Bailey, pers. comm.
Late Upper Paleolithic (LUP) Epigravettian	Grotte des enfants	GE 2	R	4.5	3.8	Henry-Gambier, 2001
	Arene Candide	AC 6	R	4.6	4.2	Formicola, pers. comm.

Arene Candide	AC 8		L	4.3	4.3	Formicola, pers. comm.

Extant populations

	side	MD	n	sd	BL	n	sd	References
American Whites	R	4,07	133	0,32	3,85	133	0,37	Black, 1978
Australian Aboriginals	R	4,43	36	0,39	4,26	26	0,34	Margetts and Brown, 1978
South Africans	R	4,22	23	0,35	3,82	23	0,35	Grine, 1984
San	R	3,97	37	0,38	3,91	35	0,36	Grine, 1984

Anatomical description

Abbreviations

In describing the dental morphology the following abbreviations have been used: Orientation: bucco-lingual (BL), mesio-distal (MD), occlusal-cervical (OC), inciso-cervical (IC). Cusps: protoconid (PR), entoconid (EN), metaconid (ME), hypoconid (HY), hypoconulid (HYPL). Other features: marginal ridge (MR), interproximal contact facet (ICF), cervical enamel line (CEL).

2931CA 15 HUM. TO 1 (Ldm$_1$)

The specimen comprises the intact crown and the remnants of the roots that have been resorbed (Figure 3). Preservation is very good, with minor post mortem cracks across the surface, not affecting the overall morphology. The occlusal wear is marked, with large, confluent areas of dentine exposed on the PR, HY, HYPL and EN, and, to a lesser extent, on the ME. Dentine is also exposed at the level of the mesial MR. The mesial ICF is very faint. A large carious lesion occupies most of the distal face, also extending on the most distal part of the occlusal surface. A chip of enamel is missing from the disto-buccal corner; flaking must have occurred *in vitam*, since the edges of the enamel are smooth. The occlusal outline is oval, with some degree of MD compression and mesio-buccal extension. The outline of all five cusps is still evident. Although

worn, PR must have been the largest cusp, followed by the EN, HY and HYPL. Distal to the ME tip, dentine exposure and enamel thickening are suggestive of the occurrence of a postmetaconulid. The PR is mesially placed to the ME. Although worn, the mesial MR must have been very thick. The anterior fovea, lingually placed to the midline, is reduced to a slit that opens lingually just in front of the ME. Remnants of what must have been a deep central fovea are evident, mesial to the EN. On the buccal face the *tuberculum molare* is fairly well developed, with a notable mesio-buccal extension. The CEL curves around the *tuberculum molare*, climbing distally at the level of the HY. The presence and extent of development of the buccal grooves cannot be ascertained because of wear. The lingual face is markedly convex MD and OC, bulging at the level of the ME. The mesial face is featureless. Only a few millimetres of the root system are present. The sharp edges of the root remnants and the scooping of its internal surface indicate that the roots have been naturally resorbed, causing the tooth to be shed. Shedding of dm_1 in modern humans occurs when the first permanent premolar emerges in the mouth, that is around 10.5-11.5 years of age (AlQahtani *et al.*, 2010).

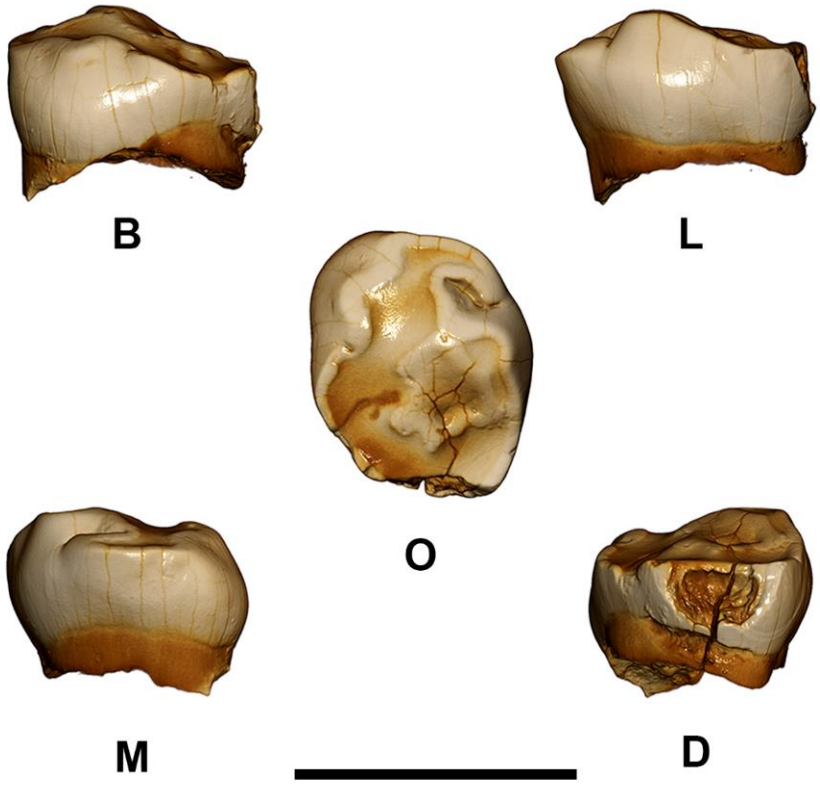

Figure 3. Three dimensional digital models of 2931CA 15 HUM. TO 1 (lower left first deciduous molar, Ldm_1). The black bar is equivalent to 1 cm. B, buccal; D, distal; L, lingual; M, mesial; O, occlusal.

2931CA 15 HUM. TO 2 (Rdi_1)

The specimen has the intact crown and remnants of the resorbed root (Figure 4). Preservation is very good, with only minor post mortem cracks across the surface, not affecting the overall morphology. The incisal wear is marked, with the flat wear plane tilted slightly distally. The exposed dentine measures 1.3 mm BL in its largest point. Its profile tapers distally, truncated by a marked, distal ICF (BL 0.8 IC 1.5). The mesial ICF is faint. The labial face has a square

shape (*sensu* Grine, 1984), in that the mesial and distal edges are almost parallel and the almost straight cervical enamel line does not extend much cervically. The face is slightly convex IC, and more so MD. The MD convexity is slightly skewed distally. Numerous microscratches cross it, with different orientations. On the lingual face the cervical eminence is well developed symmetrically placed. From it a faint median ridge moves toward the incisal edge. Both the mesial and the distal MR are weakly developed. The preserved root is subtriangular in cross section, tapering lingually. Some 4.1 mm of it are still present on the labial side and 1.1 mm on the lingual side. The root has sharp edges and its internal surface is scooped, indicating that the root has been naturally resorbed causing the shedding of the tooth. Shedding of di_1 in modern humans occurs when the first permanent incisor emerges in the mouth, that is around 5.5-6.5 years of age (AlQahtani *et al.*, 2010).

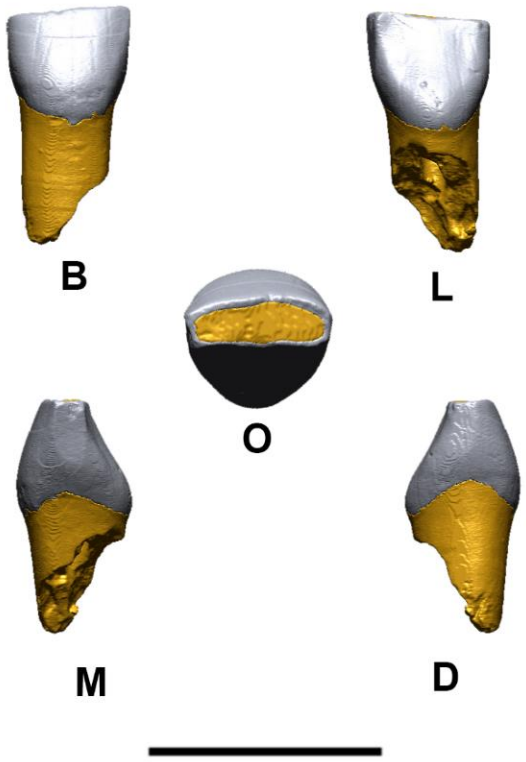

Figure 4. Three dimensional digital models of 2931CA 15 HUM. TO 2 (lower right central deciduous incisor, Rdi_1). The black bar is equivalent to 1 cm. B, buccal; D, distal; L, lingual; M, mesial; O, occlusal.

Comparative dental crown metrics

2931CA 15 HUM. TO 1 (Ldm1)

The estimated MD diameter of the Ldm_1 is 8.9 mm (8.7 mm as measured) and the BL diameter is 7.2 mm. These values fall into the variability of the other specimens of the South African MSA from Die Kelders (AP6246 and AP6291) and Diepkloof Rock Shelter (DRS 3). Together with the South African specimens, in the Late Pleistocene human fossil record a fairly good number of lower dm1 are available, thus allowing us the possibility of carrying out some

comparative analysis. Table 1 shows the mean values of MD and BL diameters for a series of specimens belonging to different populations identified here as cultural groups, plus 4 samples of modern human populations (American Whites, Australian Aboriginals, South Africans and San).

Inspection of the data indicates an interesting pattern, with some differences among groups in dental size in the mean MD diameter (Figure 5): Middle Paleolithic (MP) samples (Qafzeh and Skhul) display the highest value; South African MSA, early Upper Paleolithic Aurignacian (EUPA) and early Upper Paleolithic Gravettian (EUPG) showing similar values; late Upper Paleolithic (LUP, i.e. Epigravettian and Magdalendian) have the lowest, and not dissimilar from extant populations; Iberomaurusian (IBM) have intermediate values between the latter two. No similar differences seem to exist in the BL mean values. A scatterplot of the two variables (MD and BL) (Figure 6a) emphasizes the results.

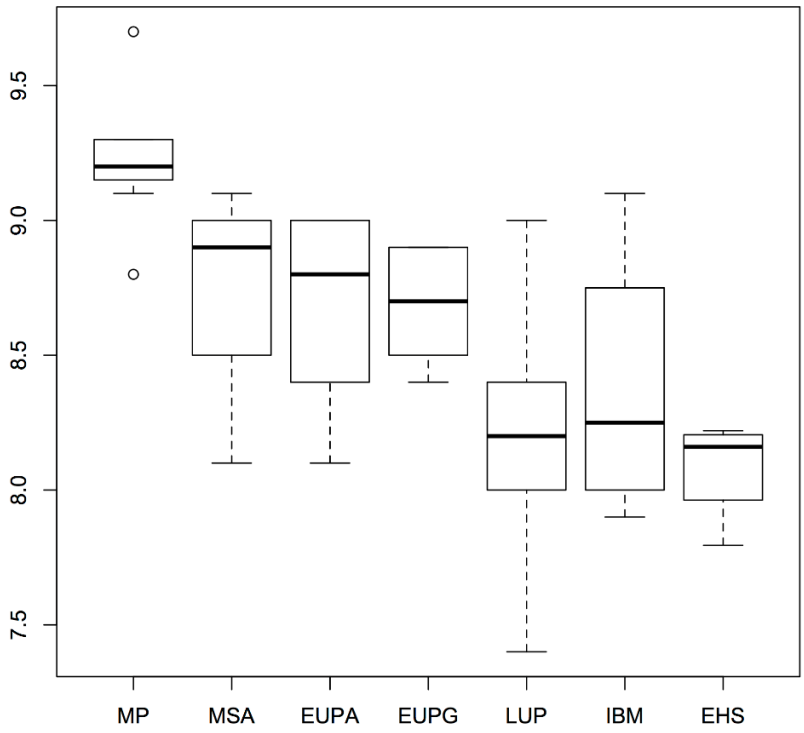

Figure 5. Boxplot of the variability in dm_1s MD diameters for each group considered. MP: Middle Paleolithic; MSA: Middle Stone Age; EUPA: Early Upper Paleolithic Aurignacian; EUPG: Early Upper Paleolithic Gravettian; LUP: Late Upper Paleolithic (Epigravettian and Magdalenian); IBM: Iberomaurusian; EHS: Extant *Homo sapiens*.

The differences observed have been tested with a MANOVA, which suggests significant differences both for the interaction of MD and BL ($p<0.01$) and for MD alone ($p<0.001$). The MP sample is the one that diverges more from the other samples and this could affect the analysis. Thus, we repeated the MANOVA excluding the MP samples to test whether the significance persists; the results give significance ($p<0.05$) only for the interaction of the two variables analysed. This means that, even if the differences observed are largely

linked to the high MD values of the MP specimens, nevertheless crown diameters reveal some differences among the groups.

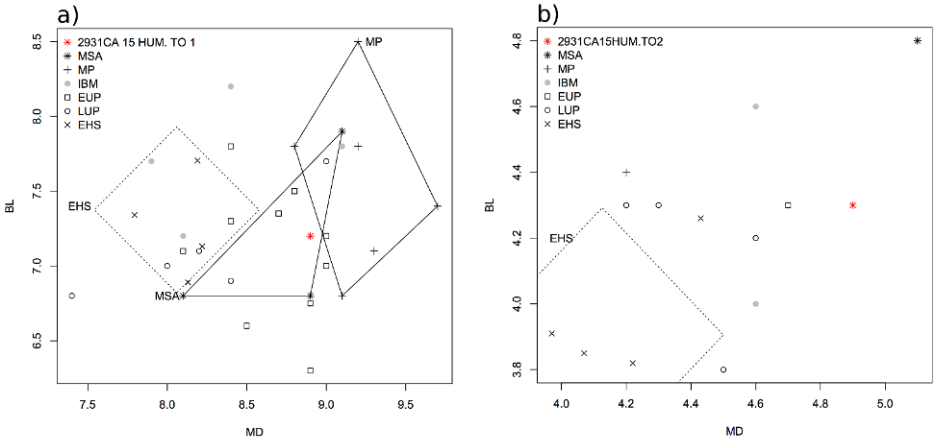

Figure 6. Bivariate plots comparing the dental dimensions (MD and BL diameters) of (a) 2931CA 15 HUM. TO 1 (Ldm_1) and (b) 2931CA 15 HUM. TO 2 (Rdi_1) to those of Late Pleistocene fossil specimens and extant samples. Specimens included and references are listed in Tables 1, Table 2 and Appendix A. The polygons encompass the variability of each group. The dashed line represents the standard deviation of the total sample of EHS. The EUP group includes both Aurignacian and Gravettian samples.

2931CA 15 HUM. TO 2 (Rdi1)

The corrected MD diameter of the Rdi_1 is 4.9 mm (4.7 mm as measured) and the BL is 4.3 mm. Compared to the other specimen of the MSA (AP6290 from Die Kelders) this specimen is smaller in both diameters (Table 2). In Figure 6b the specimens used in the comparison are plotted. Different groups seem to cluster together: MSA in the right portion of the plot, with higher MD diameter; IBM, EUP and LUP occupy the central part, with intermediate MD values; MP and EHS have low MD and stand on the left portion of the plot. The BL diameter doesn't seem to distinguish the different groups. The MANOVA

confirms these observations giving significant p-values only in the case of MD ($p<0.01$).

The Relative enamel thickness (RET) index of Rdi_1 and the comparative samples are presented in Table 3. The Z-score computed for the Rdi_1 places the tooth close to EHS at wear stage 4; however, if we also consider Late Pleistocene *H. sapiens* and Neandertals the range of RET values among these species overlaps and this specimen falls in the variability of both species.

Table 3. Values of the components of three-dimensional (3D) enamel thickness of the Rdi_1 from Sibudu (2931CA 15 HUM. TO 2), Neandertals, Upper Paleolithic *Homo sapiens* (UPHS) and recent *Homo sapiens* (RHS) di_1s. For the comparative samples (N): mean±SD (range).

	Wear stage[a]	**Enamel volume (mm^3)**	**Coronal dentine + pulp volume (mm^3)**	**EDJ surface (mm^2)**	**3D AET (mm)**	**3D RET (scale-free)**	**Z-score for RET index**
2931CA 15 HUM. TO 2	4	11.52	35.34	45.67	0.25	7.69	
Neanderthals[b](3)	1-3	12.89 ± 3.07 (9.91-16.05)	40.05 ± 0.76 (39.18-40.53)	57.40 ± 5.85 (50.65-61.06)	0.22 ± 0.04 (0.20-0.26)	6.52 ± 1.08 (5.70-7.74)	1.08

Neanderta l(1)[c]	5	10.86	42.62	53.57	0.2	5.8	
La Madeleine 4 LUP [d]	3-4	10.16	18.94	31.66	0.32	12.04	
RHS(5)[c]	2-3	11.21± 1.92 (9.45-14.45)	22.52± 1.79 (20.07-24.96)	41.21±2 .12 (38.39-43.30)	0.27±0. 03 (0.24-0.33)	9.62±1. 32 (8.52-11.83)	-1.46
RHS(4)[c]	4	8.53 ± 2.59 (5.55-10.81)	21.95 ± 3.40 (18.22-25.60)	37.49 ± 4.55 (33.15-43.37)	0.22 ± 0.04 (0.17-0.27)	7.98 ± 1.33 (6.36-9.51)	-0.21
RHS(9)[e]	5	4.78 ± 1.13 (3.12-6.19)	16.35 ± 2.63 (12.21-19.93)	22.98 ± 3.31 (16.89-27.43)	0.21 ± 0.03 (0.15-0.26)	8.15 ± 1.12 (6.11-10.28)	0.41

[a]Based on Molnar (1971).

[b]ForAbriSuard S14 and Spy VI see Bayle (2008); for Roc de Marsal see Bayle et al. (2009).

[c]Fabbri et al. (2016).

[d]Bayle (2008).

[e]Digital removal of tooth crown up to wear stage 5 (Fabbri et al., 2016).

Discussion and conclusions

The South African MSA human fossil record includes remains coming from 15 sites (Grine, 2016; Grine et al., 2017), among these, Sibudu Cave, from where a few, undescribed specimens have been reported (Plug, 2004). Thus any addition to this record, for example the two deciduous teeth described here, is important, since it allows us to better understand the anatomical features of early populations of *Homo sapiens* and their variability. Of the two deciduous teeth from Sibudu Cave, the Ldm_1 comes from the layer BS5 that is dated at around 77.2±2.2 ka and it is associated with pre-Still Bay lithic assemblages; it is thus the oldest among the four deciduous first molars from the South African MSA described so far in the literature (see above). The Rdi_1 comes from the PGS layers, which are dated at 64.7±2.3 and it is associated with a Howiesons Poort assemblage (Wadley 2015). Hence, the two specimens come not only from different individuals, but also from different populations that occupied the site in different times. The two specimens, deriving from juvenile individuals, add to the MSA deciduous dental sample from other South African sites, and confirm the observation by Grine et al. (2016) that juvenile individuals (largely represented by deciduous teeth) are relatively more abundant than adult specimens at other MSA South African sites (Die Kelders Cave 1, Blombos and Klipdrift Shelter), with the notable exception of remains from Klasies River Mouth Main Site.

The comparative metrical analysis has provided interesting results. Both teeth cluster with the other MSA specimens from South Africa, especially for MD diameters. In particular, in the metrical study of dm_1 an interesting pattern emerges with a few points that we believe particularly relevant since they derive from the analysis of deciduous teeth, that are recognized as more conservative in their morphology than permanent teeth (Brabant, 1967; von Koenigswald, 1967; Margetts and Brown, 1978; Smith, 1978; Aiello and Dean, 1990;

Hemphill, 2015; Bailey et al., 2016) and as such they are more informative when addressing taxonomic and evolutionary issues.

First, the MSA populations show similar mean MD values to EUP European populations, both Aurignacians and Gravettians, the latter two sharing almost identical mean values. Secondly, the MSA/EUP dm_1 is smaller than the mean value for MP populations. This neat difference can be explained if we consider that MP specimens probably represent an early episode of dispersal out of Africa around 120-70ka (Grove et al., 2015) that may have contributed only limitedly to the variability of later human populations (Mellars et al., 2013; Reyes-Centeno, 2014; Pagani et al., 2016). The similarities in size with Upper Paleolithic specimens, and the differences with MP sample have also been noted by Verna et al. (2013) in their description of the Diepkloof Rock Shelter (DRS 3) specimen. Thirdly, MSA/EUP samples differ from both LUP and IBM populations, both having smaller mean values of the earlier groups. Of broader significance, it is interesting to note the similarities between the MD values of the Aurignacian and Gravettian (EUP) samples and the smaller mean value of the Epigravettians and Magdalenians (LUP) – pointing to a pattern of reduction taking place between EUP and LUP already noted by Frayer (1978) for the dentition and in other aspects of cranial and postcranial dimensions (see Holt and Formicola, 2008 for a review). A similar pattern seems to exist when comparing MSA and IBM. Lastly, the mean value for the four EHS samples is even smaller, and notably distinct from all earlier samples. Although based on an admittedly small sample of fossil specimens, looking at the sequence MP – MSA/EUP – LUP and IBM – EHS an overall decrease in mean MD values is apparent, consistent with the trend towards dental size reduction in *Homo sapiens* described in the literature (eg. Brace and Mahler, 1971; LeBlanc and Black, 1974; Frayer, 1978; Calcagno, 1986; Brace et al., 1987; y'Edynak, 1989; Brace, 1995). At the same time the BL mean values do not show a similar pattern, pointing to a process of dental reduction affecting only the MD

direction. Further data are needed to support this observation. In the di_1, the MSA and the other samples are too limited to carry out an equally fine analysis, although differences between the fossil samples and the EHS are apparent, with the latter being smaller than the former.

In conclusion, the two deciduous teeth described here, a dm_1 and a di_1, contribute to expand the still limited sample of fossil human skeletal remains from the African Late Pleistocene. The analysis has shown that they are comparable in size with the other MSA specimens described in the literature. In the case of the dm_1 metrical differences among various samples of fossil and extant populations have been highlighted, that will require further investigation in the possibility that deciduous dental metrics can discriminate different fossil populations of *Homo sapiens*.

Acknowledgments

We would like to thank Shara Bailey and Vincenzo Formicola for sharing with us the raw data of the deciduous dentition from Le Figuier (S.B.) and Arene Candide (V.F.). We are grateful to Lucinda Backwell for help in many stages of the project and to Jamie Clark who first recognised that the teeth might be human when she was making a preliminary sort of the faunal remains.

References

Aiello, L. Dean, C., 1990. An introduction to human evolutionary anatomy. Academic Press, Cambridge MA.

AlQahtani, S.J., Hector, M.P., Liversidge, H.M., 2010. The London atlas of human tooth development and eruption. Am. J. Phys. Antrhopol. 142, 481-490.

Backwell, L.R., d'Errico, F., Wadley, L., 2008. Middle Stone Age bone tools from the Howiesons Poort layers, Sibudu Cave, South Africa. J. Archaeol. Sci. 35, 1566-1580.

Bailey, S.E., Benazzi, S., Buti, L., Hublin, J.-J. 2016. Allometry, Merism and tooth shape of the lower second deciduous molar and first permanent molar. Am J Phys Anthropol 159, 93-105.

Bayle, P., 2008. Analyses quantitatives par imagerie à haute résolution des séquences de maturation dentaire et des proportions des tissus des dents déciduales chez les Néanderthaliens et les Hommes modernes. Ph.D. Dissertation, University of Toulouse III.

Bayle, P., Braga, J., Mazurier, A., Macchiarelli, R. 2009. Brief communication: High resolution assessment of the dental developmental pattern and characterization of tooth tissue proportions in the late Upper Paleolithic child from La Madeleine, France. Am. J. Phys. Anthropol. 138, 493-498.

Benazzi, S., Panetta, D., Fornai, C., Toussaint, M., Gruppioni, G., Hublin, J.J., 2014. Technical note: guidelines for the digital computation of 2D and 3D enamel thickness in hominoid teeth. Am. J. Phys. Anthropol. 153, 305-313.

Black, T.K. III, 1978. Sexual dimorphism in the tooth-crown diameters of the deciduous teeth. Am. J. Phys. Anthropol. 48, 77-82.

Brabant, H., 1967. Comparison of the characteristic and anomalies of the deciduous and the permanent dentition. J. Dent. Res. 46, 897-902.

Brace, C. L., 1995. Trends in the evolution of human tooth size. In: Moggi-Cecchi J. (Ed.), Aspects of dental biology: palaeontology, anthropology and evolution. International Institute for the Study of Man, Firenze, 437 – 446.

Brace, C.L., Mahler, P.E., 1971. Post-Pleistocene changes in the human dentition. Am. J. Phys. Anthropol. 34, 191-204

Brace, C.L., Rosenberg, K.R., Hunt, K.D., 1987. Gradual change in human tooth size in the late Pleistocene and Post-Pleistocene. Evolution 41, 705-720.

Calcagno, J., 1986. Dental reduction in Post-Pleistocene Nubia. Am. J. Phys. Antrhopol. 77, 505-517.

Chase, B.M., 2010. South African palaeoenvironments during marine ocygen isotope stage 4: a context for the Howiesons Poort and Still Bay industries. J. Archaeol. Sci. 37, 1359-1366.

y'Edynak, G., 1978. Culture, diet, and dental reduction in Mesolithic forager-fishers of Yugoslavia. Curr. Anthropol. 19, 616-618.

d'Errico, F., Vanhaeren, M., Wadley, L., 2008. Possible shell beads from the Middle Stone Age layers of Sibudu Cave, South Africa. J. Archaeol. Sci. 35, 2675-2685.

Fabbri, P.F., Panetta, D., Sarti, L., Martini, F., Salvadori, P.A., Caramella, D., Fedi, M., Benazzi, S., 2016. Middle paleolithic human deciduous incisor from Grotta del Cavallo, Italy. Am. J. Phys. Anthropol. 161, 506-512.

Favati-Vanni, V., 1964. Studio antropologico dello scheletro d'un bambino del Paleolitico superiore, rinvenuto nella Grotta Maritza presso Avezzano. Atti. Soc. Toscana Sc Nat. Ser B. 71, 475 – 487.

Feldkamp, I. A., Davis, L. C., & Kress, J. W., 1984. Practical cone-beam algorithm. J Opt. Soc. Am. A. 1, 612-619.

Formicola V., 1986. Anthropologie dentaire des restes de l'Epigravettien final retrouvés dans la grotte des Arene Candide (Ligurie). Bull. Mem. Soc. Anthrop. Paris 3, (XIV, 1), 37-46.

Frayer, D.W., 1978. The Evolution of Dentition in Upper Paleolithic and Mesolithic Europe. University of Kansas Publications in Anthropology, No. 10.

Grine, F.E., 1984. The deciduous dentition of the Kalahari San, the South African Negro and the South African Plio-Pleistocene hominids. Ph.D. Dissertation, University of the Witwatersrand.

Grine, F.E., 2000. Middle Stone Age human fossils from Die Kelders Cave 1, Western Cape Province, South Africa. J. Hum. Evol. 28, 129-145.

Grine, F.E., 2016. The Late Quaternary Hominins of Africa: The Skeletal Evidence from MIS 6-2. In: Jones, S.C. and Stewart, B.A. (Eds.), Africa from MIS 6-2. Population Dynamics and Paleoenvironments. Springer, Netherlands, 323-381.

Grine, F.E., Wurz, S., Marean, C.W., 2017. The Middle Stone Age human fossil record from Klasies River Main Site. J. Hum. Evol. 103, 53-78.

Grove, M., Lamb, H., Roberts, H., Davies, S., Marshall, M., Bates, R., Huws, D., 2015. Climatic variability, plasticity, and dispersal: a case study from Lake Tana, Ethiopia. J. Hum. Evol. 87, 32-47.

Hemphill. B.E., 2015. In: Irish, J.D, Scott, G.R. (Eds.), A Companion to Dental Anthropology. Wiley-Blackwell, pp. 287-310.

Hand, D.J., Taylor, C.C., 1987. Multivariate Analysis of Variance and Repeated Measures: a practical approach for behavioural scientists. Chapman and Hall, London.

Henry-Gambier, D., 2001. Les enfants de Grimaldi (grotte des Enfants, site des Baoussé-Roussé, Italie), Anthropologie et palethnologie funéraire. CTHS/RMN, Paris.

Henry-Gambier, D., Maureille, B., White, R., 2004. Vestiges humains des niveaux de l'Aurignacien ancien du site de Brassempouy (Landes). B. Mem. Soc. Anthro. Par. 16, 49-87.

Hillson, S.W., Trinkaus, E., 2002. Comparative Dental Crown Metrics. In: Zilhão, J., Trinkaus, E. (Eds.), Portrait of the Artist as a Child. Instituto Português de Arqueologia, Lisboa, pp. 356-364.

Hodgskiss, T., 2012. Attribute analysis of the Sibudu Middle Stone Age ochre assemblage. S. Afr. Humanit. 24, 99-120.

Hodgskiss, 2013. Ochre use in the Middle Stone Age at Sibudu, South Africa: grinding, rubbing, scoring and engraving. J. Afr. Archaeol. 11, 75-95.
Holt, B.M, Formicola, V., 2008. Hunters of the Ice Age: The Biology of Upper Paleolithic People. Yearb. Phys. Anthropol. 51, 70-99.

Jacobs, Z., Roberts, R.G., Galbraith, R.F., Deacon, H.J., Grün, R., Mackay, A., Mitchell, P., Wadley, L. 2008a. Ages for the Middle Stone Age of southern Africa: implications for human behaviour and dispersal. Science 322, 733-735.

Jacobs, Z., Wintle, A.G., Duller, G.A.T., Roberts, R.G., Wadley, L. 2008b. New ages for the post-Howiesons Poort, late and final Middle Stone Age at Sibudu Cave, South Africa. J. Archaeol. Sci. 35, 1790-1807.

Jacobs, Z., Roberts, R.G., 2017. Single-grain OSL chronologies for the Still Bay and Howieson's Poort industries and the transition between them: Further analyses and statistical modelling. J. Hum. Evol. 107, 1-13.

von Koenigswald, G.H.R., 1967. Evolutionary trends in the deciduous molars of the hominidea. J. Dent. Res. 46, 779-786.

LeBlanc, S.A., Black, B., 1974. A long-term trend in tooth size in the eastern Mediterranean. Am. J. Phys. Anthropol 41, 417-422.

Lombard, M., 2007. The gripping nature of ochre: the association of ochre with Howiesons Poort adhesive and Later Stone Age mastics from South Africa. J. Hum. Evol. 53, 406-419.

Lombard, M., 2011. Quartz-tipped arrows older than 60 ka: further use-trace evidence from Sibudu, KwaZulu-Natal, South Africa. J. Archaeol. Sci. 38, 1918-1930.

Lombard, M., Phillipson, L., 2010. Indications of bow and stone-tipped arrow use 64,000 years ago in KwaZulu-Natal, South Africa. Antiquity. 84, 635-648.

Margetts, B., Brown, T., 1978. Crown diameters of the deciduous teeth in Australian Aboriginals. Am. J. Phys. Anthropol. 48, 493-502.

Mellars, P., Gori, K.C., Carr, M., Soares, P.A., Richards, M.B., 2013. Genetic and archaeological perspectives on the initial modern human colonization of southern Asia. Proc. Natl. Acad. Sci. USA 110, 10699-10704.

Molnar, S., 1971. Human Tooth Wear, Tooth Function and Cultural Variability. Am. J. Phys. Anthropol. 34, 175-190.

Pagani, L., Lawson, D.J., Jagoda, E., Mörseburg, A., Eriksson, A., Mitt, M., Clemente, F., Hudjashov, G., DeGiorgio, M., Saag, L.,Wall, J.D., Cardona, A., Mägi, R., Wilson Sayres, M.A., Kaewert, S., Inchley, C., Scheib, C.L., Järve1, M., Karmin, M., Jacobs, G.S., Antao, T., Iliescu, F.M., Kushniarevich, A., Ayub, Q., Tyler-Smith, C., Xue, Y., Yunusbayev, B., Tambets, K., Basu Mallick, C., Saag, L., Pocheshkhova, E., Andriadze, G., Muller, C., Westaway, M.C., Lambert, D.M., Zoraqi, G., Turdikulova, S., Dalimova, D., Sabitov, Z., Sultana, G.N.N., Lachance, J., Tishkoff, S., Momynaliev, K., Isakova, J., Damba, L.D., Gubina, M., Nymadawa, P., Evseeva, I., Atramentova, L., Utevska, O., Ricaut, F.X., Brucato, N., Sudoyo, H., Letellier, T., Cox, M.P., Barashkov, N.A., Škaro, V., Mulahasanović, L., Primorac, D., Sahakyan, H., Mormina, M., Eichstaedt, C.A., Lichman, D.V., Abdullah, S., Chaubey, G., Wee, J.T.S., Mihailov, E., Karunas, A., Litvinov, S., Khusainova, R., Ekomasova, N., Akhmetova, V., Khidiyatova, I., Marjanović, D., Yepiskoposyan, L., Behar, D.M., Balanovska, E., Metspalu, A., Derenko, M., Malyarchuk, B., Voevoda, M., Fedorova, S.A., Osipova, L.P., Lahr, M.M., Gerbault, P., Leavesley, M., Migliano, A.B., Petraglia, M., Balanovsky, O., Khusnutdinova, E.K., Metspalu, E., Thomas, M.G., Manica, A., Nielsen, R., Villems, R., Willerslev, E., Kivisild, T., Metspalu, M., 2016. Genomic analyses inform on migration events during the peopling of Eurasia. Nature 538, 238-242.

Panetta, D., Belcari, N., Del Guerra, A., Bartolomei, A., & Salvadori, P.A., 2012. Analysis of image sharpness reproducibility on a novel engineered MicroCT scanner with variable geometry and embedded recalibration software. Phys. Medica, 28, 166-173.

Panetta, D., Belcari, N., Del Guerra, A., Moehrs, S., 2008. An optimization-based method for geometrical calibration in cone-beam CT without dedicated phantoms. Phys. Med. Biol. 53, 3841-61.

Plug, I., 2004. Resource exploitation: animal use during the Middle Stone Age at Sibudu Cave, KwaZulu-Natal. S. A. J. Sci. 100, 151-158.

R Core Team, 2017. R: a language and environment for statistical computing. R Foundation for Statistical Computing, Vienna.

Reyes-Centeno, H., Ghirotto, S., Détroit F., Grimaud-Hervé, D., Barbujani, G., Harvati, K., 2014. Genomic and cranial phenotype data support multiple modern human dispersals from Africa and a southern route into Asia. Proc. Natl. Acad. Sci. USA 111**,** 7248-7253.

Smith, P., 1978. Evolutionary changes in the deciduous dentition of near eastern populations. J. Hum. Evol. 7, 401-408.

Soriano, S., Villa, P., Wadley, L., 2009. Ochre for the toolmaker: Shaping the Still Bay points at Sibudu (KwaZulu-Natal, South Africa). J. Afr. Archaeol. 7, 41-54.

Teschler-Nicola, M.E., Antl-Weiser, W., Prossinger, H., 2004. Two Gravettian human deciduous teeth from Grub/Kranawetberg, Lower Austria. Homo 54, 229-239.

Tillier, A.M., 1999. Les enfants moustériens de Qafzeh. Interprétation phylogénétique et paléoauxologique. CNRS Éditions, Paris.

Trinkaus, E., Bailey, S.E., Davis, S.J.M., Zilhão, J., 2011. The Magdalenian Human Remains from the Galeria da Cisterna (Almonda karstic system, Torres Novas, Portugal) and their Archaeological Context. Arqueol. Port. 1, 395-413.

Trinkaus, E., Buzhilova, A.P., Mednikova, M.B., Dorbrovolskaya, M.V., 2014. The People of Sunghir. Burials, Bodies and Behavior in the Earlier Upper Paleolithic. Oxford University Press, New York.

Verna, C., Texier, P.J., Rigaud, J.P., Poggenpoel, C., Parkington, J., 2013. The Middle Stone Age human remains from Diepkloof Rock Shelter (Western Cape, South Africa). J. Archaeol. Sci. 40, 3532-3541.

Voisin, J.L., Condemi, S., Wolpoff, M.H., Frayer, D.W., 2017. Human fossil teeth. Online database, http://anthropologicaldata.free.fr.

Wadley, L., 2012. Two ‘moments in time’ during Middle Stone Age occupations of Sibudu, South Africa. S. Afr. Humanit. 24, 79-97.
Wadley, L., 2015. Those marvellous millennia: the Middle Stone Age of Southern Africa. Azania 50, 155-226.

Wadley, L., Jacobs, Z., 2004. Sibudu Cave, KwaZulu-Natal: background to the excavations of Middl Stone Age and Iron Age occupations. S. Afr. J. Sci. 100, 145-151.

Wadley, L., Langejans, G., 2014. Preliminary study of scrapers around combustion features in layer SS, Sibudu, 58,000 years ago. S. Afr. Archaeol. Bull. 69, 19-33.

Wadley, L., Sievers, C., Bamford, M., Goldberg, P., Berna, F., Miller, C., 2011. Middle Stone Age bedding construction and settlement patterns at Sibudu, South Africa. Science. 334, 1388-1391.

Wilczyński, J., Szczepanek, A., Wojtal, P., Diakowski, M., Wojenka, M., Sobieraj, D., 2014. A Mid Upper Palaeolithic Child Burial from Borsuka Cave (Southern Poland). Int. J. Osteoarchaeol. 26, 151-162.

Appendix A. Mesiodistal and buccolingual diameters (in mm) of the Ldm_1 from Sibudu (2931CA 15 HUM. TO 1) and of deciduous first mandibular molars in Late Pleistocene *Homo sapiens* fossil specimens and extant samples.

Fossil specimens	Site	specimen	side	MD	BL	Reference
Middle Stone Age (MSA)	Sibudu cave	2931CA 15 HUM. TO 1	L	8.9	7.2	This paper
	Die Kelders	AP 6246	L	8.1	6.8	Grine 2000
		AP 6291	L	9.1	7.9	Grine 2000
	Diepkloof Rock Shelter	DRS 3	L	8.9	6.8	Verna et al. 2013
Middle Paleolithic (MP)	Qafzeh	Qafzeh 10	R	9.2	7.8	Tillier 1999
		Qafzeh 14	L	9.1	6.8	Tillier 1999
		Qafzeh 21	L	9.3	7.1	Tillier 1999
		Qafzeh 12	R	9.3	7.1	Tillier 1999
		Qafzeh 4	R	8.8	7.8	Tillier 1999
		Qafzeh 15	R	9.2	8.5	Tillier 1999
	Skhul	Skhul 1	R	9.7	7.4	Tillier 1999
Iberomaurusian (IBM)	Afalou-bou-Rhummel	Afalou 4	L	8.1	7.2	Voisin et al 2017
		Afalou 16	L	9.1	7.8	Voisin et al 2017
		Afalou 19	R	8.4	8.2	Voisin et al 2017
		Afalou 41	R	7.9	7.7	Voisin et al 2017
Early Upper Paleolithic (EUP)						
Aurignacian	Brassempouy	Brassempouy 112	L	8.4	7.8	Henry-Gambier 2004
	Isturitz 2000	Isturitz 1	R	8.1	7.1	Henry-Gambier 2004
	Cueva del Castillo	CDC 2	R	9.0	7.0	Henry-Gambier 2004
	La Quina	La Quina 761	R	9.0	7.2	Henry-Gambier 2004

	Bacho Kiro	BK 1124	L	8.8	7.5	Henry-Gambier 2004
Early Upper Paleolithic (EUP)						
Gravettian	Lagar Velho	Lagar Velho I	R	8.4	7.3	Hillson and Trinkaus 2002
	Grub/Kranawetberg	G/K1	R	8.5	6.6	Teschler-Nicola et al. 2004
	Borsuka Cave	C7/682	L	8.9	6.3	Wilczyński et al. 2014
	Kostenki	Kostenki 3	-	8.9	6.75	Wilczyński et al. 2014
	Kostenki	Kostenki 4	-	8.7	7.35	Wilczyński et al. 2014
	Sunghir	Sunghir 3	R	-	7.3	Trinkaus et al. 2014
Late Upper Paleolithic (LUP)						
Epigravettian	Grotte des Enfants	GE2	R	8.4	6.9	Henry-Gambier 2001
	Grotta Maritza	GM	L+R	8.0	7.0	Favati-Vanni 1964
	Arene Candide	AC 6	R	7.4	6.8	Formicola pers.comm.; Formicola 1986
		AC 8	R	8.2	7.1	Formicola. pers. comm.; Formicola 1986
Late Upper Paleolithic (LUP)						
Magdalenian	Galeria da Cisterna	L12-220	R	9.0	7.7	Trinkaus et al. 2011

Extant populations

	side	MD	n	sd	BL	n	sd	Reference
American Whites	R	7.80	133	0.42	7.34	133	0.46	Black. 1978
Australian Aboriginals	R	8.19	179	0.53	7.71	185	0.51	Margetts and Brown. 1978
South Africans	R	8.22	35	0.50	7.13	38	0.39	Grine. 1984
San	R	8.13	90	0.48	6.89	97	0.34	Grine. 1984

List of publications

2015:

Gregorio Oxilia, Marco Peresani, Matteo Romandini, Chiara Matteucci, Cynthianne Debono Spiteri, Amanda G. Henry, Dieter Schulz, Will Archer, Jacopo Crezzini, Francesco Boschin, Paolo Boscato, Klervia Jaouen, Tamara Dogandzic, Alberto Broglio, Jacopo Moggi-Cecchi, Luca Fiorenza, Jean-Jacques Hublin, Ottmar Kullmer & Stefano Benazzi. *Earliest evidence of dental caries manipulation in the Late Upper Palaeolithic. Sci. Rep.* **5**, 12150; doi: 10.1038/srep12150 (2015).

2016:

Cristiana Margherita, Sahra Talamo, Karin Wiltschke-Schrotta, Sascha Senck, **Gregorio Oxilia**, Rita Sorrentino, Giuseppe Mancuso, Giorgio Gruppioni, Robert Lindner, Jean-Jacques Hublin, Stefano Benazzi (2016). A reassessment of the presumed Torrener Bärenhöhle's Paleolithic human tooth. *Journal of Juman Evolution,* 30; 1e6.

Julie Arnaud, Carlo Peretto, Daniele Panetta, Maria Tripodi, Federica Fontana, Marta Arzarello, Ursula Thun Hohenstein, Claudio Berto, Benedetto Sala, **Gregorio Oxilia**, Piero A Salvadori, Stefano Benazzi (2016). A reexamination of the Middle Paleolithic human remains from Riparo Tagliente, Italy. *Quaternary International, 425;* 437-444.

2017:

Gregorio Oxilia, Flavia Fiorillo, Francesco Boschin, Elisabetta Boaretto, Salvatore A. Apicella, Chiara Matteucci, Daniele Panetta, Rossella Pistocchi, Franca Guerrini, Cristiana Margherita, Massimo Andretta, Rita Sorrentino,

Giovanni Boschian, Simona Arrighi, Irene Dori, Giuseppe Mancuso, Jacopo Crezzini, Alessandro Riga, Maria C. Serrangeli, Antonino Vazzana, Piero A. Salvadori, Mariangela Vandini, Carlo Tozzi, Adriana Moroni, Robin N. M. Feeney, John C. Willman, Jacopo Moggi-Cecchi, Stefano Benazzi. *The dawn of dentistry in the late upper Paleolithic: An early case of pathological intervention at Riparo Fredian*. Am J Phys Anthropol. 2017a; 00:1–16. https://doi.org/10.1002/ajpa.23216

Gregorio Oxilia, Flavia Fiorillo, Francesco Boschin, Elisabetta Boaretto, Salvatore A. Apicella, Chiara Matteucci, Daniele Panetta, Rossella Pistocchi, Franca Guerrini, Cristiana Margherita, Massimo Andretta, Rita Sorrentino, Giovanni Boschian, Simona Arrighi, Irene Dori, Giuseppe Mancuso, Jacopo Crezzini, Alessandro Riga, Maria C. Serrangeli, Antonino Vazzana, Piero A. Salvadori, Mariangela Vandini, Carlo Tozzi, Adriana Moroni, Robin N. M. Feeney, John C. Willman, Jacopo Moggi-Cecchi, Stefano Benazzi. (2017b). *Letter to the editor: Reply to Hardy & Buckley: Earliest evidence of bitumen from Homo sp. teeth is from El Sidron.* Am J Phys Anthropol. DOI: 10.1002/ajpa.23254.

Ella Been, Erella Hovers, Ravid Ekshtain, Ariel Malinski-Buller, Nuha Agha, Alon Barash, Daniella E. Bar-Yosef Mayer, Stefano Benazzi, Jean-Jacques Hublin, Lihi Levin, Noam Greenbaum, Netta Mitki, **Gregorio Oxilia**, Naomi Porat, Joel Roskin, Michalle Soudack, , Reuven Yeshurun, Ruth Shahack-Gross, Nadav Nir, Mareike C. Stahlschmidt, Yoel Rak, Omry Barzilai. *The first Neanderthal remains from an open-air Middle Palaeolithic site in the Levant*. Scientific Reports. 2017, 7 - 2958 doi:10.1038/s41598-017-03025-z

Cristiana Margherita, **Gregorio Oxilia**, Veronica Barbi, Daniele Panetta, Jean – Jacques Hublin, David Lordkipanidze, Tengiz Meshveliani, Nino Jakeli, Zinovi

Matskevich, Ofer Bar-Yosef, Anna Belfer-Cohen, Ron Pinhasi, Stefano Benazzi (2017). *Morphological description and morphometric analyses of the Upper Palaeolithic human remains from Dzudzuana and Satsurblia caves, western Georgia.* Journal of Human Evolution. 113; 83-90.

Carla Figus, Mirko Traversari, Lucia Martina Scalise, **Gregorio Oxilia**, Antonino Vazzana, Laura Buti, Rita Sorrentino, Giorgio Gruppioni, Stefano Benazzi (2017). *The study of commingled non-adult human remains: Insights from the 16th–18th centuries community of Roccapelago (Italy).* Journal of Archaeological Science. 14; 382-391.

Under-Review:

Luca Fiorenza, Stefano Benazzi, **Gregorio Oxilia**, Ottmar Kullmer. *Functional relationship between dental macrowear, abrasion and food preparation methods in Late Pleistocene and recent modern human populations.* (International Journal of Osteoarchaeology)

G. Oxilia, O. Kullmer, G. Townsend, J. Kaidonis, Marco Boggioni, Andrea Papini, J. Moggi-Cecchi, L. Fiorenza, S. Benazzi. *The physiological linkage between dental arch asymmetry, alveolar inclination and dental macrowear pattern.* (Journal of Dental Research).

Alessandro Riga, **Gregorio Oxilia**, Daniele Panetta, Piero A. Salvadori, Stefano Benazzi, Lyn Wadley, Jacopo Moggi-Cecchi. *Human deciduous teeth from the Middle Stone Age layers of Sibudu Cave (South Africa).* (Journal of Anthropological Sciences).

Rita Sorrentino, Eugenio Bortolini, Federico Lugli, Giuseppe Mancuso, Laura Buti, **Gregorio Oxilia**, Antonino Vazzana, Carla Figus, Maria Cristina

Serrangeli, Cristiana Margherita, Annachiara Penzo, Giorgio Gruppioni, Antonio Gottarelli, Anna Cipriani, Klaus Peter Jochum, Robin N. M. Feeney, Stefano Benazzi. *Unravelling biocultural population structure in 4th/3rd century BC Monterenzio Vecchio (Bologna, Italy) through a comparative analysis of strontium isotopes, non-metric dental evidence, and funerary practices* (Plos-One).

Antonino Vazzana, Lucia Martina Scalise, Mirko Traversari, Carla Figus, Salvatore Andrea Apicella, Laura Buti, **Gregorio Oxilia**, Rita Sorrentino, Silvia Pellegrini, Chiara Matteucci, Lucio Calcagnile, Raffaele Savigni, Robin N.M. Feeney, Giorgio Gruppioni, Stefano Benazzi (2018). *A multianalytic investigation of weapon-related injuries in a Late Antiquity necropolis, Mutina, Italy*. Journal of Archaeological Science: Reports 17:550 – 559.

ACKNOWLEDGEMENTS

First of all, I would like to thank Petra. We've just always had each other's backs. Bachelor's degree first and then master's degree. Today I got PhD. Girlfriend of my past and wife of my present and future.

I would like to thank my first supervisor, Prof. Jacopo Moggi-Cecchi who gave me the opportunity to have a PhD-position at the University of Florence. Thank you for all your advices and availability.

My thanks also go to my second supervisor, Prof. Stefano Benazzi. Your constructive advices were helpful to address difficulties faced during these years of PhD.

I also would like to thank all of my co-authors, from each one I have learned how to work in a research-team.

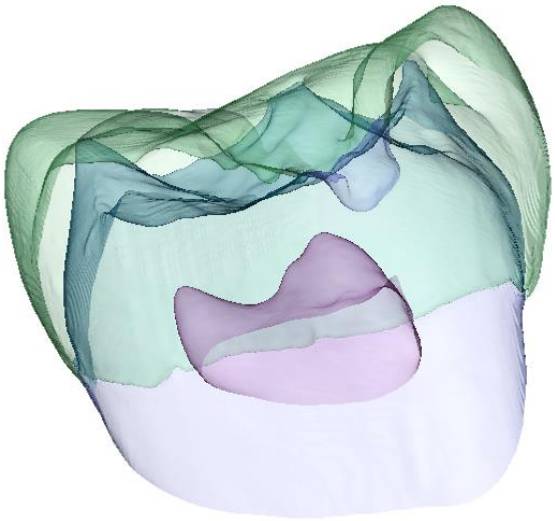

Nelle pagine seguenti saranno allegati due documenti:

1) Relazione delle attività svolte;
2) Medaglione del collegio docenti.

E’ opportuno giusticare la discrepanza che presenta la relazione delle attività svolte rispetto alla tesi.

Il motivo di tale diversità (in particolare nella struttura dell’abstract e nell’elenco pubblicazioni) è dovuto al fatto che, dalla consegna di tale documento (1) all’invio definitivo della tesi, è stato valutata la necessità di aggiungere un IX articolo (riorganizzando la struttura dell’abstract) ed aggiornare la lista delle pubblicazioni che, fortunatamente, ha subito delle variazioni (“ready to be submitted” in “under-review”).

Detto ciò, si invita i lettori a consultare i motori di ricerca internazionali per visionare lo stato di tali pubblicazioni che sicuramente subirà ulteriori aggiornamenti.

Relazione attività svolte durante il dottorato:

Human dental tissues:
Advancement in virtual dental analysis.

Dottorando: Gregorio Oxilia
Tutor: Prof. Jacopo Moggi-Cecchi
Supervisor: Prof. Stefano Benazzi

Durante questi tre anni di dottorato ho focalizzato l'attenzione sullo studio dei tessuti dentali umani prestando particolare attenzione alle nuove tecnologie e metodologie fisico/chimiche. Negli ultimi anni infatti, l'antropologia ha iniziato ad utilizzare approcci virtuali al fine di rendere più precisi e accurati i risultati ottenuti tramite metodologie tradizionali che, inevitabilmente, risultavano meno precise.

Questa tesi di dottorato documenta come un approccio virtuale 3D ed il supporto interdisciplinare scientifico nello studio antropologico, permettano di comprendere la struttura dei tessuti dentali e le alterazioni (masticatorie, para-masticatorie, para-funzionali e, una volta persi i tessuti molli, tafonomiche) che, nel corso del tempo, si sono accumulate sulla corona dentale.

La tesi presenta una raccolta di articoli (in totale 8 pubblicazioni) i quali mostrano come la complessità delle alterazioni presenti sui tessuti dentali possano essere correttamente interpretati tramite un'adeguata sequenza di analisi antropologiche con il supporto di metodi scientifici interdisciplinari.

I resti dentali sono la principale fonte di informazione in uno scavo archeologico e, a seconda del loro stato di conservazione, è possibile ottenere informazioni utili a comprendere la tassonomia, lo stile alimentare, la salute e l'igiene orale della specie identificata.

L’usura dentale consiste nella perdita di una certa quantità di tessuto dentario (smalto e/o dentina) per diversi motivi che possono essere distinti in cause para-funzionali/patologiche che producono, nel corso del tempo, una riduzione della corona dentale (stadio di usura superiore a 2, Smith, 1984) alterando la forma primaria del dente (stadio di usura 1, Smith, 1984).

Se si prende in considerazione un dente non usurato (stadio di usura 1) la struttura dentale si presenta integra, con cuspidi ben evidenti. La struttura permetterà dunque di ottenere informazioni “complete” inerenti al volume della corona dentale (smalto e dentina), utili per esempio ai fini dell’identificazione tassonomica. Con l’aumentare dell’usura molte informazioni vengono perse; in tal caso i campioni di confronto utilizzati per l’identificazione tassonomica dovranno essere calibrati sulla base dello stadio di usura del dente in esame. Questo è il caso del **Paper I** (“The first Neanderthal remains from an open-air Middle Palaeolithic site in the Levant” pubblicato recentemente su Scientific Reports – Nature), **Paper II** (“A reassessment of the presumed Torrener Barenh€ ohle's Paleolithic human tooth” pubblicato nel 2016 nel Journal of Human Evolution), **Paper III** (“A reexamination of the Middle Pa leolithic human remain s from Riparo Tagliente, Italy” pubblicato nel 2016 nel Quaternary International) e il **Paper IV** (“Morphological description and morphometric analyses of the Upper Palaeolithic human remains from Dzudzuana and Satsurblia caves, western Georgia” pubblicato recentemente nel Journal of Huan Evolution).

Grazie alle analisi dei tessuti dentali (valori volumetrici dello smalto, della dentina, oltre che della cavità pulpare e della radice), abbiamo restituito risultati utili all’identificazione tassonomica di alcuni resti umani.

Una volta superato lo stadio di usura 3 (Smith, 1984) risulta difficile procedere con le analisi tassonomiche sia per la mancanza di campioni di confronto, sia per la ridotta quantità di informazioni che i tessuti dentali possono restituire. All’aumentare dello stadio di usura (>2, Smith, 1984) e delle patologie (carie)

dunque, è possibile applicare altre metodologie; una tra tutte è la macrousura dentale.

Tramite l'identificazione delle faccette d'usura (piccoli piani inclinati sviluppati sulla superfice occlusale dei denti) è possibile rilevare informazioni inerenti alle dinamiche masticatorie, para-masticatorie e patologiche. Questo è il caso del **Paper V** ("*Earliest evidence of dental caries manipulation in the Late Upper Palaeolithic*" pubblicato nel 2015 su Scientific Reports - Nature) e **Paper VI** ("*The dawn of dentistry in the late upper Paleolithic: An early case of pathological intervention at Riparo Fredian*",pubblicato recentemente sull'American Journal of Physical Anthropology). Due casi studio in cui è stato possibile, tramite lo studio dell'usura dentale, analisi microscopiche e dei materiali residui (Scanning Electron Microscopy (SEM), Fourier transform infrared spectroscopy (FTIR), energy dispersion X-ray spectroscopy (EDS), Raman microscopy analysis), confermare i due casi più antichi di manipolazione dentale datati in un range cronologico di 14.000 – 12.000 anni, retrodatando di circa 8,000 anni i più antichi casi di cura dentale fino ad oggi noti.

La scelta di utilizzare alcune metodologie (Fourier transform infrared spectroscopy (FTIR), energy dispersion X-ray spectroscopy (EDS), and Raman microscopy analysis) rispetto ad altre (Gas chromatography) ha permesso di porre in luce una problematica ad oggi di notevole importanza: la conservazione del materiale biologico. Quali sono i criteri nella scelta dell'applicazione di tecniche invasive rispetto a quelle non-invasive?.

Questo è il topic del **Paper VII** ("*Letter to the editor: Reply to Hardy & Buckley: Earliest evidence of bitumen from Homo sp. teeth is from El Sidron*"). Una "Letter to the editor" inviata all'American Journal of physical anthropology in risposta ad alcuni ricercatori i quali ponevano in dubbio la scelta/applicazione delle metodologie chimico/fisici utilizzate per analizzare il materiale biologico estratto dalle cavità cariose identificare nei reperti del Riparo Fredian.

Infine, la tesi pone l'attenzione sulla necessità di studiare i denti animali umani, nel contesto in cui essi si sviluppano (sistema masticatorio). Il **Paper VIII** ("*The physiologicial linkage between dental arch asymmetry, alveolar inclination and dental macrowear pattern*" – pronto per la sottomissione al Journal of Dental Research) ha lo scopo di evidenziare, tramite l'utilizzo di una campione umano recente (Aborigenal – Yuemudu) una stretta correlazione tra lo sviluppo delle usure dentali e le asimmetrie palatali/alveolari. Questa alterazione dovuta a "fattori interni" contrasta con gli studi paleonutrizionali ad oggi noti che attribuiscono al cibo (fattori esterni) la principale causa dello sviluppo delle usura dentali. Questo nuovo approccio cerca di porre al centro del dibattito la corretta interpretazione dei dati ottenuti tramite le usure dentali in ambito odontoiatrico ed evolutivo umano.

Lista di pubblicazioni:

2015:

Gregorio Oxilia, Marco Peresani, Matteo Romandini, Chiara Matteucci, Cynthianne Debono Spiteri, Amanda G. Henry, Dieter Schulz, Will Archer, Jacopo Crezzini, Francesco Boschin, Paolo Boscato, Klervia Jaouen, Tamara Dogandzic, Alberto Broglio, Jacopo Moggi-Cecchi, Luca Fiorenza, Jean-Jacques Hublin, Ottmar Kullmer & Stefano Benazzi. *Earliest evidence of dental caries manipulation in the Late Upper Palaeolithic. Sci. Rep.* **5**, 12150; doi: 10.1038/srep12150 (2015).

2016:

Cristiana Margherita, Sahra Talamo, Karin Wiltschke-Schrotta, Sascha Senck, **Gregorio Oxilia**, Rita Sorrentino, Giuseppe Mancuso, Giorgio Gruppioni, Robert Lindner, Jean-Jacques Hublin, Stefano Benazzi (2016). A reassessment

of the presumed Torrener Bärenhöhle's Paleolithic human tooth. *Journal of Juman Evolution,* 30; 1e6.

Julie Arnaud, Carlo Peretto, Daniele Panetta, Maria Tripodi, Federica Fontana, Marta Arzarello, Ursula Thun Hohenstein, Claudio Berto, Benedetto Sala, **Gregorio Oxilia**, Piero A Salvadori, Stefano Benazzi (2016). A reexamination of the Middle Paleolithic human remains from Riparo Tagliente, Italy. *Quaternary International, 425;* 437-444.

2017:

Gregorio Oxilia, Flavia Fiorillo, Francesco Boschin, Elisabetta Boaretto, Salvatore A. Apicella, Chiara Matteucci, Daniele Panetta, Rossella Pistocchi, Franca Guerrini, Cristiana Margherita, Massimo Andretta, Rita Sorrentino, Giovanni Boschian, Simona Arrighi, Irene Dori, Giuseppe Mancuso, Jacopo Crezzini, Alessandro Riga, Maria C. Serrangeli, Antonino Vazzana, Piero A. Salvadori, Mariangela Vandini, Carlo Tozzi, Adriana Moroni, Robin N. M. Feeney, John C. Willman, Jacopo Moggi-Cecchi, Stefano Benazzi. *The dawn of dentistry in the late upper Paleolithic: An early case of pathological intervention at Riparo Fredian*. Am J Phys Anthropol. 2017a; 00:1–16. https://doi.org/10.1002/ajpa.23216

Gregorio Oxilia, Flavia Fiorillo, Francesco Boschin, Elisabetta Boaretto, Salvatore A. Apicella, Chiara Matteucci, Daniele Panetta, Rossella Pistocchi, Franca Guerrini, Cristiana Margherita, Massimo Andretta, Rita Sorrentino, Giovanni Boschian, Simona Arrighi, Irene Dori, Giuseppe Mancuso, Jacopo Crezzini, Alessandro Riga, Maria C. Serrangeli, Antonino Vazzana, Piero A. Salvadori, Mariangela Vandini, Carlo Tozzi, Adriana Moroni, Robin N. M. Feeney, John C. Willman, Jacopo Moggi-Cecchi, Stefano Benazzi. (2017b).

Letter to the editor: Reply to Hardy & Buckley: Earliest evidence of bitumen from Homo sp. teeth is from El Sidron. Am J Phys Anthropol. DOI: 10.1002/ajpa.23254.

Ella Been, Erella Hovers, Ravid Ekshtain, Ariel Malinski-Buller, Nuha Agha, Alon Barash, Daniella E. Bar-Yosef Mayer, Stefano Benazzi, Jean-Jacques Hublin, Lihi Levin, Noam Greenbaum, Netta Mitki, **Gregorio Oxilia**, Naomi Porat, Joel Roskin, Michalle Soudack, , Reuven Yeshurun, Ruth Shahack-Gross, Nadav Nir, Mareike C. Stahlschmidt, Yoel Rak, Omry Barzilai. The first Neanderthal remains from an open-air Middle Palaeolithic site in the Levant. Scientific Reports. 2017, 7 - 2958 doi:10.1038/s41598-017-03025-z

Cristiana Margherita, **Gregorio Oxilia**, Veronica Barbi, Daniele Panetta, Jean – Jacques Hublin, David Lordkipanidze, Tengiz Meshveliani, Nino Jakeli, Zinovi Matskevich, Ofer Bar-Yosef, Anna Belfer-Cohen, Ron Pinhasi, Stefano Benazzi (2017). Morphological description and morphometric analyses of the Upper Palaeolithic human remains from Dzudzuana and Satsurblia caves, western Georgia. *Journal of Human Evolution.* 113; 83-90.

Carla Figus, Mirko Traversari, Lucia Martina Scalise, **Gregorio Oxilia**, Antonino Vazzana, Laura Buti, Rita Sorrentino, Giorgio Gruppioni, Stefano Benazzi (2017). The study of commingled non-adult human remains: Insights from the 16th–18th centuries community of Roccapelago (Italy). *Journal of Archaeological Science*. 14; 382-391.

Ready to be Submitted:

G. Oxilia, O. Kullmer, G. Townsend, J. Kaidonis, Marco Boggioni, Andrea Papini, J. Moggi-Cecchi, L. Fiorenza, S. Benazzi. *Asymmetry, balance and*

dental macrowear patterns of Yuendumu Aboriginals: a case study. (*Journal of Dental research*).

Congressi durante il dottorato:

2017

Gregorio Oxilia, Flavia Fiorillo, Francesco Boschin, Elisabetta Boaretto, Salvatore A. Apicella, Chiara Matteucci, Daniele Panetta, Rossella Pistocchi, Franca Guerrini, Cristiana Margherita, Massimo Andretta, Rita Sorrentino, Giovanni Boschian, Simona Arrighi, Irene Dori, Giuseppe Mancuso, Jacopo Crezzini, Alessandro Riga, Maria C. Serrangeli, Antonino Vazzana, Piero A. Salvadori, Mariangela Vandini, Carlo Tozzi, Adriana Moroni, Robin N. M. Feeney, John C. Willman, Jacopo Moggi-Cecchi and Stefano Benazzi. *The dawn of dentistry in the Late Upper Paleolithic: An early case of pathological intervention at Riparo Fredian.* European Society for the Human Evolution (ESHE), 21-23 September 2017, Leiden.

Riga A., Oxilia, G., Panetta D., Salvadori P.A., Benazzi S., Wadley L., Moggi-Cecchi J. *Human deciduous teeth from the Middle Stone Age layers of Sibudu Cave (South Africa).* European Society for the Human Evolution (ESHE), 21-23 September 2017, Leiden.

Cristiana Margherita, Gregorio Oxilia, Laura Buti, Jean-Jacques Hublin, Stefano Benazzi. *3D enamel thickness in Neandertal and Homo sapiens permanent lower molars and premolars.* European Society for the Human Evolution (ESHE), 21-23 September 2017, Leiden.

Gregorio Oxilia, Flavia Fiorillo, Francesco Boschin, Elisabetta Boaretto, Salvatore A. Apicella, Chiara Matteucci, Daniele Panetta, Rossella Pistocchi, Franca Guerrini, Cristiana Margherita, Massimo Andretta, Rita Sorrentino, Giovanni Boschian, Simona Arrighi, Irene Dori, Giuseppe Mancuso, Jacopo Crezzini, Alessandro Riga, Maria C. Serrangeli, Antonino Vazzana, Piero A. Salvadori, Mariangela Vandini, Carlo Tozzi, Adriana Moroni, Robin N. M. Feeney, John C. Willman, Jacopo Moggi-Cecchi and Stefano Benazzi. *L'origine dell'odontoiatria nel Tardo Paleolitico superiore: l'antichità delle cure biomediche.* Associazione Antropologica Italiana (AAI), 6-8 September 2017, Roma.

Riga A., Oxilia, G., Panetta D., Salvadori P.A., Benazzi S., Wadley L., Moggi-Cecchi J. Nuovi resti di denti decidui dai livelli di Middle Stone Age di Sibudu Cave (Sud Africa). Associazione Antropologica Italiana (AAI), 6-8 September 2017, Roma.

Figus C., Traversari M., Vazzana A., Sorrentino R., Buti L., Scalise L.M., Oxilia G., Gruppioni G., Benazzi S. Neonatal and postnatal mortality in Roccapelago through the study of human skeletal remains and parish records. Associazione Antropologica Italiana (AAI), 6-8 September 2017, Roma.

Gregorio Oxilia, Flavia Fiorillo, Francesco Boschin, Elisabetta Boaretto, Salvatore A. Apicella, Chiara Matteucci, Daniele Panetta, Rossella Pistocchi, Franca Guerrini, Cristiana Margherita, Massimo Andretta, Rita Sorrentino, Giovanni Boschian, Simona Arrighi, Irene Dori, Giuseppe Mancuso, Jacopo Crezzini, Alessandro Riga, Maria C. Serrangeli, Antonino Vazzana, Piero A. Salvadori, Mariangela Vandini, Carlo Tozzi, Adriana Moroni, Robin N. M. Feeney, John C. Willman, Jacopo Moggi-Cecchi and Stefano Benazzi. *The dawn of dentistry in the Late Upper Paleolithic: An early case of pathological*

intervention at Riparo Fredian. American Association of Physical Anthropologist (AAPA), 19-22 April 2017, New Orleans.

2016

Cristiana Margherita, Gregorio Oxilia, Veronica Barbi, Daniele Panetta, Jean-Jacques Hublin, David Lordkipanidze, Tengiz Meshveliani, Nino Jakeli, Zinovi Matskevich, Ofer Bar-Yosef, Anna Belfer-Cohen, Ron Pinhasi, Stefano Benazzi. *Morphological description and morphometric analyses of the Upper Palaeolithic human remains from Dzudzuana and Satsurblia caves, western Georgia.* European Society for the Human Evolution (ESHE), 9-14 September 2016, Madrid.

2015

Oxilia G, Peresani M, Romandini M, Matteucci C, Spiteri CD, Henry AG, Schulz D, Archer W, Crezzini J, Boschin F, Boscato P, Jaouen K, Dogandzic T, Broglio A, Moggi-Cecchi J, Fiorenza L, Hublin JJ, Kullmer O, Benazzi S. *Earliest evidence of proto-dental treatment in the Late Upper Paleolithic.* European Society for the Human Evolution (ESHE), 10-12 September 2015, London.

Oxilia G, Peresani M, Romandini M, Matteucci C, Spiteri CD, Henry AG, Schulz D, Archer W, Crezzini J, Boschin F, Boscato P, Jaouen K, Dogandzic T, Broglio A, Moggi-Cecchi J, Fiorenza L, Hublin JJ, Kullmer O, Benazzi S. *Earliest evidence of proto-dental treatment in the Late Upper Paleolithic.* Associazione Antropologica Italiana (AAI), 3-5 September 2015, Bologna/Ravenna.

Esperienze all'estero durante il dottorato:

Settembre – Dicembre 2016	PhD student visitor at the School of Biomedical Sciences, Faculty of Medicine Nursing and Health Sciences at the Monash University (Melbourne - Australia).

Esperienza di scavo durante il dottorato:

11 Luglio 2016 – 22 Luglio 2016	Scavo Archeologico preistorico (Grotta dell'Alma Veirana – Liguria)
15 Luglio 2015 – 8 Agosto 2015	Scavo Archeologico preistorico (Grotta dell'Alma Veirana – Liguria)

Workshop seguiti durante il dottorato:

26 Giugno -07 Luglio 2017	"Acquiring and post-processing 3D data in Anthropology and Archaeology". (membro dell'organizzazione) In Ravenna (Italy), Department for Cultural Heritage_ University of Bologna.
20-21 Ottobre 2016	"Virtual reconstruction and Computational Biomechanics" In Melbourne (Australia), Department of Anatomy and Developmental Biology_ Monash University - Clayton Campus.
27 Giugno -01 Luglio 2016	"Acquiring and post-processing 3D data in Anthropology and Archaeology". (membro dell'organizzazione)

In Ravenna (Italy), Department for Cultural Heritage_ University of Bologna.

Premi:

12 Settembre 2015 (London) Premio per la miglior ricerca, European Society for the study of Human Evolution.

Posizioni accademiche:

26 Febbraio 2016 Lezioni di Antropologia dentale ed Antropologia virtuale presso la Scuola di Paleoantropologia. (Dipartimento di Fisica e Geologia, Università di Perugia).

2015 – Oggi Membro della commissione esaminatrice per I corsi di laurea di Antropologia fisica, Paleoantropologia e Bioarcheologia (Università di Bologna)

2015 - Oggi Cultore della materia in Paleoantropologia e Bioarcheologia. (Università di Bologna - campus Ravenna).

Medaglione Collegio Docenti

UNIVERSITÀ DEGLI STUDI DI FIRENZE
Dipartimento di Biologia Evoluzionistica

Dottorato di Ricerca in Biologia (DRB)

Sede amministrativa: Dipartimento di Biologia
Via G. La Pira, 4, Firenze, Italy
Tel. +39- 055 2757418

Coordinatore DREEAB e DRB: Prof. Alberto Ugolini
Tel. 055 275 5152
e-mail:alberto.ugolini@unifi.it

Verbale della riunione del Collegio dei Docenti del DRB seduta del 27 Settembre 2017 presso locali di Via Romana 17, Firenze.
La riunione inizia alle ore 9.00 con il seguente ordine del Giorno:

Seduta pubblica
1-Relazioni dei dottorandi del XXX ciclo e dei dottorandi dei cicli precedenti con rinvio della Tesi.

Seduta ristretta
2-Comunicazioni
3-Sostituzione del supervisore per la dottoranda Valeria Mazza
4-Conseguimento del titolo di "Doctor Europaeus"
5-Valutazione delle relazioni presentate dai dottorandi del XXX ciclo sull'attività triennale, formulazione dei giudizi sull'attività svolta nei 3 anni e ammissione dei dottorandi del XXX e dei dottorandi dei cicli precedenti con rinvio della Tesi alle successive procedure previste per il conseguimento del titolo.
6-Individuazione dei revisori delle Tesi
7-Composizione della commissione giudicatrice per l'esame finale del XXX ciclo e dei dottorandi con rinvio della discussione della Tesi appartenenti a cicli precedenti.
8-Varie ed eventuali

SEDUTA PUBBLICA
Inizio ore 9.00.
Presenti: Ugolini (Coordinatore e presidente di seduta), Beani , Santini, Moggi, Caramelli, Cervo, Mengoni, Dani. Zaccaroni, Lari, Fani, Foggi, Turillazzi

Assenti giustificati: Mariotti, Perito, Cirulli, Chelazzi, , Scapini, Gonnelli, Papini, Cavalieri, Coppi, Ciofi,
Assenti: Maleci, Mastromei, Cannicci, Mocali, Bazzicalupo, Stanyon,

1-Relazioni dei dottorandi del XXX ciclo e dei dottorandi dei cicli precedenti con rinvio della Tesi.
L'ordine delle presentazioni (30' di tempo) è il seguente:

Dottorando	Tutors
1 Presta Luana	Mengoni
2 Mazza Valeria	Mengoni
3 Oxilia Gregorio	Moggi

4 Ciofini Alice	Ugolini
5 Lombardi Sonia (29°)	Santini
6 Amitrano Francesca	Caramelli
7 Pilli Elena	Caramelli
8 Pepiciello Irene	Cervo

SEDUTA RISTRETTA Inizio ore 13.00
Presenti: Ugolini (Coordinatore e presidente di seduta), Beani , Santini, Moggi, Caramelli, Cervo, Mengoni, Dani. Zaccaroni, Lari, Fani, Foggi, , Ciofi,
Assenti giustificati: Mariotti, Perito, Cirulli, Chelazzi, Scapini, Gonnelli, Papini, Cavalieri, Coppi, Turillazzi
Assenti: Maleci, Mastromei, Cannicci, Mocali, Bazzicalupo, Stanyon,

.....OMISSIS.....

5-Valutazione delle relazioni presentate dai dottorandi del XXX ciclo sull'attività triennale,e formulazione dei giudizi sull'attività svolta nei 3 anni e ammissione dei dottorandi del XXX e dei dottorandi dei cicli precedenti con rinvio della Tesi alle successive procedure previste per il conseguimento del titolo.

Il Collegio Docenti, valutate le relazioni presentate dai dottorandi e sentiti i supervisori, stila i giudizi sintetici relativi all'attività triennale di ciascun dottorando. Valutata l'attività complessiva di ciascun dottorando e dei dottorandi con rinvio della Tesi, il Collegio Docenti ammette tutti i dottorandi alla prosecuzione delle procedure previste per accedere alla discussione finale della Tesi (v allegati 1 - 8).

.....OMISSIS.....

La riunione termina alle 15.05

Firenze 27 Settembre 2017

Il Coordinatore

Prof. Alberto Ugolini

Il Segretario

Prof. Alessio Mengoni

Allegato 3

Gregorio Oxilia

Valutazione dell'attività triennale

Il Dott. Gregorio Oxilia nato a Verona il 14/01/1988, si è laureato in Quaternario, Preistoria ed Archeologia (LM-2) nel 2014 presso l'Università di Ferrara.
Il candidato ha elaborato una Tesi di Dottorato dal titolo *Human dental tissues: Advancements in virtual dental analysis* che è stata svolta presso il Dipartimento di Biologia (Università di Firenze) e presso il Dipartimento di beni Culturali dell'Università di Bologna. L'opera di tutorato è stata affidata al Prof. Jacopo Moggi Cecchi.
Oggetto della ricerca sono state l'individuazione e l'applicazione delle più avanzate tecniche di analisi digitale per lo studio di reperti dentari da contesti fossili del Paleolitico superiore italiano ed europeo
La ricerca compiuta dal Dott. Oxilia ha reso possibile la messa a punto e l'approfondimento di metodi di indagine di antropologia virtuale che hanno consentito lo studio non invasivo di resti fossili. I vari metodi hanno messo in evidenze la possibilità di usare queste tecniche per ricerche di sistematica, paleopatologia e funzionalità della dinamica masticatoria.
Il dottorando ha dimostrato di saper procedere nella ricerca con autonomia nelle analisi di laboratorio, progettando in maniera indipendente le varie fasi del lavoro svolto.
Ha partecipato a cinque congressi scientifici sia nazionali che internazionali, presentando sei contributi come poster e tre come comunicazione orale. Nel 2015 ha vinto il premio come miglior poster al congresso della *European Society for the study of Human Evolution*. Ha pubblicato otto lavori scientifici su riviste internazionali indicizzate di cui due a primo nome. Ha tenuto lezioni seminariali per il corso di Antropologia fisica, Paleoantropologia e Bioarcheologia e nell'ambito della Scuola di Paleoantropologia presso l'Università di Perugia.
Il collegio dei docenti esprime il proprio compiacimento per la ricerca svolta e per l'attività triennale nel suo complesso ed approva la possibilità di accedere alle procedure di ammissione all'esame finale.